2-7-2011 12:00 AM

Synthesis of One-Dimensional And Two-Dimensional Carbon Based Nanomaterials

Mihnea Ioan Ionescu
The University of Western Ontario

Supervisor
Xueliang Sun
The University of Western Ontario

Graduate Program in Mechanical and Materials Engineering
A thesis submitted in partial fulfillment of the requirements for the degree in Doctor of Philosophy

SYNTHESIS OF ONE-DIMENSIONAL AND TWO-DIMENSIONAL CARBON BASED NANOMATERIALS

(Spine title: Synthesis of 1D and 2D Carbon based Nanomaterials)

(Thesis format: Integrated-Article)

by

Mihnea Ioan Ionescu

Graduate Program in Mechanical and Materials Engineering

A thesis submitted in partial fulfillment
of the requirements for the degree of
Doctor of Philosophy

The School of Graduate and Postdoctoral Studies
The University of Western Ontario
London, Ontario, Canada

THE UNIVERSITY OF WESTERN ONTARIO
School of Graduate and Postdoctoral Studies

CERTIFICATE OF EXAMINATION

Supervisor

Dr. Xueliang Sun

Supervisory Committee

Dr. Jun Yang

Examiners

Dr. Jeff Wood

Dr. Jun Yang

Dr. Paul Charpentier

Dr. Gu Xu

The thesis by

Mihnea Ioan Ionescu

entitled:

Synthesis of One-Dimensional and Two-Dimensional Carbon Based Nanomaterials

is accepted in partial fulfillment of the
requirements for the degree of
Doctor of Philosophy

Date

Chair of the Thesis Examination Board

ABSTRACT

Particular physical and chemical properties of carbon based nanomaterials (CBNs) have promised and exhibited great applications in manufacturing various nanodevices such as electron field emitters, sensors, one-dimensional conductors, supercapacitors, reinforcing fibres, hydrogen storage devices, and catalyst supports for fuel cells electrodes. Despite these amazing technical progresses, many challenges still remain in the development of synthesis methods suitable for commercial applications and fabricating novel functional nanostructures with complex architectures.

In this Ph.D. thesis, one-dimensional (1D), two-dimensional (2D) carbon nanostructures, and 1D/2D hybrid of carbon nanostructures have been synthesized using various chemical vapour deposition (CVD) methods. The objective of this work is to explore the potential of various CVD methods, including specially-designed CVD techniques, such as modified spray pyrolysis, plasma enhanced CVD, and magnetron sputtering deposition. By making use of these innovative methods, high density regular and nitrogen-doped nanotubes, graphite nanosheets and assemblies have been successfully obtained on conducting and semiconducting substrates. For the modified spray pyrolysis method, systematic investigation of regular carbon nanotubes (CNTs) was conducted in terms of optimizing various experimental parameters such as hydrocarbon source, temperature, and catalyst in order to control the quality and structure of CBNs. Doping of nitrogen into carbon nanotubes was also systematically studied to enhance their electrical and mechanical properties. Interestingly, a novel

structure of multi-branched nitrogen doped CNTs has been achieved by this modified spray pyrolysis method. By employing the plasma assisted CVD/sputtering hybrid system, selective growth of single and few walled CNTs have been realized. The device has also been able to produce 2D carbon nanostructures of nanosheets and a hybrid of nanosheets suspended on vertical aligned CNTs. Based on the magnetron sputtering deposition method, carbon nanowalls have been synthesized without any catalyst addition. Morphology, microstructure, and vibration properties of the CBNs were characterized by scanning electron microscopy, transmission electron microscopy, Raman spectroscopy, and X-ray photoelectron spectroscopy.

Carbon nanomaterials, grown in high densities on conducting and semiconducting substrates, promise great potential in building various nanodevices with different electron conducting requirements. In addition, CBNs provide a very high surface area for the support of platinum particles for use in hydrogen fuel cell electrodes.

Keywords: Carbon, Nanomaterials, Carbon Based Nanomaterials, Nanotubes, Doped Nanotubes, Branched Nanotubes, Graphite Sheets, Nanowalls, Chemical Vapor Deposition

CO-AUTHORSHIP

Chapter 4: Mihnea Ionescu – designed and implemented the experimental device, conducted the experiments, collected and analyzed the data, and wrote the chapter; Yong Zhang – helped to acquire the Raman spectra, reviewed, and revised the chapter; Ruying Li – helped to acquire the SEM images and acquired the TEM images; Xueliang Sun – guided the experiments and revised the chapter; Hakima Abou-Rachid – made revisions and recommendations to the chapter; Louis-Simon Lussier – revised the chapter.

Chapter 5: Mihnea Ionescu – improved the design of the experimental device, conducted the experiments, design and implemented the electrical characterization setup, collected and analyzed the data, and wrote the chapter; Yong Zhang – helped to analyze the XPS data and to acquire the Raman spectra, reviewed, and revised the chapter; Ruying Li – helped to acquire the SEM images and acquired the TEM images; Xueliang Sun – guided the experiments and revised the chapter.

Chapter 6: Mihnea Ionescu – innovated and implemented the design of the experimental device, conducted the experiments, collected and analyzed the data, and wrote the chapter; Yong Zhang – helped to acquire the Raman spectra, reviewed, and revised the chapter; Ruying Li – helped to acquire the SEM images and acquired the TEM images; Xueliang Sun – guided the experiments and revised the chapter; Hakima

Abou-Rachid – made revisions and recommendations to the chapter; Louis-Simon Lussier – revised the chapter.

Chapter 7: Mihnea Ionescu – conducted the experiments, design and implemented the electrical characterization setup, collected and analyzed the data, and wrote the chapter; Yong Zhang – helped to acquire the Raman spectra, reviewed, and revised the chapter; Ruying Li – helped to acquire the SEM images and acquired the TEM images; Xueliang Sun – guided the experiments and revised the chapter.

Chapter 8: Mihnea Ionescu – innovated and implemented the design of the experimental device, conducted the experiments, collected and analyzed the data, and wrote the chapter; Yong Zhang – helped to acquire the Raman spectra, reviewed, and revised the chapter; Ruying Li – helped to acquire the SEM images and acquired the TEM images; Xueliang Sun – guided the experiments and revised the chapter.

Chapter 9: Mihnea Ionescu – innovated and implemented the design of the experimental device, conducted the experiments, collected and analyzed the data, and wrote the chapter; Yong Zhang – helped to acquire the Raman spectra, reviewed, and revised the chapter; Ruying Li – helped to acquire the SEM images and acquired the TEM images; Xueliang Sun – guided the experiments and revised the chapter.

DEDICATION

To my dearest mother, wife, and sister for their never ending love, prayers, encouragements, and support.

ACKNOWLEDGEMENTS

I genuinely thank my research advisor, Prof. Xueliang Andy Sun, for his encouragement, support, patience, advice, and guidance during my whole study period. I am grateful for offering me the opportunity to be part of his Nanomaterials and Energy research group. I doubt that I will ever be able to convey my appreciation fully, but I owe him my deepest gratitude.

I would like to express my special thanks to Mrs. Ruying Li (Kathy), for providing me with understanding and support. Her advice, encouragement, and kindness played an essential role in the development of this thesis by helping me overcome many obstacles.

I wish to extend my sincere appreciation to Dr. Yong Zhang (Bryan), for taking time out from his busy schedule to review and revise my scientific writing. His hard work, advice, help and our fruitful discussions were crucial in finalizing and refining this thesis.

Sincere thanks to Dr. Jun Yang for following my research progress and for accepting to be part of the Supervisory Committee.

I would like to thank all my colleagues from Nanomaterials and Energy research group. They have created a friendly, highly professional, and wonderful study environment which has made the whole learning journey worthwhile.

I recognize that this research would not have been possible without the financial assistance of NSERC, the University of Western Ontario Graduate Studies, the

Department of Mechanical and Materials Engineering at the University of Western Ontario (Teaching Assistantships, Graduate Research Scholarships), and the Province of Ontario Graduate Scholarship fund, and express my acknowledgement to these agencies.

I will never have enough words of gratitude and love for my family and friends. Your love, care, and unconditional support brought happiness into my life. Thank you for showing me a great deal about who I am and who I'd like to become. Last, but certainly not least, I need to thank my wife and best friend, Betty, who surrounded me with love and encouragement. Without your help and editing assistance, I would never have managed to finish this thesis. You're a real trouper to have stuck with me through these years in my life.

TABLE OF CONTENTS

LIST OF TABELS

LIST OF FIGURES

LIST OF SYMBOLS

0D	Zero Dimensional
1D	One Dimensional
2D	Two Dimensional
AACVD	Aerosol Assisted Chemical Vapor Deposition
C60	Buckminsterfullerene
CBN	Carbon Based Nanomaterial
CNS	Carbon Nanosheet
CNT	Carbon Nanotubes
CNW	Carbon Nanowall
CNx	Nitrogen-Doped Carbon Nanotube
CVD	Chemical Vapor Deposition
DC	Direct Current
DLC	Diamond-Like Carbon
EELS	Electron-Energy Loss Spectroscopy
FCCVD	Floating Catalyst Chemical Vapor Deposition
FLG	Few-Layer Graphene
FWCNT	Few-Walled Carbon Nanotube
GLC	Glass-Like Carbon
HiPCO	High Pressure Carbon Monoxide
HOPG	Highly Oriented Pyrolytic Graphite

HPHT	High Pressure and High Temperature
ITO	Indium Tin Oxide
MWCNT	Multi-Walled Carbon Nanotube
PECVD	Plasma Enhanced Chemical Vapor Deposition
RBM	Radial Breathing Mode
RF	Radio Frequency
SEM	Scanning Electron Microscopy
SS	Stainless Steel
SWCNT	Single-Walled Carbon Nanotube
TCR	Temperature Coefficient of Resistance
TEM	Transmission Electron Microscopy
VA-CNT	Vertically Aligned Carbon Nanotube
XPS	X-ray Photoelectron Spectroscopy

CHAPTER 1

GENERAL INTRODUCTION

1.1 Nanotechnology

Nanotechnology is the study and creation process of functional and useful materials, devices, and systems through control of matter at the nanometer scale, generally between 1 to 100 nanometers in at least one dimension. The study of physical properties of nanoscale materials have led to numerous new applications. The aim of nanotechnology is to make use of these properties and efficiently manufacture and generate larger structures with fundamentally new molecular organization [1]. Theoretically, this possibility was envisioned in 1959 by Richard Feynman [2]. The term ‘nanotechnology’ was popularized by K. Eric Drexler, when he exposed ideas about building machines at the molecular scale, far smaller than a cell. Drexler spent years analyzing these incredible devices and finally published a milestone book in the 1990’s: “Nanosystems: Molecular Machinery, Manufacturing, and Computation” [3, 4]. At that time, fullerenes and nanotubes were just discovered and nanotechnology became an accepted concept [5, 6]. Nanoscale materials such as nanotubes, nanowires, and nanobelts have extraordinary properties and unique geometric features [7]. These are exciting discoveries of the last two decades which have given a great impulse to the research on nanomaterials. They have offered new opportunities of exploring distinct properties of nanoscale materials, but also issued new challenges. Utilizing their properties at the

nanoscale and bringing these properties to the macroscale are difficult tasks. For this reason, a new conceptual framework for nanotechnology development which takes into consideration the present scientific potential [8] has been envisioned. It proposes an interdisciplinary approach spanning across applied physics, materials science, engineering, mechanics, electronics, and biology. The framework describes four generations of nanotechnology development. The first generation of nanotechnology products incorporates passive nanostructures and designed materials to perform one task. The second phase introduces active nanostructures for multitasking such as actuators, drug delivery devices, and sensors. The third generation features nanosystems with thousands of interacting components built from the bottom-up, rather than manufactured using top-down fabrication methods. Such achievements would lead to the fourth generation which is expected to combine heterogeneous molecular systems. From this point of view, the contemporary research performed in this area is not nanotechnology in the original meaning of the word. Realistically, the nanotechnology development could be considered at the end of the first generation [9]. From this perspective, the synthesis of nanomaterials with controlled structure plays a crucial role in nanotechnology research towards the second generation of nanotechnology development.

1.2 Carbon nanomaterials

Nanomaterials cover various types of nanostructured materials which posses at least one dimension in the nanometer range [10]. While most microstructured materials

have similar properties to their bulk counterparts, the properties of materials with nanometer dimensions are significantly different from those of atoms and bulk materials [7]. Carbon is a unique element due to its ability to form a variety of nanomaterials ranging from zero-dimensional (0D) fullerenes to one-dimensional (1D) conducting and semiconducting carbon nanotubes, and to two-dimensional (2D) semimetallic graphenes [11]. These carbon based nanomaterials have remarkable physical properties and have received specific attention for a variety of applications. It clearly appears that carbon based materials constitute a topic of huge scientific interest and great strategic importance, in which an interdisciplinary approach is necessary [12]. Although the study of nanostructured carbon materials has recently undergone a steadily rapid development and keeps a fast moving research field, the investigation still lacks in terms of fundamental understandings of the growth mechanisms and key factors responsible for the synthesis of carbon nanomaterials. Moreover, because the carbon phase diagram is far from in-depth exploration, new forms of carbon are expected to be discovered. Carbon based nanomaterials are currently considered a milestone in nanotechnology because they provide an accelerated scientific progress with many industrial applications. Achieving an enhanced degree of controllability and tuning capacity of material properties, would lead to the accomplishment of the ultimate nanotechnological goal: the capability to design and manufacture various complex three-dimensional hierarchical assembly nanostructures and fabrication of self-assembly nanoengineered systems.

1.3 Thesis objectives and structure

Numerous studies of CNBs have previously been conducted in examining the synthesis of 1D carbon nanotubes, their physical properties, and the influence of different growth parameters. However, there have been few studies investigating the factors that influence the nanotube growth in spray pyrolysis and plasma assisted deposition methods. Less has been done with regards to the synthesis of 2D carbon nanostructures. Consequently, this study is focused on the implementation of controllable synthesis procedures and on the correlation between the applied growth parameters and the structure of the obtained carbon based nanomaterials. 1D and 2D carbon based nanostructures have been synthesized by employing different methods, such as spray pyrolysis, plasma enhanced chemical vapor deposition (PECVD), and magnetron sputtering.

The thesis consists in ten chapters organized in the following arrangement:

Chapter 1 generally introduces the background of nanotechnology and nanomaterials. The research objectives and the thesis structure are outlined.

Chapter 2 is a review of the fundamental aspects of carbon materials with respect to the structure and properties of different types of carbon materials. It also describes the most important techniques presently used for carbon nanomaterials synthesis. In addition, general considerations on doping carbon nanotubes are presented along with the growth mechanism of regular and doped nanotubes.

Chapter 3 outlines the experimental setups and provides information about the employed characterization methods and procedures.

Chapter 4 proposes a modified spray pyrolysis chemical vapor deposition (CVD) method for growing carbon nanotubes (CNTs) on electrically semiconducting and conducting substrates without hydrogen addition. The experiments have been conducted by optimizing the various parameters such as temperature, precursor flow rate, precursor volume, and catalyst concentration.

Chapter 5 considers the study of nitrogen-doping effects on the growth and structure of carbon nanotubes obtained by spray pyrolysis method. The nitrogen amount incorporated in CNTs decreases the growth rate and influences the tubes structure, from straight to corrugated nanotubes.

Chapter 6 outlines the synthesis of a new structure of nitrogen-doped and hierarchical CNTs by spray pyrolysis CVD. The structure is highly controlled and consists of aligned CNTs which have multiple-level branched structure with increasing mean diameters.

Chapter 7 focuses on the parameters effects on the growth of carbon nanotubes using PECVD method. The parametric study includes the variation of the inductive power, temperature, catalyst thickness, and plasma to substrate distance.

Chapter 8 proposes the synthesis of a hybrid of 1D/2D carbon nanostructures in a single step by PECVD method. The hybrid is composed of two-dimensional carbon nanosheets suspended on vertically aligned carbon nanotubes. The carbon nanosheets are detached from the substrate by the first generation of vertical align CNTs and are covered by arrays of a new CNT generation.

Chapter 9 explores a new method of growing two-dimensional carbon nanowalls. In this study, the magnetron sputtering technique is proposed for growing carbon nanowalls, on semiconducting substrates, without catalyst addition.

Chapter 10 concludes and summarizes the findings from these studies. It also presents experimental considerations for further improvements in future work.

1.4 References

[1] L.E. Foster, *Nanotechnology: Science, Innovation, and Opportunity*, Prentice Hall, 2009.

[2] R. Feynman, "There's plenty of room at the bottom," *Journal of Microelectromechanical Systems,* vol. 1, 1992, pp. 60-66.

[3] E. Drexler, *Engines of Creation: The Coming Era of Nanotechnology*, Anchor, 1987.

[4] K.E. Drexler, *Nanosystems: Molecular Machinery, Manufacturing, and Computation*, Wiley, 1992.

[5] H.W. Kroto, J.R. Heath, S.C. O'Brien, R.F. Curl, and R.E. Smalley, "C60: Buckminsterfullerene," *Nature*, vol. 318, Nov. 1985, pp. 162-163.

[6] S. Iijima, "Helical microtubules of graphitic carbon," *Nature*, vol. 354, Nov. 1991, pp. 56-58.

[7] G. Cao, *Nanostructures and Nanomaterials: Synthesis, Properties & Applications*, Imperial College Press, 2004.

[8] D.M. Bowman and G.A. Hodge, "Nanotechnology: Mapping the wild regulatory frontier," *Futures*, vol. 38, Nov. 2006, pp. 1060-1073.

[9] M.A. Ratner and D. Ratner, *Nanotechnology: a gentle introduction to the next big idea*, Prentice Hall PTR, 2003.

[10] D. Vollath, *Nanomaterials: An Introduction to Synthesis, Properties and Applications,* Wiley-VCH, 2008.

[11] T.C. Dinadayalane and J. Leszczynski, “Remarkable diversity of carbon–carbon bonds: structures and properties of fullerenes, carbon nanotubes, and graphene,” *Structural Chemistry*, 2010.

[12] A.L. Porter and J. Youtie, “How interdisciplinary is nanotechnology?,” *Journal of Nanoparticle Research*, vol. 11, 2009, pp. 1023-1041.

CHAPTER 2

LITERATURE REVIEW

2.1 Carbon materials

Carbon is a fascinating chemical element with unique properties. It is one of the few elements known and used since antiquity. The name comes from Latin language word “carbo” which means coal. No other element in the periodic table occurs in so many different forms [1]. Coal, soot, graphite, and diamond are all nearly pure forms of carbon. While graphite is soft enough to be used in pencils, diamond ranks among the hardest materials known. Carbon has been used from ancient times, in charcoal form for bronze production or as candle soot mixed with olive oil for writing. Some of the earliest cave paintings, at Lascaux or Altamira, were realized using a mixture of charcoal and soot [2, 3]. Carbon based nanomaterials refer to solid carbon materials with structural units on a nanometer scale in at least one direction. These materials have a large surface to volume ratio reflected in their unique and remarkable properties. Carbon is accepted to be as important for nanotechnology as silicon is for electronics [4]. The morphology of carbon nanomaterials ranges from fullerenes to carbon nanotubes, from graphene to nanocones or nanodiamonds. Carbon, the common element of these materials, continues to arouse the interest and attention of researchers all over the world. This chapter is a review of the most important aspects of the carbon materials, carbon nanomaterials, and their synthesis methods.

2.1.1 Electronic structure of a single carbon atom

Carbon is the chemical element with symbol C, atomic number 6. It is found in the periodic table as a member of group 14. A carbon atom has six electrons with a $1s^2 2s^2 2p^2$ electronic ground state configuration. The two electrons contained in the 1s orbital are strongly bound electrons and are called core electrons. The other four electrons which occupy the $2s^2 2p^2$ orbitals, are weakly bound electrons, and are called valence electrons (Figure 2.1a). The actual location of electrons in a carbon atom cannot be determined with certainty and the diagram can be misleading. A better way to look at the carbon atom is by using an energy level chart shown in Figure 2.1b. The electrons are represented by arrows while the direction of the arrow represents the spin of the electron. Two electrons are found in the 1s orbital close to the nucleus. These two electrons, which spin in opposite directions, have the lowest possible energy. They fill the K shell or first shell as principal quantum number; K (n=1). Being filled, the K shell is completely stable and its two electrons do not take part in any bonding. The four electrons belong to the L shell; L (n=2). The L-shell has two different sub-shells, s and p. Two electrons fill the 2s orbital and have opposite spin. The last two electrons partially fill the 2p orbital and have parallel spin. The 2s and the 2p electrons have different energy levels. The 2p electrons located in the outer orbital are the only electrons available for bonding to other atoms. These electrons are the valence electrons.

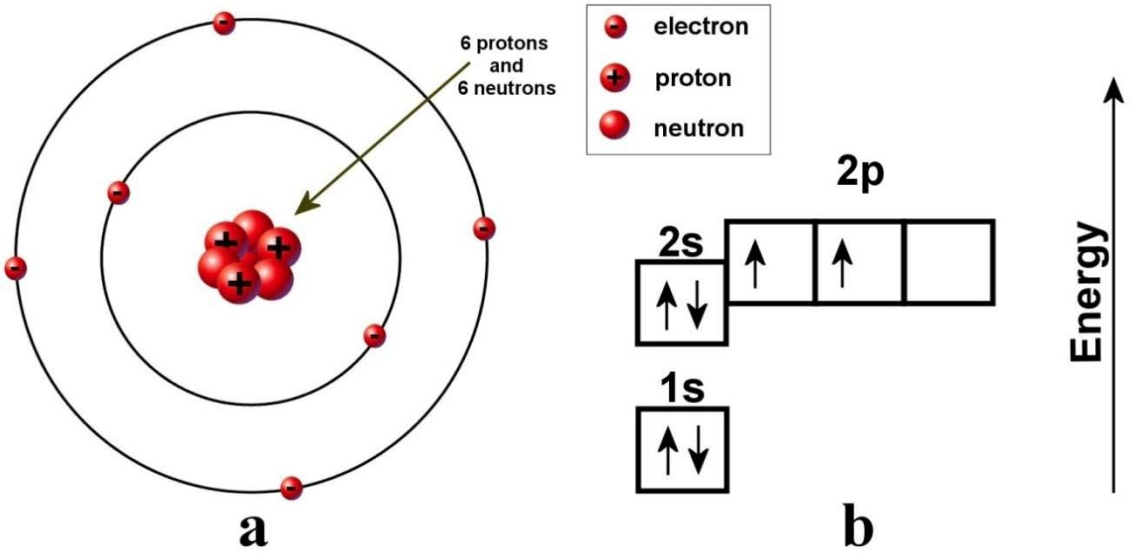

Figure 2.1 Diagram of the electronic structure of the carbon atom in the ground state (a) and the energy level chart (b).

In this state carbon is divalent because only two electrons are available for bonding. Divalent carbon is found in carbene, a class of highly reactive molecules. In contrast, carbon allotropes and polymorphs are tetravalent and four valence electrons are present for bonding the carbon atoms [5]. The description of how carbon electron valence is increased to form carbon allotropes is outlined below.

2.1.2 Hybridization of carbon atoms

The electron configuration of the carbon atom has to be modified in order to allow carbon atoms to combine themselves. The configuration of the carbon atom must be altered to a state with four instead of two valence electrons. This modification implies

mixing the orbitals of the outer shell of the atom in the ground state and, consequently, forming new hybrid atomic orbitals. The concept is called hybridization. For carbon, one 2s electron is promoted into the 2p orbital. The remaining 2s orbital is spherically symmetrical while the formed three 2p orbitals are oriented along the three axes perpendicular to each other. The way of combining these different orbitals gives different carbon hybridization types.

2.1.2.1 *sp* hybridization

In *sp* hybridization one s and one p ($2p_x$) orbital from the outer shell are altered to form two equivalent orbitals called '*sp*' hybrid orbitals directed towards the 'x' axis. This hybridization is often known as diagonal hybridization as the two sp orbitals are at 180^o due to mutual repulsion of their electron clouds. The remaining $2p_y$ and $2p_z$ orbitals do not take part in hybridization and are directed along the 'y' and 'z' axes, perpendicular to the two sp orbitals (Figure 2.2). The linear orientation of the sp orbitals is available to form high strength sigma (σ) bonds while the non-hybridized p orbitals are available to form pi (π) bonds. Carbon, in its *sp* hybridization, forms carbine or polyyne.

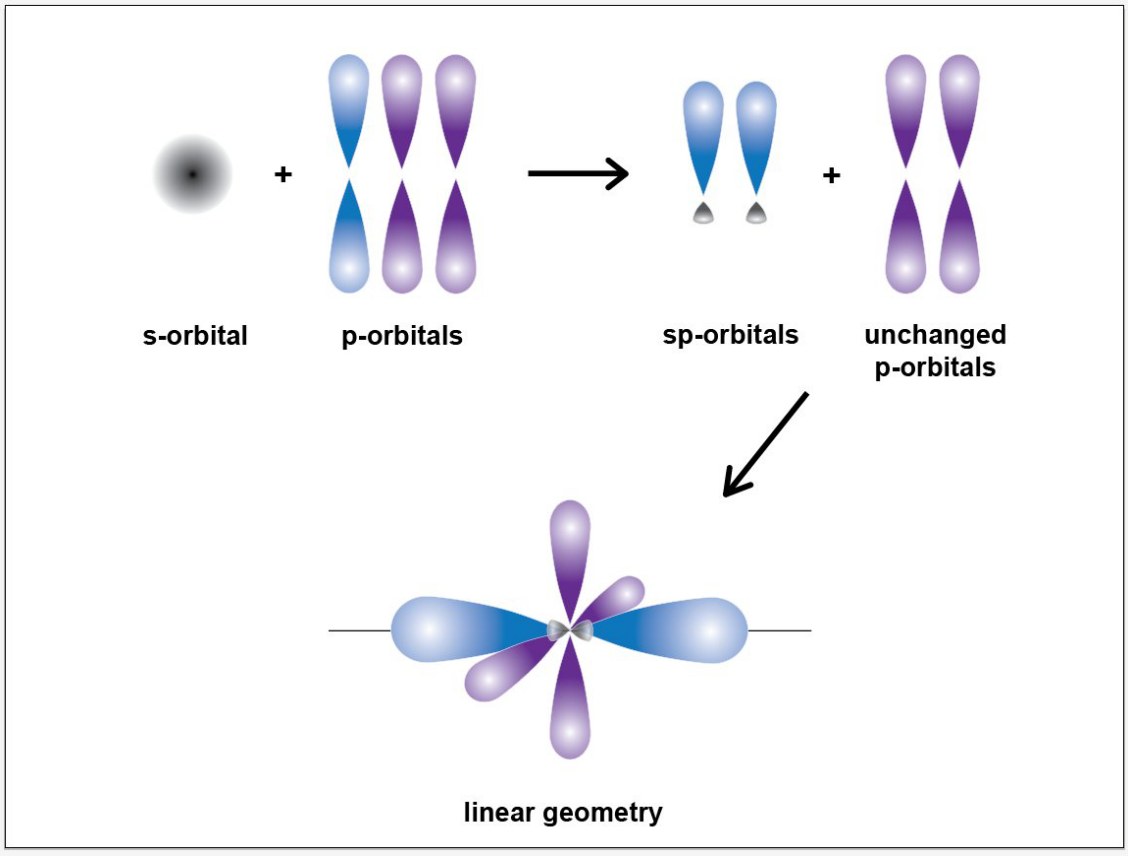

Figure 2.2 *sp* hybridization of carbon.

2.1.2.2 sp^2 hybridization

In this type of hybridization, one s and two p orbitals ($2p_x$ and $2p_y$) get hybridized to form three equivalent orbitals called 'sp^2' hybrid orbitals. These identical orbitals are in the same plane and their orientation is at 120^o angle (Figure 2.3). Graphite is the typical structure for sp^2 hybridization of carbon. The planar orientation of the sp^2 orbitals is available to form σ bonds with three other sp^2-hybridized carbon atoms.

The un-hybridized orbital $2p_z$ of carbon is oriented in a plane perpendicular to the plane containing the three hybridized orbitals and is available to form π bonds.

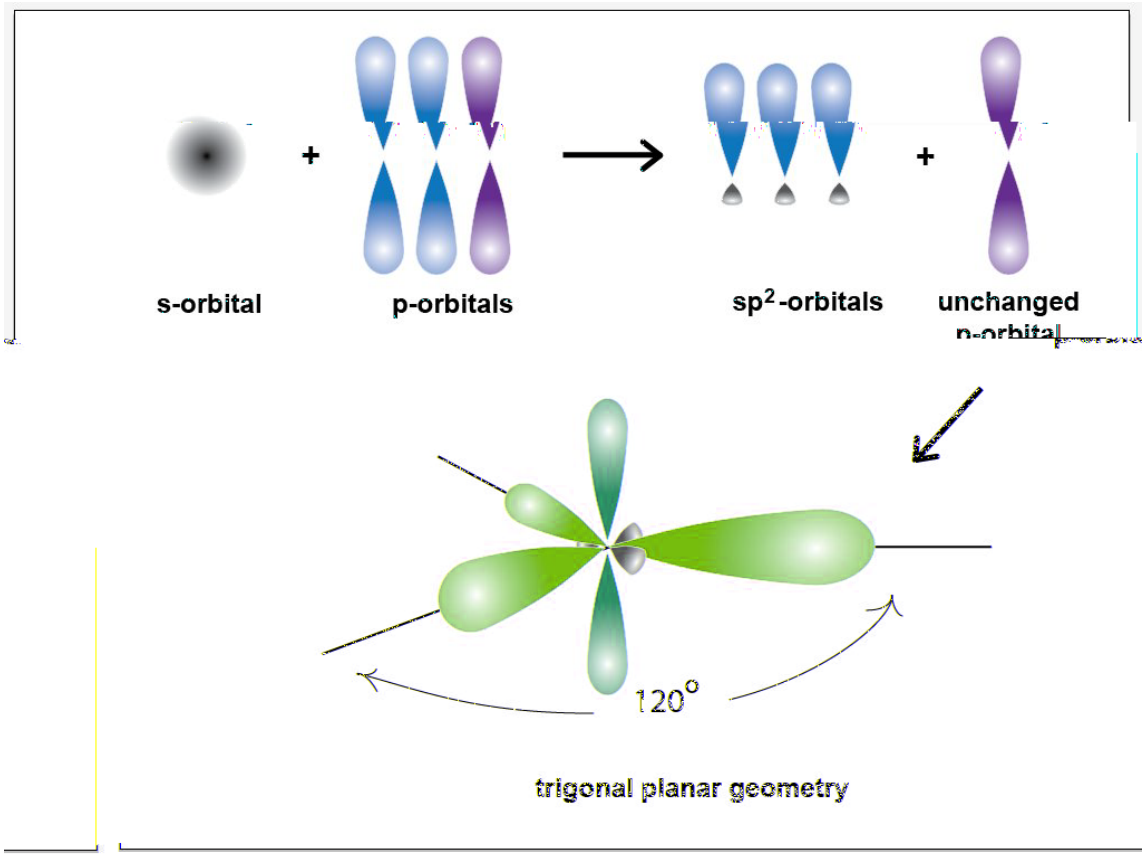

Figure 2.3 sp^2 hybridization of carbon.

2.1.2.3 sp^3 hybridization

In the sp^3 hybridization, the carbon atom has four sp^3 orbitals of equivalent energies formed from one s orbital and three p orbitals. These orbitals, due to mutual

repulsion of the electron clouds, are directed towards the four corners of a regular tetrahedron with the carbon atom in the center. The angle between the hybrid orbitals is approximately 109.5°. This structure is the basis of the diamond crystal. The four sp^3 valence electrons of the hybrid carbon atom, in combination with the small size of the atom, cause strong covalent σ bonds. Each tetrahedron of the hybridized carbon atom (shown in Figure 2.4) combines with other four hybridized carbon atoms to form a three-dimensional lattice structure.

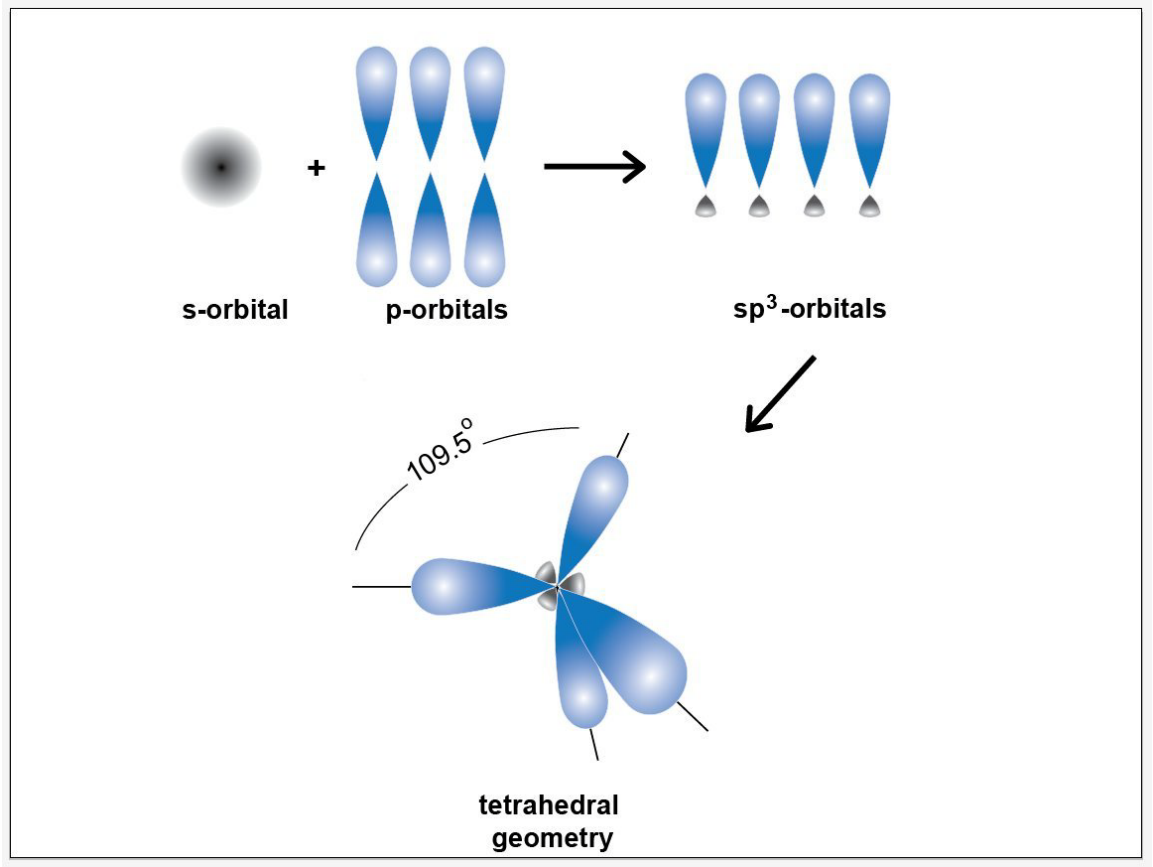

Figure 2.4 sp^3 hybridization of carbon.

2.1.3 Carbon allotropes

Allotropes are defined as the structural modifications of an element. Allotropism is the property of chemical elements to exist in two or more different forms. The concept of allotropy was originally proposed by the Swedish scientist Baron Berzelius in 1841 who reviewed the monoclinic and rhombic forms of sulfur [6]. Carbon has three main allotropes: diamond, graphite, and carbyne. These forms represent the three types of carbon hybridization: *sp*, sp^2, and sp^3. Fullerenes are a recently discovered form of pure carbon and take the form of a hollow sphere, ellipsoid, or tube. Fullerene hybridization falls between graphite (sp^2) and diamond (sp^3) due to the curvature of the surface [7] and will be reviewed in a later paragraph.

2.1.3.1 Carbyne

Elemental carbon exists in three bonding states according to its hybridization. Each type of hybridization should correspond to a certain form of carbon. Only two forms of carbon related to the sp^2 and sp^3 hybridization were known up to 1960: graphite and diamond. Therefore, it was reasonable to assume the existence of a material with one-dimensional structure formed by carbon atoms sp hybridized [8]. For a long time finding this carbon allotrope was the subject of great interest of both theoretical and experimental research. At the end of the 19^{th} century, several approaches were reported in attempt to synthesize one-dimensional polymers of carbon. C.Glaser used the oxidative

coupling reaction of ethynyl compounds as starting monomer. These experiments were systematically investigated in 1959-1960 and culminated with the discovery of the linear allotropic form of carbon [9]. This form was labeled carbyne from the Latin word “carboneum” (carbon) and the suffix “yne” used in organic chemistry to designate an acetylenic bond. Carbyne occurs in two forms: polyyne and cumulene. Polyyne is a linear chain-like form of alternating single and triple bonds $(–C{\equiv}C–)_n$, while cumulene contains double bonds of carbon atoms $(=C=C=)_n$ [10]. Carbyne was found as a natural mineral in 1968 in the Ries meteorite crater (Germany) and was named “chaoite” in the honor of the respected scientist E. Chao. Carbynes have drawn considerable interest in nanotechnology as its Young's modulus is forty times that of diamond [11]. To date, the longest polyyne synthesized is a chain of 44 carbon atoms [12].

2.1.3.2 Graphite

Graphite, the sp^2 hybridized form of carbon, was named in 1789 from the Greek word “graphein” (to draw, to write). Graphite has a layered hexagonal planar structure. The hexagonal layers are held parallel with each other by Van der Waals forces. In each layer, the hexagonal lattice is formed by carbon atoms with separation of 0.142 nm, and the distance between planes is 0.335 nm [13]. The chemical bonds within the layers are covalent with sp^2 hybridization. Two forms of graphite are known, hexagonal and rhombohedral. Although these have graphene layers which stack differently, they have similar physical properties. The thermodynamically stable form of graphite is hexagonal

graphite with an ABAB stacking sequence of the graphene layers (Figure 2.5). The unit cell dimensions are a=0.2456 nm and c=0.6708 nm [14]. Hexagonal graphite is thermodynamically stable below approximately 2600 K and 6 GPa [15]. The rhombohedral graphite is thermodynamically unstable with an ABCABC stacking sequence of the layers. The unit cell constants are a=0.2566 nm and c=1.0062 nm [16]. This form has not been isolated in pure form. It is always mixed with the hexagonal form in variable amounts which can be increased up to 40% of rhombohedral content. Heating to above 1600 K progressively transforms rhombohedral graphite to hexagonal graphite, which shows that the hexagonal phase is thermodynamically more stable [17].

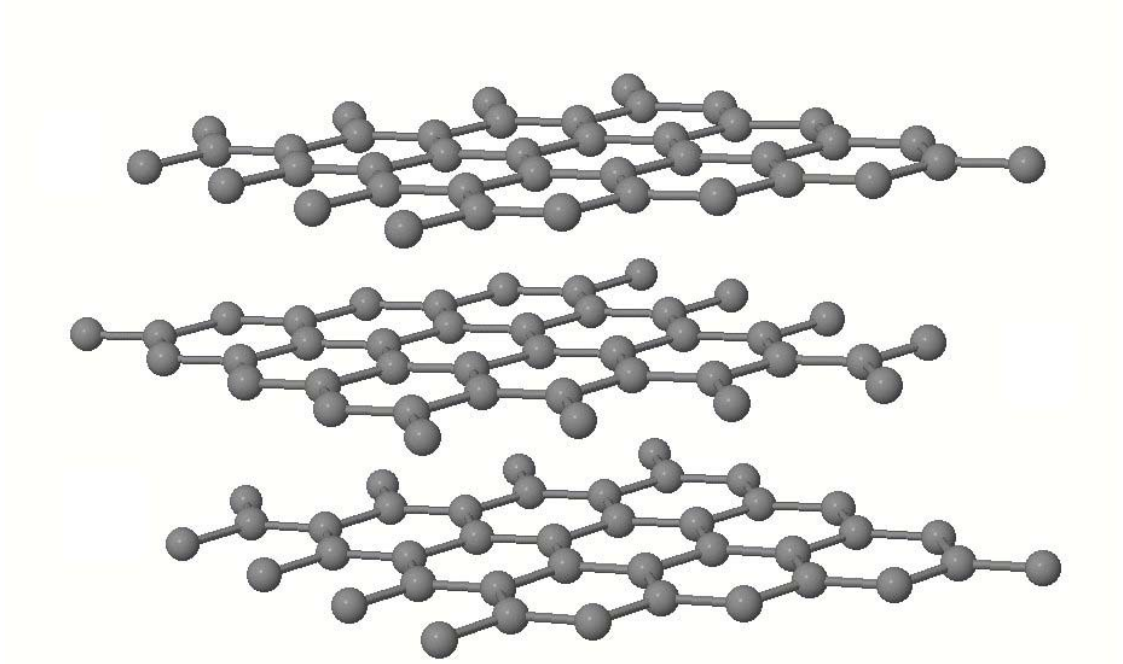

Figure 2.5 The hexagonal form of graphite.

2.1.3.3 Diamond

Diamond is an allotrope of carbon. Diamonds were discovered in India about 6000 years ago in the riverbeds of the region. The name diamond is derived from the ancient Greek "adamas" meaning unbreakable, untamed and unconquerable. In 1772, it was proved that diamond is composed of carbon [18]. It is the hardest naturally occurring mineral and ranks among the rarest materials known. Most natural diamonds are formed at high-pressure and high-temperature conditions in the Earth mantle and are brought close to the surface through volcanic eruptions. Diamonds can also be produced synthetically by processes which simulates the conditions in the Earth mantle or by chemical vapor deposition [19]. Despite its hardness, the chemical bonds that hold together the carbon atoms are weaker in diamond than in graphite. The difference is that in diamond the covalent bonding between the carbon atoms has sp^3 hybridization and forms an inflexible and strong three-dimensional lattice. In graphite, the atoms are strongly bonded in sheets, but the sheets are weakly bonded and slide easily [20]. Two forms of diamond are known with cubic and hexagonal crystal structure. Frequently, diamond is found in the cubic form which is thermodynamically stable at pressures above 6 GPa at room temperature and metastable at atmospheric pressure. At low pressures cubic diamond converts rapidly to graphite at temperature above 1900 K in an inert atmosphere [21]. Under ambient conditions such transformation is negligibly slow. In the cubic form, each carbon atom is linked to four other carbon atoms in a tetrahedral array (Figure 2.6). The bond length between two carbon atoms is 0.154 nm [22]. Pure diamond transmits visible light and appears as a clear colorless crystal. The other form of diamond

is called lonsdaleite or hexagonal diamond. It is thought to occur when meteoric graphite falls to Earth. The heat and stress from the impact transform the graphite into a structure similar to diamond. The properties of this material are not well known due to the limited existent amount of lonsdaleite. Using computer simulation techniques, it was shown that lonsdaleite withstands 58% more stress than diamond. If the result is experimentally confirmed, hexagonal diamond would be far harder than any substance ever measured [23].

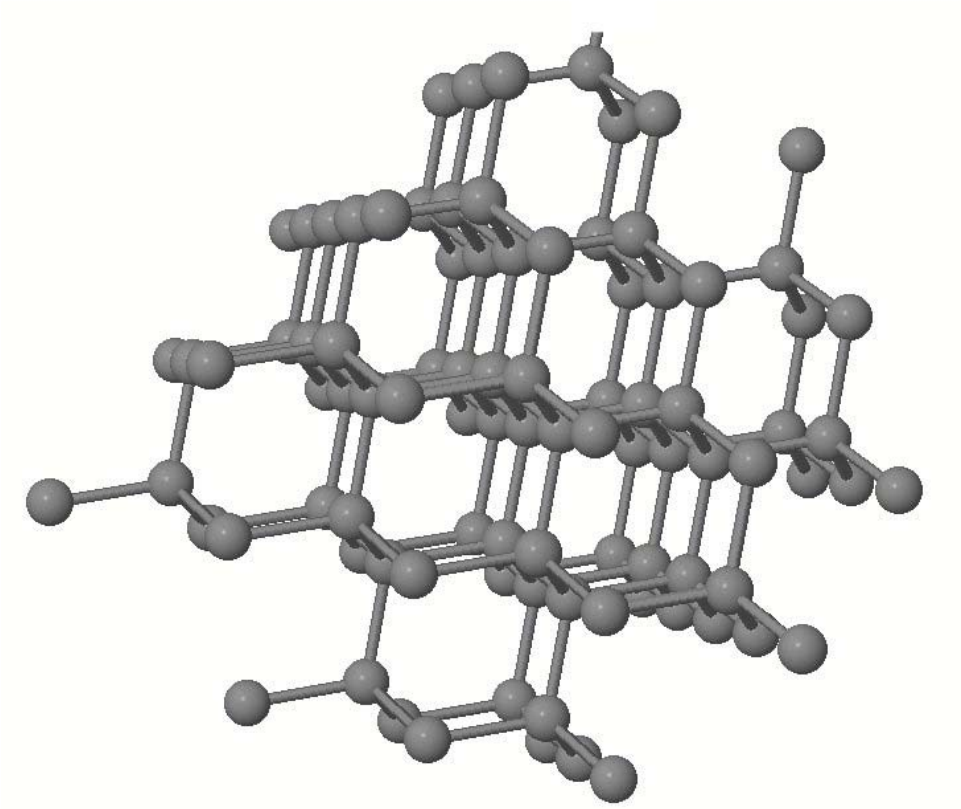

Figure 2.6 The cubic form of diamond.

2.1.4 Other forms of carbon

2.1.4.1 Amorphous carbon

Amorphous carbon is a carbon material without long-range crystalline order. Short-range order exists and it is related to the graphite and diamond lattices. These varieties of disordered structures are formed because carbon is able to exist in three hybridizations. Amorphous carbon presents deviations in both bonding distances and angles for the sp^2 as well as for the sp^3 configuration (Figure 2.7) due to a high concentration of dangling bonds [24].

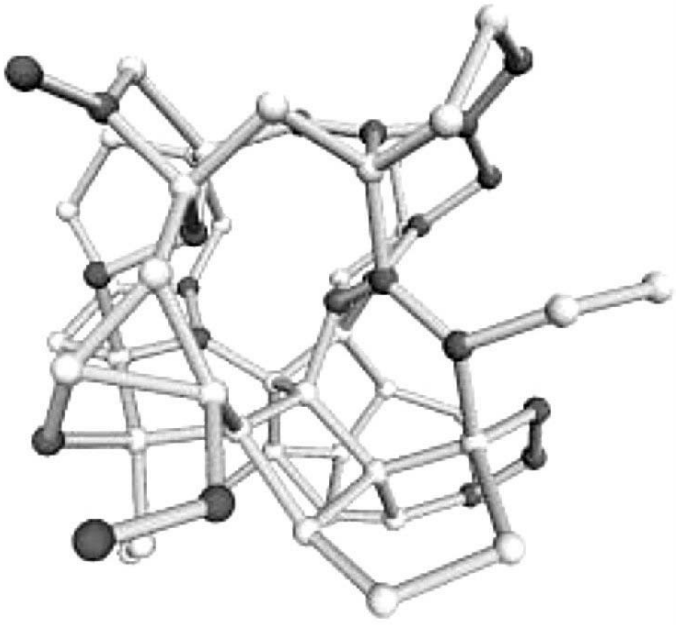

Figure 2.7 View of a-C network showing deviations in both bonding distances and angles for the sp^2 and sp^3 hybridized atoms [25].

These characteristics are inconsistent with any other allotrope of carbon. Two specific amorphous forms of carbon exist distinguished by their macroscopic and microscopic properties. These forms are graphite-like (*a*-C) and diamond-like (DLC) amorphous carbon. They are identified by the ratio of sp^2 to sp^3 hybridization contained in the material. The diamond-like amorphous carbon is transparent and much harder than graphite-like form. Depending on the deposition conditions, DLC films can be fully amorphous or contain diamond crystallites. Usually, diamond-like carbon films contain a significant amount of hydrogen especially when they are obtained by the chemical vapor deposition method. Atomic hydrogen is considered one of the most critical components in the gas phase mixture for obtaining diamond films. Synthetic diamonds can be grown when the synthesis conditions enhance the formation of sp^3 over sp^2 bonds. Diamond films have been prepared on a variety of substrates, including quartz, Si, Ni, and W. The films grown by these techniques are usually polycrystalline, consisting of randomly oriented, small diamond crystallites. The deposited material is called diamond if it is proved to have a full three-dimensional crystalline lattice of diamond [26].

2.1.4.2 Glass-like carbon

Glass-like carbon (GLC) is a very high isotropic carbon-based material. The structure of this material has been a subject of debate for a long time. Early models assumed that its structure contains both sp^2 and sp^3 bonded atoms. Presently, it is known that glassy carbon possesses exclusively sp^2 bonded atoms consisting in small graphite-

like hexagonal layers with no true graphitic orientation between layers [27]. Several models have been proposed for the structure of GLC, but none of these are generally accepted (Figure 2.8) [27, 28]. Glass-like carbon intermediates between glass and carbon in respect of both thermal and electrical conductivity and can be described as a conductive ceramic. It has a high resistance to corrosion, erosion, and a high impermeability to gases and liquids. Due to its resistance to chemical agents, glass-like carbon is used for the manufacture of special laboratory analytical equipment such as crucibles and beakers [29].

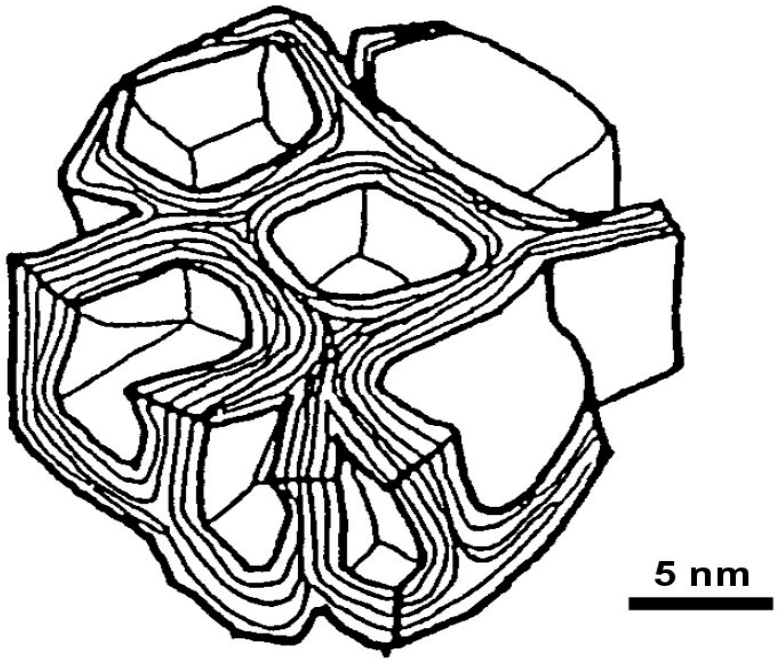

Figure 2.8 Schematic diagram for the microstructure of the closed pore structure model for glassy carbon [30].

2.1.4.3 Carbon blacks

Carbon blacks represent finely divided carbon particles with sizes of 100 nm or higher. A characteristic signature associated with carbon blacks is the concentric organization of the graphite layers in each individual particle [31]. The concentric graphitic layers are found to be more pronounced in the region close to the particle surface (Figure 2.9).

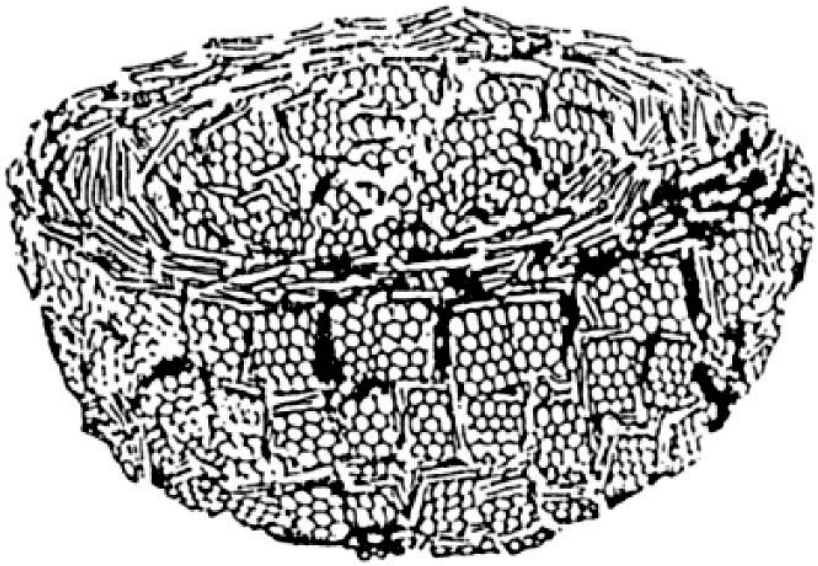

Figure 2.9 Schematic view of a carbon black particle showing short graphitic segments [33].

They are widely used in industry as a filler to modify mechanical, electrical, and optical properties of the materials in which they are dispersed. There are various types of

processes by which they are produced: thermal decomposition of natural gas, decomposition of acetylene, partial combustion of oil droplets, and decomposition of ethylene in a plasma arc. On a laboratory scale, special processes are used, such as laser ablation of graphite and laser pyrolysis of acetylene [32]. These synthesis routes produced types of carbons blacks with different physical and chemical properties.

2.1.5 Phase diagram of carbon

The large binding energy between atoms of carbon is reflected in the extremely high melting temperatures (~4000 K) of carbon allotropes. In addition, very high temperatures are required to transform one solid phase of carbon to another. The phase diagram of carbon reveals multiple crystallographic transitions in the solid phase. Initially, the diagram was traced knowing only graphite and diamond as allotropes of carbon. The experimental data accumulated in experiments done at high pressure and high temperature (HPHT) revealed that graphite could be transformed in diamond and diamond remained stable under ambient conditions [34, 35]. In principle, it very slowly transforms back to the thermodynamically stable form of solid carbon, which is graphite. In the phase diagram proposed by F.P. Bundy (Figure 2.10a), along with diamond and graphite, the hexagonal diamond and liquid carbon were emphasized.

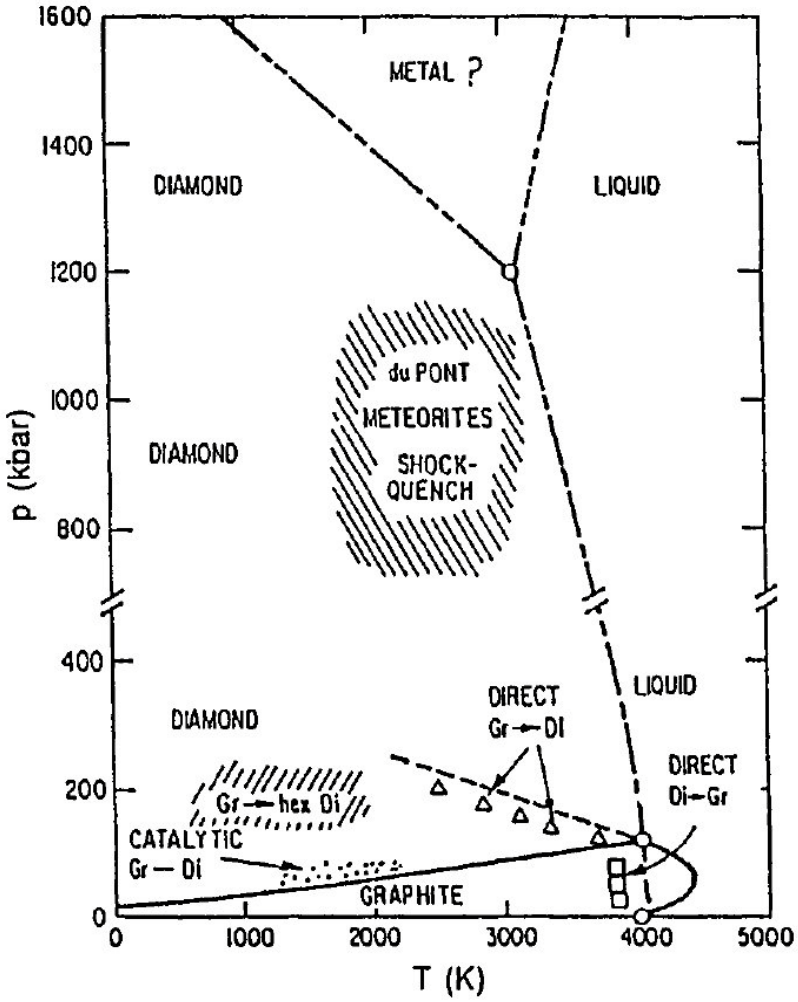

Figure 2.10 Phase diagram of carbon after F.P. Bundy [36].

The liquid carbon phase at high pressures is still unexplored and is indicated in the diagram as metallic carbon (Figure 2.10b) [36]. Many new things have been learned during the past few decades about physical forms of carbon and its properties over a wide range of pressure and temperature. Nevertheless, in order to probe the results obtained at HPHT with increased accuracy and sensitivity, the development of more precise experimental methods is needed. The investigation of new forms of carbon and of new

synthesis procedures proved experimentally that carbon materials could be obtained at low pressure via CVD method. Unfortunately, low pressure experimental results and carbon structures such as carbyne or amorphous carbon (*a*-C) have not been localized on the phase diagram. Consequently, a review of the carbon phase diagram is necessary for a deeper understanding of the current results and would serve as a tool in finding new carbon structures.

2.1.6 Carbon based nanomaterials

Nanomaterials refer to solid materials which have at least one physical dimension limited to the nanoscale. While most micro-structured materials have similar properties to the corresponding bulk materials, the properties of materials with nanometer dimensions are significantly different from their bulk counterparts. The large surface to volume ratio and the nanometer size of the materials determine the characteristics which do not exist in the corresponding bulk materials, i.e. high surface energy, spatial confinement, reduced imperfections [37]. As a result, the material properties differ significantly on the nanometer scale. For example, the lattice constants are reduced [37], the melting point becomes lower [38], the photoluminescence process occurs [39]. Carbon based nanomaterials (CBNs) cover various types of nanostructured carbons. The most representative ones are nanodiamonds, fullerenes, nanotubes, nanofibres, and graphene. Variations of these nanostructures are nanocones, nanorings, branched nanotubes, and nanofibres. By the early 1980s, although the majority of carbon based nanomaterials were

almost unknown, carbon science was widely considered to be a mature discipline, unlikely to produce any major surprises. However, this situation changed in 1985 due to the synthesis of first all-carbon molecule, buckminsterfullerene. It was the discovery of Harry Kroto, Richard Smalley, and their colleagues, which led to the synthesis of carbon nanotubes and which made carbon science so fashionable [40].

2.1.6.1 Fullerenes

Fullerenes are a class of molecules composed entirely of carbon, in a spherical, ellipsoidal, or cylindrical arrangement. They are closed hollow cages consisting of carbon atoms interconnected in pentagonal and hexagonal rings. Spherical fullerenes are also called buckyballs, and cylindrical ones are called carbon nanotubes or buckytubes.

2.1.6.1.1 Spherical fullerenes

Spherical fullerenes are zero-dimensional molecules since all dimensions are limited to nanoscale. The chemical formula of spherical fullerenes is C_n, where n represents the number of atoms in the molecule. Among the isolated stabile fullerenes are C_{60}, C_{70}, C_{76}, C_{80}, C_{84} and the series extends to gigantic fullerenes [41] and onion fullerenes [42]. The number of carbon atoms in gigantic fullerene is larger than 100 (C_n, $n>100$) and the structure is similar to that of spherical fullerene. Onion fullerenes have

similar hollow-cage structure formed by multiple concentric shells. The most famous fullerene is C_{60}, also called buckminsterfullerene after the architect R. Buckminster Fuller, whose geodesic dome is constructed on the same structural principles (Figure 2.11).

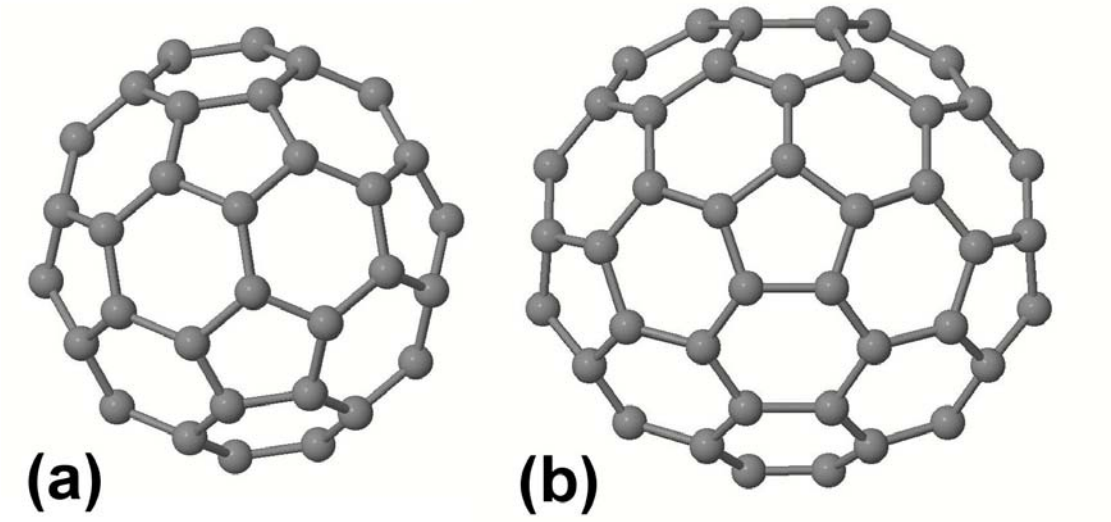

Figure 2.11 View of stable fullerenes C_{60} (a) and C_{76} (b).

Buckminsterfullerene is the most common and most stable fullerene. It is also the smallest carbon molecule with pentagonal faces isolated from each other. Their average diameter is 0.683 nm. The arrangement of its 60 carbon atoms resembles a truncated icosahedron similar to a soccer ball. Fullerenes are chemically stable, but they are less dynamically stable than graphite. The sp^2-hybridized carbon atoms must be bent to form closed spheres in comparison to planar graphite in which the atoms are at their minimum energy level. Fullerenes have been studied as a main material in various applications. Some examples are solar cells [43], photodetectors [44], field effect transistors [45], and

additives in polymers [46]. Originally, fullerenes were produced using arc discharge and laser ablation methods. These methods do not produce the quantities of fullerenes needed for research. The combustion method can produce fullerene continuously by burning hydrocarbon fuel at low pressures and is considered more suitable for mass production.

2.1.6.1.2 Carbon nanotubes

Carbon nanotubes (CNTs) are members of the fullerene structural family. Similar to spherical fullerenes, the sp^2-hybridized carbon atoms must be bent to form cylindrical structures. Early studies, published before transmission electron microscope (TEM) invention, reported about the possibility of forming carbon filaments from thermal decomposition of hydrocarbons [47]. Unfortunately, due to the lack of resolution of the available microscopy tools, it was not possible to reveal an inner cavity of the produced filaments. Since mid 20^{th} century, there have been many reports about tubular structures similar to CNTs thanks to the invention of TEM. The first commercial version was produced by Siemens in 1939. TEM evidence of tubular nanosized carbon filaments was published in 1952 by L.V. Radushkevich and V.M. Lukyanovich [48]. Similar images and results were recorded by Oberlin et al. in 1976 [49]. The report of S. Ijima from 1991 was the first unambiguous evidence of growing CNTs without any catalyst [50] and brought nanotubes into the awareness of the scientific audience. Different techniques have been developed to produce nanotubes. These include arc discharge [51], laser ablation [52], high pressure carbon monoxide (HiPCO) [53], and chemical vapor

deposition [54, 55]. CVD growth of CNTs can be realized in vacuum or at atmospheric pressure. The research efforts in finding suitable catalysts and scalable growth methods have resulted in the development of continuous growth processes. Consequently, large quantities of nanotubes can be synthesized making the CNTs commercially viable. CNTs have a close relation to graphite as their structure can be conceptualized as a rolled-up monolayer of graphite. If only one layer forms the tube wall, the tube type is single-walled carbon nanotube (SWCNT). CNTs with multiple rolled layers of graphite are called multi-walled carbon nanotubes (MWCNTs). MWCNTs have more than one wall or concentric tubes and the inter-tube spacing is 0.34 nm, which corresponds to the inter-layer distance of 0.35 nm in graphite [56]. While the diameter of CNTs is in the range of several hundred nanometers down to 0.3 nm [57], the length can be up to several centimeters [58]. Since only one direction is not limited to nanoscale, CNTs are 1D nanomaterials. Following the concept of forming a CNT by wrapping a one atom-thick layer of graphite into a cylinder, the structure of a SWCNT can be represented by a chiral vector C_h. The chiral vector C_h is defined by two integers (n,m) as well as two base vectors a_1 and a_2 [59, 60]. The description of a specific SWCNT is given by (n, m) indices when the graphite layer is bent in such a way that both ends of the vector lie on top of each other. When indices are taken in consideration as criteria, SWCNTs are categorized as follows: armchair tubes (n,n) when m=n, zig-zag tubes (n,0) for m=0,and chiral tubes for any other (n,m). The pair of integer indices (n,m) determine the diameter and the chiral angle of the tube. The chirality of SWCNTs is related to their electrical properties. A tube is metallic when (m-n)/3 is an integer. All other SWCNTs are

semiconducting. This means that m and n determine the diameter, the chirality, and the physical properties of SWCNTs [61] (Figure 2.12).

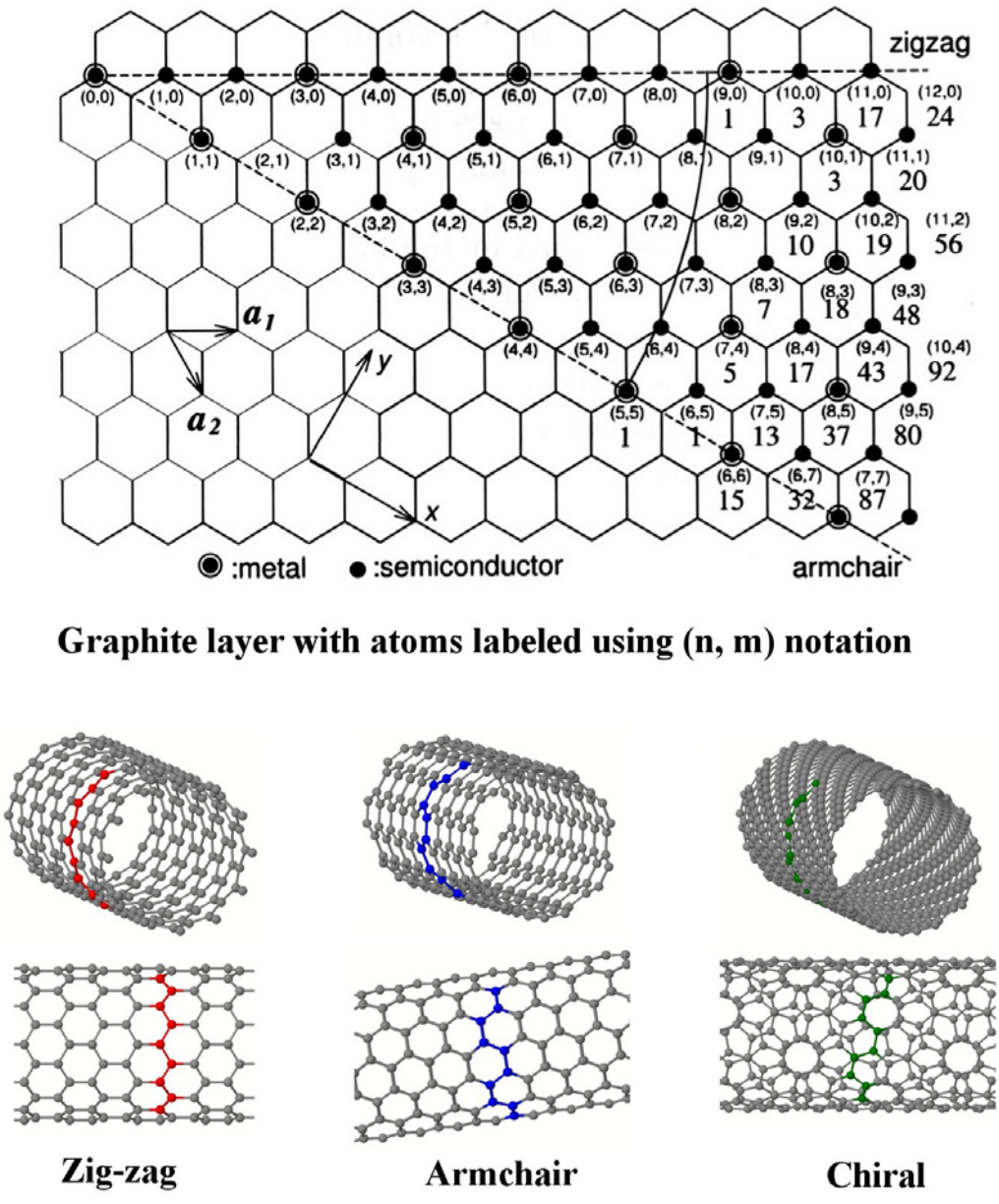

Figure 2.12 Graphite layer with atoms labeled using (n, m) notation [59] and different types of CNTs.

Nevertheless, CNTs have proven to be a versatile material due to other characteristics. The resistivity of nanotube ropes measured at room temperature has shown that single walled nanotube ropes are the most conductive carbon fibers known with tolerance for very high current densities [62]. The small diameter and high aspect ratio of CNTs is very favorable for field emission. CNTs develop at their free end a strong electric field even for moderate voltages [63, 64]. Since the basal plane elastic modulus of graphite is one of the largest of any known material, CNTs are expected to be among the high-strength fibers. CNTs are stiffer than steel and very resistant to damage from physical forces. Recently, it was proved that the Damascus blades from the seventeenth century, the sharpest swords in history, were made from steel that contained fullerene molecules [65]. Using atomic force spectroscopy, high values of tensile strength and Young's modulus were reported. Pressing on the tip of a nanotube causes bending without damaging the tip. When the force is removed, the nanotube returns to its original state. This property makes CNTs very useful as probe tips for high-resolution scanning probe microscope [66, 67]. CNT arrays have a lower thermal resistance which might serve as the interface material for thermal management in high power microelectronic devices [68]. Another property of carbon nanotubes is the chemical stability due to their highly hydrophobic nature and very regular structure. Recently, CNTs have been used to support platinum in proton exchange membrane fuel cell electrodes [69, 70]. In lithium ion batteries, CNTs are used as electrodes because they exhibit high reversible capacity [71]. There are several other areas of technology where carbon nanotubes are already being used. These include composite materials [72], flat-panel displays [73], and sensing devices [74, 75]. Introduction of defects can also result in various new structures such as

Y-branches, T-branches, or heterojunctions between normal and doped nanotubes [76]. These defects can be introduced in a controlled way by adjusting the synthesis procedures. Defects are studied with great effort since even more interesting properties than their original forms occur. The unique properties of carbon nanotubes will undoubtedly lead to many more applications and CNTs will become one of the most important raw materials in the near future.

2.1.6.2 Carbon nanofibers

Carbon nanofibers are graphitic filamentous structures which differ from nanotubes in the orientation of the graphite monolayer planes. In CNTs, the graphite monolayer planes are parallel to the tube axis. In nanofibers, the graphite layers are arranged perpendicular to the fiber axis (stacked form) or at an angle to the axis (herringbone form) [10]. The structure of these nanofibers is illustrated in Figure 2.13. Carbon nanofibers are produced by catalytic exposure of gaseous hydrocarbons to high temperatures, similar to CNTs. The fiber structure is dictated by the chemical nature of the catalyst particle, the composition of the reactant gas, and the synthesis temperature. High strength combined with their superior stiffness has made carbon fibers an attractive material for high performance composite structures [29].

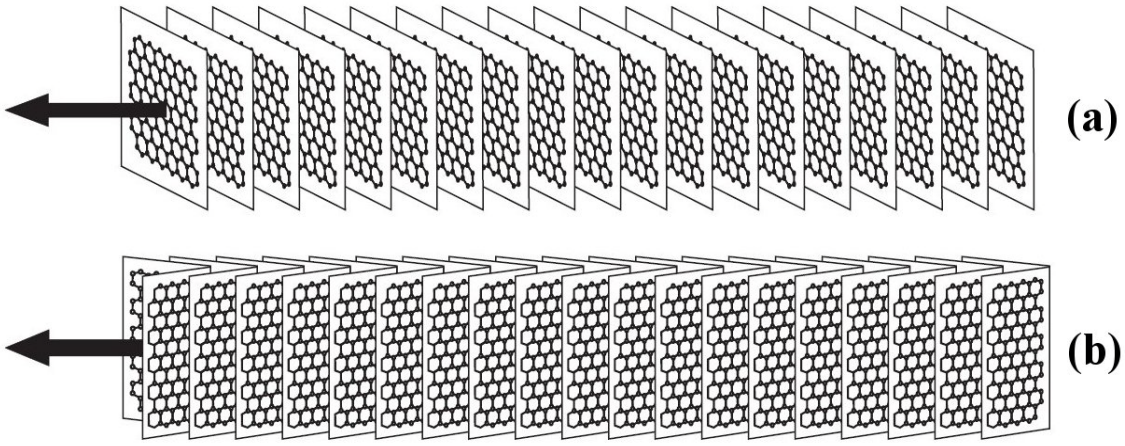

Figure 2.13 The structure of “stacked” (a) and “herringbone” (b) nanofibers (the arrow indicates the fiber axis) [10].

2.1.6.3 Graphenes

Graphenes represent the 2D carbon nanomaterials formed by one or several monolayers of graphite. Similar to the graphite structure, the sp^2-bonded carbon atoms are densely packed in a honeycomb crystal lattice with the bond length of about 0.142 nm. A single sheet is called a graphene sheet, while several graphene sheets, stacked with an interplanar spacing of 0.335 nm, are called few-layer graphene (FLG). Graphene is the basic structural element of the other carbon based nanomaterials, as it can be wrapped up to form 0D spherical fullerenes or rolled to form 1D nanotubes (Figure 2.14) [77].

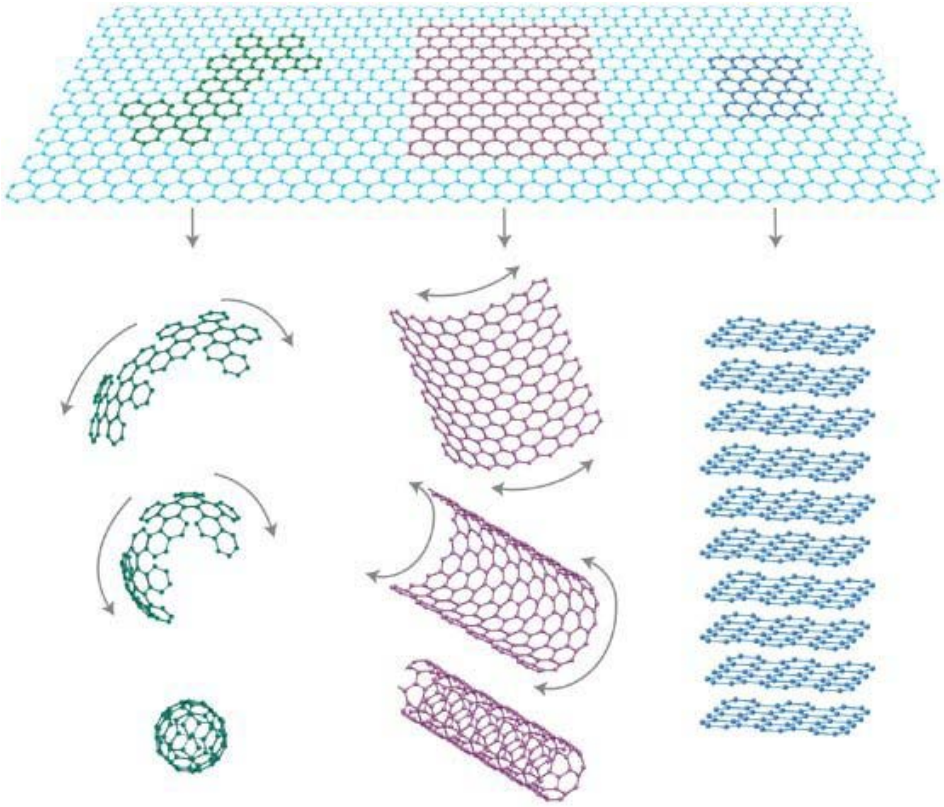

Figure 2.14 Graphene as a 2D building material for carbon materials of all other dimensionalities: 0D fullerenes, 1D nanotubes or 3D graphite.

Graphene has been studied theoretically for many years [78]. It was believed to be unstable, and presumed not to exist in the free state [79]. Free standing graphene layers are difficult to be obtained, as they have the tendency to roll and form scrolls with respect to its lower energy state [80]. First method of graphene synthesis was reported in 1962 by P.Boehm. In this work, it was demonstrated the existence of monolayer of reduced graphene oxide flakes [81]. The produced graphene had low quality due to incomplete removal of various functional groups. Between 1990 and 2004, many efforts were made to create very thin films of graphite by mechanical exfoliation [82] but nothing less than several tens of layers were produced. In 2004, A. Geim and K. Novoselov obtained

single-atom thick graphene from bulk graphite by using a process called micromechanical cleavage [83]. To date, different methods have been developed to produce single-layer or few-layer graphene such as mechanical exfoliation [83], oxidation of graphite [84], liquid-phase exfoliation [85, 86], by chemical vapor deposition [87, 88], thermal decomposition of silicon carbide [89, 90], and cutting open nanotubes [91]. Unfortunately, many challenges have to be addressed in graphene synthesis for practical application since these methods suffer from limited controllability over the size, shape, edge, or location of graphene. The reason why graphenes have drawn so much attention to scientists arises from their remarkable properties. Experimental results from electronic transport measurements show that graphene has remarkably high electron mobility at room temperature [77]. A single layer of graphene has a high Young's modulus of more than 1 TPa [92] and is one of the stiffest known materials. It absorbs approximately 2.3% of white light demonstrating a very high opacity for an atomic monolayer [93]. The thermal conductivity of graphene was recently measured and exceeds the thermal conductivity for carbon nanotubes or diamond [94]. Graphene research is still at the very beginning and many experimental and theoretical results are expected to elucidate the physical characteristics of this important material.

2.1.6.4 Carbon nanowalls

Carbon nanowalls (CNWs) or carbon nanosheets are two-dimensional self-supported networks of vertically aligned graphitic walls. The edges of CNWs consist of

plane graphene sheet stacks standing almost vertically on the substrate [95]. They provide an important model of a two-dimensional graphite structure with strong anisotropy in physical properties. Isolated carbon sheets or petal-like carbon structures were previously reported as byproducts during fullerene and nanotube preparations [96, 97]. However, they coexisted with other carbon forms and had low controllability. Recently, this type of carbon nanomaterial has been effectively synthesized on various substrates using PECVD [98, 99]. Free-standing and vertically oriented carbon nanowalls have a very high surface to volume ratio and sharp edges [100]. These properties are attractive for electron field emission devices. CNWs could also be used as catalyst support in proton exchange membrane fuel cells.

2.2 Synthesis methods review on carbon based nanomaterials

2.2.1 Synthesis of zero-dimensional spherical fullerenes

The first techniques used for spherical fullerene production were arc discharge and laser ablation. These methods produce small quantities of fullerenes and are not suitable for mass production. These processes will be discussed in detail in the next subchapter about the synthesis of carbon nanotubes. Fullerenes are mainly produced by the combustion method which is able to generate soot with a high yield of fullerenes. The process is continuous and scalable. Occurrence of combustion is caused by mixing toluene, acetylene, or benzene with oxygen. The growth mechanism of fullerenes in a

combustion process is still unclear and further investigations are needed [101]. The device is composed of three major components. First part, called the combustion chamber, contains a burner enclosed within a temperature insulated chamber. The combustion chamber is connected to a soot collection chamber, which is the second main part of the system. Finally, a heat exchanger cools the exhaust gases before they enter the vacuum pump. The soot collection chamber includes a filter which prevents the soot from entering in the pump. The filter can be cleaned with a nitrogen jet pulse without interrupting the production, and the soot is collected in a collecting tank (Figure 2.15). Fullerenes can be continuously produced by this method without halting the synthesis process [102].

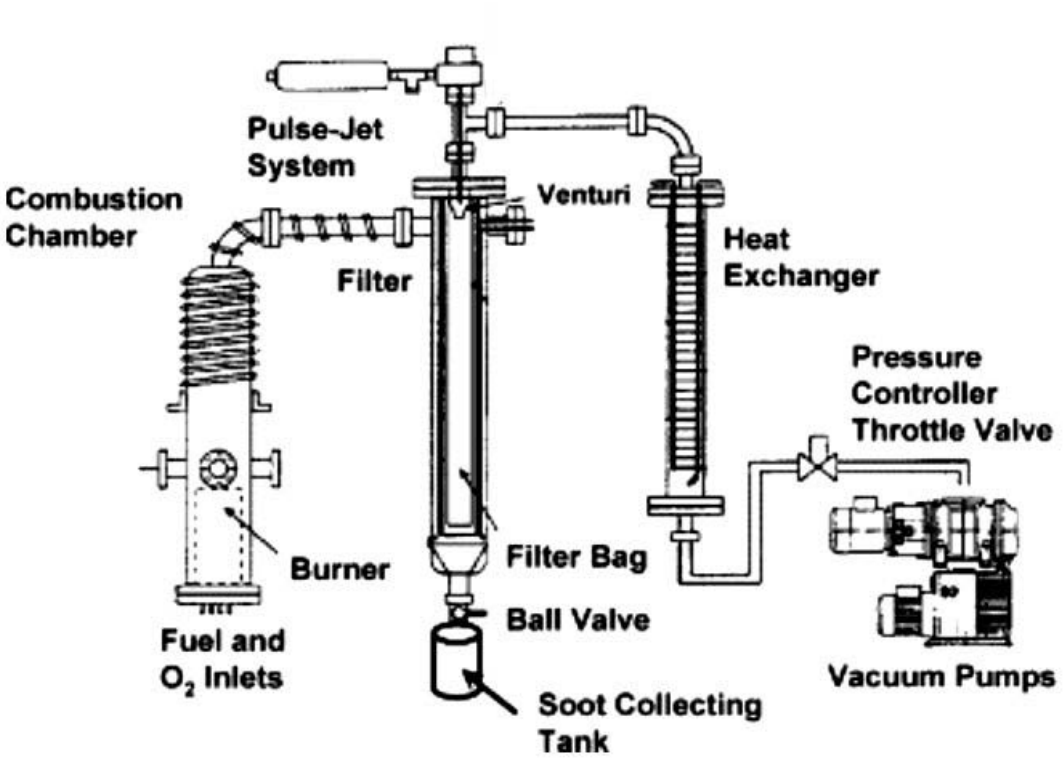

Figure 2.15 Schematic diagram of fullerene synthesis device - combustion method [102].

2.2.2 Synthesis of one-dimensional carbon nanotubes

2.2.2.1 Synthesis of regular CNTs

Arc discharge, laser ablation, and chemical vapor deposition (CVD) are the main techniques that have been developed to produce carbon nanotubes. In the first two cases, a solid piece of graphitic carbon is heated to a very high temperature, at which carbon atoms are separated and reassemble either on the cathode in the case of arc discharge or on a cooled collector in the case of laser vaporization. During this reassembly process, highly ordered nanotubes are formed. Catalytic chemical vapor deposition follows a different process. Instead of starting with a solid piece of carbon, CVD methods employ feedstock of hydrocarbon gas, which dissociates either thermally or in the presence of plasma. There are several derivative methods related to thermal CVD such as floating catalyst, aerosol assisted, and spray pyrolysis. CVD methods feature simple, economical, and adaptable to different experimental conditions. These catalytic techniques also enable nanotube synthesis to be achieved under relatively mild conditions, giving more control over the growth process. In addition, CVD methods make it possible to grow arrays of aligned nanotubes on different substrates. Although MWCNTs produced by catalytic CVD methods are structurally inferior to those made by the high-temperature arc and laser techniques, catalytically produced SWCNTs still have a high degree of structural perfection. With these considerations, CVD methods are strong candidates for large production of CNTs. In the following paragraphs, various synthesis methods of obtaining regular CNTs are thoroughly reviewed.

2.2.2.1.1 Arc discharge method

The carbon arc discharge method was initially used for producing C60 fullerenes [50]. A typical arc discharge device is composed of a vacuum chamber inside which two graphite electrodes are held at a short distance apart (Figure 2.16). In the deposition process, the chamber is usually filled with inert gas at low pressure. A direct current driven by a potential difference creates a high temperature discharge between the two graphite electrodes. The position of the anode is adjustable in a way that as the anode is consumed, the gap width between the two electrodes can be held constant [51].

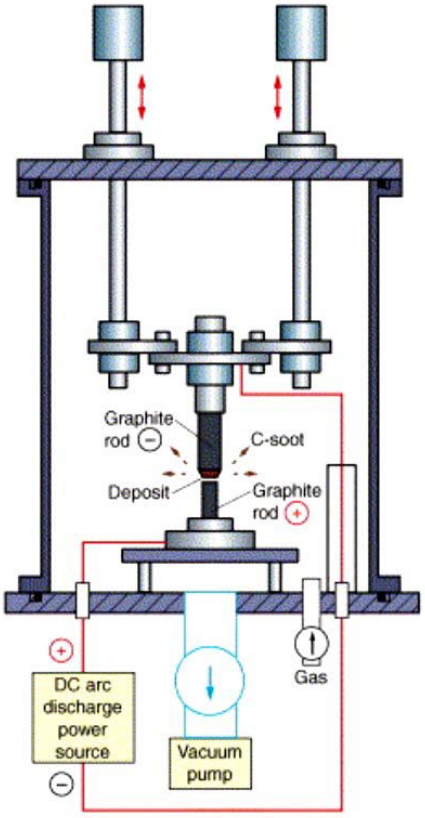

Figure 2.16 Schematic diagram of CNT formation apparatus by the arc-discharge method [104].

This rather simple technique produces a complex mixture of components. The deposit formed on the cathode contains SWCNTs and MWCNTs as well as carbon nanoparticles [103]. The typical nanotubes developed during the arc discharge exhibit a good crystalline structure with few structural defects due to the very high temperature, around 3000 ^{o}C. In order to make use of these nanotubes, additional steps are required since they have to be separated from the cathode, purified, and manipulated onto a substrate.

2.2.2.1.2 Laser ablation method

Very high temperatures are reached during nanotube production in the laser ablation method, which is similar to that in the arc discharge method. A graphite target, placed in the deposition chamber in a flow of inert gas, is heated to around 1200 ^{o}C by a furnace. A high-power laser is pointed to a target to generate vaporized material which is carried by gas into a cooled collector (Figure 2.17), where the vaporized material condenses [105]. Laser vaporization can produce up to 90% highly ordered nanotubes, aligned along a common axis. The average nanotube diameter and size distribution can be controlled by varying the growth temperature and other process parameters. SWCNTs have been produced by using a composite target of graphite and metal catalyst particles. The best yield has been obtained from a cobalt and nickel mixture [106]. On the other hand, laser ablation method along with arc discharge has several drawbacks. First, the nanotubes are mixed with unwanted forms of carbon and additional steps for purifying

the CNTs are required. Second, the equipment requirements and the large energy consumed qualify these methods as less favorable for mass production [103].

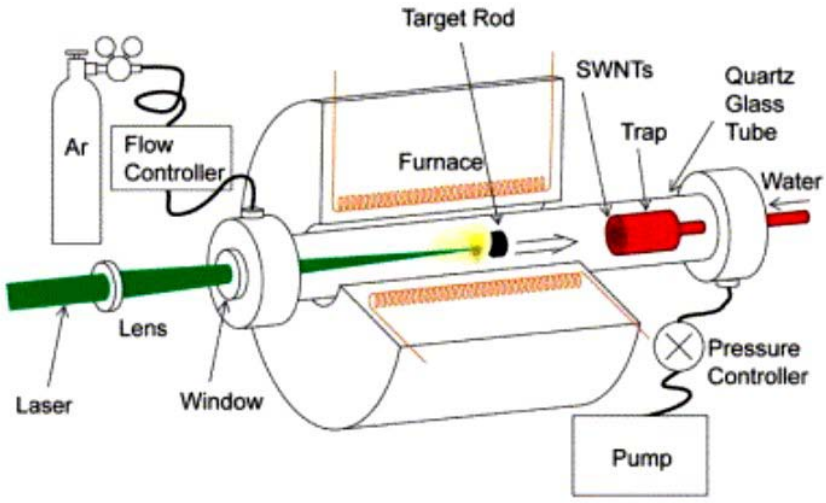

Figure 2.17 Schematic diagram of the laser-furnace apparatus [104].

2.2.2.1.3 Thermal chemical vapor deposition method

A basic thermal CVD apparatus consists of a quartz tube connected to a gaseous carbon source and placed in a tubular furnace (Figure 2.18). In a typical thermal CVD process, a substrate is exposed to one or more volatile hydrocarbon precursors, which thermally decompose and react on the substrate surface to produce CNT deposit. Usually gaseous precursors are used. Before synthesis, a metal catalyst is deposited onto the substrate. The key point to deposit CNTs is to create *in-situ* nano-sized catalyst particles

during the growth process. The most studied catalysts used for growing CNTs by thermal CVD method are iron, cobalt, and nickel. The commonly used carbon precursors are carbon monoxide and hydrocarbons such as methane, ethane, ethylene, and acetylene. The growth behavior of CNTs relates to the catalyst preparation, growth temperature, carbon source type, and feeding rate. In a typical growth process, air in the deposition tube is firstly removed by purging an inert gas and the furnace is heated until the substrate reaches the desired temperature. Then carbon precursors, metered trough a flow controller, are introduced into the system for a specific growth period. Finally, the carbon source is turned off and the reactor is cooled down to room temperature in a flow of inert gas before exposing the product to air. The main advantages of this method are its simplicity and adaptability. Moreover, the growth temperature is much lower than that achieved in arc discharge and laser ablation procedures. The disadvantage is the necessity of catalyst preparation prior to the deposition process.

Figure 2.18 Schematic diagram of a thermal CVD setup.

2.2.2.1.4 Floating catalyst chemical vapor deposition method

Floating catalyst CVD (FCCVD) method derives from the thermal CVD method. In a FCCVD process, catalyst and carbon source are introduced into the system reactor simultaneously, which is different from that of common thermal CVD. This method usually uses gaseous precursors as carbon source and solid organometallic species as catalyst source. The organometallic species decompose at temperatures lower than those used for CNT growth and can be placed in the same furnace or in a separate one (Figure 2.19). The most popular catalyst precursor is ferrocene, but other types of metallocenes have also been studied. The catalyst is formed by vaporization of organometallic precursors and transported to the substrate by carrier gas flows. Catalyst particles are deposited on the substrate in high densities and vertically aligned arrays of CNTs are subsequently obtained. The advantage of FCCVD method is the elimination of extra step of the catalyst preparation. A drawback of this method resides in less controllability of the evaporation rate over metallocene precursors.

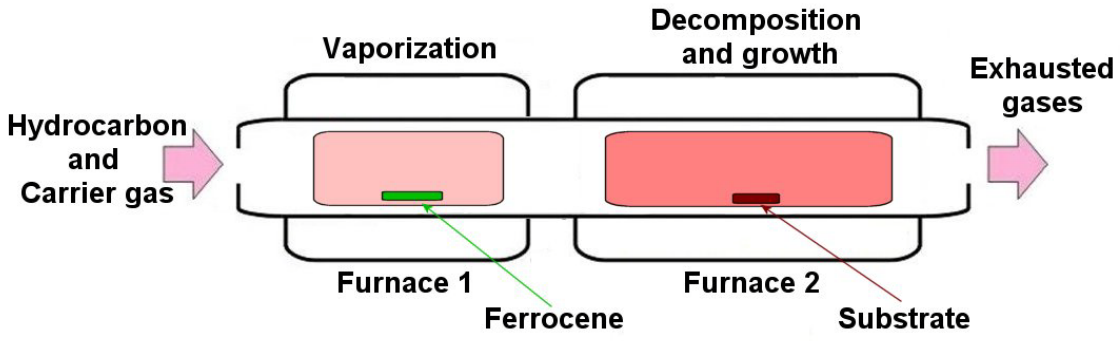

Figure 2.19 Schematic diagram of a FCCVD setup.

2.2.2.1.5 Aerosol assisted chemical vapor deposition method

Aerosol assisted CVD (AACVD) method involves the atomization of precursor solution, in which fine aerosol droplets are generated and delivered by a flow of inert carrier gas into the reaction zone. The atomization is realized using an ultrasonic nebulizer (Figure 2.20). The precursor solution is prepared by dissolving organometallic species, as catalyst source, in carbonaceous liquids. When the precursor reaches the high temperature zone, the solvent evaporates and organometallic species decomposes to provide the catalyst particles. The metallic particles are deposited onto substrates and act as active nucleation centers for nanotube growth [107]. This process generates clean and aligned CNTs since the catalyst particles are deposited on the substrate in high densities [108].

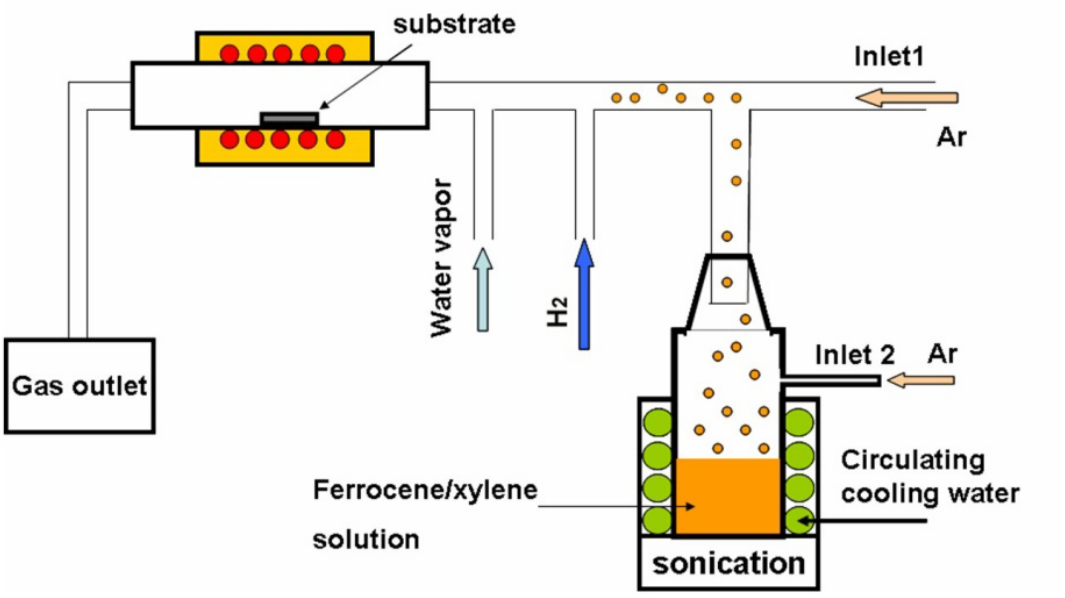

Figure 2.20 Schematic diagram of an AACVD setup [107].

The main advantages of this method are: 1) the substrate is continuously fed with both carbon and catalyst; 2) a wide range of precursors can be used since even non-volatile liquids can be ultrasonicated [109]; 3) the commonly employed process of catalyst preparation is spared. However, AACVD method gives a limited control over the solution feeding rate and requires large quantities of precursors to protect the ultrasonic nebulizer.

2.2.2.1.6 Spray pyrolysis chemical vapor deposition method

Spray pyrolysis CVD is a process in which CNTs are deposited by spraying an active solution on a heated surface. The precursor solution is sprayed through a nozzle located in the reaction zone (Figure 2.21) [110]. Similar to AACVD, the active solution is prepared by dissolving organometallic species in carbonaceous liquids. At high temperature, the solvent evaporates and acts as carbon source, while the organometallic species decomposes to provide the catalyst particles. The metallic particles act as active nucleation centers for the nanotube growth [111]. This method generates long and aligned CNTs deposited in high densities. Among various techniques, spray pyrolysis CVD provides a controlled way of spraying complex carbonaceous liquids directly into the deposition chamber, spares the intermediate stage for catalyst preparation, and ensures semi-continuous growth of CNTs [112]. These advantages give the possibility of scale-up production of CNTs at commercially viable prices.

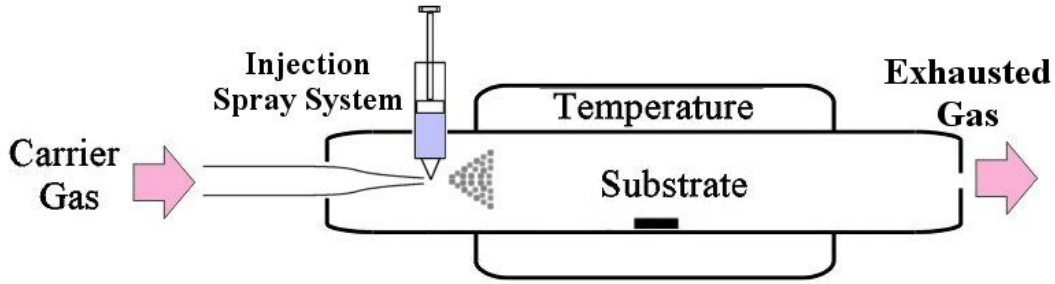

Figure 2.21 Schematic diagram of spray pyrolysis CVD setup.

2.2.2.1.7 Plasma-enhanced chemical vapor deposition method

Plasma-enhanced CVD (PECVD) is a process of depositing CNTs from a gas state, using electrical energy to generate a glow discharge in which the energy is transferred into a gaseous carbon source. Usually, the discharge is realized in vacuum. A basic PECVD reactor is shown in Figure 2.22. The plasma generated energy decomposes and transforms the gas molecules into reactive radicals, ions, and different types of related molecules. These reactive species interact with the heated substrate and the deposition process occurs. Since the gas molecule decomposition occurs before reaching the substrate, deposition is possible at lower temperatures than that other CVD processes require. Although this is the major advantage of PECVD process, the true role of the plasma in CNT growth is not clear yet. Recent reports indicate that PECVD facilitates the growth of CNTs with better vertical orientation and at lower temperatures in comparison with thermal CVD method [113, 114]. Some other advantages of PECVD method in growing CNTs are good adhesion, coverage, and uniformity of the product [115].

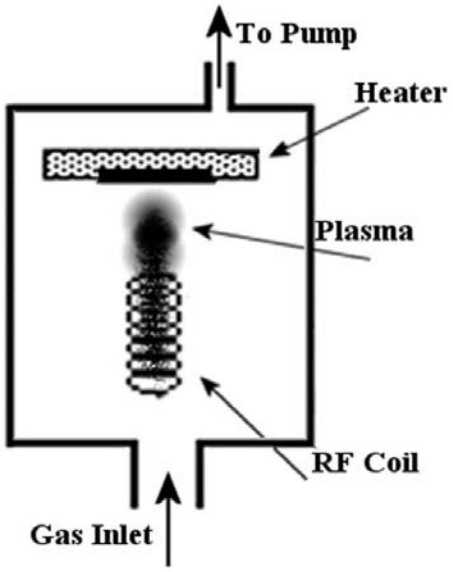

Figure 2.22 Schematic diagram of PECVD deposition system.

2.2.2.1.8 Other methods used for CNT production

Besides the techniques discussed above, CNTs can also be produced using other methods such as ball milling and diffusion flame synthesis. Ball milling and subsequent annealing is a simple method for CNT production. In this method, graphite powder is placed into a stainless steel container along with several hardened steel balls. Argon is introduced into the stainless steel container and the milling is carried out at room temperature for several days. The powder resulted from milling process is annealed in an inert gas flow at high temperatures. The mechanism to form CNTs using this process is not clear yet, but it is thought that the ball milling forms nanotube nuclei, and the annealing process activates nanotube growth. The main products obtained by using this

method are MWCNTs [116]. Flame synthesis method uses a hydrocarbon gas for CNT production. The combustion of a portion of the hydrocarbon gas provides an elevated temperature and the remaining fuel serves as the required hydrocarbon reagent. Hence, the flame constitutes an efficient source of both energy and hydrocarbon raw material [117]. Combustion synthesis can be scaled for high-volume commercial production. The additional step required for purification is the main disadvantage of these methods.

2.2.2.1.9 Growth mechanism of CNTs

Physical properties of CNTs are directly related to the structure of the nanotube and it is essential to understand what controls the diameter, the number of shells, the helicity, and the defects of the nanotubes during synthesis. It can be assumed that the growth mechanism depends greatly on the technique employed. Growth mechanism of nanotube formation is assumed to be similar for arc-discharge [118] and laser ablation [119] techniques, since both of them use a graphite-metal mixture as starting materials and involve the vaporization of this mixture followed by condensation in an inert gas. Although different models have been proposed, it is generally accepted that the growth of CNTs using these methods follows a solid phase growth model (Figure 2.23) [120]. In the early stage of evaporation and at very high temperatures of approximately 2500 ^{o}C, small carbon and metal clusters are formed. As the temperature of the system is reduced and reaches the eutectic temperature of metal-carbon alloy, the metal clusters are supersaturated with carbon and their surface is covered with carbon clusters such as

hemispherical fullerene-like structures. Below this temperature carbon starts to precipitate out of the metal-carbon mixture and grows as a tube. At this stage, if the temperature is just below the eutectic temperature (approximately 1200 ^{o}C), nanotubes in a high yield are produced [121]. The fact that metal particles are not found at the tip of the resulted tubes indicates that the mechanism follows a base growth mode [120].

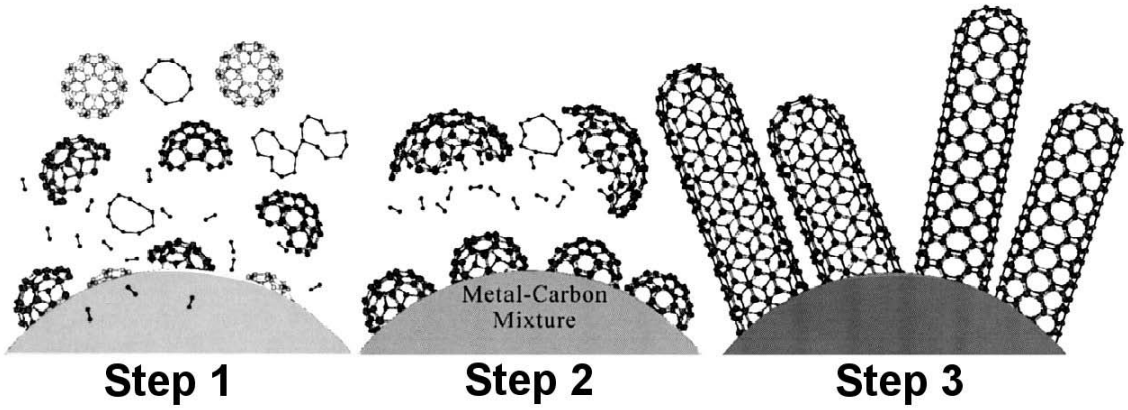

Figure 2.23 Diagram of the growth model of CNTs for arc discharge and laser ablation methods [119].

Up to now, the way in which nanotubes are formed in the catalytic CVD process has not been precisely determined and is still a subject of controversy. In a typical CVD process, a hydrocarbon gas is flowed over a substrate covered by a catalyst material and situated at high temperatures in inert atmosphere. The most effective catalysts have been shown repeatedly to be iron, nickel and cobalt [122]. A generally accepted growth model presumes that spherical or semispherical catalyst nanoparticles are formed on the substrate due to high temperature. In the growth process, the catalytic activity of the

formed nanoparticles enhances the decomposition of volatile carbon compounds. The carbon atoms diffuse through and over the metal particles rapidly [106]. The metal clusters become supersaturated with carbon and carbon precipitates out from the particle surface. If the carbon supply is not stopped, the carbon precipitation on the catalyst nanoparticles continues and leads to the formation of nanotubes. Depending on the adhesion of catalyst particles to the substrate, different growth modes take place. For a weak adhesion between the catalyst particles and substrate, the carbon precipitation occurs at the bottom surface of the particle and the tubes lift the catalyst particle as it grows. In this case the formed nanotube wraps the catalyst particle at its top end. This type of growth mode is called “tip growth” (Figure 2.24a).

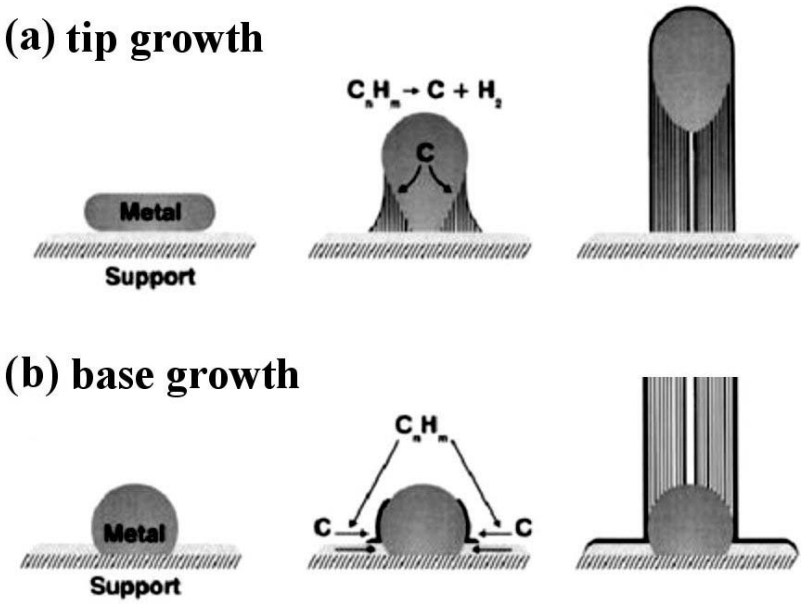

Figure 2.24 Diagram of the CNTs tip growth model (a) and base growth model (b) [32].

In the case of strong adhesion between the catalyst particles and substrate, the carbon precipitates at the top surface of the particle and the tube continues to grow while the catalyst particle remains attached to the substrate. This growth model of nanotube is called “base growth” (Figure 2.24b). The catalyst particle size determines the size of the nanotube. When the particle diameter is reduced bellow several nanometers, SWCNTs can be obtained [123].

2.2.2.2 Doped CNTs

2.2.2.2.1 General review on doped CNTs

Theoretical and experimental studies reveal that it is possible to tune the physical and chemical properties of CNTs by incorporating hetero atoms within the carbon lattice [124, 125]. Boron and nitrogen are frequently studied dopants because their atom size is similar to that of carbon [126].The substitution of carbon atoms in the hexagonal lattice of a CNT by atoms with a different valence number has an important impact upon the electronic structure and the electronic transport of CNTs [127]. The substitution of a carbon atom by a nitrogen atom, into the CNT lattice of a metallic SWCNT, modifies the Fermi-energy of the SWCNT. Since nitrogen has five valence electrons and carbon only has four, the nitrogen-doped SWCNT state shifts above the Fermi-energy of the undoped SWCNT. In the case of substituting a carbon atom by a boron atom, the boron-doped SWCNT state shifts below the Fermi-energy of the undoped SWCNT, due to the reduced

valence of boron [128]. Doping carbon nanotubes also effects their structure and chemical reactivity [129]. The hetero atoms produce localized defects, which are energetically less stable than perfect carbon lattice. This makes the tube surface chemically active and facilitates chemical functionalization [130]. Methods of obtaining doped CNTs are similar to those used for regular nanotube production. Incorporation of hetero atoms within the graphitic walls of CNTs depends on various growth parameters such as precursor, catalyst, pressure, and reaction temperature. In order to meet the requirements of practical applications, it is necessary to refine an appropriate method to produce doped CNTs in large amounts at commercially viable prices, with a strong control over their diameter, length, and dopant amount.

2.2.2.2.2 Nitrogen doped CNTs

Nitrogen doped carbon nanotubes (CN_x) exhibit distinct morphologies from their undoped counterparts. This is understandable if the substitutional nitrogen atoms are considered as localized defects in the carbon lattice. Analysis of the experimental results yielded that nitrogen doped SWCNTs generally have straight walls, similar to undoped SWCNT morphology [131]. On the other hand, nitrogen doped MWCNTs exhibit a distinct structure in comparison with their undoped counterparts. These tubes contain a regularly spaced array of internal carbon walls called ‘bamboo’ structure. The walls are usually corrugated and irregular. Alignment and number of nanotube walls depend on catalyst used and dopant concentration [132]. Theoretical studies of the bonding

configuration of nitrogen within CN_x proposed various structural models. There are three primary types: substitutional or 'graphitic' nitrogen where a nitrogen atom replaces a carbon atom (Figure 2.25a), pyrrole-like nitrogen where the substitutional nitrogen atom sits in a five-fold ring (Figure 2.25b), and pyridine-like nitrogen where the nitrogen atom is two-fold coordinated (Figure 2.25c). These theoretical models were demonstrated experimentally using different characterization methods such as X-ray photoelectron spectroscopy (XPS) and combination of elemental mapping with electron-energy loss spectroscopy (EELS). By using these methods, it was observed that gaseous nitrogen can be also trapped in the interior region of CN_x. Encapsulation of nitrogen molecules in CNTs takes place during a growth process. Nitrogen atoms participate in the growth process of CN_x. A part of the nitrogen atoms are trapped in the hollow zone of the tubes as molecular nitrogen [133] or remain intercalated between the inner layers [134] while the rest of the atoms substitute the carbon atoms in the described configurations [135]. The methods developed for the synthesis of nitrogen doped CNTs are similar to the methods used for regular nanotubes production. Using the arc-discharge method, CN_x were produced by the evaporation of the graphite rod in a nitrogen and helium atmosphere [136] or by utilizing a composite anode containing nitrogen rich precursor in helium atmosphere [131]. Around 1.0 at.% of nitrogen was incorporated into the tubes by using this procedure. The most common technique for CN_x synthesis is CVD method. Different variations were considered such as thermal CVD [137], AACVD [138], FCCVD [139], and PECVD [140]. The maximum nitrogen content reported in CN_x is approximately 20 at.% obtained from acetonitrile pyrolysis via AACVD method [138].

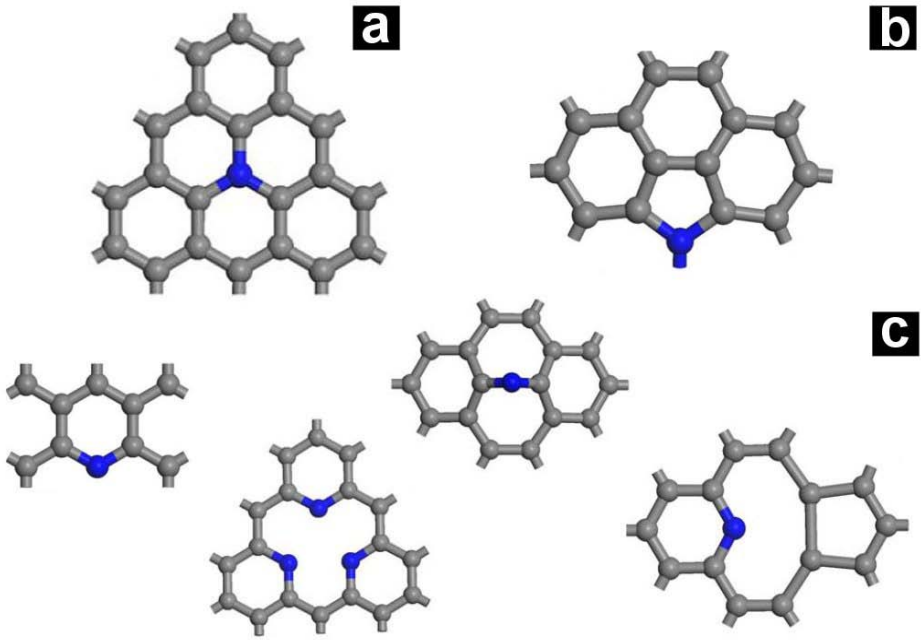

Figure 2.25 Bonding configurations for nitrogen atoms in CNTs; graphitic nitrogen (a), pyrrolic-type nitrogen (b), pyridine-like nitrogen (c) [141].

2.2.2.2.3 Growth mechanism of nitrogen doped CNTs

The nanotube growth model described for regular nanotubes cannot explain the regular internal ‘bamboo’ cavities of nitrogen doped MWCNTs. An alternative growth model for these nitrogen-doped tubes was proposed after investigation of CN_x using transmission electron microscopy and electron energy loss spectroscopy chemical mapping analysis (Figure 2.26) [142]. Similar to the mechanism of regular CNT formation, catalyst nanoparticles are formed on the substrate due to high temperature during the growth process, allowing carbon atoms to diffuse through and over catalyst particles. The catalyst nanoparticles become supersaturated and carbon precipitates out from the particle surface. The difference between the growth model of regular CNTs and

that of CN_x consists in the way how the catalyst particles are engaged in the process. In the case of growing CN_x, the catalyst particles are forced out of the graphitic tubular structure and migrate rapidly to the tube tip, due to the accumulated stress which arises from the internal walls. As the number of layers increases, the catalyst particle is pressurized until it is ejected from the cavity and the process is repeated. Since both carbon and nitrogen are soluble in iron, both diffuse through the catalyst particle. When the molten catalyst particle is supersaturated with carbon and nitrogen, they precipitate and form CN_x nanotubes [32]. This model is supported by the observation that the bamboo periodicity decreases when the catalyst particle size becomes smaller [142].

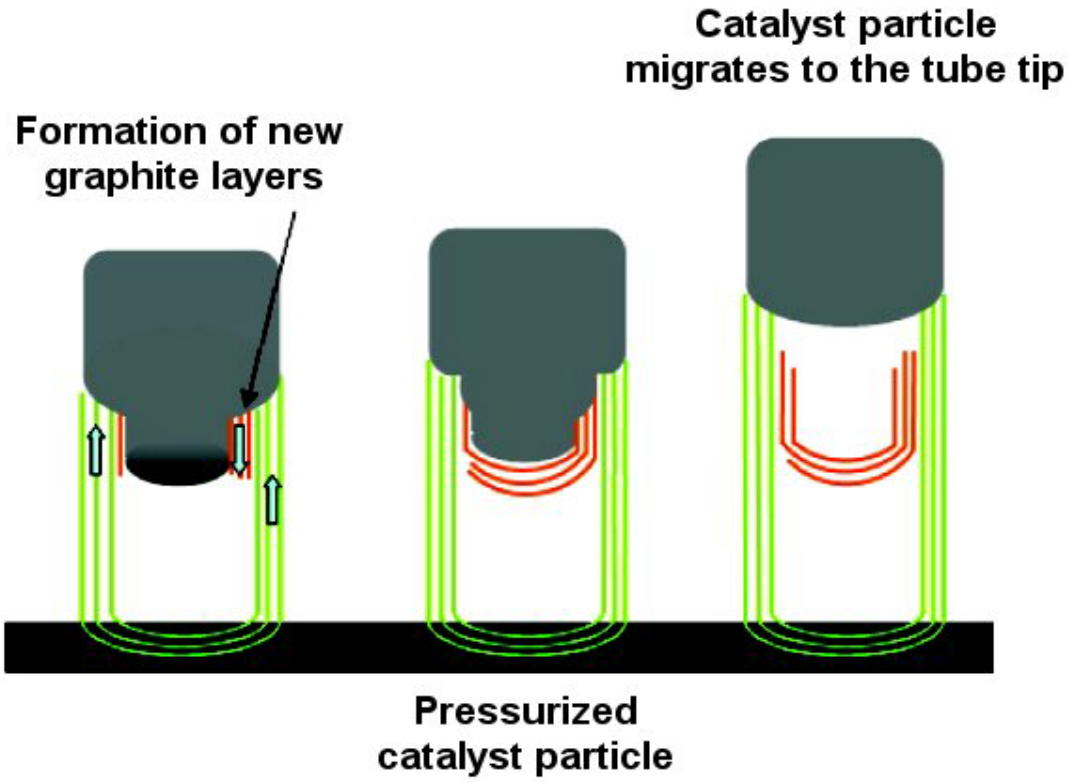

Figure 2.26 Diagram of the formation of a bamboo cavity in CN_x [143].

2.2.3 Synthesis of two-dimensional graphenes

The current major challenges in the nanomaterial synthesis are large-scale production and controlled growth of graphene [144]. Presently, scientific research on graphene is performed using mechanically exfoliated graphene obtained from natural or highly-oriented pyrolytic graphite (HOPG) flakes [145]. This low-tech method is not suitable for electronics production, but it was proved to deliver high-quality material for testing and measuring a whole wealth of physical phenomena [146]. Mechanical exfoliation was the first reported and repeatable synthesis method to isolate graphene for studying their physical properties. The method relies on isolating graphene from graphite by destroying Van der Waals force between graphite layers. In this graphene synthesis process, highly oriented pyrolytic graphite sheets are etched in oxygen plasma. After this step, a cohesive tape is used to split graphite crystals into thinner pieces. The tape with attached flakes is dissolved in acetone, and the flakes including graphite monolayers are sedimented on a silicon wafer. The technique has been followed and improved along with efforts to develop new processing routes for efficient synthesis of large scale graphene. An improved method is chemical cleavage from graphite. Graphenes are fabricated from graphite oxide obtained by treating graphite with strong oxidizers. Atomic planes of graphite are partially detached due to intercalation of oxide groups. By using ultrasonic treatment, the oxidized graphenes are exfoliated and ready to be reduced to graphene chemically or by thermal annealing [147]. A different and new method for graphene synthesis is thermal CVD. Graphene were grown, at high temperatures, on nickel substrates using a precursor mixture of methane and hydrogen [148]. Nickel has a good

solubility for carbon atoms and the graphene formation is attributed to the precipitation of carbon atoms on nickel surface at moderate cooling rates. Graphene films were also fabricated on copper foils [149]. It was concluded that the thickness of graphene films is independent on deposition time due to low solubility of carbon in copper. In this case, the precipitation mechanism does not work and needs additional studies. Graphenes were also obtained using plasma enhanced CVD. Single-layer and few-layer graphene were grown on different type of substrates by radio frequency PECVD using a gas mixture of methane and hydrogen, high plasma powers, and high temperatures [150]. These achievements in graphene synthesis confirmed the reproducibility of results and created routes to a better control over the thickness of graphene layers and large scale production. However, in order to achieve better control of graphene growth and explore its potential for manufacturing different nanodevices, further investigations of graphene growth mechanism are necessary.

2.3 The future of carbon based nanomaterials

Physical properties of carbon based nanomaterials are related to the hardest material known (diamond) and to one of the softest (graphite). They can act as semiconductors, metals, and dielectrics. The band gap of semiconducting nanotubes or nanodiamonds can be tuned by changing the size and/or the doping elements. These materials can be transparent or opaque, and their surfaces may be passive (basal planes of graphite) or chemically active (edge planes of graphite). Thus, numerous variations of

mechanical, electrical, or chemical properties can be achieved by using carbon nanomaterials and controlling their structure and surface chemistry. Combinations of these carbon materials enlarge the area of their application. For example, solar cells based on mixture of carbon nanotubes and carbon fullerenes [151] demonstrated enhanced efficiency, while SWCNTs filled with fullerenes [152, 153] have been realized and are expected to have a crucial influence in computing architectures.

The ultimate goal of nanotechnology is not only to develop materials with amazing properties, but also to realize mechanical systems at nanoscale level. The possibility of creating mechanical systems has been experimentally demonstrated by successfully controlling and manipulating the formation of a single iron carbonyl molecule [154]. In order to take advantage of nanotechnology, a better molecular control of complex structures is required. Unfortunately, this is far from reality at this moment. Fragile attempts have been done in this area of research. Examples are the synthesis of nanobuds which are a combination of nanotubes and fullerene [155], and the branched nanotubes [156]. Although the construction of a nanoscale electromechanical actuator using multi-walled carbon nanotube as the motion element has been successful [157], even less has been done in realizing molecular machineries. Since carbon is the common element of these achievements, there are premises that visionary views of R. Feyman and E. Drexler will be accomplished in the future.

2.4 References

[1] E. Roston, *The Carbon Age: How Life's Core Element Has Become Civilization's Greatest Threat*, Walker & Company, 2009.

[2] P. Harris, "On charcoal," *Interdisciplinary Science Reviews*, vol. 24, 1999, pp. 301-306.

[3] M. Faraday, *The chemical history of a candle*, New York: Collier Books, 1962.

[4] Y. Gogotsi, *Carbon Nanomaterials*, CRC Press, 2006.

[5] H.O. Pierson, *Handbook of Carbon, Graphite, Diamonds and Fullerenes: Processing, Properties and Applications*, William Andrew, 1995.

[6] W.B. Jensen, "The Origin of the Term Allotrope," *Journal of Chemical Education*, vol. 83, Jun. 2006, p. 838.

[7] R.C. Haddon, R.E. Palmer, H.W. Kroto, and P.A. Sermon, "The Fullerenes: Powerful Carbon-Based Electron Acceptors [and Discussion]," *Philosophical Transactions: Physical Sciences and Engineering*, vol. 343, Apr. 1993, pp. 53-62.

[8] R.B. Heimann, "Carbon allotropes: a suggested classification scheme based on valence orbital hybridization," *Carbon*, vol. 35, pp. 1654-1658.

[9] R. Heimann, S. Evsyukov, and L. Kavan, *Carbyne and Carbynoid Structures*, Springer, 1999.

[10] G. Messina and S. Santangelo, *Carbon: The Future Material for Advanced Technology Applications*, Springer, 2006.

[11] L. Itzhaki, E. Altus, H. Basch, and S. Hoz, "Harder than Diamond: Determining the Cross-Sectional Area and Young's Modulus of Molecular Rods," *Angewandte Chemie International Edition*, vol. 44, 2005, pp. 7432-7435.

[12] W.A. Chalifoux and R.R. Tykwinski, "Synthesis of polyynes to model the sp-carbon allotrope carbyne," *Nat Chem*, vol. 2, Nov. 2010, pp. 967-971.

[13] B.T. Kelly, *Physics of Graphite*, Springer, 1981.

[14] D. Chung, "Review: Graphite," *Journal of Materials Science*, vol. 37, 2002, pp. 1475-1489.

[15] C. Cousins, "Formal elasticity of four carbon allotropes: I. The inner elastic

constants, internal strain tensors, and zone-centre optic mode frequencies and their pressure dependences," *Journal of Physics Condensed Matter*, vol. 14, 2002, pp. 5091-5113.

[16] L. Samuelson, I.P. Batra, and C. Roetti, "A comparison of electronic properties of various modifications of graphite," *Solid State Communications*, vol. 33, Feb. 1980, pp. 817-820.

[17] S. Flandrois and B. Simon, "Carbon materials for lithium-ion rechargeable batteries," *Carbon*, vol. 37, Feb. 1999, pp. 165-180.

[18] R.M. Hazen, *The Diamond Makers*, Cambridge University Press, 1999.

[19] M. Werner and R. Locher, "Growth and application of undoped and doped diamond films," *Reports on Progress in Physics*, vol. 61, Dec. 1998, pp. 1665-710.

[20] B.T. Kelly, *Physics of Graphite*, Springer, 1981.

[21] P. John, N. Polwart, C.E. Troupe, and J.I.B. Wilson, "The oxidation of (100) textured diamond," *Diamond and Related Materials*, vol. 11, Mar. , pp. 861-866.

[22] C. Cousins, "Elasticity of carbon allotropes. I. Optimization, and subsequent modification, of an anharmonic Keating model for cubic diamond," *Physical Review B - Condensed Matter and Materials Physics*, vol. 67, 2003, pp. 241071-2410713.

[23] L. Itzhaki, E. Altus, H. Basch, and S. Hoz, "Harder than Diamond: Determining the Cross-Sectional Area and Young's Modulus of Molecular Rods," *Angewandte Chemie International Edition*, vol. 44, 2005, pp. 7432-7435.

[24] S. Elliot, *Physics of Amorphous Materials*, Longman, 1990.

[25] N.A. Marks, D.R. McKenzie, B.A. Pailthorpe, M. Bernasconi, and M. Parrinello, "Microscopic Structure of Tetrahedral Amorphous Carbon," *Physical Review Letters*, vol. 76, Jan. 1996, p. 768.

[26] J. Robertson, "Diamond-like amorphous carbon," *Materials Science and Engineering: R: Reports*, vol. 37, May. 2002, pp. 129-281.

[27] P.J.F. Harris, "Fullerene-related structure of commercial glassy carbons," *Philosophical Magazine*, vol. 84, 2004, p. 3159.

[28] F. Cowlard, "Vitreous carbon - a new form of carbon," *Biological Engineering Society 10 anniversary conference, recent advances in bio-medical engineering, 7-10 April 1970*, London, UK: Biological Engng. Soc, 1970, p. 1 pp.

[29] P. Morgan, *Carbon Fibers and Their Composites*, CRC Press, 2005.

[30] A. Yoshida, Y. Kaburagi, and Y. Hishiyama, "Microtexture and magnetoresistance of glass-like carbons," *Carbon*, vol. 29, 1991, pp. 1107-1111.

[31] J. Donnet, *Carbon Black*, CRC Press, 1993.

[32] P.L. Walker and P.A. Thrower, *Chemistry and Physics of Carbon, Volume 14*, Marcel Dekker, 1978.

[33] G. Benedek, P. Milani, and V. Ralchenko, *Nanostructured Carbon for Advanced Applications*, Springer, 2001.

[34] F.P. Bundy, "The P, T Phase and Reaction Diagram for Elemental Carbon, 1979," *Journal of Geophysical Research*, vol. 85, pp. PP. 6930-6936.

[35] F.P. Bundy, W.A. Bassett, M.S. Weathers, R.J. Hemley, H.U. Mao, and A.F. Goncharov, "The pressure-temperature phase and transformation diagram for carbon; updated through 1994," *Carbon*, vol. 34, 1996, pp. 141-153.

[36] F. Bundy, *Solid State Physics Under Pressure: Recent Advances with Anvil Devices*, edited by S. Minomura, Kluwer Academic Publishers, 1985.

[37] G. Cao, *Nanostructures and Nanomaterials: Synthesis, Properties & Applications*, Imperial College Press, 2004.

[38] K.K. Nanda, S.N. Sahu, and S.N. Behera, "Liquid-drop model for the size-dependent melting of low-dimensional systems," *Physical Review A*, vol. 66, Jul. 2002, p. 013208.

[39] S. Graham, K. Pichler, R. Friend, W. Romanow, J. McCauley, N. Coustel, J. Fischer, and A. Smith, "Photoluminescence in solid films of C60," Switzerland: 1992, pp. 531-5.

[40] H.W. Kroto, J.R. Heath, S.C. O'Brien, R.F. Curl, and R.E. Smalley, "C60: Buckminsterfullerene," *Nature*, vol. 318, Nov. 1985, pp. 162-163.

[41] H.W. Kroto and K. McKay, "The formation of quasi-icosahedral spiral shell carbon particles," *Nature*, vol. 331, Jan. 1988, pp. 328-331.

[42] D. Ugarte, "Curling and closure of graphitic networks under electron-beam irradiation," *Nature*, vol. 359, Oct. 1992, pp. 707-709.

[43] C. Deibel and V. Dyakonov, "Polymer–fullerene bulk heterojunction solar cells," *Reports on Progress in Physics*, vol. 73, 2010, p. 096401.

[44] X. Wang, O. Hofmann, R. Das, E.M. Barrett, A.J. deMello, J.C. deMello, and D.D.C. Bradley, "Integrated thin-film polymer/fullerene photodetectors for on-chip microfluidic chemiluminescence detection," *Lab on a Chip*, vol. 7, Jan. 2007, pp. 58-63.

[45] R.C. Haddon, A.S. Perel, R.C. Morris, T.T.M. Palstra, A.F. Hebard, and R.M. Fleming, "C60 thin film transistors," *Applied Physics Letters*, vol. 67, 1995, p. 121.

[46] G. Agostini, L. Pasimeni, M. Ruzzi, S. Monti, M. Maggini, M. Prato, I. Lamparth, and A. Hirsch, "Fullerene derivatives embedded in poly(methylmethacrylate): a laser flash photolysis and time-resolved EPR study," *Chemical Physics*, vol. 253, Feb. 2000, pp. 105-113.

[47] M. Monthioux and V.L. Kuznetsov, "Who should be given the credit for the discovery of carbon nanotubes?," *Carbon*, vol. 44, Aug. 2006, pp. 1621-1623.

[48] L.V. Radushkevich and V.M. Lukyanovich, "O strukture ugleroda, obrazujucegosja pri termiceskom razlozenii okisi ugleroda na zeleznom kontakte," *Zhurnal Fizicheskoi Khimii*, vol. 26, 1952, pp. 88-95.

[49] A. Oberlin, M. Endo, and T. Koyama, "Filamentous growth of carbon through benzene decomposition," *Journal of Crystal Growth*, vol. 32, 1976, pp. 335-349.

[50] S. Iijima, "Helical microtubules of graphitic carbon," *Nature*, vol. 354, Nov. 1991, pp. 56-58.

[51] T.W. Ebbesen and P.M. Ajayan, "Large-scale synthesis of carbon nanotubes," *Nature*, vol. 358, Jul. 1992, pp. 220-222.

[52] T. Guo, P. Nikolaev, A.G. Rinzler, D. Tomanek, D.T. Colbert, and R.E. Smalley, "Self-Assembly of Tubular Fullerenes," *The Journal of Physical Chemistry*, vol. 99, Jul. 1995, pp. 10694-10697.

[53] P. Nikolaev, M. Bronikowski, K. Bradley, F. Rohmund, D. Colbert, K. Smith, and R. Smalley, "Gas-phase catalytic growth of single-walled carbon nanotubes from carbon monoxide," *Chemical Physics Letters*, vol. 313, Nov. 1999, pp. 91-7.

[54] N. Inami, M. Ambri Mohamed, E. Shikoh, and A. Fujiwara, "Synthesis-condition dependence of carbon nanotube growth by alcohol catalytic chemical vapor deposition method," *Science and Technology of Advanced Materials*, vol. 8, 2007, pp. 292-295.

[55] A. Eftekhari, P. Jafarkhani, and F. Moztarzadeh, “High-yield synthesis of carbon nanotubes using a water-soluble catalyst support in catalytic chemical vapor deposition,” *Carbon*, vol. 44, Jun. 2006, pp. 1343-1345.

[56] H. Dai, “Carbon nanotubes: opportunities and challenges,” *Surface Science*, vol. 500, Mar. 2002, pp. 218-241.

[57] X. Zhao, Y. Liu, S. Inoue, T. Suzuki, R.O. Jones, and Y. Ando, “Smallest Carbon Nanotube Is 3 Å in Diameter,” *Physical Review Letters*, vol. 92, Mar. 2004, p. 125502.

[58] Q. Wen, R. Zhang, W. Qian, Y. Wang, P. Tan, J. Nie, and F. Wei, “Growing 20 cm Long DWNTs/TWNTs at a Rapid Growth Rate,” *Chemistry of Materials*, vol. 22, Feb. 2010, pp. 1294-1296.

[59] M.S. Dresselhaus, G. Dresselhaus, and P. Avouris, *Carbon nanotubes: synthesis, structure, properties, and applications*, Springer, 2001.

[60] S. Reich, C. Thomsen, and J. Maultzsch, *Carbon Nanotubes: Basic Concepts and Physical Properties*, Wiley-VCH, 2004.

[61] E. Ivchenko and B. Spivak, “Chirality effects in carbon nanotubes,” *Physical Review B (Condensed Matter and Materials Physics)*, vol. 66, Oct. 2002, pp. 155404-1.

[62] T.W. Ebbesen, H.J. Lezec, H. Hiura, J.W. Bennett, H.F. Ghaemi, and T. Thio, “Electrical conductivity of individual carbon nanotubes,” *Nature*, vol. 382, Jul. 1996, pp. 54-56.

[63] J. Bonard, J. Salvetat, T. Stockli, W.A. de Heer, L. Forro, and A. Chatelain, “Field emission from single-wall carbon nanotube films,” *Applied Physics Letters*, 1998.

[64] R. Seelaboyina, S. Boddepalli, K. Noh, M. Jeon, and W. Choi, “Enhanced field emission from aligned multistage carbon nanotube emitter arrays,” *Nanotechnology*, vol. 19, 2008, p. 065605.

[65] M. Reibold, P. Paufler, A. Levin, W. Kochmann, N. Patzke, and D. Meyer, “Materials: Carbon nanotubes in an ancient Damascus sabre,” *Nature*, vol. 444, 2006, p. 286.

[66] M.M.J. Treacy, T.W. Ebbesen, and J.M. Gibson, “Exceptionally high Young's modulus observed for individual carbon nanotubes,” *Nature*, vol. 381, Jun. 1996, pp. 678-680.

[67] M. Yu, B.S. Files, S. Arepalli, and R.S. Ruoff, “Tensile Loading of Ropes of Single Wall Carbon Nanotubes and their Mechanical Properties,” *Physical Review Letters*, vol. 84, Jun. 2000, p. 5552.

[68] K. Zhang, M. Yuen, J. Gao, and B. Xu, “Fabrication of High Thermal Conductivity Carbon Nanotube Arrays by Self Assembled Fe3O4 particles,” *CIRP Annals - Manufacturing Technology*, vol. 56, 2007, pp. 245-248.

[69] M.S. Saha, R. Li, X. Sun, and S. Ye, “3-D composite electrodes for high performance PEM fuel cells composed of Pt supported on nitrogen-doped carbon nanotubes grown on carbon paper,” *Electrochemistry Communications*, vol. 11, Feb. 2009, pp. 438-441.

[70] X. Sun, R. Li, D. Villers, J.P. Dodelet, and S. Désilets, “Composite electrodes made of Pt nanoparticles deposited on carbon nanotubes grown on fuel cell backings,” *Chemical Physics Letters*, vol. 379, Sep. 2003, pp. 99-104.

[71] B. Gao, A. Kleinhammes, X.P. Tang, C. Bower, L. Fleming, Y. Wu, and O. Zhou, “Electrochemical intercalation of single-walled carbon nanotubes with lithium,” *Chemical Physics Letters*, vol. 307, Jul. 1999, pp. 153-157.

[72] V.G. Gavalas, R. Andrews, D. Bhattacharyya, and L.G. Bachas, “Carbon Nanotube Sol−Gel Composite Materials,” *Nano Letters*, vol. 1, Dec. 2001, pp. 719-721.

[73] Y. Nakayama and S. Akita, “Field-emission device with carbon nanotubes for a flat panel display,” *Synthetic Metals*, vol. 117, Feb. 2001, pp. 207-210.

[74] O.K. Varghese, P.D. Kichambre, D. Gong, K.G. Ong, E.C. Dickey, and C.A. Grimes, “Gas sensing characteristics of multi-wall carbon nanotubes,” *Sensors and Actuators B: Chemical*, vol. 81, Dec. 2001, pp. 32-41.

[75] W. Jiang, S. Xiao, H. Zhang, Y. Dong, and X. Li, “Capacitive humidity sensing properties of carbon nanotubes grown on silicon nanoporous pillar array,” *Science in China Series E: Technological Sciences*, vol. 50, 2007, pp. 510-515.

[76] L.F. Su, J.N. Wang, F. Yu, and Z.M. Sheng, “Continuous synthesis of Y-junction carbon nanotubes by catalytic CVD,” *Chemical Vapor Deposition*, vol. 11, 2005, pp. 351-354.

[77] A.K. Geim and K.S. Novoselov, “The rise of graphene,” *Nature Materials*, vol. 6, Mar. 2007, pp. 183-191.

[78] P.R. Wallace, “The Band Theory of Graphite,” *Physical Review*, vol. 71, May. 1947, p. 622.

[79] E. Fradkin, “Critical behavior of disordered degenerate semiconductors. II. Spectrum and transport properties in mean-field theory,” *Physical Review B*, vol. 33, Mar. 1986, p. 3263.

[80] S.F. Braga, V.R. Coluci, S.B. Legoas, R. Giro, D.S. Galvão, and R.H. Baughman, “Structure and Dynamics of Carbon Nanoscrolls,” *Nano Letters*, vol. 4, May. 2004, pp. 881-884.

[81] H.P. Boehm, A. Clauss, G.O. Fischer, and U. Hofmann, “Das Adsorptionsverhalten sehr dunner Kohlenstoff-Folien,” *Zeitschrift fur anorganische und allgemeine Chemie*, vol. 316, 1962, pp. 119-127.

[82] A.K. Geim and P. Kim, “Carbon Wonderland,” *Scientific American*, vol. 298, 2008, pp. 90-97.

[83] K.S. Novoselov, A.K. Geim, S.V. Morozov, D. Jiang, Y. Zhang, S.V. Dubonos, I.V. Grigorieva, and A.A. Firsov, “Electric Field Effect in Atomically Thin Carbon Films,” *Science*, vol. 306, Oct. 2004, pp. 666-669.

[84] D.A. Dikin, S. Stankovich, E.J. Zimney, R.D. Piner, G.H.B. Dommett, G. Evmenenko, S.T. Nguyen, and R.S. Ruoff, “Preparation and characterization of graphene oxide paper,” *Nature*, vol. 448, Jul. 2007, pp. 457-460.

[85] Y. Hernandez, V. Nicolosi, M. Lotya, F.M. Blighe, Z. Sun, S. De, McGovernI. T., B. Holland, M. Byrne, Y.K. Gun'Ko, J.J. Boland, P. Niraj, G. Duesberg, S. Krishnamurthy, R. Goodhue, J. Hutchison, V. Scardaci, A.C. Ferrari, and J.N. Coleman, “High-yield production of graphene by liquid-phase exfoliation of graphite,” *Nat Nano*, vol. 3, 2008, pp. 563-568.

[86] M. Lotya, Y. Hernandez, P.J. King, R.J. Smith, V. Nicolosi, L.S. Karlsson, F.M. Blighe, S. De, Z. Wang, I.T. McGovern, G.S. Duesberg, and J.N. Coleman, “Liquid Phase Production of Graphene by Exfoliation of Graphite in Surfactant/Water Solutions,” *Journal of the American Chemical Society*, vol. 131, Mar. 2009, pp. 3611-3620.

[87] A. Reina, X. Jia, J. Ho, D. Nezich, H. Son, V. Bulovic, M.S. Dresselhaus, and J. Kong, “Large Area, Few-Layer Graphene Films on Arbitrary Substrates by Chemical

Vapor Deposition," *Nano Letters*, vol. 9, Jan. 2009, pp. 30-35.

[88] C. Di, D. Wei, G. Yu, Y. Liu, Y. Guo, and D. Zhu, "Patterned Graphene as Source/Drain Electrodes for Bottom-Contact Organic Field-Effect Transistors," *Advanced Materials*, vol. 20, 2008, pp. 3289-3293.

[89] C. Berger, Z. Song, X. Li, X. Wu, N. Brown, C. Naud, D. Mayou, T. Li, J. Hass, A.N. Marchenkov, E.H. Conrad, P.N. First, and W.A. de Heer, "Electronic Confinement and Coherence in Patterned Epitaxial Graphene," *Science*, vol. 312, May. 2006, pp. 1191-1196.

[90] H. Huang, W. Chen, S. Chen, and A.T.S. Wee, "Bottom-up Growth of Epitaxial Graphene on 6H-SiC(0001)," *ACS Nano*, vol. 2, Dec. 2008, pp. 2513-2518.

[91] L. Jiao, X. Wang, G. Diankov, H. Wang, and H. Dai, "Facile synthesis of high-quality graphene nanoribbons," *Nat Nano*, vol. 5, May. 2010, pp. 321-325.

[92] C. Lee, X. Wei, J.W. Kysar, and J. Hone, "Measurement of the Elastic Properties and Intrinsic Strength of Monolayer Graphene," *Science*, vol. 321, Jul. 2008, pp. 385-388.

[93] A.B. Kuzmenko, E. van Heumen, F. Carbone, and D. van der Marel, "Universal Optical Conductance of Graphite," *Physical Review Letters*, vol. 100, Mar. 2008, p. 117401.

[94] A.A. Balandin, S. Ghosh, W. Bao, I. Calizo, D. Teweldebrhan, F. Miao, and C.N. Lau, "Superior Thermal Conductivity of Single-Layer Graphene," *Nano Letters*, vol. 8, Mar. 2008, pp. 902-907.

[95] M. Hiramatsu and M. Hori, *Carbon Nanowalls: Synthesis and Emerging Applications*, Springer, 2010.

[96] Y. Ando, X. Zhao, and M. Ohkohchi, "Production of petal-like graphite sheets by hydrogen arc discharge," *Carbon*, vol. 35, 1997, pp. 153-8.

[97] S. Iijima, T. Wakabayashi, and Y. Achiba, "Structures of carbon soot prepared by laser ablation," *Journal of physical chemistry*, vol. 100, 1996, pp. 5839-5843.

[98] Y. Wu, P. Qiao, T. Chong, and Z. Shen, "Carbon Nanowalls Grown by Microwave Plasma Enhanced Chemical Vapor Deposition," *Advanced Materials*, vol. 14, 2002, pp. 64-67.

[99] K. Shiji, M. Hiramatsu, A. Enomoto, M. Nakamura, H. Amano, and M. Hori,

"Vertical growth of carbon nanowalls using rf plasma-enhanced chemical vapor deposition," *Diamond and Related Materials*, vol. 14, 2005, pp. 831-834.

[100] Y. Wu, B. Yang, B. Zong, H. Sun, Z. Shen, and Y. Feng, "Carbon nanowalls and related materials," *Journal of Materials Chemistry*, vol. 14, 2004, p. 469.

[101] J.B. Howard, K.D. Chowdhury, and J.B.V. Sande, "Carbon shells in flames," *Nature*, vol. 370, 1994, p. 603.

[102] H. Takehara, M. Fujiwara, M. Arikawa, M.D. Diener, and J.M. Alford, "Experimental study of industrial scale fullerene production by combustion synthesis," *Carbon*, vol. 43, 2005, pp. 311-319.

[103] P.G. Collins and P. Avouris, "Nanotubes for electronics," *Scientific American*, vol. 283, Dec. 2000, pp. 62-69.

[104] Y. Ando, X. Zhao, T. Sugai, and M. Kumar, "Growing carbon nanotubes," *Materials Today*, vol. 7, Oct. 2004, pp. 22-29.

[105] A. Thess, R. Lee, P. Nikolaev, H. Dai, P. Petit, J. Robert, C. Xu, Y.H. Lee, S.G. Kim, A.G. Rinzler, D.T. Colbert, G.E. Scuseria, D. Tomanek, J.E. Fischer, and R.E. Smalley, "Crystalline Ropes of Metallic Carbon Nanotubes," *Science*, vol. 273, Jul. 1996, pp. 483-487.

[106] R. Baker, "Catalytic growth of carbon filaments," *Carbon*, vol. 27, 1989, pp. 315-323.

[107] Y. Zhang, R. Li, H. Liu, X. Sun, P. Mérel, and S. Désilets, "Integration and characterization of aligned carbon nanotubes on metal/silicon substrates and effects of water," *Applied Surface Science*, vol. 255, Feb. 2009, pp. 5003-5008.

[108] M. Pinault, M. Mayne-L'Hermite, C. Reynaud, O. Beyssac, J.N. Rouzaud, and C. Clinard, "Carbon nanotubes produced by aerosol pyrolysis: growth mechanisms and post-annealing effects," *Diamond and Related Materials*, vol. 13, Apr. , pp. 1266-1269.

[109] M. Mayne, N. Grobert, M. Terrones, R. Kamalakaran, M. Rühle, H.W. Kroto, and D.R.M. Walton, "Pyrolytic production of aligned carbon nanotubes from homogeneously dispersed benzene-based aerosols," *Chemical Physics Letters*, vol. 338, Apr. 2001, pp. 101-107.

[110] L. Tapasztó, K. Kertész, Z. Vértesy, Z. Horváth, A. Koós, Z. Osváth, Z. Sárközi,

A. Darabont, and L. Biró, “Diameter and morphology dependence on experimental conditions of carbon nanotube arrays grown by spray pyrolysis,” *Carbon*, vol. 43, 2005, pp. 970-977.

[111] C.P. Deck and K. Vecchio, “Growth mechanism of vapor phase CVD-grown multi-walled carbon nanotubes,” *Carbon*, vol. 43, Oct. 2005, pp. 2608-2617.

[112] R. Kamalakaran, M. Terrones, T. Seeger, P. Kohler-Redlich, M. Ruhle, Y.A. Kim, T. Hayashi, and M. Endo, “Synthesis of thick and crystalline nanotube arrays by spray pyrolysis,” *Applied Physics Letters*, 2000.

[113] S. Hofmann, B. Kleinsorge, C. Ducati, A.C. Ferrari, and J. Robertson, “Low-temperature plasma enhanced chemical vapour deposition of carbon nanotubes,” *Diamond and Related Materials*, vol. 13, Apr. , pp. 1171-1176.

[114] M. Bell, K. Teo, and W. Milne, “Factors determining properties of multi-walled carbon nanotubes/fibres deposited by PECVD,” *Journal of Physics D: Applied Physics*, vol. 40, 2007, pp. 2285-2292.

[115] Ren, Huang, Xu, Wang, Bush, Siegal, and Provencio, “Synthesis of large arrays of well-aligned carbon nanotubes on glass,” *Science (New York, N.Y.)*, vol. 282, Nov. 1998, pp. 1105-1107.

[116] N. Pierard, A. Fonseca, Z. Konya, I. Willems, G. Van Tendeloo, and J. B.Nagy, “Production of short carbon nanotubes with open tips by ball milling,” *Chemical Physics Letters*, vol. 335, Feb. 2001, pp. 1-8.

[117] S. Nakazawa, T. Yokomori, and M. Mizomoto, “Flame synthesis of carbon nanotubes in a wall stagnation flow,” *Chemical Physics Letters*, vol. 403, 2005, pp. 158-162.

[118] P.J.F. Harris, S.C. Tsang, J.B. Claridge, and M.L.H. Green, “High-resolution electron microscopy studies of a microporous carbon produced by arc-evaporation,” *Journal of the Chemical Society, Faraday Transactions*, vol. 90, 1994, p. 2799.

[119] H. Kataura, Y. Kumazawa, Y. Maniwa, Y. Ohtsuka, R. Sen, S. Suzuki, and Y. Achiba, “Diameter control of single-walled carbon nanotubes,” *Carbon*, vol. 38, 2000, pp. 1691-7.

[120] P. Harris, “Solid state growth mechanisms for carbon nanotubes,” *Carbon*, vol. 45, Feb. 2007, pp. 229-39.

[121] R. Sen, S. Suzuki, H. Kataura, and Y. Achiba, “Growth of single-walled carbon nanotubes from the condensed phase,” *Chemical Physics Letters*, vol. 349, Dec. 2001, pp. 383-388.

[122] F. Derbyshire, A. Presland, and D. Trimm, “Graphite formation by the dissolution - precipitation of carbon in cobalt, nickel and iron,” *Carbon*, vol. 13, Apr. 1975, pp. 111-113.

[123] S.B. Sinnott, R. Andrews, D. Qian, A.M. Rao, Z. Mao, E.C. Dickey, and F. Derbyshire, “Model of carbon nanotube growth through chemical vapor deposition,” *Chemical Physics Letters*, vol. 315, Dec. 1999, pp. 25-30.

[124] S. Latil, S. Roche, D. Mayou, and J. Charlier, “Mesoscopic Transport in Chemically Doped Carbon Nanotubes,” *Physical Review Letters*, vol. 92, Jun. 2004, p. 256805.

[125] M. Terrones, P. Ajayan, F. Banhart, X. Blase, D. Carroll, J. Charlier, R. Czerw, B. Foley, N. Grobert, R. Kamalakaran, P. Kohler-Redlich, M. Rühle, T. Seeger, and H. Terrones, “N-doping and coalescence of carbon nanotubes: synthesis and electronic properties,” *Applied Physics A: Materials Science & Processing*, vol. 74, 2002, pp. 355-361.

[126] O. Stephan, P. Ajayan, C. Colliex, Redlich Ph., J. Lambert, P. Bernier, and P. Lefin, “Doping graphitic and carbon nanotube structures with boron and nitrogen,” *Science*, vol. 266, 1994, pp. 1683-1685.

[127] R. Sen, B.C. Satishkumar, A. Govindaraj, K.R. Harikumar, G. Raina, J. Zhang, A.K. Cheetham, and C.N.R. Rao, “B-C-N, C-N and B-N nanotubes produced by the pyrolysis of precursor molecules over Co catalysts,” *Chemical Physics Letters*, vol. 287, May. 1998, pp. 671-676.

[128] J. Wei, H. Hu, H. Zeng, Z. Zhou, W. Yang, and P. Peng, “Effects of nitrogen substitutional doping on the electronic transport of carbon nanotube,” *Physica E: Low-dimensional Systems and Nanostructures*, vol. 40, Jan. 2008, pp. 462-466.

[129] P. Nemes-Incze, N. Daróczi, Z. Sárközi, A. Koós, K. Kertész, O. Ţiprigan, Z. Horváth, A. Darabont, and L. Biró, “Synthesis of bamboo - structured multiwalled carbon nanotubes by spray pyrolysis method, using a mixture of benzene and pyridine,” *Journal of Optoelectronics and Advanced Materials*, vol. 9, 2007, pp.

1525-1529.

[130] A.H. Nevidomskyy, G. Csányi, and M.C. Payne, “Chemically Active Substitutional Nitrogen Impurity in Carbon Nanotubes,” *Physical Review Letters*, vol. 91, 2003, p. 105502.

[131] M. Glerup, J. Steinmetz, D. Samaille, O. Stéphan, S. Enouz, A. Loiseau, S. Roth, and P. Bernier, “Synthesis of N-doped SWNT using the arc-discharge procedure,” *Chemical Physics Letters*, vol. 387, Mar. 2004, pp. 193-197.

[132] M. Yudasaka, R. Kikuchi, Y. Ohki, and S. Yoshimura, “Nitrogen-containing carbon nanotube growth from Ni phthalocyanine by chemical vapor deposition,” *Carbon*, vol. 35, 1997, pp. 195-201.

[133] M. Terrones, R. Kamalakaran, T. Seeger, and M. Rühle, “Novel nanoscale gas containers: encapsulation of N2 in CNx nanotubes,” *Chemical Communications*, 2000, pp. 2335-2336.

[134] H.C. Choi, J. Park, and B. Kim, “Distribution and Structure of N Atoms in Multiwalled Carbon Nanotubes Using Variable-Energy X-Ray Photoelectron Spectroscopy,” *The Journal of Physical Chemistry B*, vol. 109, Mar. 2005, pp. 4333-4340.

[135] C. Ewels and M. Glerup, “Nitrogen doping in carbon nanotubes,” *Journal of Nanoscience and Nanotechnology*, vol. 5, Sep. 2005, pp. 1345-63.

[136] R. Droppa, P. Hammer, A.C.M. Carvalho, M.C. dos Santos, and F. Alvarez, “Incorporation of nitrogen in carbon nanotubes,” *Journal of Non-Crystalline Solids*, vol. 299-302, Apr. 2002, pp. 874-879.

[137] C. Tang, Y. Bando, D. Goldberg, and Fangfang Xu, “Structure and nitrogen incorporation of carbon nanotubes synthesized by catalytic pyrolysis of dimethylformamide,” *Carbon*, vol. 42, 2004, pp. 2625-33.

[138] M. Glerup, M. Castignolles, M. Holzinger, G. Hug, A. Loiseau, and P. Bernier, “Synthesis of highly nitrogen-doped multi-walled carbon nanotubes,” *Chemical Communications (Cambridge, England)*, Oct. 2003, pp. 2542-2543.

[139] H. Liu, Y. Zhang, R. Li, X. Sun, S. Désilets, H. Abou-Rachid, M. Jaidann, and L. Lussier, “Structural and morphological control of aligned nitrogen-doped carbon nanotubes,” *Carbon*, vol. 48, Apr. 2010, pp. 1498-1507.

[140] E. Wang, “A New Development in Covalently Bonded Carbon Nitride and Related Materials,” *Advanced Materials*, vol. 11, 1999, pp. 1129-1133.

[141] V.B.A.E. Basiuk, *Chemistry of Carbon Nanotubes*, American Scientific Publishers, 2008.

[142] S. Trasobares, O. Stéphan, C. Colliex, W. Hsu, H. Kroto, and D. Walton, “Compartmentalized CNx nanotubes: Chemistry, morphology, and growth,” *Journal of Chemical Physics*, vol. 116, 2002, pp. 8966-8972.

[143] Ming Lin, J. Tan, C. Boothroyd, Kian Ping Loh, Eng Soon Tok, and Yong-Lim Foo, “Dynamical observation of bamboo-like carbon nanotube growth,” *Nano Letters*, vol. 7, 2007, pp. 2234-8.

[144] M. Segal, “Selling graphene by the ton,” *Nat Nano*, vol. 4, Oct. 2009, pp. 612-614.

[145] K.S. Novoselov, A.K. Geim, S.V. Morozov, D. Jiang, Y. Zhang, S.V. Dubonos, I.V. Grigorieva, and A.A. Firsov, “Electric Field Effect in Atomically Thin Carbon Films,” *Science*, vol. 306, Oct. 2004, pp. 666-669.

[146] K.S. Novoselov, A.K. Geim, S.V. Morozov, D. Jiang, M.I. Katsnelson, I.V. Grigorieva, S.V. Dubonos, and A.A. Firsov, “Two-dimensional gas of massless Dirac fermions in graphene,” *Nature*, vol. 438, Nov. 2005, pp. 197-200.

[147] X. Lu, H. Huang, N. Nemchuk, and R.S. Ruoff, “Patterning of highly oriented pyrolytic graphite by oxygen plasma etching,” *Applied Physics Letters*, vol. 75, 1999, p. 193.

[148] S. Bae, H. Kim, Y. Lee, X. Xu, J. Park, Y. Zheng, J. Balakrishnan, T. Lei, H. Ri Kim, Y.I. Song, Y. Kim, K.S. Kim, B. Ozyilmaz, J. Ahn, B.H. Hong, and S. Iijima, “Roll-to-roll production of 30-inch graphene films for transparent electrodes,” *Nat Nano*, vol. 5, 2010, pp. 574-578.

[149] K.S. Kim, Y. Zhao, H. Jang, S.Y. Lee, J.M. Kim, K.S. Kim, J. Ahn, P. Kim, J. Choi, and B.H. Hong, “Large-scale pattern growth of graphene films for stretchable transparent electrodes,” *Nature*, vol. 457, Feb. 2009, pp. 706-710.

[150] J.J. Wang, M.Y. Zhu, R.A. Outlaw, X. Zhao, D.M. Manos, B.C. Holloway, and V.P. Mammana, “Free-standing subnanometer graphite sheets,” *Applied Physics Letters*, vol. 85, 2004, p. 1265.

[151] Cheng Li, Yuhong Chen, S. Ntim, and S. Mitra, “Fullerene-multiwalled carbon nanotube complexes for bulk heterojunction photovoltaic cells,” *Applied Physics Letters*, vol. 96, Apr. 2010, p. 143303 (3 pp.).

[152] D.A. Britz, A.N. Khlobystov, J. Wang, A.S. O'Neil, M. Poliakoff, A. Ardavan, and G.A.D. Briggs, “Selective host-guest interaction of single-walled carbon nanotubes with functionalised fullerenes,” *Chemical Communications (Cambridge, England)*, Jan. 2004, pp. 176-177.

[153] A.N. Khlobystov, D.A. Britz, J. Wang, S.A. O'Neil, M. Poliakoff, and G.A.D. Briggs, “Low temperature assembly of fullerene arrays in single-walled carbon nanotubes using supercritical fluids,” *Journal of Materials Chemistry*, vol. 14, 2004, p. 2852.

[154] H.J. Lee and W. Ho, “Single-Bond Formation and Characterization with a Scanning Tunneling Microscope,” *Science*, vol. 286, Nov. 1999, pp. 1719-1722.

[155] A.G. Nasibulin, P.V. Pikhitsa, H. Jiang, D.P. Brown, A.V. Krasheninnikov, A.S. Anisimov, P. Queipo, A. Moisala, D. Gonzalez, G. Lientschnig, A. Hassanien, S.D. Shandakov, G. Lolli, D.E. Resasco, M. Choi, D. Tomanek, and E.I. Kauppinen, “A novel hybrid carbon material,” *Nat Nano*, vol. 2, Mar. 2007, pp. 156-161.

[156] L.P. Biró, R. Ehlich, Z. Osváth, A. Koós, Z.E. Horváth, J. Gyulai, and J.B. Nagy, “From straight carbon nanotubes to Y-branched and coiled carbon nanotubes,” *Diamond and Related Materials*, vol. 11, Mar. , pp. 1081-1085.

[157] A.M. Fennimore, T.D. Yuzvinsky, W. Han, M.S. Fuhrer, J. Cumings, and A. Zettl, “Rotational actuators based on carbon nanotubes,” *Nature*, vol. 424, Jul. 2003, pp. 408-410.

CHAPTER 3

EXPERIMENTAL PROCEDURES

In this chapter, general experimental procedures are described. Further detailed information will be provided in each corresponding chapter.

3.1 Synthesis processes

The experimental set-ups used to synthesize carbon nanomaterials followed the CVD process. The deposition was carried on conducting materials such as carbon fiber papers and stainless steel plates, or on semiconducting materials such as silicon wafers. Catalyst nanoparticles were produced either by physical vapor deposition prior to synthesis process [1], or by thermal decomposition of catalyst precursors during synthesis [2]. Each procedure is described in detail in the corresponding chapters.

3.1.1 Catalyst preparation

The physical vapor deposition coatings of substrates was realized using magnetron sputtering at room temperature, at the pressure of 15 mTorr, with a argon flow of 15 sccm. For some experiments, a 30 nm-thick aluminum film was used as an under-

layer to effectively prevent the catalyst from aggregation [3]. The aluminum film was deposited using a radio frequency type magnetron at the power of 200 W. The metallic catalyst material was deposited by a direct current type magnetron at a power of 100 W. The thickness for the catalyst film was in the range of 0.5–10 nm monitored by a quartz crystal microbalance [4]. The deposition was realized in a custom made plasma enhanced CVD/sputtering hybrid system. The same system was used for PECVD experiments. The following subchapter describes the deposition system and outlines the PECVD procedures.

3.1.2 The growth based on plasma enhanced CVD system

The PECVD/sputtering hybrid system utilized for carbon nanomaterials synthesis is illustrated in Figure 3.1. The plasma discharge source, situated inside the deposition chamber, was operated in inductively coupled mode [5]. It consisted of a copper coil around the outside of one inch quartz tube coupled with the feed-gas entrance (A). The inductive coil was powered by a 13.56 MHz RF generator which could generate the maximum power of 300 W. The coil was connected to a matching network (B) to minimize the reflected power. A moving substrate holder allowed free positioning of substrates along the axis of the quartz tube. The substrates (up to 2 inch in diameter) were attached to a resistive heating element that could be moved at different distances from the plasma source by a vertical movement device (C). The growth temperature was calibrated and monitored by an implanted thermocouple [6]. The assembly acted like a remote

plasma reactor as there was no direct contact between the plasma and the substrate. The minimum substrate-to-plasma distance that could be achieved was 8 cm. Gases were fed directly into the plasma source and controlled by mass flow controllers (D).

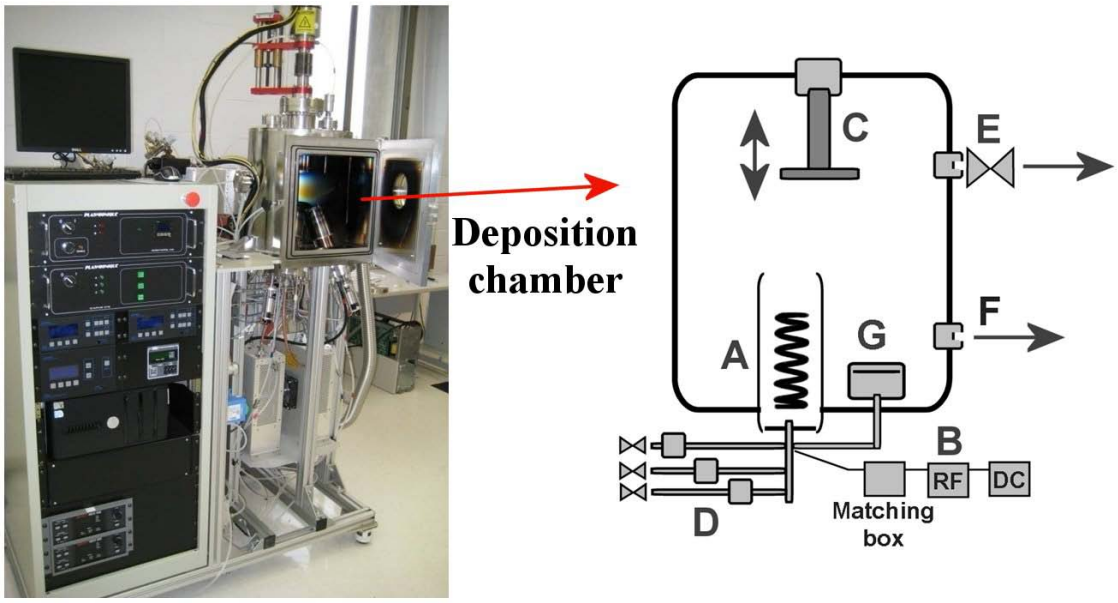

Figure 3.1 Image and schematic diagram of PECVD/sputtering hybrid deposition system.

The deposition pressure was obtained by a vacuum pump (E), measured with a vacuum transducer (F), and controlled by either an electronic or a manual valve. The system also comprised of an RF and two DC magnetron sputtering guns (G) for catalyst and/or under-layer material deposition.

The growth process consisted in several steps. First, the reactor was continuously flushed with argon during loading and unloading the samples. Before the growth process, the pressure was decreased to 10^{-5} Torr to remove the undesired species from the deposition chamber. After this procedure, the pressure was increased to the required

growth value and the substrate stage was heated up. When the desired temperature was reached, additional 10 minutes were allowed for temperature equilibration. The nanomaterials growth started with the admission of the precursor gas mixture in the deposition chamber. After 5 minutes the plasma was ignited. Last, the reactor was allowed to cool down under vacuum and an inert atmosphere before exposure to air.

3.1.3 The growth based on spray pyrolysis CVD system

The spray pyrolysis CVD system consisted in an electronically controlled furnace with 300 mm effective heating length, a quartz reactor tube (i.d. 25.4 mm), and a spraying setup, respectively (Figure 3.2a). The spraying device consisted in a micro nozzle (i.d. 0.29 mm) connected with the carrier gas tube (i.d. 4.2 mm) and situated in front of a sealed inner tube (i.d. 1.5 mm) that carried the active solution. The device was capable of spraying liquids injected at low flow rates. The pressure formed inside the carrier gas tube pulverized the solution, through the nozzle, inside the deposition chamber, up to the substrate surface situated in the middle of the quartz tube (Figure 3.2b). The schematic diagram of spray pyrolysis deposition system is presented in Figure 3.2c. Before starting the growth, the reactor was flushed with argon. Then, the temperature was increased to the desired value. Once the desired temperature was reached, the growth process was initiated. The active solution, composed of ferrocene ($Fe(C_5H_5)_2$) dissolved in carbonaceous liquids, was injected into the spraying device [7]. Ferrocene was used to produce metallic iron particles and to act as catalyst, while the

carbonaceous liquid provided the carbon feedstock. In the spraying process, argon was used as the carrier gas. A carrier gas flow rate of 175 sccm was sufficient to continuously spray the solution into the quartz reactor. After the growth, the reactor was allowed to cool down under argon flow before exposure to air.

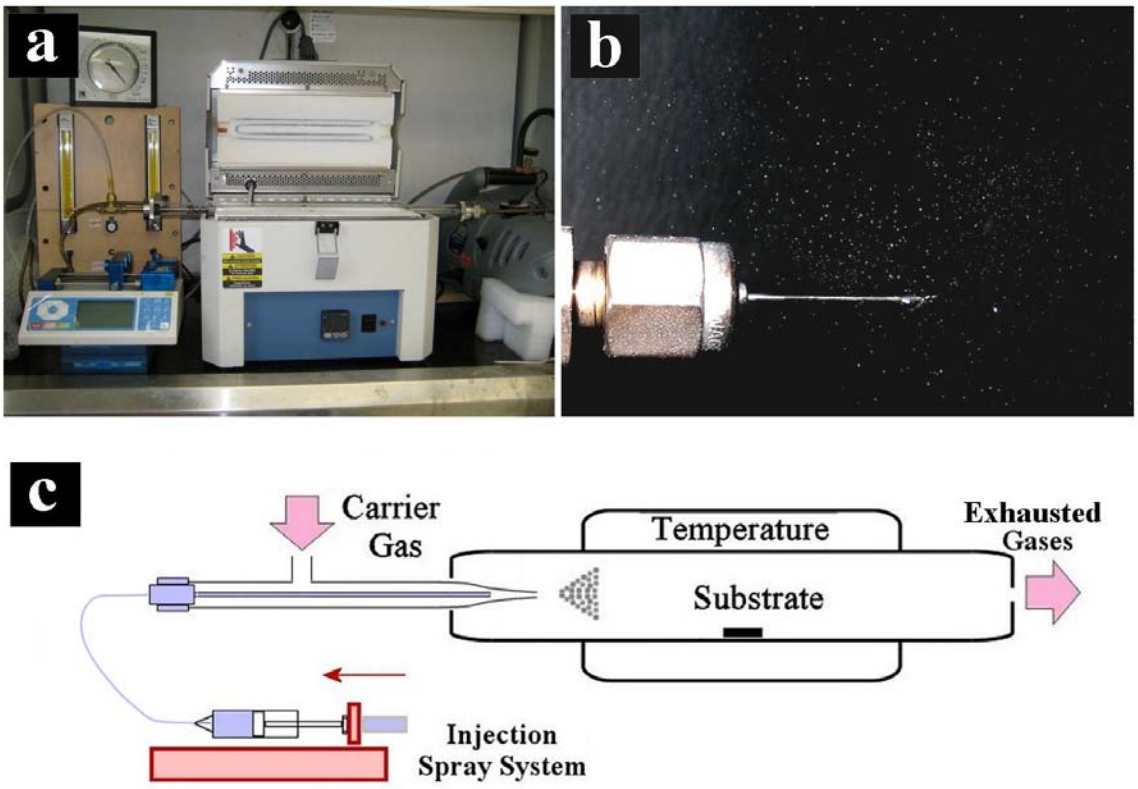

Figure 3.2 Image of spray pyrolysis deposition system (a), view of the pulverized droplets (b), and schematic diagram of deposition system (c).

3.2 Microstructure characterization

The synthesized carbon based nanomaterials were characterized using different techniques including electron microscopy, electron spectroscopy, and Raman spectroscopy. The surface topography of the materials was investigated using scanning electron microscopy (SEM - Hitachi S-4800). Details of the material structure were examined by transmission electron microscopy (TEM - Philips CM-10). The atomic percentage ratio of nitrogen and carbon for the obtained nitrogen doped nanostructures was determined by X-ray photoelectron spectroscopy (XPS - Kratos AXIS Ultra, Al Kα). The quality, crystalline perfection, and vibrational properties of the material were studied using Raman spectroscopy (Horiba Jobin Yvon - LabRAM HR800).

3.3 Property evaluation

3.3.1 Evaluation techniques

The *I–V* characteristics of bulk carbon nanomaterials were measured following the two-points probe model [8]. The measurement system contained a DC power supply (Agilent E3644A) and a digital multimeter (Agilent 34410A). The field emission properties of carbon nanomaterials were investigated using a planar diode configuration [9]. The measurement system contained a high voltage DC power supply (Polaron 3kV) and a digital multimeter (Agilent 34410A).

3.3.2 Microprobes sensing elements fabrication

The electrical resistance of bulk carbon nanomaterials, such as ohmic *I-V* characteristics, was measured following a two-points probe model. The measurements were conducted in the same oven used for the CVD process, at temperatures between 35 ^{o}C and 125 ^{o}C, monitored by a K type thermocouple. In order to achieve thermal equilibrium, the temperature of the system was kept for 10 minutes after the target temperature had been reached. Mechanical pressure was used to make the contacts between the carbon nanotube powder and the conducting terminals. The microprobes were obtained by inserting the carbon nanotube powder into a polytetrafluoroethylene (Teflon) enclosure and confining the powder under a pressure of 60 kPa using a mechanical press (Figure 3.3).

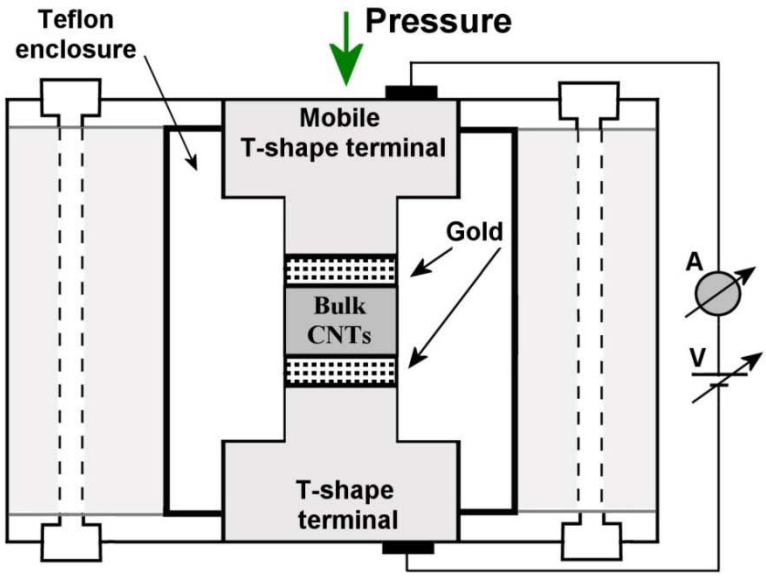

Figure 3.3 Schematic diagram of the two-points microprobe fabrication.

"T" shape gold plated aluminum conductors were used. The conductors confined the powder, made a good mechanical contact, and acted as microprobes terminals. Following a similar procedure, the change of electrical resistance with pressure was measured. The measurements were done at room temperature for the pressure interval of 40-139 kPa.

3.3.2 Field emission measurements

The emission characteristics of the CNT arrays were investigated in vacuum at a base pressure of 10^{-6} Torr. The measurements were carried out using a planar diode configuration (Figure 3.4).

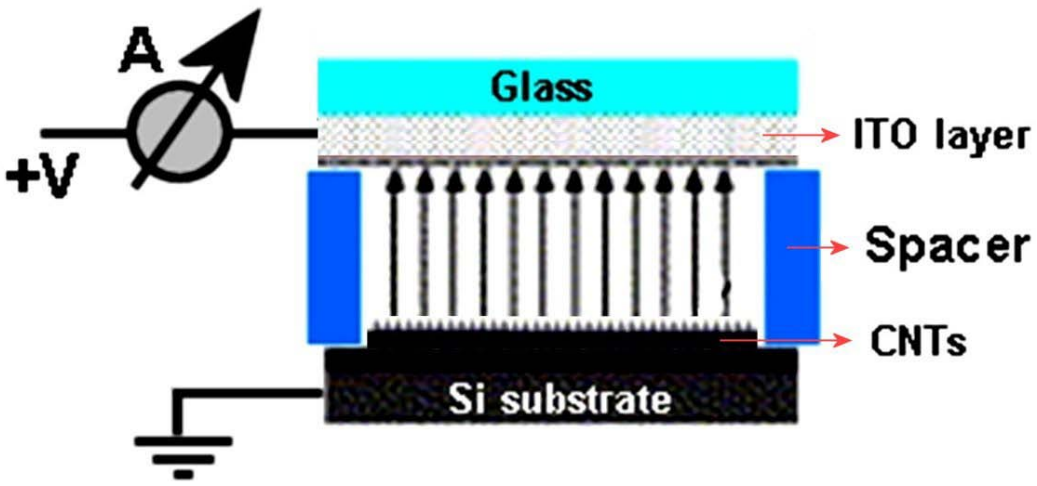

Figure 3.4 Schematic diagram of the planar diode configuration.

In a typical experiment, the active area of electrodes was around 35 mm^2 and an anode-to-sample spacing 200 μm. A glass plate, covered by indium-tin-oxide (ITO) thin film using magnetron sputtering, acted as anode to collect the emitted electrons.

3.4 References

[1] S. Hofmann, B. Kleinsorge, C. Ducati, A.C. Ferrari, and J. Robertson, "Low-temperature plasma enhanced chemical vapour deposition of carbon nanotubes," *Diamond and Related Materials*, vol. 13, Apr. , pp. 1171-1176.

[2] R.A. Afre, T. Soga, T. Jimbo, M. Kumar, Y. Ando, M. Sharon, P.R. Somani, and M. Umeno, "Carbon nanotubes by spray pyrolysis of turpentine oil at different temperatures and their studies," *Microporous and Mesoporous Materials*, vol. 96, Nov. 2006, pp. 184-190.

[3] H. Su, K. Shin, K. Leou, and C. Tsai, "On the roles of multilayered metal catalysts in the synthesis of high-quality single-walled carbon nanotubes," *Emerging Technologies - Nanoelectronics, 2006 IEEE Conference on*, 2006, pp. 108-112.

[4] S. Pisana, M. Cantoro, A. Parvez, S. Hofmann, A. Ferrari, and J. Robertson, "The role of precursor gases on the surface restructuring of catalyst films during carbon nanotube growth," *Physica E: Low-dimensional Systems and Nanostructures*, vol. 37, Mar. 2007, pp. 1-5.

[5] Y. Li, D. Mann, M. Rolandi, W. Kim, A. Ural, S. Hung, A. Javey, J. Cao, D. Wang, E. Yenilmez, Q. Wang, J.F. Gibbons, Y. Nishi, and H. Dai, "Preferential Growth of Semiconducting Single-Walled Carbon Nanotubes by a Plasma Enhanced CVD Method," *Nano Letters*, vol. 4, Feb. 2004, pp. 317-321.

[6] E.J. Bae, Y. Min, D. Kang, J. Ko, and W. Park, "Low-Temperature Growth of Single-Walled Carbon Nanotubes by Plasma Enhanced Chemical Vapor Deposition," *Chemistry of Materials*, vol. 17, Oct. 2005, pp. 5141-5145.

[7] M.S. Mohlala, X. Liu, J.M. Robinson, and N.J. Coville, "Organometallic Precursors

for Use as Catalysts in Carbon Nanotube Synthesis," *Organometallics*, vol. 24, Feb. 2005, pp. 972-976.

[8] G. Rimbu, C. Jackson, and K. Scott, "Platinum / carbon / polyaniline based nanocomposites as catalysts for fuel cell technology," *Journal of Optoelectronics and Advanced Materials*, vol. 8, 2006, pp. 611-616.

[9] K. Yeong and J. Thong, "The effects of adsorbates on the field emission properties of multiwall carbon nanotubes," *Vacuum Electronics, 2003 4th IEEE International Conference on*, 2003, pp. 126-127.

CHAPTER 4

SPRAY PYROLYSIS CHEMICAL VAPOR DEPOSITION METHOD FOR THE CARBON NANOTUBE GROWTH: PARAMETRIC STUDIES

4.1 Abstract

Spray pyrolysis chemical vapor deposition (CVD) in the absence of hydrogen at low carrier gas flow rates has been used for the growth of carbon nanotubes. A parametric study of the carbon nanotube growth has been conducted by optimizing various parameters such as temperature, precursor flow rate, precursor volume, and catalyst concentration. Experimental observations and characterizations reveal that the growth rate, size and quality of the carbon nanotubes are significantly dependent on the reaction parameters. Scanning electron microscopy, transmission electron microscopy, and Raman spectroscopy techniques were employed to characterize the morphology, structure and crystallinity of the carbon nanotubes. The synthesis process can be applied to both semiconducting silicon wafer and conducting substrates such as carbon microfibers and stainless steel plates. This approach promises great potential in building various nanodevices with different electron conducting requirements. In addition, the absence of hydrogen and the relatively low synthesis temperature (typically 750 ^{o}C) qualify the spray pyrolysis CVD method as a safe and easy way to scale up the CNT growth, which is applicable in industrial production.

4.2 Introduction

Carbon nanotubes (CNTs) have been extensively studied due to their outstanding electrical, mechanical and optical properties [1-4] which has led to numerous applications of carbon nanotubes as device components, such as sensors [5-6], fuel cells [7-10], field emission devices [11], transistors, and logic circuits [12-14]. Up to now, different techniques including arc discharge, laser ablation and chemical vapor deposition (CVD) have been employed for the CNT growth [15-19]. CVD methods are particularly attractive due to the large area deposition capability, aligned CNT growth, and low costs [20–22]. Among various CVD techniques, spray pyrolysis CVD reveals promising results in CNT synthesis. It provides a controlled way of spraying complex carbonaceous liquids mixed with catalyst containing molecules (metallocene powders) directly into the deposition chamber [23] and ensures semi-continuous growth of CNTs, which gives the possibility to scale up the method for production of CNTs at commercially viable prices. Up to date, high carrier gas flow rates (more than 8000 sccm) have been used in spray pyrolysis experiments and it is still a challenge to obtain catalyst free CNTs with uniform diameters [24, 25]. When low carrier gas flow rates were used, the reactant solution could not be sprayed and fully evaporated, leaving behind metallocene residues [26]. To achieve controlled growth of high quality CNTs with uniform size and high yield, a parametric study on the CNT growth in a spray pyrolysis process is necessary. In addition, controlled growth of CNTs on suitable substrates is one of the key impediments in building various nanodevices. Besides CNT growth on conventional silicon substrates, direct growth of CNTs on conducting substrates has been exploited to improve properties

of electrode materials. This approach has provided *in situ* electrical end-connection for the individual CNTs and, consequently, promises potential applications in fuel-cells, lithium-ion batteries, supercapacitors, sensors, and field emission devices [27]. However, the CNT synthesis on metallic substrates is difficult to achieve mainly due to the degradation of catalytic nanoparticles under the reactive CNT growth conditions, i.e. the hydrogen environment at elevated temperatures. Previously investigated procedures to synthesize CNTs on stainless steel (SS) require intermediated steps associated with substrate preparation prior to CNT growth [28-30].

In this work, vertically aligned MWCNTs have been achieved on semiconducting Si, conducting carbon microfiber, and stainless steel substrates using a modified spray pyrolysis CVD method without hydrogen addition. Low flow rates of argon carrier gas (175 sccm) were used for micro spraying mixtures of ferrocene in xylene at different concentrations, over substrates situated at growing temperature. Parametric studies on the CNT growth indicated that the nanotube growth was significantly affected by the involved factors such as temperature, precursor flow rate, precursor volume, and concentration of catalyst in carbonaceous precursors. The method offers several significant advantages, i.e. controlling carrier gas flows without affecting the spraying process, the possibility to use complex mixtures of volatile precursors, the absence of complex substrate preparation, and the setup simplicity. Morphology, structure and crystallinity of nanotubes were investigated using scanning electron microscopy (SEM), transmission electron microscopy (TEM) and Raman techniques. The absence of H_2 as a carrier gas and a relatively low synthesis temperature qualify the spray pyrolysis CVD method as a safe and easy way to scale up route for industrial production.

4.3 Experimental

The experimental setup was composed of an electronically controlled furnace with 300 mm effective heating length, a quartz reactor tube (i.d. 25.4 mm), and a spraying setup, respectively. The device developed for spraying liquids injected at low flow rates consisted of a carrier gas tube (i.d. 4.2 mm) which ended with a spraying nozzle (i.d. 0.5 mm) and a sealed inner tube (i.d. 1.5 mm) that carried the active solution. The pressure formed inside the carrier gas tube pulverized the solution evenly at low flow rates, through the nozzle, inside the deposition chamber, up to the substrate surface situated in the middle of the quartz tube. The deposition system and the injection device are presented in Figure 4.1.

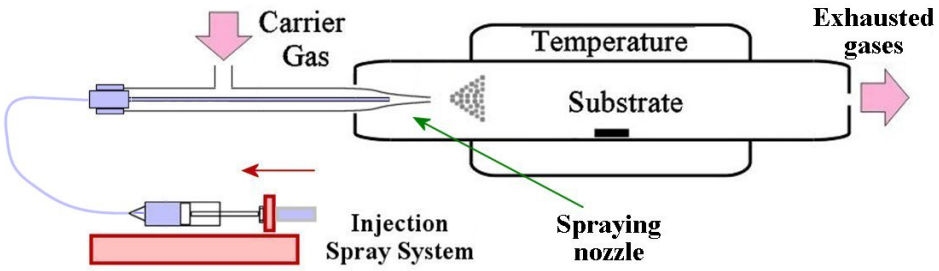

Figure 4.1 Schematic diagram of spray pyrolysis CVD system.

In this parametric study, oriented n-type Si (100) silicon wafers were used as a substrate, without removing the native oxide layer. An aluminum (Al) under-layer, with the thickness of 30 nm, was magnetron sputtered on the Si substrate to effectively prevent the catalyst particles from aggregation. Effects of growth conditions have been systematically examined by changing one of the following parameters while keeping the others fixed. The investigated parameters were as follows: the growth temperature,

precursor flow rate, concentration of ferrocene in xylene, and volume of active solution injected. In the spraying process, argon was used as carrier gas at a flow rate of 175 sccm. After the growth, the reactor was allowed to cool down under argon flow before exposure to air. The same procedure has been used for CNT deposition on conducting substrates. Samples were characterized by scanning electron microscopy (SEM - Hitachi S-4800), Raman spectroscopy (Renishaw Raman spectrometer with laser excitation of 785 nm), and transmission electron microscopy (Philips CM-10). The TEM samples were prepared by sonicating a small amount of as-grown nanotubes in ethanol for 10 min and drying few drops of suspension on a Cu micro-grid.

4.4 Results and discussion

In order to optimize the growth process on Si wafers and conducting substrates, a parametric study was carried out involving perturbation of substrate temperature, precursor flow rate, concentration of catalyst in carbon precursor, and injected volume, while keeping other parameters fixed as described in the experimental part.

4.4.1 Effect of temperature

CNTs were grown at deposition temperatures in the range of 600-900 °C. All other parameters were kept constant: volume of injected solution at 3 ml, flow rate of

carrier argon at 175 sccm, ferrocene/xylene concentration at 1%, and precursor flow rate at 0.75 ml/min. Figure 4.2 shows SEM images of the products obtained at these temperatures. The CNTs could not be produced at 600 °C and only catalyst particles were found on the substrate (Figure 4.2a). This suggests that there was insufficient hydrocarbon decomposition below 600 °C and the catalyst particle activity was very low, hindering the CNT formation [31]. SEM image of the sample done at 900°C revealed a substrate covered by amorphous carbon (Figure 4.2b), indicating that the iron particles lost their catalytic activity at high temperature. On the other hand, vertically aligned CNT arrays were obtained for all experiments done between these temperatures. The average tube length was 12 μm for 700 °C, increased to 51 μm for 750 °C, and presented a maximum of 63 μm for 800 °C (Figure 4.2c). The average diameter of CNTs (Figure 4.2d) presented a maximum of 54 nm for tubes synthesized at 700 °C (Figure 4.2f) and sharply decreased to 28 nm for tubes grown at 750 °C down to 19 nm for the ones grown at 800 °C (Figure 4.2g). At 800 °C, the CNTs were disordered, non-uniform in size, and the diameter distribution was wider due to the agglomeration of the catalyst particles. The Raman spectra for the nanotubes synthesized at 750 °C and 800 °C confirm the degree of crystallinity of the products. The intensity of the D-peak relative to G-peak (I_D/I_G=0.68, Figure 4.2e curve (1)) indicates a higher structural order of tubes synthesized at 750 °C.

In comparison, the tubes grown at 800 °C had a weaker peak around 1580 cm^{-1} (I_D/I_G=0.93, Figure 4.2e curve (2)) which is a signature of defects contained in graphene walls and a low degree of crystallinity [32].

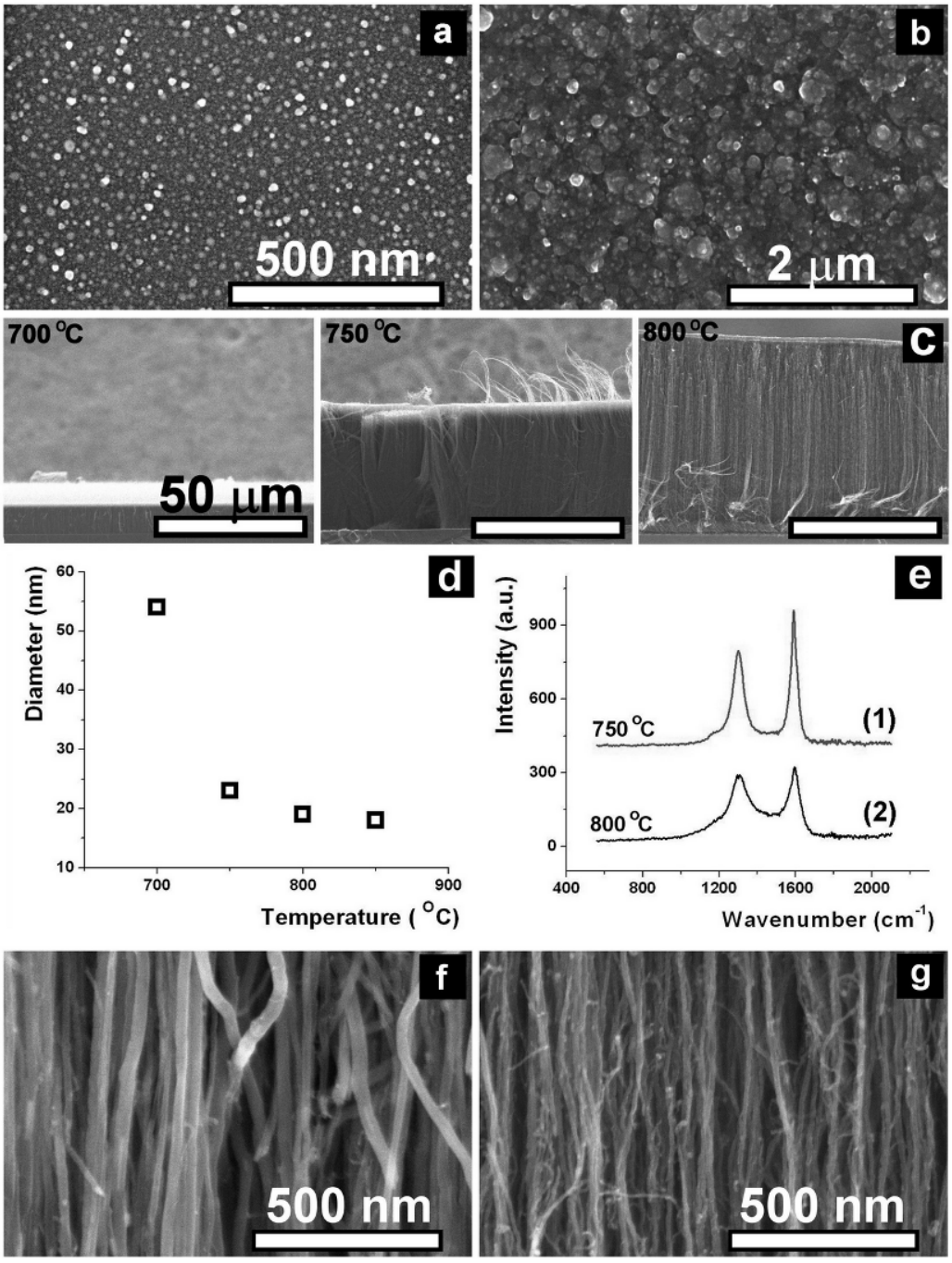

Figure 4.2 SEM images of the products obtained at 600 °C (a); 900 °C (b); SEM images of cross-sectional view of the VA-CNT arrays obtained at 700 °C, 750 °C, and 800 °C (c); Diagrammatic relationship between the average CNT diameter and growth temperature (d); Raman spectra of the nanotubes synthesized at 750 °C and 800 °C (e); SEM image of CNTs with 54 nm average diameter obtained at 700 °C (f); SEM image of CNTs with 19 nm average diameter obtained at 800 °C (g).

These results punctuate the temperature influence on the structure of the CNTs. At temperatures lower than 700 °C, the tube growth is inhibited by the low concentration of carbon atoms. Increase of the temperature promotes the decomposition of carbonaceous liquid and CNTs are formed in a process of dissolving, diffusing, and precipitating the carbon atoms through the catalyst iron particles. The dissolving and diffusion rates increase with temperature and consequently the CNT yield becomes larger. At 900 °C and above, the carbon concentration is too high and the dissolving rate becomes higher than diffusing and precipitating rates. The catalyst particles lose their catalytic activity and the carbon atoms accumulate on the particle surface as amorphous carbon which terminates the CNT growth.

This part of the study demonstrates that vertically aligned MWCNTs can be synthesized at temperatures in the range of 700 °C - 800 °C. While a maximum tube length was obtained at 800 °C, the temperature of 750 °C was the optimum one to grow quality and well-aligned CNT arrays and was considered for the following experiments.

4.4.2 Effect of precursor flow rate

The effect of precursor flow rate on the CNT growth was examined in the range of 0.05-1.0 ml/min while keeping other parameters constant. The volume of solution injected was 3 ml, the carrier argon flow rate was 175 sccm, the temperature was 750 °C, and the ferrocene/xylene concentration was 1%. The SEM images show that vertically aligned CNT arrays were obtained for all experiments (Figure 4.3a).

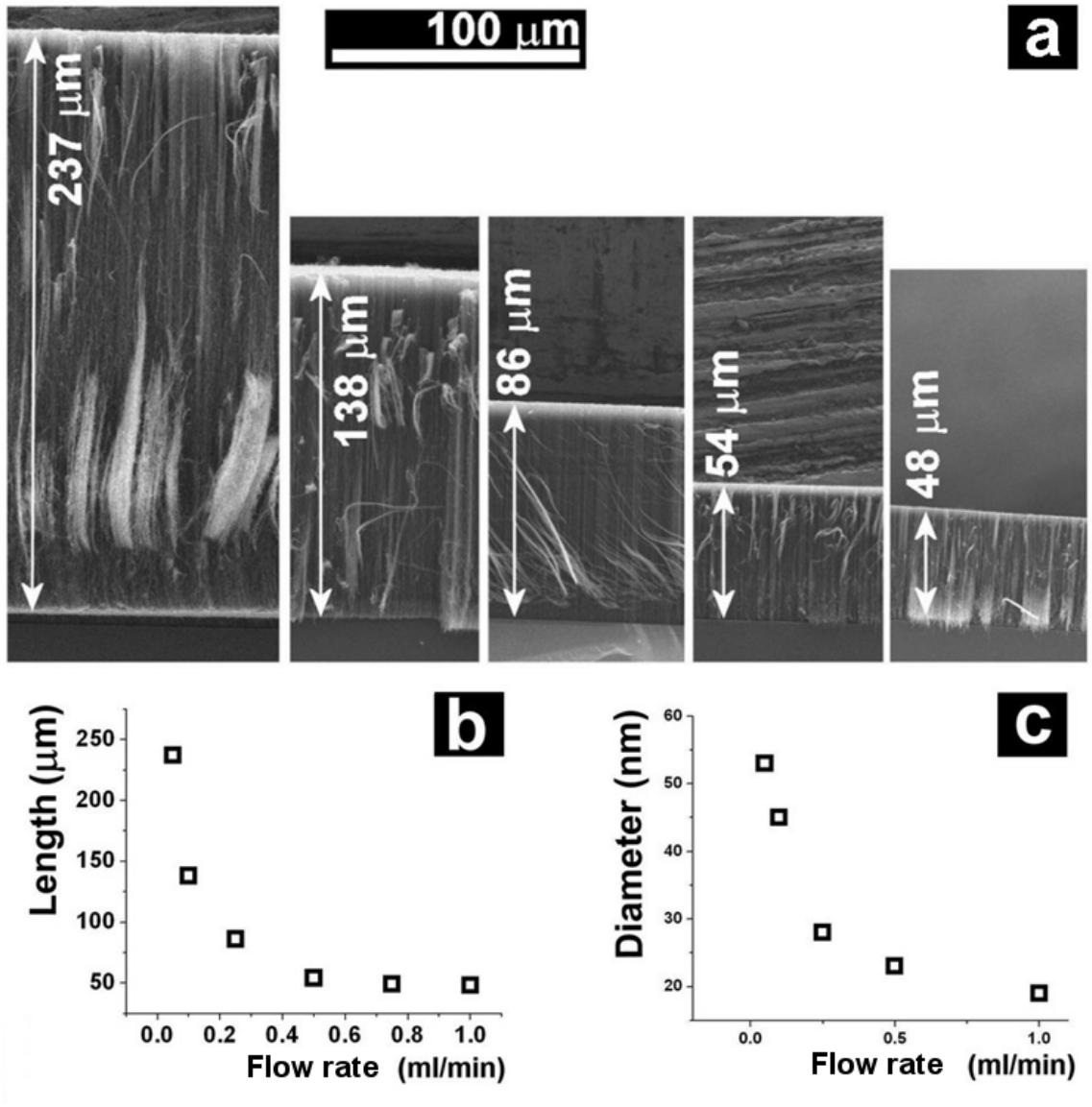

Figure 4.3 SEM image of cross-sectional view of VA-CNT arrays obtained at 0.05, 0.1, 0.25, 0.5, and 1.0 ml/min - scale 100 μm (a); average nanotube length function of precursor flow rate (b); average nanotube diameter function of flow rate (c).

By increasing the precursor flow rate, the tubes became shorter. The average tube length presented a maximum of 237 μm for experiments performed at 0.05 ml/min and decreased to 48 μm for experiments done at flow rate of 1 ml/min (Figure 4.3b). A higher

precursor flow rate shortened the reaction time of the carbonaceous species with the catalyst particles and moderated the catalyst activity. This effect was also reflected on the change of CNT diameters. At low flow rates, the collisions of the active catalyst nanoparticles were promoted and the iron particles coalesced and formed CNTs with thicker diameters. This effect was weakened for a high precursor flow rate. The average tube diameter was 52 nm for experiments done at the flow rate of 0.05 ml/min and decreased to 18 nm for experiments done at that of 1 ml/min (Figure 4.3c). By increasing the flow rate, the length and the average diameter of the CNTs decreased. These are in agreement with previously reported results [33] and indicate that the precursor flow rate has a direct influence over the average length and diameter of CNTs. For the following experiments, the precursor flow rate of 0.1 ml/min was preferred by taking in consideration the length and diameter of obtained CNTs and the easiness to control the precursor flow rate.

4.4.3 Effect of catalyst concentration

Ferrocene in xylene concentrations in the range of 0.1% and 5% were used to study the influence of the catalyst concentration on the CNT growth. All other parameters were kept constant: volume of solution injected at 3 ml, carrier argon flow rate at 175 sccm, temperature at 750 °C, and the precursor flow rate at 0.1 ml/min. From the SEM images, it can be seen that vertically aligned CNTs arrays were obtained for all experiments (Figure 4.4a).

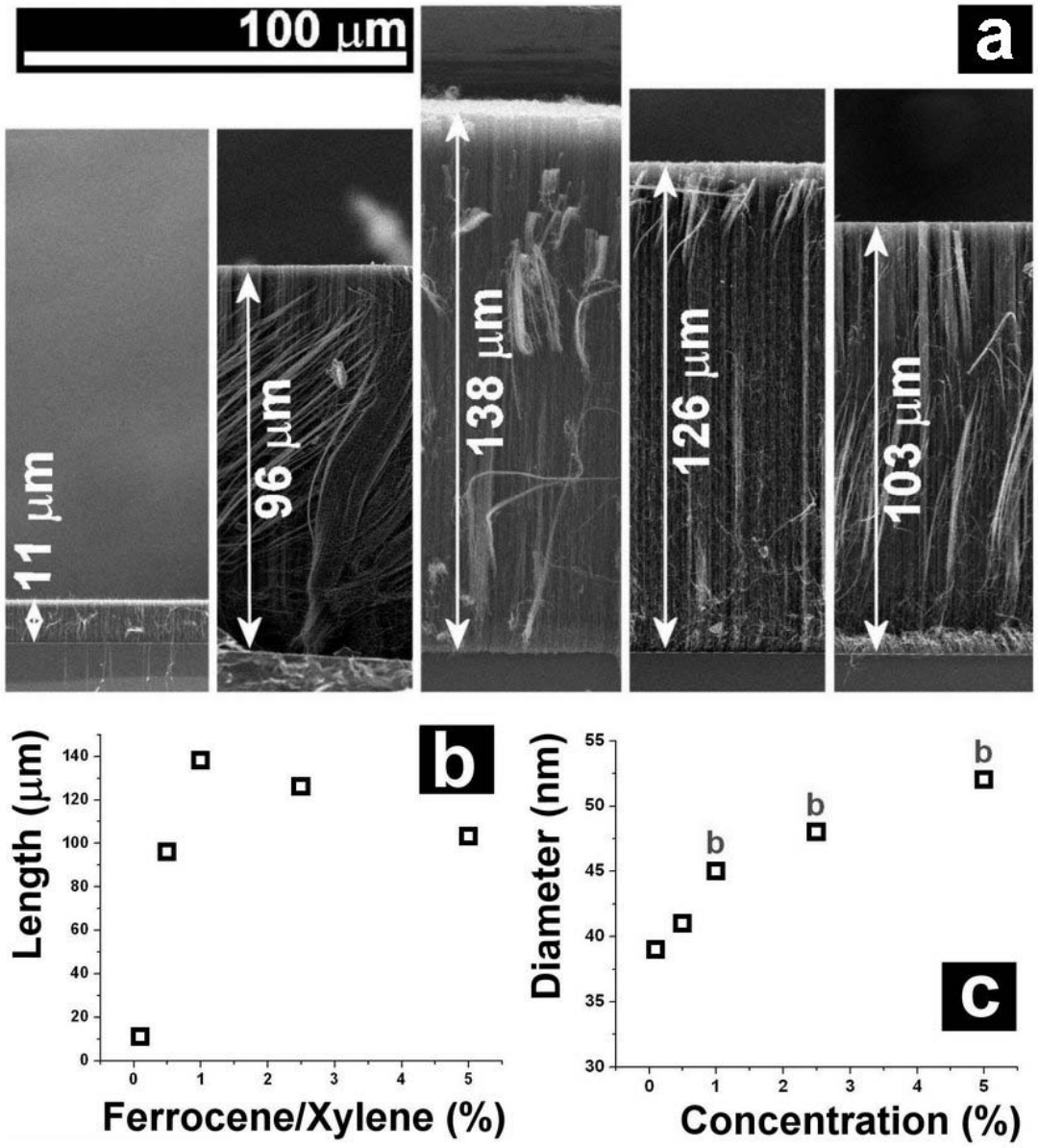

Figure 4.4 SEM images of cross-sectional view of VA-CNT arrays obtained using 0.1% ferrocene in xylene, 0.5%, 1%, 2.5%, and 5% (a); diagrammatic relationship between the average nanotube length and ferrocene concentration (b); diagrammatic relationship between the average nanotube diameter and ferrocene in xylene concentration, and the occurrence of bimodal diameter distribution (c).

The average tube length for experiments performed at 0.1% ferrocene in xylene was 11 μm. By increasing the Fe catalyst concentration, the average tube length increased to a maximum of 138 μm for experiments performed at 1% ferrocene in xylene. A future increase of ferrocene concentration decreased the average tube length to 103 μm for experiments done at 5% ferrocene in xylene. These results suggest that an optimum density of iron catalyst nanoparticles and carbon clusters for the nanotube nucleation and growth are obtained when spraying solution with the concentration of 1% ferrocene in xylene (Figure 4.4b). In the growth process, some of the sprayed catalyst particles could not reach the substrate and were deposited on the external walls of the formed tubes. Nucleation sites for smaller diameter CNTs are generated and reflected in a bimodal diameter distribution of the samples [34]. The bimodal diameter distribution was observed for all samples synthesized using ferrocene concentrations above 1%. At lower ferrocene concentrations, the bimodal diameter distribution disappeared (Figure 4.4c).

SEM and TEM micrographs in figure 4.5 show differences in structure between nanotubes synthesized at 5 % and 0.5 % ferrocene in xylene concentrations. For high concentrations, the CNTs are non-uniform in size and the diameter distribution is wider. Besides large nanotubes with the average diameter of 58 nm, the presence of thin nanotubes with the average outer diameter of approximately 24 nm indicates the bimodal diameter distribution of the products (Figure 4.5a-b). The larger diameter tubes are spatially aligned while the smaller diameter tubes are entangled. At low ferrocene in xylene concentrations, the CNTs are uniform, with an average diameter of 42 nm diameters, and the bimodal diameter distribution is absent (Figure 4.5c-d).

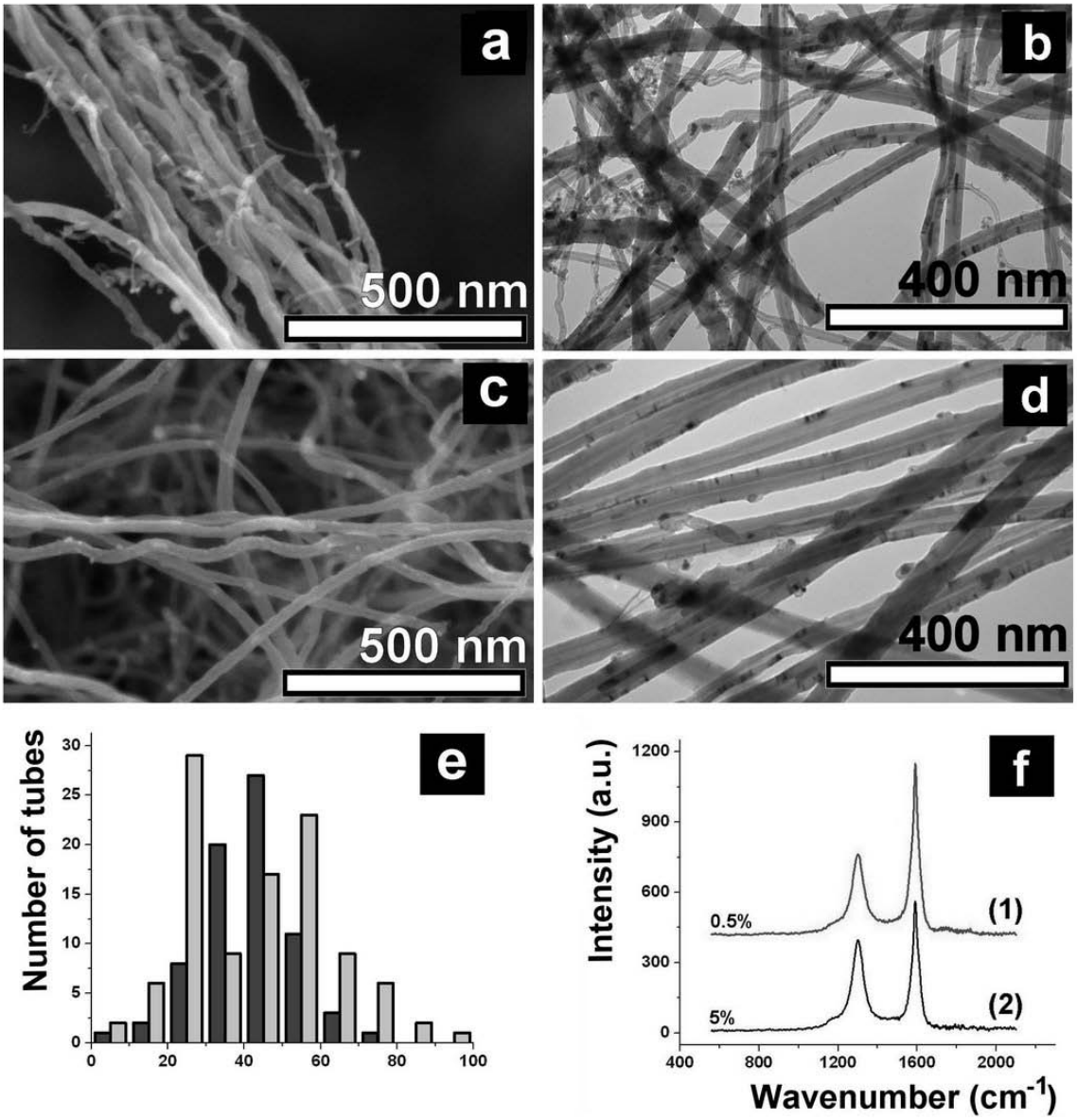

Figure 4.5 SEM image for nanotubes synthesized at 5 % ferrocene in xylene concentration (a); TEM image for nanotubes synthesized at 5 % ferrocene in xylene concentration (b); SEM image for nanotubes synthesized at 0.5 % ferrocene in xylene concentration (c); TEM image for nanotubes synthesized at 0.5 % ferrocene in xylene concentration (d); diameter distribution of nanotubes obtained at 0.5 % and 5 % ferrocene in xylene concentrations (e); Raman spectra of nanotubes synthesized at 0.5 % and 5 % ferrocene in xylene concentrations (f).

The diameter distribution diagram (Figure 4.5e) indicates a slight increase of tube diameter and confirms the occurrence of bimodal diameter distribution at high ferrocene concentrations. The Raman spectra for the nanotubes synthesized at 5 % and 0.5 % concentrations support the TEM observations. The intensity of the D band relative to G band is slightly lower for the nanotubes synthesized at the 0.5 % ferrocene in xylene concentration (I_D/I_G=0.49, Figure 4.5f curve (1)) in comparison with the nanotubes synthesized at the 5 % ferrocene in xylene (I_D/I_G=0.67, Figure 4.5f curve (2)) and indicates that the tubes obtained at lower catalyst concentrations present fewer defects and have a higher degree of crystallinity.

4.4.4 Effect of injected volume

In previous studies, the influence of several reaction parameters on the CNT length was examined by injecting a constant volume of 3 ml solution for all experiments. By changing the volume of the injected precursor, using an active solution of 1% concentration, and keeping the other parameters constant as described in the previous experiment, a direct correlation between nanotube length and the injected volume was observed. The nanotube length could be controlled at a range of about three orders of magnitude. The length increases from 1.7 μm, when only 0.3ml carbon source was injected (Figure 4.6a), to 1.5 mm when precursor of 30ml was injected (Figure 4.6b). The variation of the injected volume related to the reaction time indicates almost constant growth rates during the reaction (Figure 4.6c). The SEM image of the nanotube array root

shows that the catalyst remains on the substrate during the growth process (Figure 4.6d). These observations are consistent with all experiments and indicate that the tubes grow upwards following a base growth mechanism.

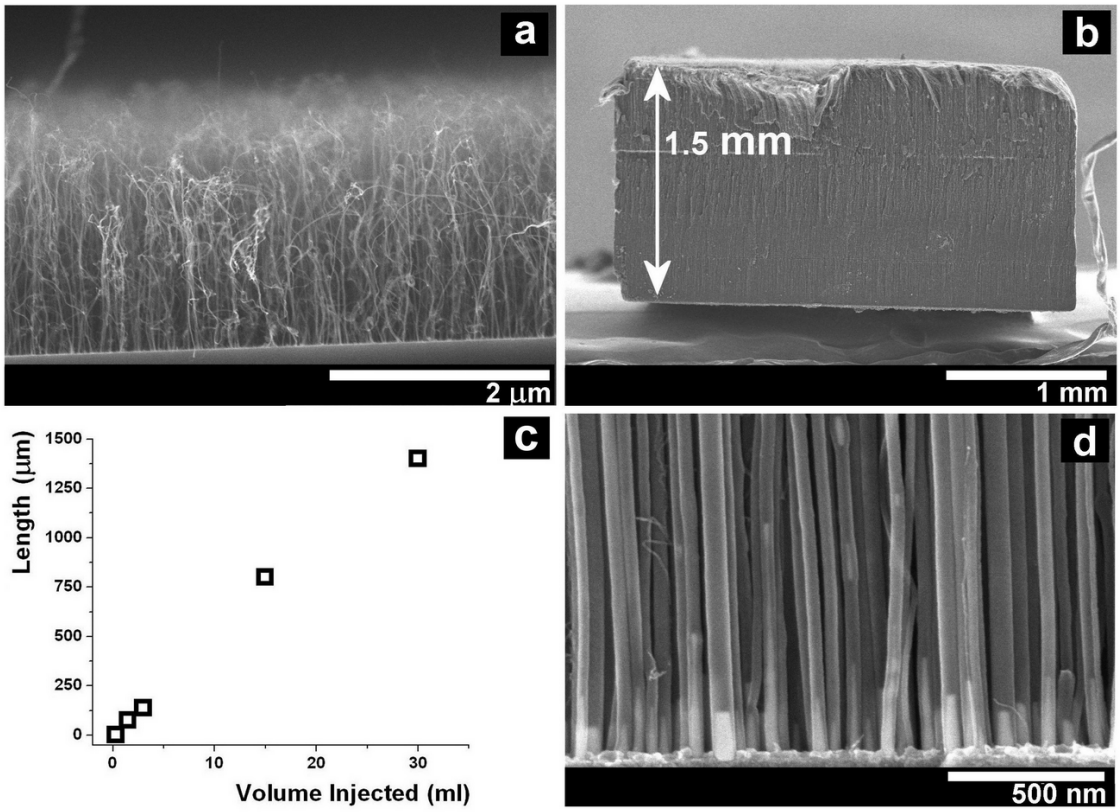

Figure 4.6 SEM image of the nanotubes synthesized using 0.3 ml active solution (a); 30 ml active solution (b); diagrammatic relationship between the average nanotube length and volume of the injected solution (c); SEM image of the nanotube roots (d).

4.4.5 Effect of substrate

The substrate preparation and growth procedure previously described were applied to conducting substrates, such as carbon paper (CP) and stainless steel 304 (SS).

Aluminum was sputtered on CP substrates as previously described. A sheet of SS (Brown Metals Comp.) was cut in 1cm x 1cm pieces and used as a substrate without additional treatment. The optimized growth conditions used for growing nanotubes on conducting substrates were: ferrocene in xylene concentration of 1%, carrier argon flow rate of 175 sccm, temperature of 750 °C, and precursor flow rate of 0.1 ml/min. Figure 7 presents SEM images and Raman spectra of the CNTs synthesized by injecting 3 ml volume of solution. A low magnification image of CNTs grown on CP reveals that the substrate was a totally covered with densely aligned tubes with 80-85 μm in length (Figure 4.7a) and 5 to 48 nm in diameter (Figure 4.7b), growing along the length of substrate fibres. CNT layer obtained on SS substrate presented dense CNT bundles with the size ranging from one to tens of micrometers (Figure 4.7c). The nanotubes were vertically aligned, had lengths up to 30-40 μm, a narrow diameter distribution, and an average diameter of 43 nm (Figure 4.7d). Besides the average length, there were no major differences between the obtained products related to TEM images and Raman spectra. The TEM image of the tubes on SS reveals minor structural defects (Figure 4.7e) similar to the tubes grown on CP (not shown). This can be assigned to the deficiency of sprayed catalyst to coalesce in uniform particles due to the substrate roughness in comparison with the growth on the Si substrate. The fact that the tubes present more defects is confirmed by Raman investigation which reveals a higher intensity of the D band relative to G band for the tubes grown both on the CP substrate (I_D/I_G=1.28, Figure 4.7f curve (1)) and SS substrate (I_D/I_G=1.47, Figure 4.7f curve (2)).

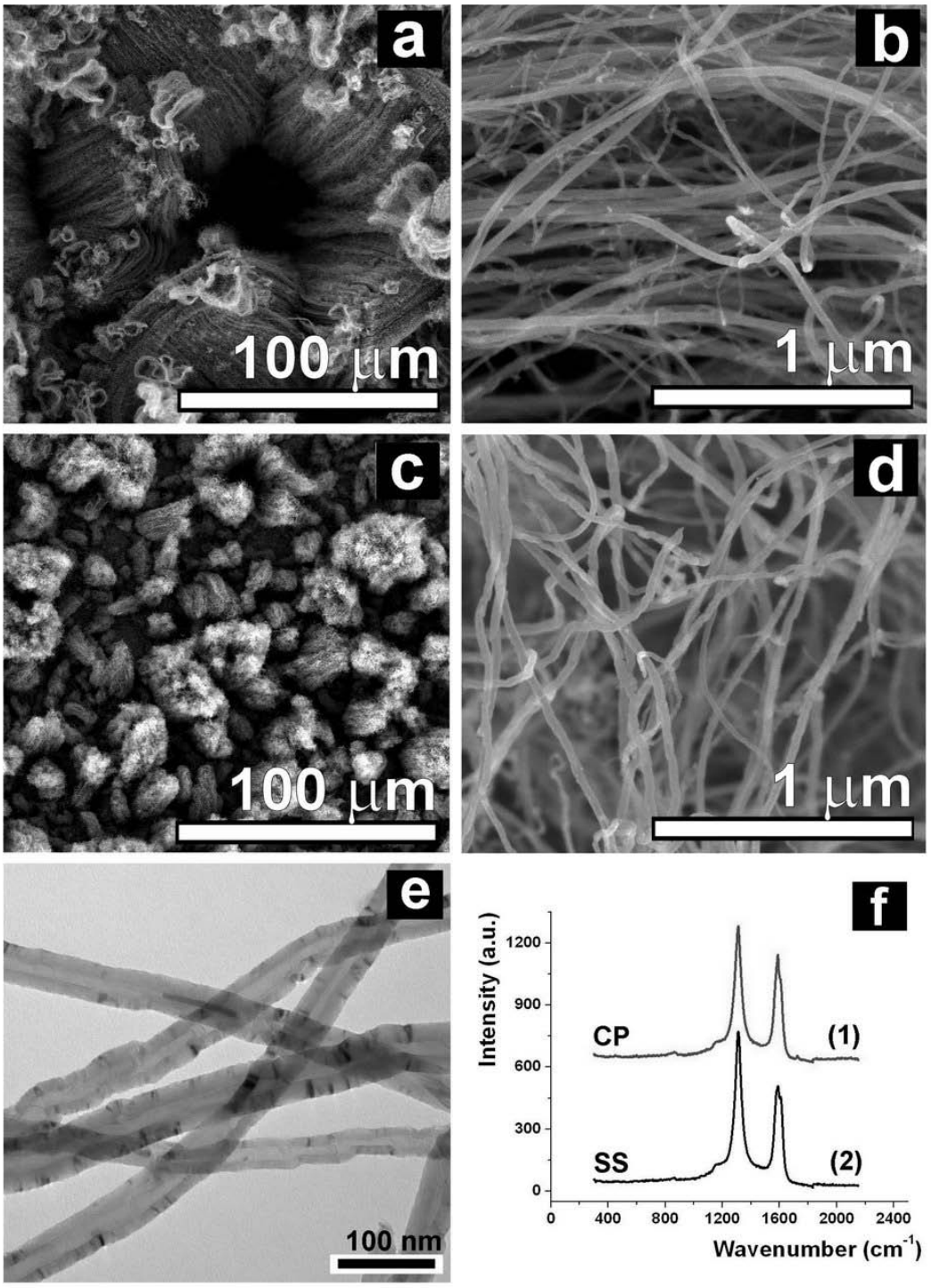

Figure 4.7 SEM image of CNTs grown on CP (a, b); SEM image of CNTs grown on SS (c, d); TEM image of CNTs grown on SS (e); Raman spectra of nanotubes synthesized on CP and SS (f).

Previously investigated procedures in terms of synthesizing CNTs on SS conducting substrates have required substrate treatment prior to CNT growth. Typical SS treatment includes acid etching, plasma etching, or treatment in hydrogen atmosphere [28-30]. The spray pyrolysis method reported here does not require additional pre-treatment for SS and provides a high CNT yield considering the volume of carbon source used. The catalyst preparation is also bypassed because the catalyst is directly and continuously sprayed over the substrate along with the carbon source. These observations indicate that both CP and SS are efficient conducting substrates for the CNT growth by using spray pyrolysis CVD method.

4.5 Conclusions

A modified spray pyrolysis chemical vapor deposition has been built in this study. CNTs have been synthesised by the modified spray pyrolysis chemical vapor deposition without hydrogen addition at a low flow rate of carrier gas (175 sccm of argon). The effects of temperature, precursor flow rate, precursor volume, and catalyst/carbon source concentration, have been systematically investigated for optimizing the nanotube growth. The average length and diameter of the carbon nanotubes decreased with temperature and precursor flow rate indicating the possibility of the nanotube growth with controlled structure. The perturbation of catalyst concentration could bring the growth of nanotubes with bimodal diameter distribution and minor effect on tube diameter variation. The optimized growth conditions were applied to semiconducting silicon, conducting carbon paper, and stainless steel substrates. Carbon nanotube forests have been successfully

grown on untreated stainless steel substrates. The versatility of this method and the absence of hydrogen usage recommend it as a safe, economical, and easy to scale up route for large-scale production of quality CNTs on different substrates.

4.6 References

[1] M.S. Dresselhaus, G. Dresselhaus, and P.C. Eklund, “Science of Fullerenes and Carbon Nanotubes,” Academic Press, 1995.

[2] Saito R, Dresselhaus G and Dresselhaus M S 1998 *Physical Properties of Carbon Nanotubes* (London: Imperial College Press)

[3] J. Bernholc, D. Brenner, M.B. Nardelli, V. Meunier, C. Roland, ”MECHANICAL AND ELECTRICAL PROPERTIES OF NANOTUBES”,

Annu. Rev. Mater. Res. 32, 347 (2002).

[4] Jorio A, Dresselhaus G and DresselhausM S 2008 *CarbonNanotubes: Advanced Topics in the Synthesis, Structure,Properties and Applications* (Berlin: Springer)

[5] Kong, J., Franklin, N.R., Zhou, C., Chapline, M.G., Peng, S., Dai, K.C.H., “Nanotube molecular wires as chemical sensors”, Science 2000, 287, 622.

[6] Ghosh, S.; Sood, A.K.; Kumar, N. Carbon nanotube flow sensors, Science 2003, 299, 1042.

[7] Sun, X., Li, R., Villers, D., Stansfield, B.L., Dodelet J.P., and Désilets, S., “Composite Electrode Made of Pt Nanoparticles Deposited on Carbon Nanotubes Grown on Fuel Cell Backings”, Chemical Physics Letters, 379, 99-104 (2003).

[8] Saha, M., Li, R.,_Sun, X., Ye, S. “3-D Composite Electrodes of Pt Supported Nitrogen-Doped Carbon Nanotubes Grown on Carbon Paper for High Performance PEM Fuel Cells”. Electrochemistry Communications, 11, *438-441* (2008).

[9]Saha, M., Li, R., Sun, X. “High Loading of Pt Nanoparticles on Carbon Nanotubes as Electrodes for PEM Fuel Cells”. J. Power Sources, 177, 314-322 (2008).

[10] Yougui Chen, Jiajun Wang, Hao Liu, Ruyin Li, Xueliang Sun, Siyu Ye and Shanna Knights. “Enhanced Stability of Pt Electrocatalysts by Nitrogen Doping in CNTs for PEM Fuel Cells”. Electrochemistry Communications, 11, 2071-2076 (2009).

[11] Zhu W, Bower C, Zhou O, Kochanski G and Jin S 1999 *Appl. Phys. Lett.* 75 873.

[12] T. Rueckes, K. Kim, E. Joselevich, G.Y. Tseng, C.L. Cheung, C.M. Lieber, Science 289, 94 (2000).

[13] Postma, H. W. C., Teepen, T., Yao, Z., Grifoni, M. & Dekker, C. Carbon nanotube single-electron transistors at room temperature. Science 293, 76–79 (2001).

[14] A. Bachtold, P. Hadley, T. Nakanishi, C. Dekker, “Logic Circuits with Carbon Nanotube Transistors”, Science 294, 1317 (2001). doi:10.1126/science.1065824

[15] S. Iijima and T. Ichihashi, Nature 363 (1993), p. 603.

[16] C. Journet, W.K. Maser, P. Bernier, A. Loiseau, M. Lamy de la Chapelle, S. Lefrant, P. Deniard, R. Lee and J.E. Fischer, Nature 388 (1997), p. 756.

[17] Thess A., Lee R., Nikolaev P., Dai H., Petit P., Robert J., Xu C., Young Hee Lee, Seong Gon Kim, Andrew G. Rinzler, Daniel T. Colbert, Gustavo E. Scuseria, David Tománek, John E. Fischer, Smalley R.E. Crystalline ropes of metallic carbon nanotubes (1996) Science, 273 (5274), pp. 483-487.

[18] J. Kong, A.M. Cassel and H. Dai, Chem. Phys. Lett. 292 (1998), p. 567.

[19] Cassel, A.M.; Raymarkers, J.A.; Kong, J. & Dai, H. Large Scale CVD Synthesis of singlewalled carbon nanotubes. J. Phys. Chem. B, 1999, 103(31), 6484-492.

[20] Hata K, Futaba D N, Mizuno K, Namai T, Yumura M and Iijima S 2004 *Science* 306 1362

[21] Kayastha V K, Wu S, Moscatello J and Yap Y K 2007 *J. Phys.Chem.* C 111 10158

[22] R. Andrews, D. Jacques, A. M. Rao, F. Derbyshire, D. Qian, X. Fan, E. C. Dickey, and J. Chen, “Continuous production of aligned carbon nanotubes: a step closer to commercial realization”, Chem. Phys. Lett. 303, 467 (1999)

[23] R. Kamalakaran, M. Terrones, T. Seeger, P.K. Redlich, M. Ruhle, Y.A. Kim, T. Hayashi, and M. Endo, “Synthesis of thick and crystalline nanotube arrays by spray pyrolysis”, Appl. Phys. Lett. 77, 3385 (2000).

[24] Christian P. Decka and Kenneth Vecchio, “Growth mechanism of vapor phase CVD-grown multi-walled carbon nanotubes”, Carbon, Volume 43, Issue 12, October 2005, Pages 2608-2617

[25] L. P. Biró, Z. E. Horváth, A. A. Koós, Z. Osváth, Z. Vértesy, Al. Darabont, K. Kertész,

C. Neamtu, Zs. Sárközi, L. Tapasztó, “Direct synthesis of multi-walled and single-walled carbon nanotubes by spray- pyrolysis”, Journal of Optoelectronics and Advanced Materials Vol. 5, No. 3, September 2003, p. 661 - 666

[26] CHRISTIAN P. DECK, GREGG S.B. MCKEE, and KENNETH S. VECCHIO, “Synthesis Optimization and Characterization of Multiwalled Carbon Nanotubes”, Journal of ELECTRONIC MATERIALS, Vol. 35, No. 2, 2006

[27] Hyung Seok Kim, Byungwoo Kim, Byeongdu Lee, Haegeun Chung, Cheol Jin Lee, Ho Gyu Yoon, and Woong Kim, “Synthesis of Aligned Few-Walled Carbon Nanotubes on Conductive Substrates”, The Journal of Physical Chemistry C 2009 113 (42), 17983-17988

[28] D. Park, Y.H. Kim and J.K. Lee, Pretreatment of stainless steel substrate surface for the growth of carbon nanotubes by PECVD, J Mater Sci 38 (24) (2003), pp. 4933–4939.

[29] C. Masarapu and B. Wei, Direct growth of aligned multiwalled carbon nanotubes on treated stainless steel substrates, Langmuir 23 (17) (2007), pp. 9046–9049.

[30] M.D. Abad, J.C. Sánchez-López, A. Berenguer-Murcia, V.B. Golovko, M. Cantoro, A.E.H. Wheatley, A. Fernández, B.F.G. Johnson, J. Robertson, Catalytic growth of carbon nanotubes on stainless steel: Characterization and frictional properties, Diamond & Related Materials 17 (2008) 1853–1857

[31] A. Gohier, T.M. Minea, A.M. Djouadi, J. Jiménez and A. Granier, “Growth kinetics of low temperature single-wall and few walled carbon nanotubes grown by plasma enhanced chemical vapor deposition”, Physica, E, Low-dimens. syst. nanostruct. 37 (2007), p. 34.

[32] M. S. Dresselhaus, G. Dresselhaus, R. Saito and A. Jorio (2005). "Raman Spectroscopy of Carbon Nanotubes" Physics Reports (2005) 409: 47.

[33] Tapasztó L., Kertész K., Vértesy Z., Horváth Z. E., Koós A. A., Osváth Z., Sárközi Zs., Darabont Al.,. Biró L. P., “Diameter and morphology dependence on experimental conditions of carbon nanotube arrays grown by spray pyrolysis”, Carbon 43 (2005) 970–977.

[34] C. Singh, M.S. Shaffer and A.H. Windle, Production of controlled architectures of aligned carbon nanotubes by an injection chemical vapour deposition method, Carbon 41 (2) (2003), pp. 359–368.

CHAPTER 5

NITROGEN-DOPING EFFECTS ON THE GROWTH, STRUCTURE, AND ELECTRICAL PERFORMANCE OBTAINED BY SPRAY PYROLYSIS METHOD

5.1 Abstract

Vertically aligned nitrogen-doped carbon nanotubes with modulated nitrogen content have been synthesized in a large scale by using spray pyrolysis chemical vapor deposition. The effects of nitrogen doping on the growth, structure and electrical performance of carbon nanotubes have been systematically examined. Field emission scanning electron microscopy, transmission electron microscopy, X-ray photoelectron spectroscopy, and Raman techniques have been employed to characterize the morphology, composition, and vibrational properties of the nanotubes. The results indicate that incorporated nitrogen significantly influences the growth rate, morphology, size, and structure of the nanotubes. Electrical measurement investigation of the nanotubes indicates that the change in electrical resistance increases with temperature and pressure as the nitrogen concentration increases inside the tubes. This work presents a versatile, safe, and easy way to scale up route of growing carbon nanotubes with controlled nitrogen content and modulated structure, and may provide an insight in developing various nitrogen-doped carbon based nanodevices.

5.2 Introduction

During the past decade carbon nanotubes (CNTs) have been extensively studied due to their outstanding electrical and mechanical properties [1-4]. Numerous applications have been developed by using CNTs as device components in sensors [5, 6], fuel cells [7-10], field emission devices [11], transistors, and logic circuits [12-14]. Nitrogen-doped carbon nanotubes (CN_x) have attracted considerable attention due to the possibility to tailor and improve the physical properties of pure carbon nanotubes [15-17]. The presence of additional lone pairs of electrons facilitates the injection of the electrons into the conduction band [18]. Low concentration doping of nitrogen into CNTs would make possible the enhancement of the electronic conductance and surface reactivity of the tubes without deteriorating the mechanical properties [19]. However, the correlation between the nitrogen doping, microstructure and electrical transport behaviors of the low nitrogen doped CNTs still needs to be carefully investigated. These factors are key points in the development of CN_x-based functional components such as improved catalyst support materials in proton exchange membrane fuel cells and durable composite materials. Various techniques have been used for CN_x synthesis including arc discharge [20], ion implantation [21], and diverse techniques based on chemical vapor deposition (CVD) [22, 23]. Among these techniques, spray pyrolysis CVD reveals promising results in CNT synthesis. It provides a controlled way of spraying complex carbonaceous liquids mixed with catalyst containing molecules (metallocene powders) directly into the deposition chamber and ensures semi-continuous growth of CNTs [24]. Spray pyrolysis experiments usually require high flow rates of carrier gas and display difficulties in

obtaining catalyst free CNTs with uniform diameters [25]. When low flow rates of carrier gas were used, the reactant solution could not be sprayed and fully evaporated, leaving behind metallocene residues [26]. Nevertheless, practical applications of doped nanotubes necessitate a precise and controlled introduction of dopants and a fairly large amount of material preferably in aligned configuration.

In this work, vertically aligned CNTs with modulated nitrogen concentration have been grown on semiconducting Si using a modified spray pyrolysis CVD method without hydrogen addition. Mixtures of ferrocene, xylene, and acetonitrile were directly sprayed over the substrate at a low flow rate of carrier gas (175 sccm) without affecting the spraying process or the evaporation of the catalyst. The correlation between the nitrogen doping concentration, nitrogen chemical environment, structure and crystallinity of the nanotubes was investigated and the dependence of the electrical transport properties of the nanotubes on the nitrogen content, temperature, and pressure was also addressed.

5.3 Experimental

The CVD system used in this study consisted of an electronically controlled furnace with 300 mm effective heating length, a quartz reactor tube (i.d. 25.4 mm), and a spraying setup. The device developed for spraying liquids at low precursor flow rates consisted of a carrier gas tube (i.d. 4.2 mm) which ended with a spraying nozzle (i.d. 0.5 mm) and a sealed inner tube (i.d. 1.5 mm) carrying the active solution. The pressure formed inside the carrier gas tube pulverized the solution even at low flow rates, through

the nozzle, inside the deposition chamber, up to the substrate surface situated in the middle of the quartz tube. The deposition system and the injection device are presented in Figure 5.1.

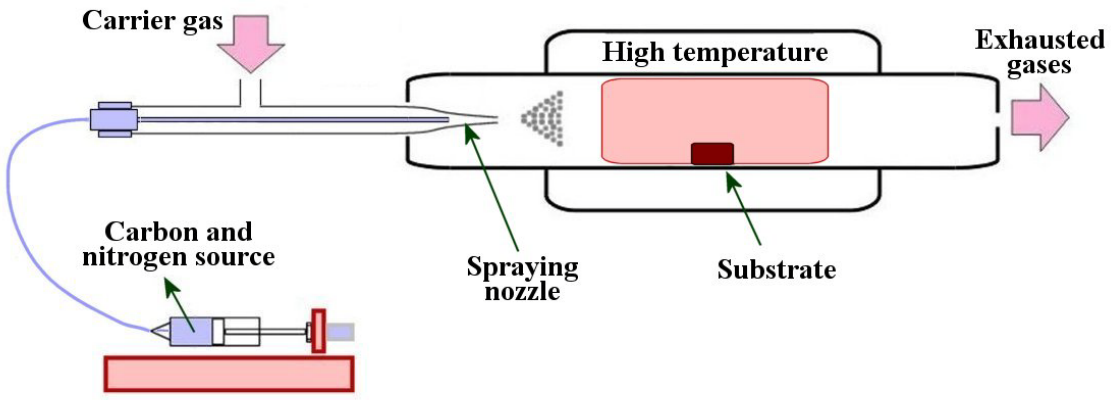

Figure 5.1 Schematic diagram of spray pyrolysis CVD system for CN_x synthesis.

In this study, oriented n-type (1, 0, 0) silicon (Si) wafers were used as a substrate, without removing the native oxide layer. An aluminum (Al) under-layer, with the thickness of 30 nm, was magnetron sputtered on the Si substrate to effectively prevent the catalyst particles from aggregation. The active solution of 0.01 g/ml concentration was prepared by dissolving ferrocene ($Fe(C_5H_5)_2$) into mixture of xylene ($C_6H_4(CH_3)_2$) and acetonitrile (CH_3CN). Ferrocene was used to produce metallic iron particles and to act as catalyst during the synthesis process and the xylene:acetonitrile mixture produced the C:N feedstock. The solution was continuously sprayed into the quartz reactor when the temperature reached 750 °C. In the spraying process, argon was used as the carrier gas at a flow rate of 175 sccm. The reaction was maintained for 4 min to inject a total amount of

3 ml solution at a feed rate of 0.75 ml/min in the CVD system. After the growth, the reactor was allowed to cool down under argon flow before exposure to air. Samples were characterized by scanning electron microscopy (SEM - Hitachi S-4800), Raman spectroscopy (Raman - Renishaw 785 nm laser excitation), and transmission electron microscopy (TEM - Philips CM-10). The TEM samples were prepared by sonicating a small piece of as-grown nanotubes in ethanol for 10 min and drying a few drops of suspension on a Cu micro-grid. The nitrogen amount was determined by X-ray photoelectron spectroscopy (XPS - Kratos AXIS Ultra, AlKα). *I–V* characteristics of the nitrogen-doped nanotubes were measured following a two-point probe model. The measurement system contained a DC power supply (Agilent E3644A) and a digital multimeter (Agilent 34410A). The carbon nanotubes were collected from substrates and 3 mg of powder was confined between gold plated aluminum conductors (2.5 mm diameter) and pressed at 60 kPa. The use of this method led to the manufacture of microprobes containing nanotubes from experiments with different acetonitrile concentrations.

5.4 Results and discussion

The nitrogen doping effects have been systematically examined by changing the concentration of acetonitrile in xylene. Five sets of experiments were conducted for a range of acetonitrile:xylene ratios of 0: 100, 25: 75, 50: 50, 75: 25, and xylene free.

5.4.1 Structure and composition of CNx

SEM observation revealed an overall carpet-like deposit, containing highly dense and vertically aligned CNT arrays, for all samples. Acetonitrile was used as the nitrogen feedstock and had a crucial influence on the tube growth. The length of the tubes ranged from 133 μm to 12 μm depending on the acetonitrile concentration (Figure 5.2). The maximum average tube length was obtained when acetonitrile was absent from the solution. For experiments with 25 vol% acetonitrile in xylene, the average tube length sharply decreased to 47 μm. The average tube length continued to decrease to 33 μm for 50 vol% acetonitrile in xylene down to a minimum of 12 μm for experiments done by using acetonitrile only (Figure 5.2a). These observations indicate that the introduction of nitrogen species inhibits the nanotube growth and are in concordance with previous theoretical and experimental results [27, 28]. The theoretical calculation has shown that nitrogen saturates the tube edge at the growing end, favors the defect formation, and inhibits the tube growth. The SEM image of the nanotube array root shows that the catalyst remains on the substrate during the growth process (Figure 5.2b). These observations are consistent with all experiments and indicate that the tubes grow upwards following a base growth mechanism. Figures 5.2c-d show TEM images of a nanotube at the bottom and tip part confirming that the nanotubes followed a base growth mode. Further TEM analysis reveals more detailed structural characteristics of CN_x. TEM investigations indicate that the samples contain neglected amount of amorphous carbon or catalyst particles encapsulated in the inner core or attached upon the nanotube surface.

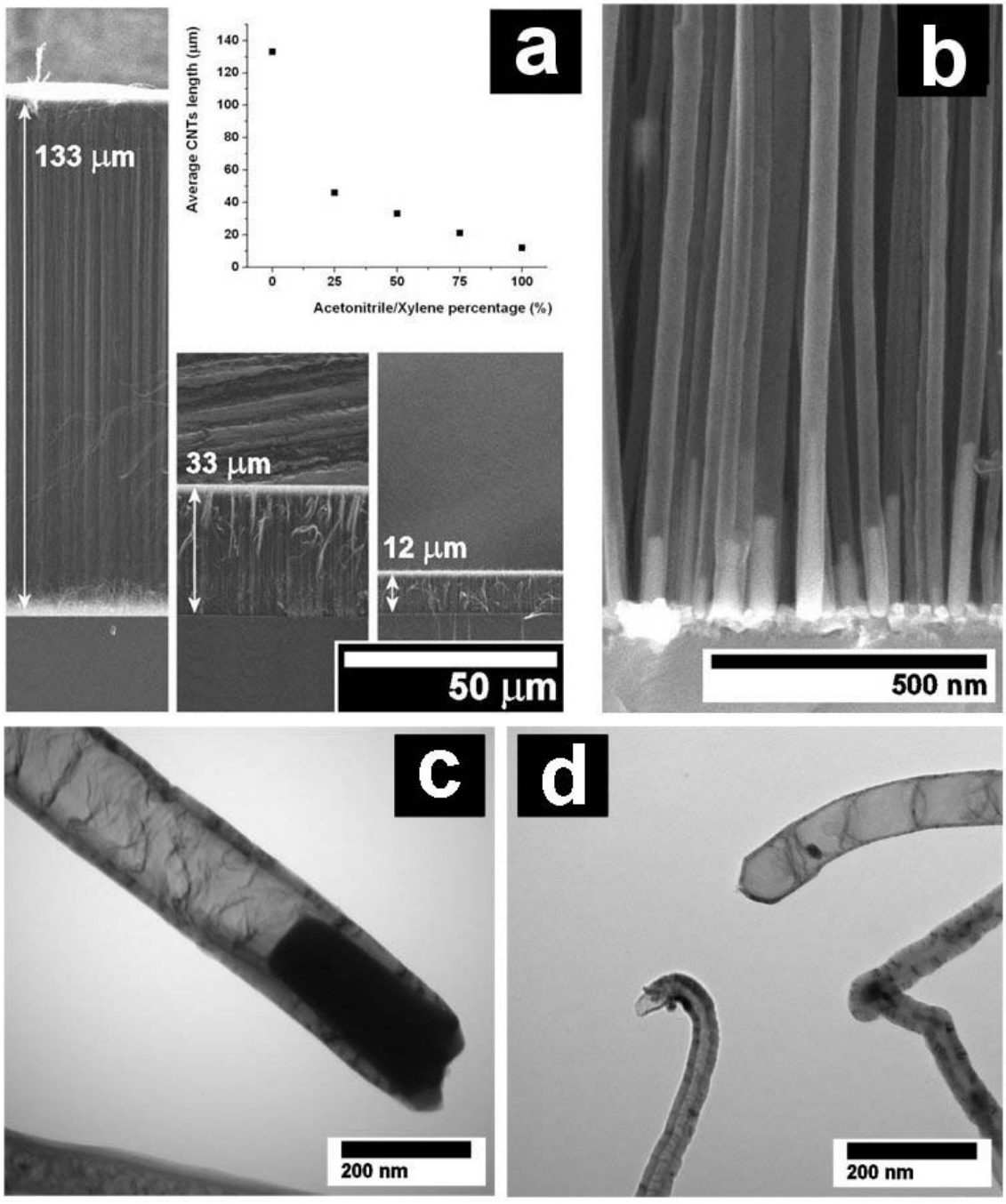

Figure 5.2 Electron microscopic images showing average CNT length (a) (inset: diagram of the relationship between acetonitrile:xylene concentration and average CNT length) and nanotubes at the bottom (b,c) and tip part (d).

The nanotubes present typical defects occurred in a CVD process regardless to the structure changes caused by the incorporation of nitrogen. The change of the nanotube structure is presented in Figure 5.3 using representative TEM images and Raman spectra of samples produced at 0 %, 50 %, and 100 % acetonitrile concentrations. The micrographs of nanotubes produced from sole xylene are typical ones for regular carbon nanotubes produced by spray pyrolysis [25] and exhibit relatively well defined graphitic shells parallel to the tube axis (Figure 5.3a-b). From the plotted diameter distribution on the basis of TEM images, the average outer diameter of the tubes is 42 nm (Figure 5.3c) and the wall thickness is around 20 nm. Raman spectrum (Figure 5.3d) indicates a strong band around 1583 cm^{-1}, which is referred to as the G-band. The G-band corresponds to the optical phonon modes of E_{2g} symmetry in graphite and indicates the formation of well graphitized carbon nanotubes. The D-band at 1352 cm^{-1} originates from defects that occur in the curved graphene layers and at the tube ends. For estimating the defect concentration in carbon nanotubes, the intensity of D-band is usually normalized to the intensity of G-band. The intensity ratio of the D-band relative to G-band (I_D/I_G=0.41) from the Raman spectrum witnesses the structural order and the degree of perfection of the tubes. The presence of acetonitrile in the precursor changed the inner structure of the nanotubes. The tubes produced from precursors containing 25 vol% (not shown) and 50 vol% acetonitrile become compartmentalized with lateral segmentation and exhibit stack-cone or bamboo structure (Figure 5.3e-f). The average outer diameter of the tubes increases to 51 nm (Figure 5.3g) while the wall thickness slightly decreases to 16 nm.

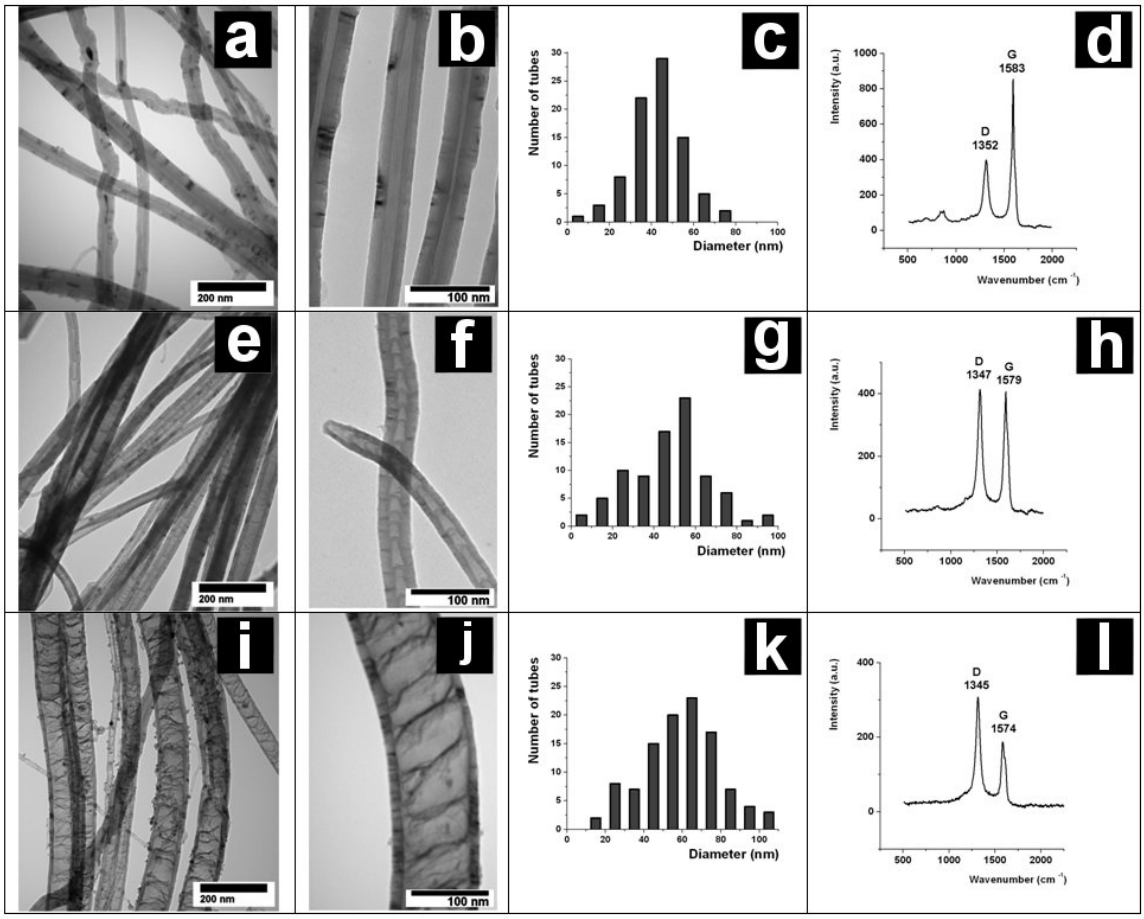

Figure 5.3 TEM images of the CNT structure, schematic diameter distribution, and Raman spectrum for samples produced using pure xylene (a-d), 50 vol% concentration of acetonitrile in xylene (e-h), and pure acetonitrile (i-l).

The I_D/I_G ratio from the Raman spectra of samples obtained from nitrogen containing precursors could be considered strongly dependent on the defect fraction originating from nitrogen incorporation. The Raman spectrum of the samples produced from precursor containing 50:50 acetonitrile and xylene (Figure 5.3h) shows an increase to 1.02 of the I_D/I_G ratio and indicates that the tubes present lattice defects and disorders derived from nitrogen doping. The nanotubes produced from precursors containing 75 vol%

acetonitrile (not shown) and from acetonitrile 100 vol% (Figure 5.3i-j) present irregular and inter-linked corrugated structure. The average wall thickness of tubes decreases around 12 nm and the average outer diameter increases to 63 nm (Figure 5.3k). These are reflected in a larger I_D/I_G ratio of 1.54 in the Raman spectrum (Figure 5.3l). These observations indicate that the degree of long-range crystalline perfection of carbon nanotubes decreases with nitrogen presence in the synthesis process. They are in agreement with previous reported observations resulted from pyrolysis of different nitrogen contained precursors such as melamine or benzylamine [23, 28]. It can be observed that adding acetonitrile in the precursor mixture used for nanotube synthesis leads to a down-shift of the G-band from 1583 cm^{-1} (0% acetonitrile) to 1574 cm^{-1} (100% acetonitrile). Since the G-band is not related to the structural defects, the shift can be attributed to a modification in the electronic structure of the nitrogen doped tubes [29]. The correlation between the structure of nitrogen doped carbon nanotubes grown with various acetonitrile concentrations and incorporated nitrogen, has been investigated by XPS measurements. The nitrogen doping concentration was determined from the atomic percentage ratio of nitrogen and carbon in the XPS measurements. Since the growth of CNTs was carried in Ar instead of N_2 flow, the nitrogen incorporation in the nanotubes walls is a result of acetonitrile decomposition and is increased with the acetonitrile concentration in the feedstock. Adding 25 vol %, 50 vol%, and 75 vol% acetonitrile in the precursor resulted in doped nanotubes with 2 at.%, 2.3 at.%, and 3.6 at.% of nitrogen, respectively. Synthesis of doped nanotubes from pure acetonitrile resulted in about 4 at.% nitrogen incorporation. The XPS N1s deconvoluted spectra of the nanotubes were fitted by three Lorenzian-like components with binding energies of 398.8 ± 0.3 eV (N1), 402.1

± 0.3 eV (N2), and 405.5 ± 0.3 eV (N3). In addition, a new peak at 398.6 eV ± 0.3 (N4) could be detected from the nanotubes in the case of using 25 vol% acetonitrile. The spectra of the nanotubes produced from 25 vol%, 50 vol% acetonitrile and from pure acetonitrile are presented in Figure 5.4. The low-energy N1 peak is less intensive and corresponds to pyridinic nitrogen. The peaks N2 and N3 are more dominant and are attributed to graphitic nitrogen and molecular nitrogen, respectively. Molecular nitrogen is intercalated between the nanotube layers or encapsulated in the central nanotube hollow and thus it should have no influence on the structural characteristics of nanotubes [29]. The peak N4 can be assigned to the tetrahedral nitrogen bonded to sp^3-C probably due to un-decomposed N-H bond, which is similar to the case using octadecylamine as the precursor [30]. Furthermore, the ratio of pyridinic nitrogen to graphitic nitrogen increases with acetonitrile concentration from I_{N1}/I_{N2}=0.37 (25 vol% acetonitrile) to 0.65 (50 vol% acetonitrile) and presents a maximum of 0.73 for pure acetonitrile. This suggests that the pyridine-like nitrogen doping increases with the acetonitrile concentration. The pyridine-like sites is considered to be responsible for the wall roughness and interlinked morphologies [31]. As the number of pyridinic nitrogen increases within the tubes, the roughness of tube walls and compartment layers also increases. These results are consistent with the TEM and Raman analyses and confirm that the defects and disorders of the tubes are dependent on the content of pyridinic nitrogen in the CNTs. The changes in tube morphology with the nitrogen concentration are summarized in Table 5.1.

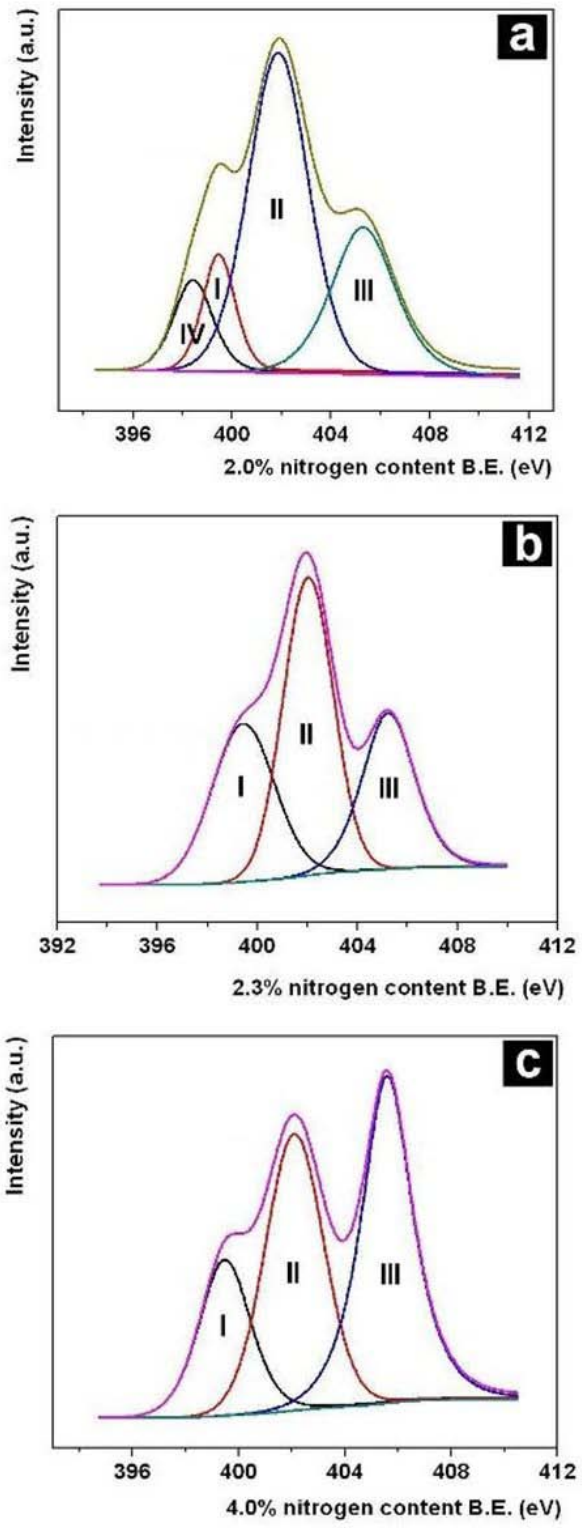

Figure 5.4 XPS spectra of the nanotubes produced from 25 vol% (a), 50 vol% (b), and pure acetonitrile (c).

Table 5.1 Dependence of nitrogen doping, structure and size of the CN_x on ratios of acetonitrile:xylene.

Acetonitrile:Xylene	Nitrogen amount (at.%)	CNTs Walls Structure	Average Outer Diameter and Wall Thickness (nm)	Average CNTs length (μm)
0:100	-	Straight	42/20	133
25:75	2	Straight and Bamboo	44/19	46
50:50	2.3	Bamboo and Corrugated	51/16	33
75:25	3.6	Corrugated	56/15	21
100:0	4.0	Corrugated	63/12	12

5.4.2 Electrical resistivity of bulk CNx

Bulk resistance of CN_x as ohmic *I–V* characteristics was measured following a two-point probe model. The measurements were conducted in the same oven used in the CVD process, at temperatures between 35 ^{o}C and 125 ^{o}C, monitored by a K type thermocouple. In order to achieve thermal equilibrium, the temperature of the system was kept for 10 minutes after the target temperature had been reached. For every step of temperature a set of *I–V* measurements were done (Figure 5.5a). For the temperature of 35 ^{o}C, all microprobes had almost the same electrical resistivity of 7.27×10^{-3} Ω*m. With increasing temperature, the resistivity of the microprobes decreased monotonically. At the temperature of 85 ^{o}C, the resistivity of regular nanotubes produced from xylene was 7.10×10^{-3} Ω*m and that of the nanotubes produced using pure acetonitrile was 7.02×10^{-3}

Ω*m. At 125 ^{o}C, the resistivity of regular nanotubes was 6.96×10^{-3} Ω*m, whereas that of the probe contained nanotubes obtained from pure acetonitrile was as low as 6.83×10^{-3} Ω*m (Figure 5.5b). These differences represent a change in resistivity of more than 29% between regular nanotubes and the tubes produced from pure acetonitrile, indicating a better conductivity of CN_x. The temperature coefficient of resistance (TCR) gave the resistance change factor per degree of temperature change and was calculated from the formula $R = R_0 [1+\alpha(T-T_0)]$. The resulted TCR was $-4.7280*10^{-4}$ K^{-1} for regular nanotubes, increased to $-5.7879*10^{-4}$ K^{-1} for nanotubes obtained from 50 vol% acetonitrile, and presented a maximum value of $-6.6915*10^{-4}$ K^{-1} for the nanotubes achieved using pure acetonitrile.

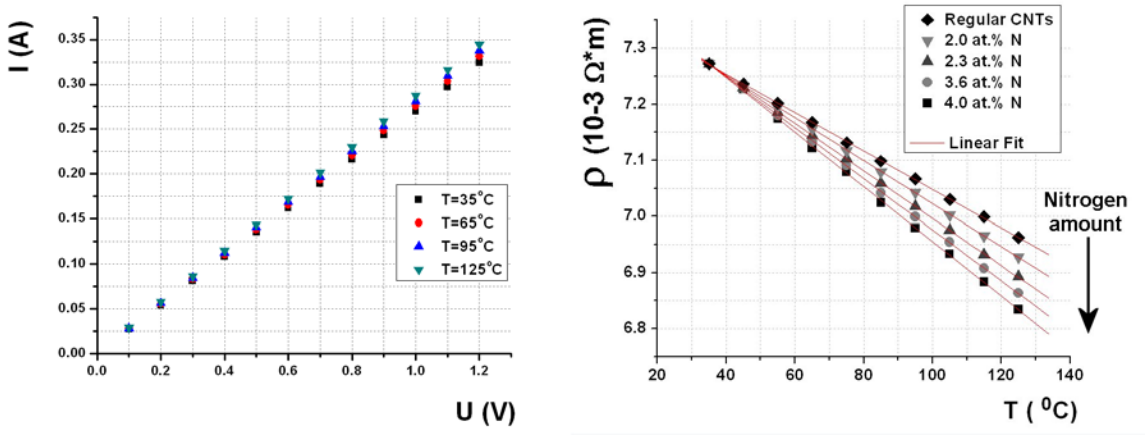

Figure 5.5 *I–V* characteristics of regular nanotubes for temperatures between 35 ^{o}C and 125 ^{o}C (a). A plot of resistivity vs. temperature for bulk CNTs with different nitrogen content (b).

The change of electrical resistance with pressure was measured following a similar procedure. The measurements were done at room temperature for the pressure interval of 40-139 kPa. The change of electrical resistance increased with the nitrogen amount (Figure 5.6) and the difference between regular nanotubes and the tubes produced from pure acetonitrile was about 20%. These measurements are in agreement with the results obtained by other groups [32-35], but could depend on sample preparation, material impurities, and the measuring conditions. It was indicated that the conduction occurs at the cross section of the nanotubes and is affected by inner structure of the tubes and by the applied compressive stress. While many factors influence the measurement results, this method is highly repeatable and a relatively simple tool to quantify the resistivity of bulk CNTs.

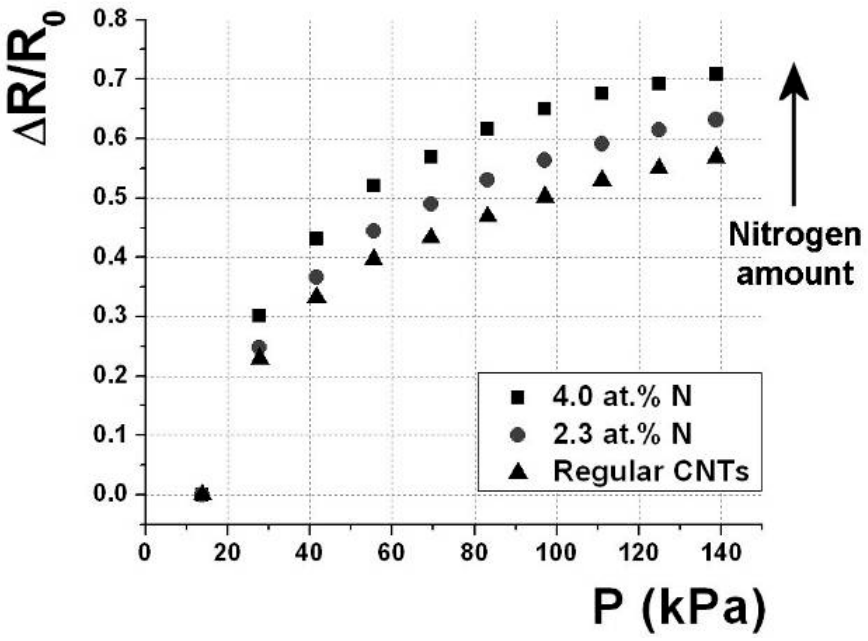

Figure 5.6 A plot of electrical resistance vs. pressure for bulk CNTs with different nitrogen content.

5.5 Conclusions

Vertically aligned CNTs with tuning nitrogen content have been synthesized on silicon wafers by a modified spray pyrolysis CVD method. The nitrogen concentration was tailored by changing the concentration ratio of nitrogen/carbon source during the spraying process. The incorporated nitrogen significantly influenced the tube structure from straight to corrugated nanotubes, caused defects within the CN_x, and decreased the growth rate. The ratio of pyridinic nitrogen to graphitic nitrogen in CN_x increased with acetonitrile/xylene ratio. Electrical measurements of the CN_x with temperature and pressure indicate a better conductivity of bulk CN_x as the nitrogen concentration inside the tubes increased. The present work introduces a versatile method of growing vertical aligned doped nanotubes and demonstrates that CNTs with modulated nitrogen, controlled structure, and controlled electrical transport properties can be obtained. It provides useful information in terms of both fundamental understandings and practical applications of CN_x nanotubes in developing various CN_x nanotube-based nanodevices.

5.6 References

[1] P. Ajayan, "Nanotubes from carbon," *Chemical Reviews,* vol. 99, 1999, pp. 1787-1800.

[2] R. Tenne, "Inorganic nanotubes and fullerene-like nanoparticles," *Nature Nanotechnology,* vol. 1, Nov. 2006, pp. 103-111.

[3] J. Bernholc, D. Brenner, M. Buongiorno Nardelli, V. Meunier, and C. Roland, "Mechanical and electrical properties of nanotubes," *Annual Review of Materials Science*, vol. 32, 2002, pp. 347-375.

[4] L. Qu and L. Dai, "Gecko-foot-mimetic aligned single-walled carbon nanotube dry adhesives with unique electrical and thermal properties," *Advanced Materials*, vol. 19, 2007, pp. 3844-3849.

[5] Jing Kong, N. Franklin, Chongwu Zhou, M. Chapline, Shu Peng, Kyeongjae Cho, and Hongjie Dai, "Nanotube molecular wires as chemical sensors," *Science*, vol. 287, Jan. 2000, pp. 622-625.

[6] S. Ghosh, A. Sood, and N. Kumar, "Carbon nanotube flow sensors," *Science*, vol. 299, Feb. 2003, pp. 1042-1044.

[7] X. Sun, R. Li, D. Villers, J. Dodelet, and S. Desilets, "Composite electrodes made of Pt nanoparticles deposited on carbon nanotubes grown on fuel cell backings," *Chemical Physics Letters*, vol. 379, Sep. 2003, pp. 99-104.

[8] M. Saha, Ruying Li, Xueliang Sun, and Siyu Ye, "3-D composite electrodes for high performance PEM fuel cells composed of Pt supported on nitrogen-doped carbon nanotubes grown on carbon paper," *Electrochemistry Communications*, vol. 11, Feb. 2009, pp. 438-441.

[9] M.S. Saha, R. Li, and X. Sun, "High loading and monodispersed Pt nanoparticles on multiwalled carbon nanotubes for high performance proton exchange membrane fuel cells," *Journal of Power Sources*, vol. 177, Mar. 2008, pp. 314-322.

[10] Y. Chen, J. Wang, H. Liu, R. Li, X. Sun, S. Ye, and S. Knights, "Enhanced stability of Pt electrocatalysts by nitrogen doping in CNTs for PEM fuel cells," *Electrochemistry Communications*, vol. 11, 2009, pp. 2071-2076.

[11] S. Srivastava, V. Vankar, and V. Kumar, "Excellent field emission properties of short conical carbon nanotubes prepared by microwave plasma enhanced CVD process," *Nano Scale Research Letters*, vol. 3, Jan. 2008, pp. 25-30.

[12] T. Rueckes, K. Kim, E. Joselevich, G. Tseng, C. Cheung, and C. Lieber, "Carbon nanotube-based nonvolatile random access memory for molecular computing," *Science*, vol. 289, Jul. 2000, pp. 94-97.

[13] H. Postma, T. Teepen, Zhen Yao, M. Grifoni, and G. Dekker, "Carbon nanotube single-electron transistors at room temperature," *Science*, vol. 293, Jul. 2001, pp. 76-79.

[14] A. Bachtold, P. Hadley, T. Nakanishi, and C. Dekker, "Logic circuits with carbon nanotube transistors," *Science*, vol. 294, Nov. 2001, pp. 1317-1320.

[15] M. Terrones, P. Ajayan, F. Banhart, X. Blase, D. Carroll, J. Charlier, R. Czerw, B. Foley, N. Grobert, R. Kamalakaran, P. Kohler-Redlich, M. Ruhle, T. Seeger, and H. Terrones, "N-doping and coalescence of carbon nanotubes: synthesis and electronic properties," *Applied Physics A (Materials Science Processing)*, vol. A74, Mar. 2002, pp. 355-361.

[16] M. Terrones, A. Jorio, M. Endo, A. Rao, Y. Kim, T. Hayashi, H. Terrones, J. Charlier, G. Dresselhaus, and M. Dresselhaus, "New direction in nanotube science," *Materials Today*, vol. 7, 2004, pp. 30-45.

[17] C. Ewels and M. Glerup, "Nitrogen doping in carbon nanotubes," *Journal of Nanoscience and Nanotechnology*, vol. 5, Sep. 2005, pp. 1345-1363.

[18] Y. Huang, J. Gao, and R. Liu, "Structure and electronic properties of nitrogen-containing carbon nanotubes," *Synthetic Metals*, vol. 113, Jul. 2000, pp. 251-255.

[19] R. Sen, B.C. Satishkumar, A. Govindaraj, K.R. Harikumar, G. Raina, J. Zhang, A.K. Cheetham, and C.N.R. Rao, "B-C-N, C-N and B-N nanotubes produced by the pyrolysis of precursor molecules over Co catalysts," *Chemical Physics Letters*, vol. 287, May. 1998, pp. 671-676.

[20] M. Glerup, J. Steinmetz, D. Samaille, O. Stephan, S. Enouz, A. Loiseau, S. Roth, and P. Bernier, "Synthesis of N-doped SWNT using the arc-discharge procedure," *Chemical Physics Letters*, vol. 387, Mar. 2004, pp. 193-197.

[21] J. Kotakoski, A. Krasheninnikov, Y. Ma, A. Foster, K. Nordlund, and R. Nieminen, "B and N ion implantation into carbon nanotubes: insight from atomistic simulations," *Physical Review B (Condensed Matter and Materials Physics)*, vol. 71, May. 2005, pp. 205408-205408-6.

[22] C. Tang, Y. Bando, D. Goldberg, and Fangfang Xu, "Structure and nitrogen incorporation of carbon nanotubes synthesized by catalytic pyrolysis of dimethylformamide," *Carbon*, vol. 42, 2004, pp. 2625-2633.

[23] Hao Liu, Yong Zhang, Ruying Li, Xueliang Sun, S. Desilets, H. Abou-Rachid, M. Jaidann, and L. Lussier, "Structural and morphological control of aligned nitrogen-doped carbon nanotubes," *Carbon*, vol. 48, Apr. 2010, pp. 1498-1507.

[24] O. Tiprigan, A. Koós, P. Nemes-Incze, Z. Horváth, Z. Sárközi, S. Simon, A. Darabont, and L. Biró, "Obtaining bamboo-structured, multiwalled carbon nanotubes using the spray pyrolysis method," *Journal of Optoelectronics and Advanced Materials*, vol. 9, 2007, pp. 617-620.

[25] L. Biró, Z. Horváth, A. Koós, Z. Osváth, Z. Vértesy, A. Darabont, K. Kertész, C. Neamţu, Z. Sárközi, and L. Tapasztó, "Direct synthesis of multi-walled and single-walled carbon nanotubes by spray-pyrolysis," *Journal of Optoelectronics and Advanced Materials*, vol. 5, 2003, pp. 661-666.

[26] C. Deck, G. Mckee, and K. Vecchio, "Synthesis optimization and characterization of multiwalled carbon nanotubes," *Journal of Electronic Materials*, vol. 35, 2006, pp. 211-223.

[27] B.G. Sumpter, V. Meunier, J.M. Romo-Herrera, E. Cruz-Silva, D.A. Cullen, H. Terrones, D.J. Smith, and M. Terrones, "Nitrogen-Mediated Carbon Nanotube Growth: Diameter Reduction, Metallicity, Bundle Dispersability, and Bamboo-like Structure Formation," *ACS Nano*, vol. 1, Nov. 2007, pp. 369-375.

[28] A. Koos, M. Dowling, K. Jurkschat, A. Crossley, and N. Grobert, "Effect of the experimental parameters on the structure of nitrogen-doped carbon nanotubes produced by aerosol chemical vapour deposition," *Carbon*, vol. 47, Jan. 2009, pp. 30-37.

[29] L. Bulusheva, A. Okotrub, I. Kinloch, I. Asanov, A. Kurenya, A. Kudashov, X. Chen, and H. Song, "Effect of nitrogen doping on Raman spectra of multi-walled carbon nanotubes," *Physica Status Solidi B*, vol. 245, Oct. 2008, pp. 1971-1974.

[30] K. Ghosh, M. Kumar, T. Maruyama, and Y. Ando, "Micro-structural, electron-spectroscopic and field-emission studies of carbon nitride nanotubes grown from cage-like and linear carbon sources," *Carbon*, vol. 47, May. 2009, pp. 1565-1575.

[31] Hyun Chul Choi, Jeunghee Park, and Bongsoo Kim, "Distribution and structure of N atoms in multiwalled carbon nanotubes using variable-energy X-ray photoelectron

spectroscopy," *Journal of Physical Chemistry B*, vol. 109, Mar. 2005, pp. 4333-4340.

[32] P. Singjai, S. Changsarn, and S. Thongtem, "Electrical resistivity of bulk multi-walled carbon nanotubes synthesized by an infusion chemical vapor deposition method," *Materials Science & Engineering A (Structural Materials: Properties, Microstructure and Processing)*, vol. 443, Jan. 2007, pp. 42-46.

[33] L. Chen, C. Qin, X. Shi, S. Bai, and L. Wang, "High temperature electrical and thermal properties of the bulk carbon nanotube prepared by SPS," *Materials Science & Engineering A (Structural Materials: Properties, Microstructure and Processing)*, vol. 420, Mar. 2006, pp. 208-211.

[34] R. Ma, C. Xu, B. Wei, J. Liang, D. Wu, and D. Li, "Electrical conductivity and field emission characteristics of hot-pressed sintered carbon nanotubes," *Materials Research Bulletin*, vol. 34, Mar. 1999, pp. 741-747.

[35] Yan-Hui Li, Jinquan Wei, Xianfeng Zhang, Cailu Xu, Dehai Wu, Li Lu, and Bingqing Wei, "Mechanical and electrical properties of carbon nanotube ribbons," *Chemical Physics Letters*, vol. 365, Oct. 2002, pp. 95-100.

CHAPTER 6

CONTROLLED SYNTHESIS OF A NOVEL CLASS OF CARBON NANOSTRUCTURES: MULTIPLE-LEVEL HIERARCHICAL N-DOPED CARBON NANOTUBES*

6.1 Abstract

A new structure of hierarchical nitrogen-doped carbon nanotubes (CNTs) has been synthesized by an innovated spray pyrolysis chemical vapor deposition (CVD). The structure consists of aligned CNTs which have multiple-level branched structure with increasing mean diameters from 10nm (first-level) to 210nm (final-level). The multi-level hierarchical, nitrogen doped carbon nanotubes have been characterized by scanning electron microscopy (SEM) and transmission electron microscopy (TEM). The formation mechanism is explained by the gradual coalescence of the catalyst particles on the substrate during growth process, finally generating large diameter nanotubes. The branching process is highly controllable and the multiple branched N-doped carbon nanotubes may have potential applications for electronic and nanoenergetic materials.

* US patent is pending for the results presented in this chapter

6.2 Introduction

Continuous requirements of miniaturization and complex nanoscale devices have generated an increasing interest in developing novel nanomaterials with complicated structures. CNTs have drawn considerable attention due to their outstanding electrical and mechanical properties [1-4]. Furthermore, their complex spatial architecture has contributed to their potential applications in sensors, fuel cells, field emission devices, transistors, and logic circuits [5-9]. In order to integrate nanomaterials with different properties into functional systems, much attention has been focused on branched CNTs [10-12]. Up to now, many techniques have been employed to produce branched carbon nanotubes. Initially, Y-shape CNTs were synthesized by arc discharge [13] and alumina template [14, 15]. A high-intensity electron beam was used to join crossed CNTs [16]. Another approach was to attach catalyst particles to the grown CNTs during the CVD growth process to initialize and sustain branches formation [17, 18]. Recently, more complicated branched CNTs have been reported by using a pyrolysis method, in which gas flow fluctuation has been considered the key factor that influences the branch occurrence [19, 20]. These studies have presented valuable information about the synthesis process and opened new routes in finding novel properties of nanostructured carbon. However, these methods have the disadvantages of inconsistent repeatability and introduction of external templates or additional steps that make the process complex and difficult to control.

In this study, we report an innovative, simple, one-step spray pyrolysis CVD method to synthesize, for the first time, multi-level hierarchical nitrogen doped carbon

nanotubes. Along the length direction of the nanotubes, from top to bottom, the height of the final-level nanotubes can be well controlled. The first-level nanotubes at the top part exhibited branched nanotubes with much thinner diameter than the final-level nanotubes. During the experiments, it was found that the precursor and substrate type, growth time, catalyst concentration, and temperature were important factors in the formation of the branches. The detailed growth mechanisms are also discussed.

6.3 Experimental

Silicon (Si n-type (1, 0, 0)) wafers were used as a substrate, without removing the native oxide layer. An aluminum (Al) under-layer, with the thickness of 30 nm, was magnetron sputtered on the Si substrate to effectively prevent the catalyst particles from aggregation. The substrate was introduced into a CVD deposition chamber composed of a quartz tube inside an oven. The temperature was increased in a nitrogen atmosphere. Ferrocene powder dissolved in acetonitrile (3.0 wt%) was used as iron catalyst, carbon, and nitrogen sources. When the substrate reached the desired temperature (700 $^{\circ}$C), the injection pump was started at very low precursor flow rate (0.06 ml/min). The volume of active solution (3 ml) was pulverized inside the deposition chamber through a micro spraying nozzle (Figure 6.1). Aligned arrays of nitrogen doped multi-branched CNTs were produced by spray pyrolysis of acetonitrile and ferrocene mixtures using nitrogen as carrier gas. The temperature of the substrate could be varied between room temperature and 800 °C, while the liquid injection flow rate could be controlled between 1 ml/min

and 1 μl/min by an injection pump. For spraying liquids at such a low injection rate, a device was built and consisted in a mixture chamber located in front of a micro nozzle. The pressure of the carrier gas, inside the mixture chamber, pulverized the liquid through the nozzle inside the deposition chamber to the substrate surface. After experiments, the deposition chamber was kept in nitrogen atmosphere to cool down to room temperature.

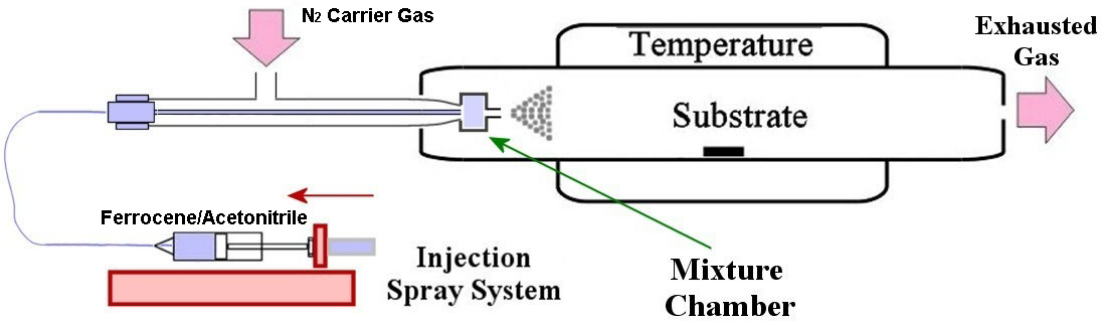

Figure 6.1 Schematic diagram of the spray pyrolysis CVD apparatus with the injection device.

6.4 Results and discussion

Figure 6.2 shows SEM images of the hierarchically branched carbon nanotubes. The product consists of vertical aligned and multi-branched carbon nanotubes with a length of 5 μm. Catalyst particles are observed on the bottom ends of the CNTs, indicating a base-growth mode of the nanotubes. The CNTs have diameters ranged from 147 nm to 450 nm (Figure 6.2b), indexed here as the final-level CNTs.

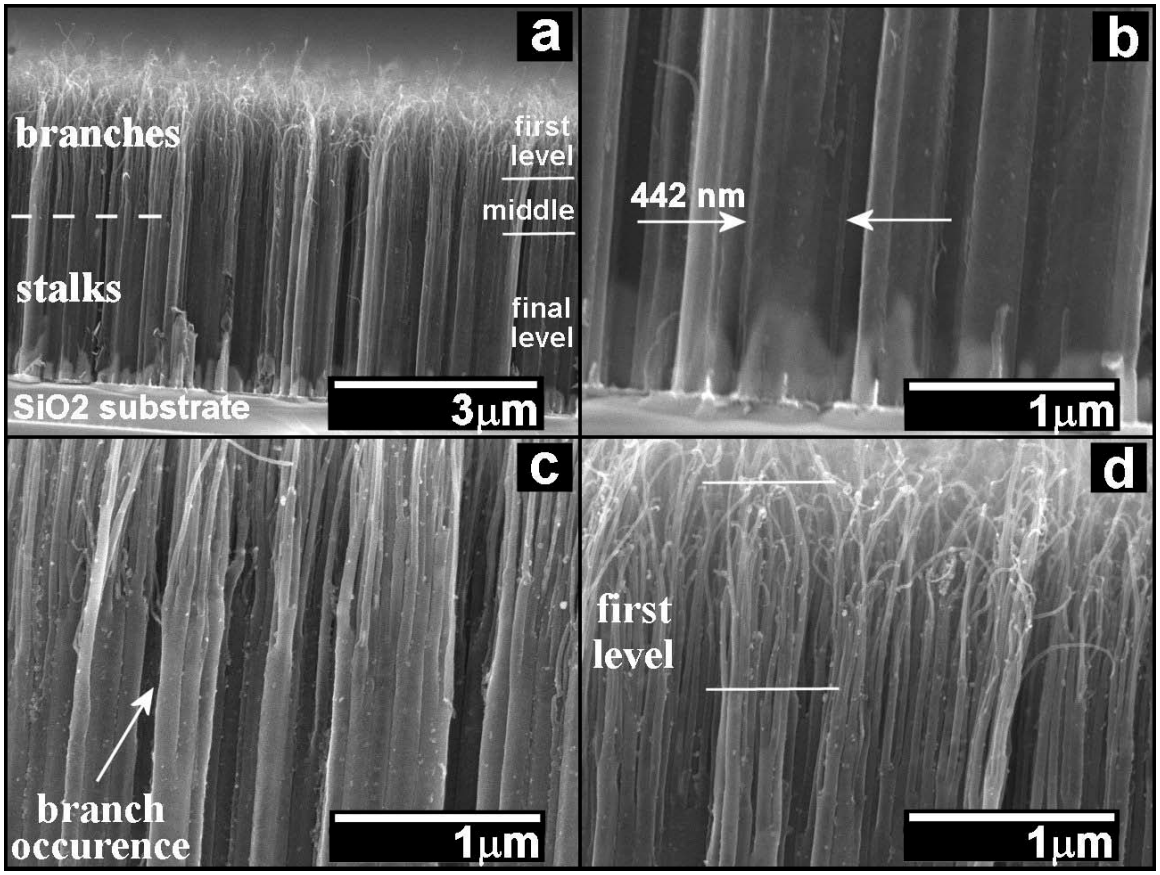

Figure 6.2 SEM image of a well-aligned branched CNTs array (a); view of catalyst particles at the bottom ends of CNTs (b); nanotube branch occurence at the same height (c); view of the top part of branched CNTs (d).

The increased magnification SEM image of the middle part (marked in Figure 6.2a) shows that the nanotube branches are at the same height (Figure 6.2c). The hierarchical CNTs with thinner diameter of 56 nm are observed, indicating synchronous growth of different nanotubes. At the top part, more branched CNTs are observed (Figure 6.2d), featuring nanotube bundles with much thinner diameter. From the SEM images, it can be seen that the final-level nanotubes have large diameters, up to 450 nm, due to the

mergence of the branched nanotubes. The size of the nanotube bundle from the originally formed nanotube branches is almost equal to the diameter of the later formed stalk nanotube due to van der Waals force that keeps the tubes together. TEM observation provides more insight into the fine structure of the branched CNTs. Figure 6.3a shows three typical images of the branched CNT bundle, obviously indicating a morphology transition from thinner branch nanotubes to thicker stalk nanotubes. Figure 6.3b shows a bottom image of the nanotube with a catalyst. The mean diameter of the stalk nanotube is around 210 nm. Figure 6.3c shows the image of the junction part between the branched and stalk nanotubes. The diameter of the nanotubes increases from 70 nm of the branched nanotubes to 210 nm of the stalk nanotubes. As marked in the picture, individual nanotubes from the branched nanotubes have smaller diameters which gradually increase from the tip to the base and form multiple branches over their length. It is possible to form multi-level branched nanotubes between the thinnest branched nanotubes and the thickest stalk nanotubes. Figure 6.3d shows the typical image of the first-level nanotubes. Their diameters, which are around 10 nm, are much smaller than the second-level (70 nm) and third-level (210 nm) nanotube diameters. In addition, the first-level nanotubes feature a closed tip without any visible catalyst particle, confirming the base-growth mode of the branched CNTs in this case. Further experiments have been performed in order to investigate the growth mechanism of the multi-level branched CNTs, including the effect of precursor and substrate type, growth time, catalyst concentration, and temperature, while keeping other parameters fixed as described in the experimental section.

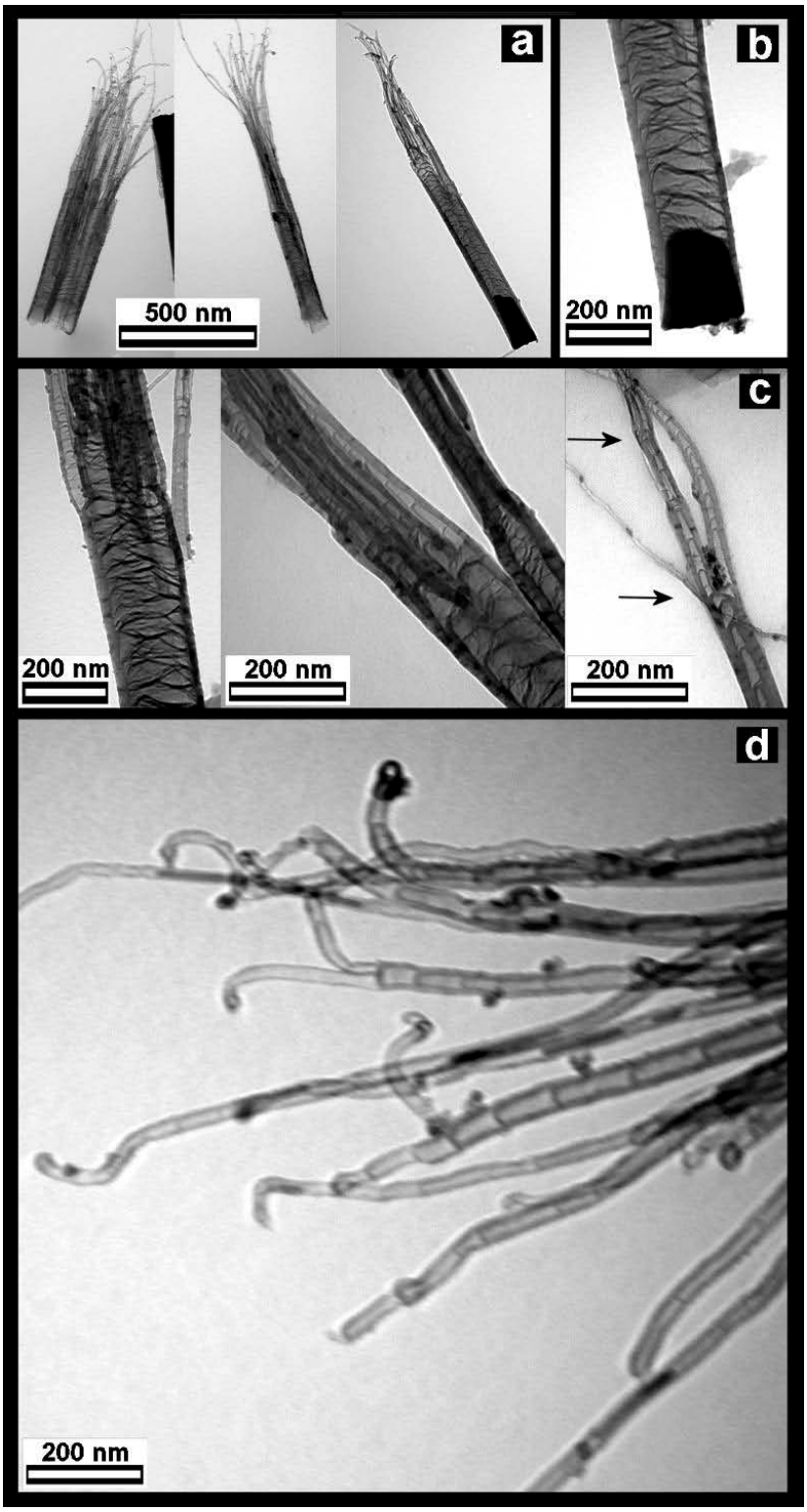

Figure 6.3 TEM images of the branched CNTs (a); view of the stalk nanotube with a catalyst inclusion (b); view of the nanotube branch occurrence (c); view of the first-level nanotubes (d).

6.4.1 Effect of precursors

During experiments, it has been found that the formation of the multi-level branched carbon nanotubes depends greatly on the employed spray precursors. We have investigated the effect of nitrogen-containing or nitrogen-free precursors on the formation of branched nanotubes. When we used acetonitrile as nitrogen-contained precursor, multi-level branched nanotubes were obtained in a controlled way. Figure 6.4a and Figure 6.4b show two representative SEM images of the CNTs using xylene and ethanol as the nitrogen-free precursors. In both cases, no branched nanotubes were observed. The precursor of ethylene gave nanotubes with a dual diameter distribution (Figure 6.4a), while that of ethanol brought nanotubes with narrow diameter distribution (Figure 6.4b). When ethanol dissolved with melamine was used as the precursor, the morphology of the nanotubes showed better alignment compared to the case without melamine, but no branched structure was generated (Figure 6.4c). However, when melamine was dissolved in pyridine to provide nitrogen, branched nanotubes appeared (Figure 6.4d). Compared with multi-level branched nanotubes grown using acetonitrile as the precursor, the stalk nanotubes grown using pyridine dissolved with melamine have much smaller diameters (50 nm) and present fewer branched nanotubes. It indicates that the achievement of multi-level hierarchical CNTs is highly selective in precursors, and nitrogen doping may be a crucial factor in inducing the formation of the branched nanotubes. A further study of these factors will be performed in the near future.

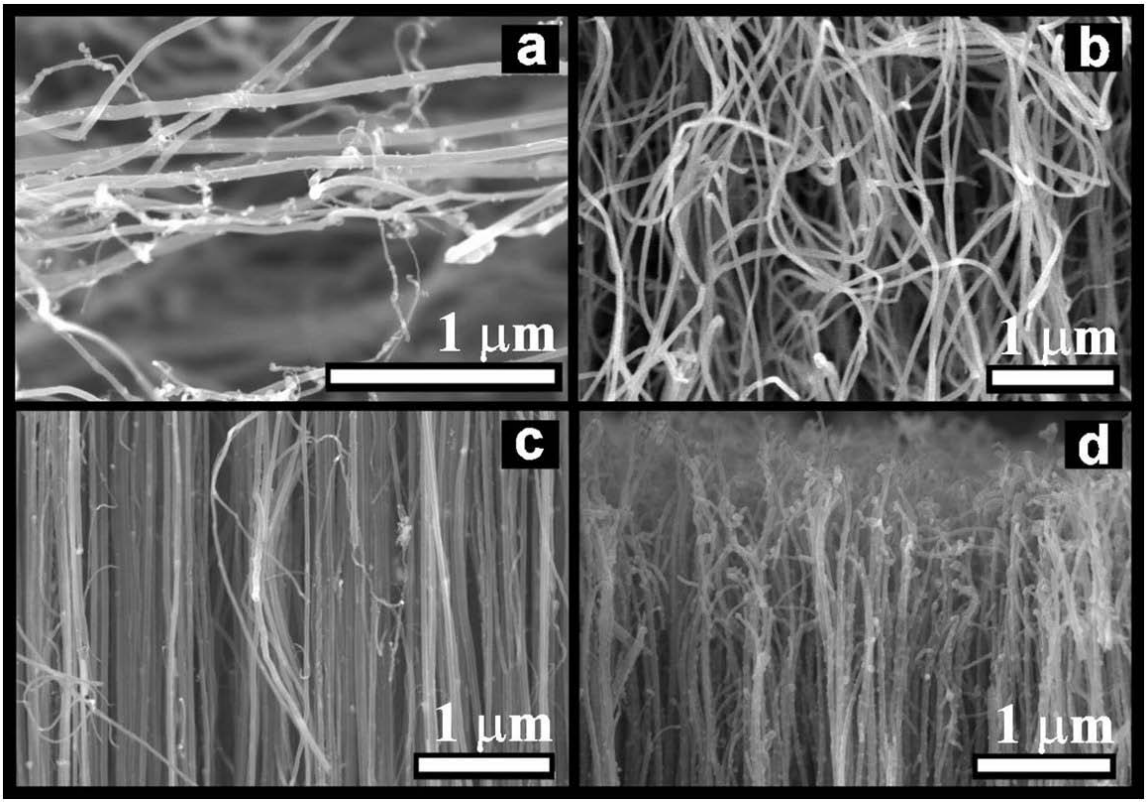

Figure 6.4 SEM images of the CNTs using different precursors: xylene (a), ethanol (b), melamine in ethanol (c), and melamine in pyridine (d).

6.4.2 Effect of growth time

In order to understand the formation process of different hierarchies of the multi-level branched CNTs, effect of growth time was investigated. Figure 6.5 shows the cross-sectional SEM images of the nanotubes with the growth time of 10, 20, 30, 40 and 60 min, respectively. In the reaction process, the carbonaceous liquid mixed with catalyst particles was pulverized over the substrate at low rates. Initially, the catalyst particles adhered to the substrate and formed catalyst clusters. Carbon and nitrogen species absorption and precipitation promoted the nanotube growth. In short time, the density of

catalyst particles became large enough to form aligned multiwall nanotubes. Figure 6.5a shows the initial growth stage of the nanotubes at the growth time of 10 min. The nanotubes are dense, short, and thin. The average length of the nanotubes is around 100 nm, though some longer leading nanotubes are also observed. The diameter of the nanotubes in this stage is around 10 nm, which is equivalent to the size of the first-level branched nanotubes, as observed in Figure 6.3d. With time, continuous feeding of catalyst made the original catalyst particles larger on the substrate and caused an increased diameter of the CNTs. The catalyst particles not only enlarged in volume, but also became closer to each other. Moreover, confining the catalyst particles into the formed CNTs resulted in the elongation of the catalyst particles and the formation of catalyst rods with conical shape. The different diffusion distances of carbon and nitrogen species along the conical catalyst rods raised the probability of defect occurrence. This was reflected by the different thickness of the CNT walls around the catalyst rod. In this way, the obstacle of the nanotube walls between adjacent catalyst particles was overcome, promoting the coalescence and the junction formation. The coalescence of three or more particles caused the formation of multi-terminal branched junctions. Figure 6.5b shows the picture of the nanotubes at the growth time of 20 min. The diameter of the bottom part of the nanotubes becomes thicker and junctions of branched structures appear, implying later formation of the bottom nanotubes. This can be attributed to the mergence of the thinner nanotubes due to the aggregation of the catalyst particles, which witnesses the base growth mode of the branched nanotubes (corresponding to second generation).

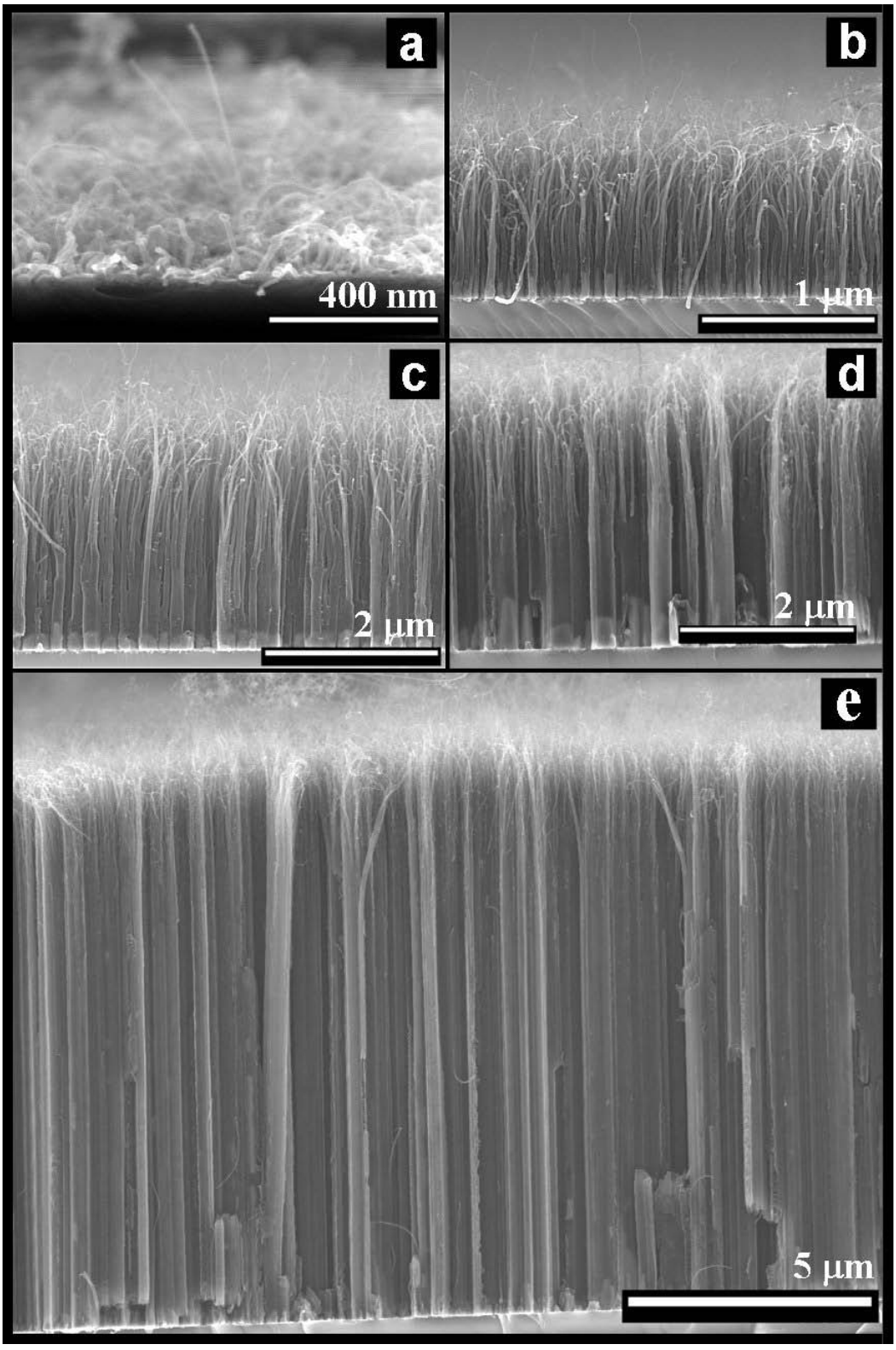

Figure 6.5 SEM images of the CNTs obtained after a growth time of 10 min (a), 20 min (b), 30 min (c), 40 min (d), and 60 min (e).

Figure 6.5c shows the SEM image at the growth time of 30 min. A further increase of the catalyst particle size can be seen, and new level thicker nanotubes are observed at the same height due to aggregation of the catalyst particles (third generation – formation in the end). With a further increase of the growth time to 40 min, as shown in Figure 6.5d, the stalk nanotubes are unable to form further branches, which may be due to their large diameters, thick walls, and strong adhesion to the substrate. As shown in Figure 6.5e, which presents the SEM image of the nanotubes with the growth time of 60 min, no further branch is observed.

6.4.3 Effect of precursor flow rate

Usually, precursor flow rate over 0.1 ml/min is used for growing carbon nanotubes in a spray pyrolysis method. In our experiments, it has been found that a lower flow rate favored the formation of branched CNTs. As shown in Figure 6.6a, the branched nanotubes with length of 4.5 μm and stalk part of approximately 2.1 μm were obtained at a precursor flow rate of 0.02 ml/min. The diameters of the stalk nanotube ranged from 147 nm to 450 nm. The number of the branches connected to one stalk nanotube could reach 17 branches on average and a maximum of 30 branches. A higher precursor flow rate of 0.06 ml/min, as shown in Figure 6.6b, gave shorter branched nanotubes with the whole length of 3.1 μm and a stalk length of about 1.3 μm. At this flow rate, the diameter of the stalk nanotubes and the number of nanotubes generated by a stalk remained almost unchanged based on the cross sectional view of SEM image.

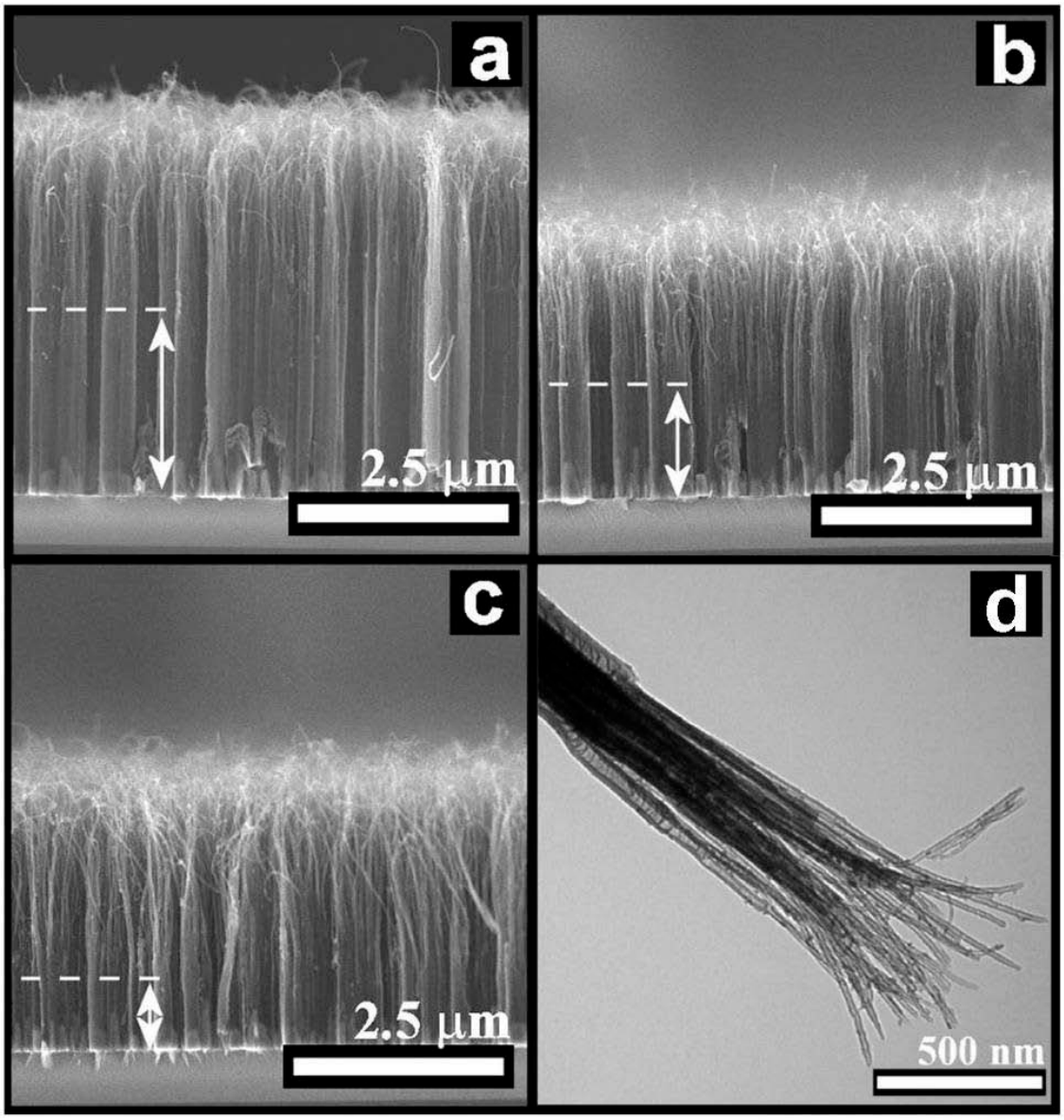

Figure 6.6 SEM images of the branched nanotubes obtained at different precursor flow rates: 0.02 ml/min (a), 0.06 ml/min (b), and 0.1 ml/min (c). TEM image of the branched nanotubes showing the amount of branches derived from a single stalk nanotube obtained at a flow rate of 0.06 ml/min (d).

When the precursor flow rate was increased to 0.1 ml/min, as shown in Figure 6.6c, evident change of the branch density was observed. The average number of the nanotubes

connected to one stalk nanotube decreased to 9 branches. Compared to the sample with the flow rate of 0.06 ml/min, the nanotubes using the flow rate of 0.1ml/min do not present evident change in the total length, but much shorter stalk nanotubes of 0.8 μm. The diameter of the stalk nanotubes decreased and ranged between 97 nm and 211 nm. TEM image in Figure 6.6d clearly demonstrates the amount of the branches from a single stalk nanotube obtained at a rate of 0.06 ml/min. It indicates that the density of the branches from a single stalk nanotube may be adjusted to some extent by tuning the flow rate of the spray.

6.4.4 Effect of catalyst concentration

In our experiments, ferrocene was used as the catalyst for the nanotube growth. It has been found that the amount of ferrocene can evidently affect the branching behavior of the nanotube growth. The optimized concentration for the branched structure growth was 3.0 wt% ferrocene in acetonitrile. No obvious changes were observed for a higher concentration of ferrocene (3.5 wt%, not shown). By decreasing the ferrocene concentration to 2.5 wt%, nanotubes with a longer length of 6 μm and smaller stalk diameter of 200 nm were obtained (Figure 6.7a). The branched nanostructure is still visible (Figure 6.7b).

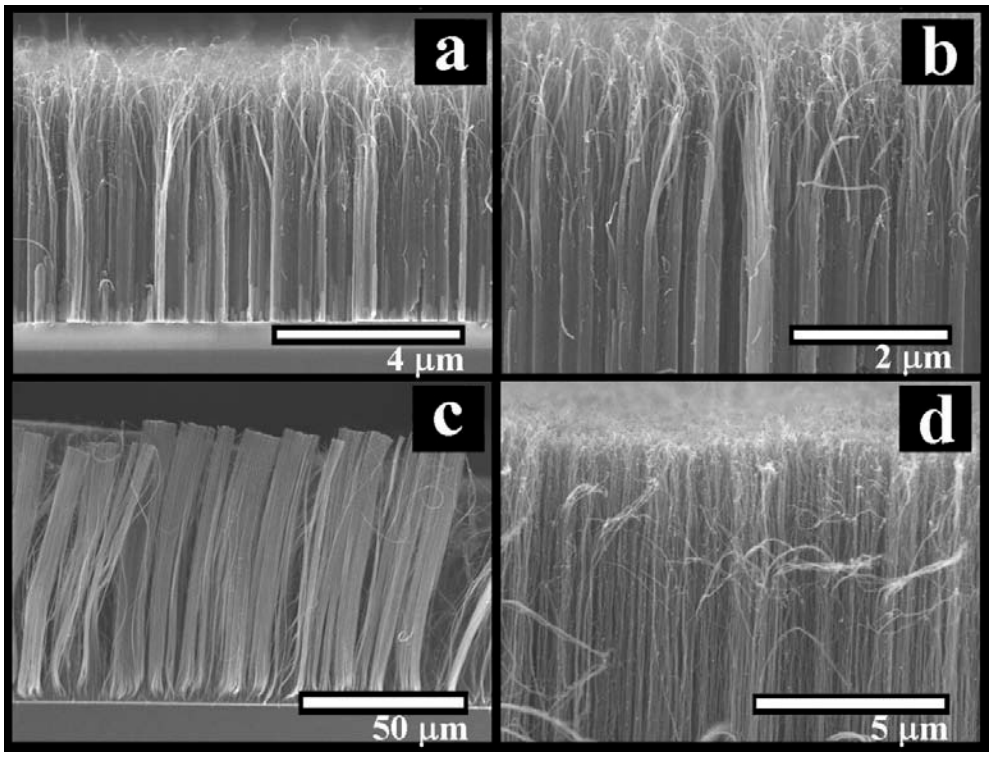

Figure 6.7 SEM images of the CNTs using different concentrations of ferrocene: 2.5 wt% (a) and (b), 0.5 wt% (c) and (d).

The branched structures almost disappeared for a further decrease of the ferrocene concentration down to 0.5 wt%. The nanotubes became much longer (Figure 6.7c) and thinner (Figure 6.7d), with the length of 70 μm and diameter of 45 nm (based on magnified SEM observation, not shown here).

6.4.5 Effect of temperature

The optimized temperature for growing multi-level hierarchical carbon nanotubes was 700 °C. The structure could not be produced at a lower temperature (650 °C - not

shown). By increasing the temperature to 800 °C, the length of the nanostructure increased to around 15 μm (Figure 6.8a).

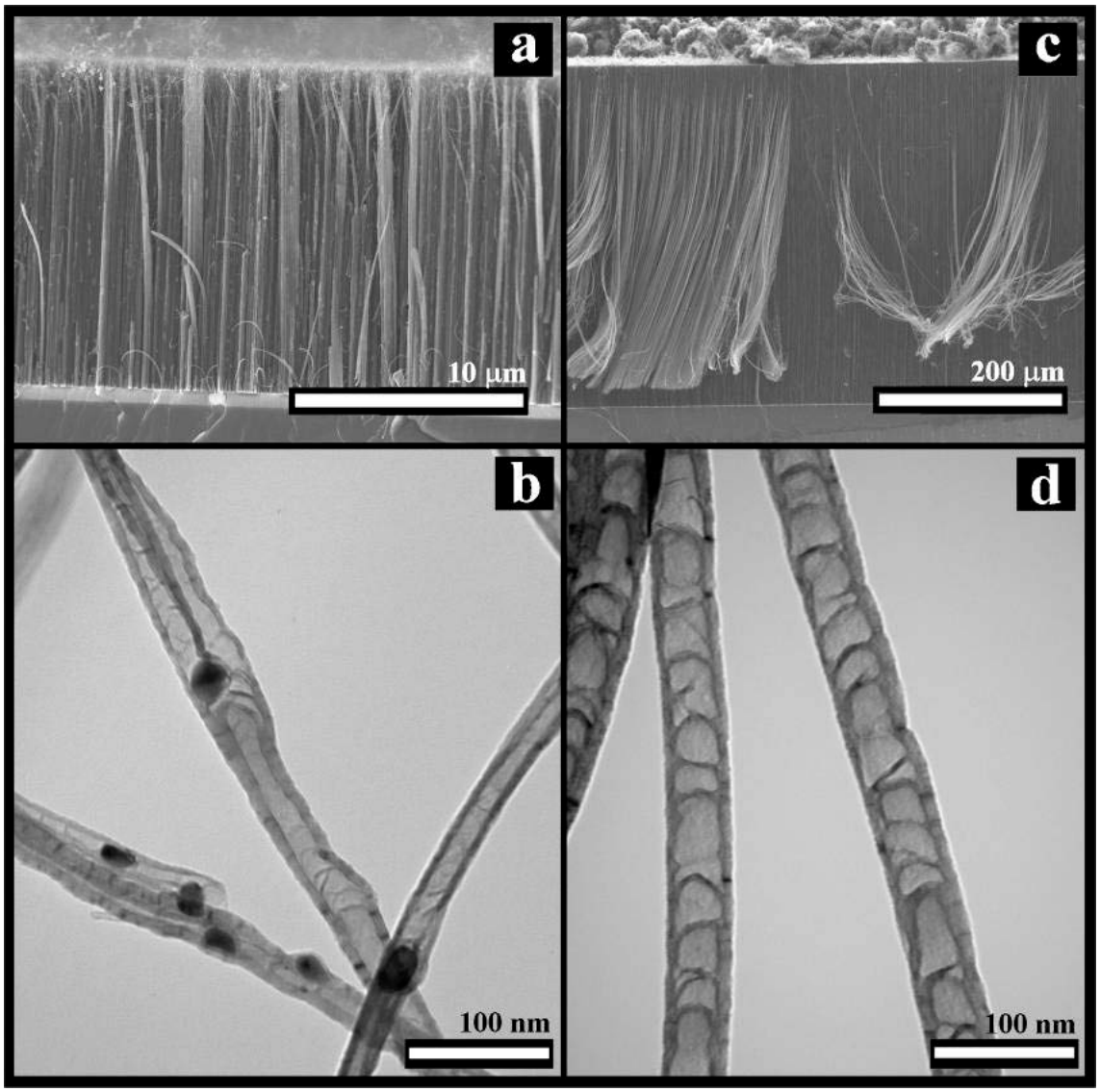

Figure 6.8 SEM (a) and TEM (b) images of the CNTs deposited at 800 °C; SEM (c) and TEM (d) images of the CNTs deposited at 900 °C.

The obtained nanotubes had the diameter around 80 nm and presented fewer branches (Figure 6.8b). With further increase of the growth temperature to 900 °C, the length of

the nanotubes increased to 380 μm (Figure 6.8c). The branched structure disappeared and only nanotubes with a diameter of 50 nm were formed (Figure 6.8d).

6.4.6 Effect of substrates

We assumed that the low roughness of the silicon wafer might contribute to the aggregation of catalyst particles and thereby trigger the formation of branched nanotubes. To compare the effect of substrates, a carbon paper substrate composed of rod-like carbon fibers (5-10 μm in diameter) with rough surface was used to replace the silicon wafer, keeping other synthesis parameters the same. Figure 6.9 shows SEM images of the nanotubes grown on the carbon paper. Much less and irregular branched nanotubes are observed, which may be due to lower mobility of the catalyst particles on the rough substrate.

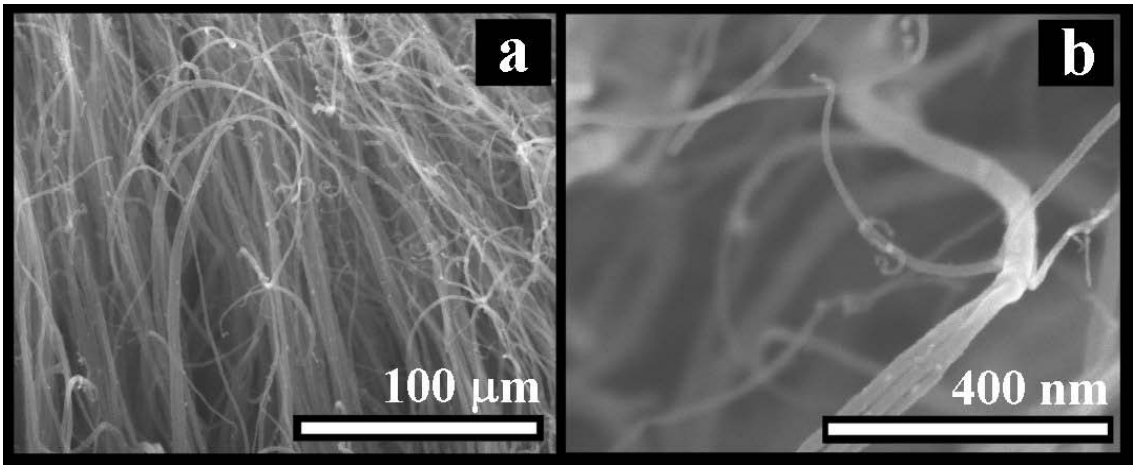

Figure 6.9 SEM images of the CNTs grown on the carbon paper substrate at low magnification (a) and high magnification (b).

6.4.7 Growth Mechanism

It has been observed that the catalyst particles were located at the base of the nanotubes and no catalyst could be found on the tip of the first-level nanotubes, suggesting that the growth mechanism followed a base growth mode. Based on these observations and the synthesis conditions, a formation mechanism of branched and multi-level CNTs is proposed.

1) The decomposition of acetonitrile/ferrocene droplets by spray pyrolysis produces Fe clusters on the substrate and an atmosphere rich in C_xH_y, CN_x species, N_2, and H_2 molecules. Fe clusters adhere to the substrate, start to form nanoparticles, and react with C_xH_y, CN_x species, and N_2 molecules (Figure 6.10a).

2) C and CN_x species are absorbed and precipitate on the Fe catalyst particles to form individual capped CNTs. The small and reactive metal particles give a strong interaction with precipitated species and form a graphene cap that stops the carbon source flux over the catalyst. The carbon source can be provided only at the catalyst/substrate interface along with more catalyst particles. The Fe particle density and adhesion to the substrate are large enough to sustain vertically aligned nanotubes and a base type growth (Figure 6.10b).

3) During the CNT growth, elongation of the catalyst particle increases its strain energy. This results in pushing the capped nanotubes away from the substrate and in forming bamboo structures. Continuing spraying the precursors at low rates increases the catalyst size and, consequently, the diameter of the formed CNTs is gradually increased (Figure 6.10c). This leads to the generation of the first-level CNTs.

4) At this stage, the flow fluctuations around the substrate are large enough to overcome the adhesion from the substrate and promote the coalescence of adjacent catalyst particles. The coalescence happens when the interaction between the catalyst particles with larger diameter is enhanced due to surface tensions. After the Fe catalyst particles become larger, the CNTs with larger diameter are formed (Figure 6.10d). This results in the production of the second-level CNTs.

5) Following the similar process, the third-level CNTs is formed (Figure 6.10e).

6) By continuing the growth process, the stalk nanotubes are unable to generate further branches due to their large diameters, thick walls, and strong adhesion to the substrate, leaving the branch formation at the same distance from the substrate.

This structure presents several important characteristics: 1) the stalk nanotube has a large diameter; 2) the branch formation occurs at the same distance from the substrate; 3) it has large numbers of branched junctions.

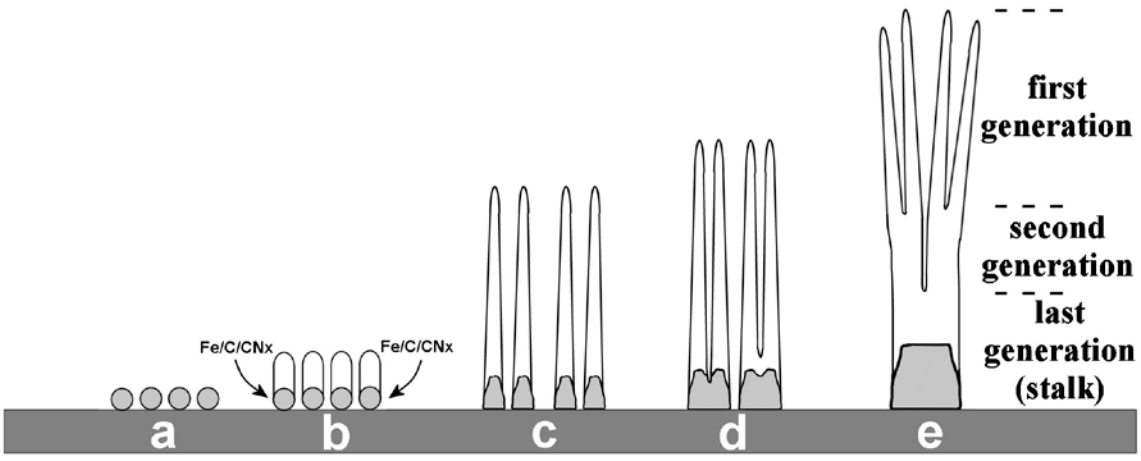

Figure 6.10 Schematic diagram of the growth mechanism of the multi-level N-doped carbon nanotubes.

6.5 Conclusions

We have, for the first time, successfully synthesized multi-level hierarchical nitrogen-doped carbon nanotubes by a highly controlled spray pyrolysis chemical vapor deposition method. The mean diameter of the CNTs from the first-level to the final-level changes from 10 nm to 210 nm. The formation mechanism of the multi-level hierarchical CNTs can be attributed to the coalescence of the catalyst particles on the substrate during the growth process. The new findings of this study can be summarized as following:

1) Multi-level hierarchical carbon nanotubes can be controllably obtained by spray pyrolysis chemical vapor deposition method.

2) Depending on the diameter of the stalk nanotubes, up to 30 branches can be generated from a single stalk nanotube, showing novel structure compared to the previous branched CNTs. To the best of our knowledge, it is reported for the first time that such a large number of branched CNTs can be generated from a single stalk CNT.

3) The critical point of transition from branched nanotubes to stalk nanotubes can be well controlled at the same spatial level.

4) A finite regulation of the branches in density can be realized by tuning the precursor flow rate.

5) The growth mechanism of the multi-level branched CNTs may follow a base-growth mode, which can be evidenced by the morphology and size changes of the CNTs with the growth time.

Effects of various parameters on the growth of the branched CNTs have been systematically investigated, such as precursor and substrate type, growth time, catalyst

concentration, temperature, and flow rate of the active solution. The multiple-level hierarchical nitrogen-doped carbon nanotubes may have potential applications for electronic and nanoenergetic materials.

6.6 References

[1]S.J. Tans, A.R.M. Verschueren, and C. Dekker, "Room-temperature transistor based on a single carbon nanotube," *Nature*, vol. 393, May. 1998, pp. 49-52.

[2]Jing Kong, N. Franklin, Chongwu Zhou, M. Chapline, Shu Peng, Kyeongjae Cho, and Hongjie Dai, "Nanotube molecular wires as chemical sensors," *Science*, vol. 287, Jan. 2000, pp. 622-625.

[3]T. Rueckes, K. Kim, E. Joselevich, G. Tseng, C. Cheung, and C. Lieber, "Carbon nanotube-based nonvolatile random access memory for molecular computing," *Science*, vol. 289, Jul. 2000, pp. 94-97.

[4]H. Postma, T. Teepen, Zhen Yao, M. Grifoni, and G. Dekker, "Carbon nanotube single-electron transistors at room temperature," *Science*, vol. 293, Jul. 2001, pp. 76-79.

[5]D. Wei and Y. Liu, "The intramolecular junctions of carbon nanotubes," *Advanced Materials*, vol. 20, 2008, pp. 2815-2841.

[6]F. Kim, S. Kwan, J. Akana, and P. Yang, "Langmuir-Blodgett nanorod assembly," *Journal of the American Chemical Society*, vol. 123, 2001, pp. 4360-4361.

[7]Yu Huang, Xiangfeng Duan, Qingqiao Wei, and C. Lieber, "Directed assembly of one-dimensional nanostructures into functional networks," *Science*, vol. 291, Jan. 2001, pp. 630-633.

[8]Dongmok Whang, Song Jin, Yue Wu, and C. Lieber, "Large-scale hierarchical organization of nanowire arrays for integrated nanosystems," *Nano Letters*, vol. 3, Sep. 2003, pp. 1255-1259.

[9]S.G. Rao, L. Huang, W. Setyawan, and S. Hong, "Large-scale assembly of carbon nanotubes," *Nature*, vol. 425, 2003, pp. 36-37.

[10] A.M. Song, A. Lorke, A. Kriele, J.P. Kotthaus, W. Wegscheider, and M. Bichler, “Nonlinear Electron Transport in an Asymmetric Microjunction: A Ballistic Rectifier,” *Physical Review Letters*, vol. 80, Apr. 1998, pp. 3831-3834.

[11] S. Reitzenstein, L. Worschech, P. Hartmann, M. Kamp, and A. Forchel, “Capacitive-Coupling-Enhanced Switching Gain in an Electron Y-Branch Switch,” *Physical Review Letters*, vol. 89, Nov. 2002, pp. 226804-226804-4.

[12] S. Ami and C. Joachim, “Intramolecular circuits connected to N electrodes using a scattering matrix approach,” *Physical Review B*, vol. 65, Apr. 2002, pp. 155419-155419-155414.

[13] D. Zhou and S. Seraphin, “Complex branching phenomena in the growth of carbon nanotubes,” *Chemical Physics Letters*, vol. 238, Jun. 1995, pp. 286-289.

[14] J. Li, C. Papadopoulos, and J. Xu, “Growing Y-junction carbon nanotubes,” *Nature*, vol. 402, 1999, pp. 253-254.

[15] G. Meng, Y.J. Jung, A. Cao, R. Vajtai, and P.M. Ajayan, “Controlled fabrication of hierarchically branched nanopores, nanotubes, and nanowires,” *Proceedings of the National Academy of Sciences of the United States of America*, vol. 102, May. 2005, pp. 7074 -7078.

[16] M. Terrones, F. Banhart, N. Grobert, J. Charlier, H. Terrones, and P.M. Ajayan, “Molecular Junctions by Joining Single-Walled Carbon Nanotubes,” *Physical Review Letters*, vol. 89, Jul. 2002, pp. 075505-075505-4.

[17] N. Gothard, C. Daraio, J. Gaillard, R. Zidan, S. Jin, and A.M. Rao, “Controlled Growth of Y-Junction Nanotubes Using Ti-Doped Vapor Catalyst,” *Nano Letters*, vol. 4, Feb. 2004, pp. 213-217.

[18] J.F. AuBuchon, L. Chen, C. Daraio, and S. Jin, “Multibranching Carbon Nanotubes via Self-Seeded Catalysts,” *Nano Letters*, vol. 6, Feb. 2006, pp. 324-328.

[19] D. Wei, Y. Liu, L. Cao, L. Fu, X. Li, Y. Wang, G. Yu, and D. Zhu, “A New Method to Synthesize Complicated Multibranched Carbon Nanotubes with Controlled Architecture and Composition,” *Nano Letters*, vol. 6, Feb. 2006, pp. 186-192.

[20] J. Su, Y. Yu, and R. Che, “Aligned array of N2-encapsulated multilevel branched carbon nanotubes,” *Applied Physics A: Materials Science Processing*, vol. 90, Jan. 2008, pp. 135-139.

CHAPTER 7

SELECTIVE GROWTH, CHARACTERIZATION, AND FIELD EMISSION PERFORMANCE OF SINGLE-WALLED AND FEW-WALLED CARBON NANOTUBES BY PLASMA ENHANCED CHEMICAL VAPOR DEPOSITION

7.1 Abstract

Single-walled carbon nanotubes (SWCNTs) and few-walled carbon nanotubes (FWCNTs) have been selectively synthesized by plasma enhanced chemical vapor deposition at a relative low temperature (550 ^{o}C) by tuning the thickness of iron catalyst. The parametric study and the optimization of the nanotube growth were undertaken by varying inductive power, temperature, catalyst thickness, and plasma to substrate distance. When an iron film of 3-5 nm represented the catalyst thickness for growing FWCNT arrays, SWCNTs were synthesized by decreasing the catalyst thickness to 1 nm. The nanotubes were characterized by field emission scanning electron microscopy, transmission electron microscopy, and Raman spectroscopy. Electron field emission properties of the nanotubes indicate that the SWCNTs exhibit lower turn-on field and higher field emission β factor compared to the FWCNTs, implying better field emission performance.

7.2 Introduction

Carbon nanotubes (CNTs) have drawn considerable attention for researchers due to their outstanding electrical, mechanical and optical properties [1-4] which lead to numerous applications of nanotubes as nanodevice components. Currently, various methods have been implemented to enable carbon nanotube synthesis such as arc discharge [5, 6], laser ablation [7], and catalytic chemical vapor deposition [8]. The chemical vapor deposition (CVD) provides a reliable approach to grow nanotubes on different substrates and is suitable for scaled growth of high purity multi-walled and singled-walled carbon nanotubes. In addition, CVD operates at substantially lower temperature than that in laser ablation and arc discharge processes [9].

In terms of applications of carbon nanotubes in semiconductor technology, vertically aligned CNTs exhibit potential applicability in electronics such as sensors [10, 11], field emission devices [12], transistors, and logic circuits [13-15]. Therefore, in order to promote the development of nanotube devices integrated in silicon technology, it is essential to explore the synthesis and the assembly of vertical CNT arrays at low temperatures, on silicon substrates. Compared to the commonly-used thermal chemical vapor deposition [16, 17], plasma enhanced chemical vapor deposition (PECVD) presents significant advantages in terms of favouring vertically aligned growth of carbon nanotubes at low temperatures due to efficiency of precursor decomposition in the plasma sheath. Moreover, this procedure is compatible with the integrated circuits manufacturing process [18-21]. Despite successful development of PECVD using various plasma sources such as inductive coupled radio frequency, microwave, and direct current, there

are still some issues to be addressed. Preventing the catalyst nanoparticles from agglomeration, maintaining the catalytic activity during the growth process, and abatement of ion damage to both catalyst nanoparticles and growing CNTs, are main requirements for PECVD methods [22, 23]. One strategy in overcoming these problems is to generate plasma away from the substrate. This procedure reduces the plasma ion bombardment on the substrate and growing tubes [24]. However, detailed understanding of parametric effect on substrates exposed to the discharge is far from being achieved. Moreover, the reduction of synthesis temperature down to 500 °C is still a challenging task. Taking these into account and the fact that the inductive coupled plasma (IPC) sources can generate homogenous and stable plasma for uniform deposition, we proposed generating plasma away from the substrate for depositing vertically aligned carbon nanotubes (VA-CNTs). Recent studies have shown that CNTs have good electron field emission performances [25-27]. Many groups focused on vertically well-aligned multi-walled CNTs because of the difficulty to obtain well-aligned SWCNTs arrays. Moreover, previous comparisons of field emission for FWCNTs and SWCNTs are rare, most of which investigated field emission of MWCNTs and SWCNTs obtained by different synthesis procedures [28, 29].

In this paper we have systematically investigated the effects of the growth parameters on CNT synthesis. By controlling the plasma conditions during the growth process, vertically aligned SWCNTs and FWCNTs have been selectively synthesized by tuning the thickness of catalyst at low substrate temperatures. Field emission properties of the SWCNTs and FWCNTs indicate that both types of the nanotubes are potential

candidates for field emission applications, and the SWCNTs promise better field emission performance.

7.3 Experimental

The VA-CNTs were synthesized using the PECVD system schematically illustrated in Figure 7.1. The plasma discharge source was controlled in inductively coupled mode and consisted of a copper coil wound around the outside of one inch quartz tube coupled with the feed-gas entrance (A). The inductive coil, powered by a 13.56 MHz RF generator (max 300 W), was connected to a matching network (B). The position of substrates along the axis of the quartz tube was set by a moving substrate holder. The substrates (up to 2 inch in diameter), attached to a resistive heating element, were placed at different distances from the plasma source by a vertical movement device (C). A thermocouple, implanted into the substrate holder, was used to calibrate and monitor the growth temperature. The assembly acted like a remote plasma reactor as no direct contact is between the plasma and the substrate. The system design allowed a minimum substrate to plasma distance of 8 cm. Mass flow controllers (D) were utilized to control the gas feeding directly into the plasma source. The deposition pressure was obtained by a vacuum pump (E), measured with a vacuum transducer (F), and controlled by either an electronic or a manual valve. For catalyst and/or under-layer material deposition the system was equipped with magnetron sputtering guns (G).

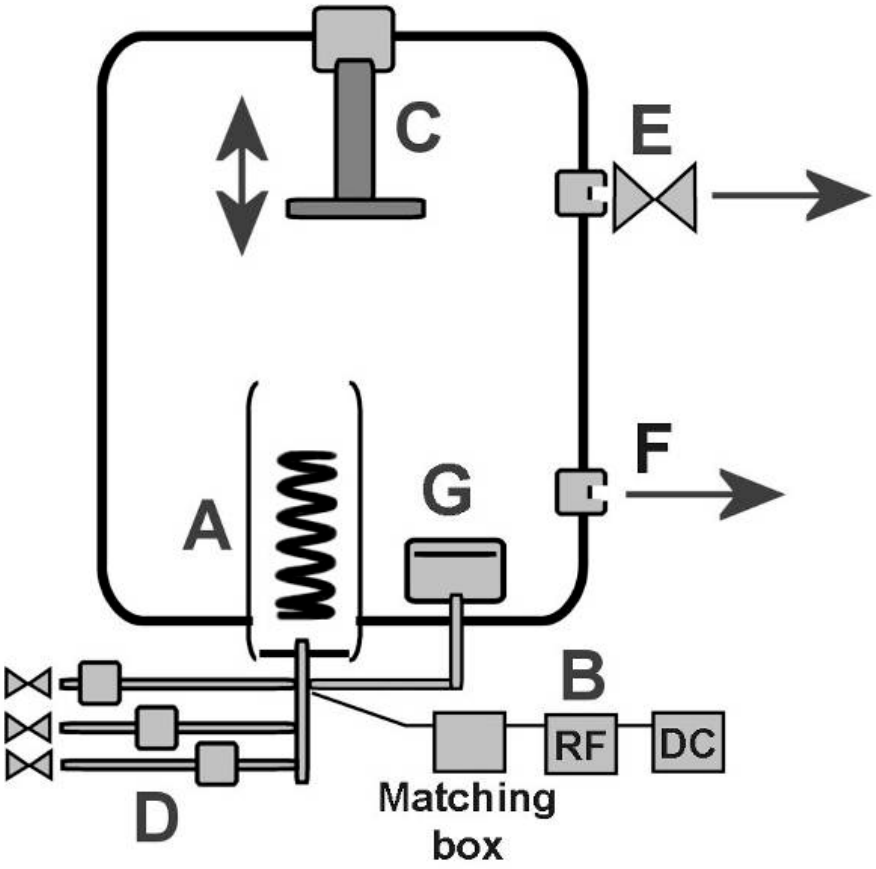

Figure 7.1 Schematic diagram of PECVD deposition system – RF plasma source (A); matching box, and generators (B); substrate heating element with vertical movement (C); mass flow controller for gas inlets (D); connection to vacuum pump (E); connection to vacuum gauge (F); magnetron (G).

In this study, oriented n-type (1, 0, 0) silicon (Si) wafers were used as a substrate, without removing the native oxide layer. The reactor was continuously flushed with argon during loading and unloading of samples. The growth process could be divided into two main steps: the physical vapor deposition (PVD) of the catalyst followed by the PECVD growth of CNTs, without breaking the vacuum. In the first step, using magnetron

sputtering, a 30nm-aluminum (Al) under-layer was deposited on the Si substrate followed by sputtering iron (Fe) catalyst film. The thickness was monitored by a quartz crystal microbalance and the catalyst film was in the range of 0.5–7 nm. The aluminum film was used to effectively prevent the Fe catalyst particles from aggregation. For the second step, the pressure was increased to about 0.1 Torr and the substrate stage was heated up to the desirable temperature, allowing 10 minutes for temperature equilibration. Then the hydrogen–methane gas mixture (H_2:CH_4 = 1:11, total flow rate = 60 sccm) was admitted and the reactor pressure was set to 2 Torr. The inductive power to the coil was turned on, and plasma was ignited. After 15 min of growth time, the reactor was allowed to cool down under vacuum before exposure to air. For the optimization of growth conditions, one of the following parameters was varied while keeping the other parameters fixed. The optimum conditions were: 550 °C of the growth temperature, 200 W of the inductive power, and 10 cm of the substrate to plasma distance. The samples were characterized by scanning electron microscopy (SEM - Hitachi S-4800), Raman spectroscopy (Renishaw Raman spectrometer with laser excitation wavelength of 785 nm), and transmission electron microscopy (TEM - JEOL 2010F). The TEM samples were prepared by sonicating a small piece of as-grown nanotubes in ethanol for 10 min and drying few drops of suspension on a Cu micro-grid. Field emission performance of the samples was studied in a vacuum system with a base pressure of 10^{-6} Torr. The field emission curves were obtained using a digital multimeter (Agilent 34410A). The measurements were carried out in a planar diode configuration with 34.2 mm^2 active area and with the anode to sample spacing of 200 μm. A glass plate, covered by a layer of indium-tin-oxide (ITO) thin film, was used as anode to collect the emitted electrons.

7.4 Results and discussion

The parametric study for this work evolved from efforts to obtain vertically oriented nanotubes with a narrow diameter distribution at relatively low temperatures. It involved perturbation of substrate temperature, plasma power, substrate distance, and catalyst thickness while keeping other parameters fixed as described in the experimental.

7.4.1 Influence of substrate temperature

In this study, nanotubes were grown at deposition temperatures in the range of 400-700 °C while all other parameters were kept constant. The plasma-heating effect could be ignored in these experiments, as the plasma was operated at moderate gas pressures [22] and large plasma to substrate distances. This aspect was verified by a thermocouple located directly under the sample holder. At 400 °C no deposit was found on the substrate. Figure 7.2 shows SEM images for the nanotubes grown at 450 °C, 550 °C, and 700 °C respectively, for 15 min. The CNTs produced at 450 °C were vertically aligned, uniform in size, with a length of 3 μm (Figure 7.2a-b). Compared with the results obtained at 550 °C (Figure 7.2c-d), the tubes were much shorter, less dense, and larger in diameter. Considering the facts that no deposit occurred at 400 °C and plasma power was unchanged for these experiments, it suggests that hydrocarbon gas decomposed insufficiently on the substrate at temperature below 450 °C and the catalyst particle activity was too low to trigger the growth of CNT array [30].

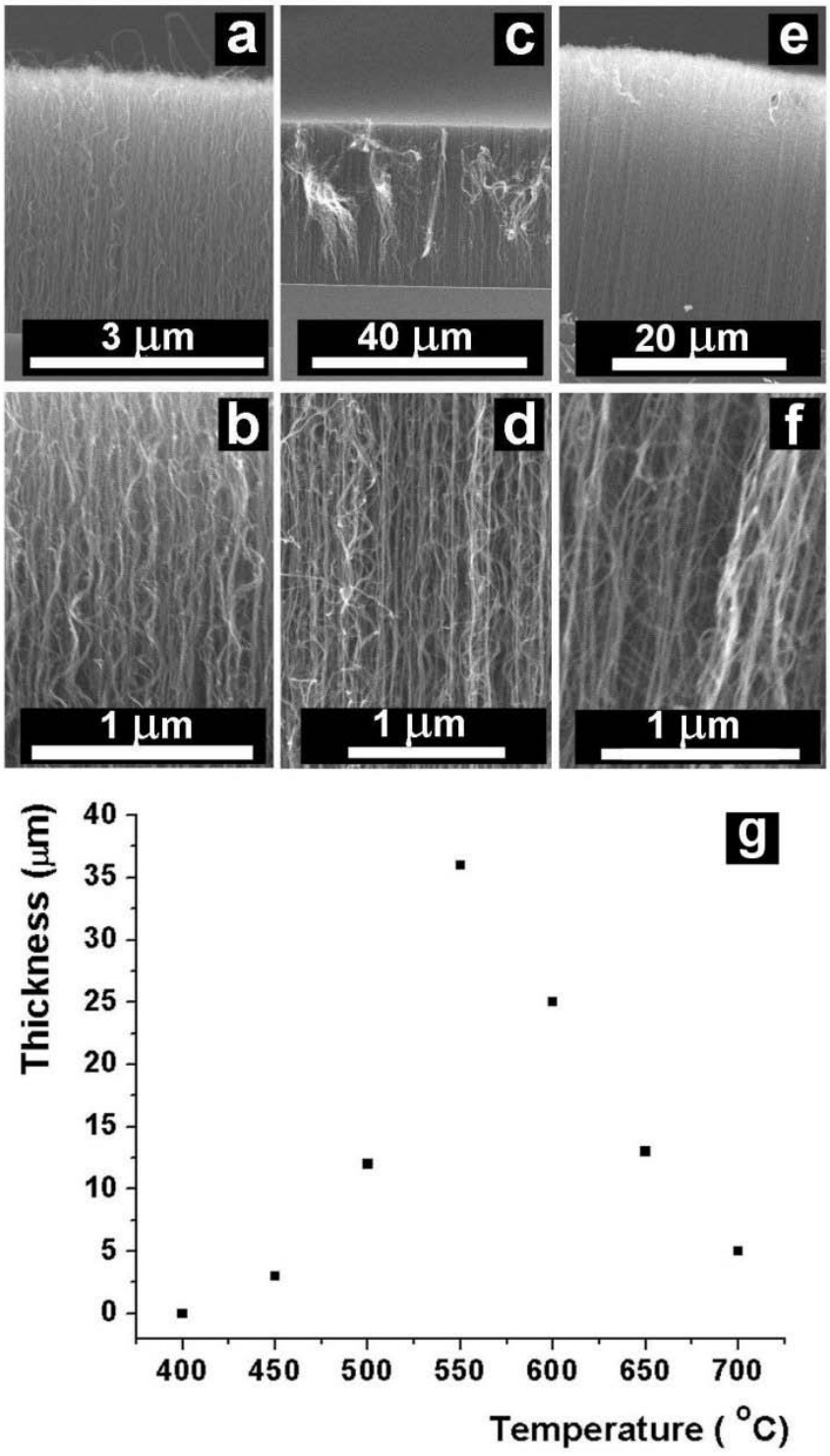

Figure 7.2 SEM images of the CNTs obtained at 450 °C (low magnification) (a); 450 °C (high magnification) (b); 550 °C (low magnification) (c); 550 °C (high magnification) (d); 700 °C (low magnification) (e); 700 °C (high magnification) (f); illustration of the average tube length with temperature (g).

The nanotubes grown at 550 °C were well-aligned and more uniform in diameter and height. The average tube length (Figure 7.2g) presented a maximum of 36 μm at this temperature. When the deposition temperature was increased to 700 °C, the process of catalyst etching and agglomeration was accelerated. As a result, shorter CNTs were grown with twist morphology, more disorders, and poorer uniformity in size (Figure 7.2e-f).

This systematic study demonstrated that quality VA-CNTs can be synthesized at relatively low temperatures. Even though the temperature as low as 450 °C was able to guarantee the achievement of CNT arrays, 550 °C was chosen as the optimum temperature in order to obtain well-aligned CNT arrays.

7.4.2 Influence of plasma power and substrate to plasma distance

Figure 7.3 shows SEM images and schematic growth rate of the nanotubes under different plasma powers. It can be seen that the nanotube growth rate increases with increasing plasma power (Figure 7.3a-b). This can be attributed to the fact that the increase of plasma power accelerated the decomposition of methane and, consequently, generated a larger amount of atomic hydrogen. In addition, the dehydrogenation of the adsorbed hydrocarbons and the carbon diffusion on the catalyst particles intensified and influenced the growth morphology [31-33]. At a low plasma power, less carbon species reacted with the catalyst particles to form nanotubes, reducing the growth rate, density, and alignment of CNTs (Figure 7.3a).

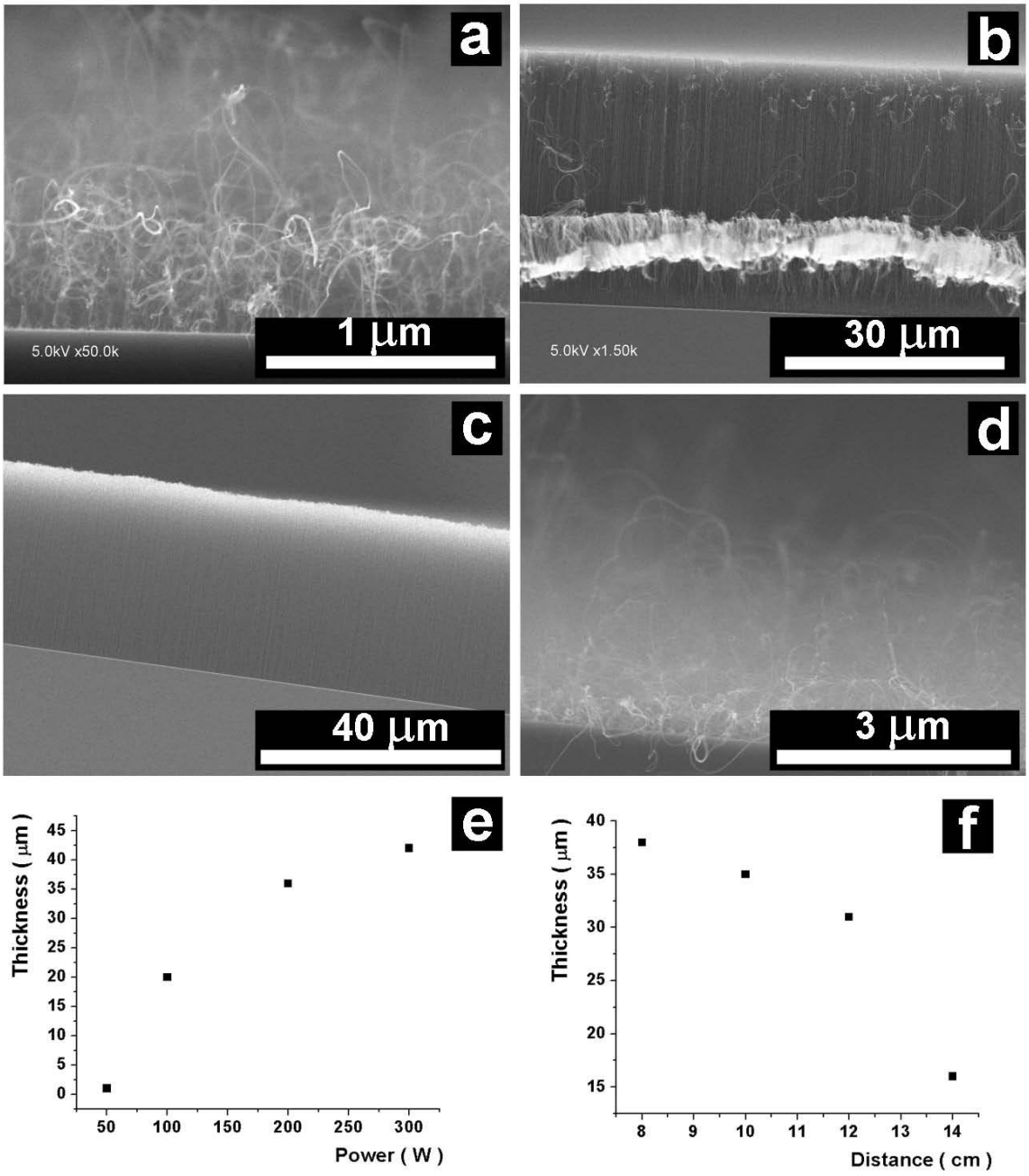

Figure 7.3 SEM images of the CNTs obtained at 50 W plasma power (a) and 300 W (b); plasma to substrate distance of minimum 8 cm (c), and 16 cm (d). Plots of average nanotube length vs. plasma power (e) and substrate to plasma distance (f).

The change of the distance between substrate and plasma had similar results (Figure 7.3c-d). As shown in Figure 7.3c, a short substrate to plasma distance of 8 cm produced long nanotubes. This growth was favoured by a high amount of atomic hydrogen and reactive carbon radicals in the proximity of catalyst surface. The atomic hydrogen made the catalyst particles active. By increasing the substrate to plasma distance to 16 cm, the carbon radicals formed in the plasma sheath recombined before reaching the catalyst particles, yielding insufficient growth, low density, and poor alignment of the nanotubes (Figure 7.3d). Figure 7.3e and Figure 7.3f present the average nanotube length as function of plasma power and substrate to plasma distance. The CNT length increased by intensifying the plasma power and by decreasing the substrate distance to plasma.

7.4.3 Influence of catalyst thickness

Size of catalyst particles has been shown to have a key role in controlling the tube diameter, length, and density in thermal CVD [34, 35]. In order to examine the effect of catalyst film thickness on the morphology of CNT arrays, different initial thicknesses of Fe films, between 0.5 nm and 7 nm, were implemented in the nanotube growth. To diminish the ion bombardment effect over the substrate, the plasma power was set as 200 W and the substrate to plasma distance was located at 10 cm. SEM micrographs of nanotubes grown on 7 nm-thick Fe film reveal that the tubes are tangled and not densely packed (Figure 7.4a-b). The wide diameter distribution can be attributed to the uneven fragmentation of the catalyst layer during the heating process [36].

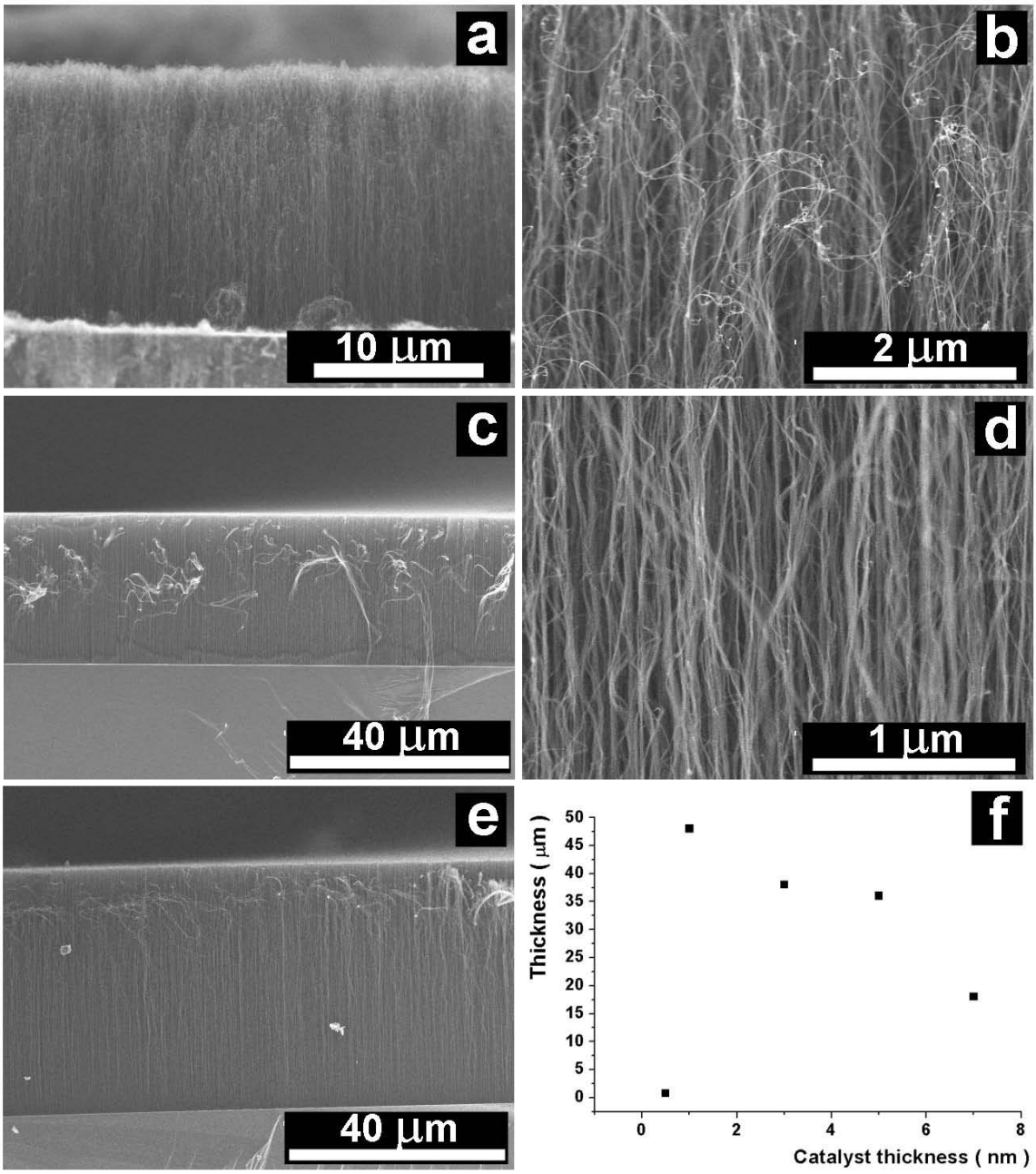

Figure 7.4 SEM images of the carbon nanotubes grown with the thickness of 7 nm Fe (low magnification) (a); 7 nm Fe (high magnification) (b); 3 nm Fe (low magnification) (c); 3 nm Fe (high magnification) (d); 1 nm Fe (e); A plot of CNT average thickness vs. catalyst thickness (f).

By decreasing the catalyst film thickness to 3 nm and 5 nm, the tubes became longer, aligned, uniform in height and diameter, as shown in Figure 7.4c-d. When the catalyst film thickness was down to 1 nm, thinner nanotubes were obtained with alignment and uniform size (Figure 7.4e). However, the nanotubes were so thin and sensitive to the electron beam of SEM that they were not able to be clearly imaged at high magnification. Figure 7.4f shows the influence of catalyst thickness on the length of the CNTs. Average CNT length increased by decreasing the catalyst thickness and reached a peak value (48 μm) when the thickness of Fe film was about 1 nm. For the catalyst film with the thickness of about 0.5 nm, no arrays were observed. The tubes were distorted and non-uniform in diameter. The suppression of CNT growth can be attributed to the reduced solubility of carbon in iron nanoparticles when the particle size is decreased [37]. It is also worth mentioning that no nanotube growth was observed in the absence of the catalyst film.

7.4.4 Structure characterization of FWCNTs and SWCNTs

A comprehensive investigation of the obtained nanotubes by TEM indicated that selective growth of FWCNTs and SWCNTs with uniform diameter could be realized by tuning the catalyst thickness based on optimized parameters. FWCNTs with outer diameter of 4-8 nm and inner diameter of about 2-5 nm could be obtained by using 3-5 nm thick iron catalyst layer, revealing relatively well defined graphitic shells parallel to

the tube axis (Figure 7.5a-b). The number of walls observed is in general between 3 and 6 walls.

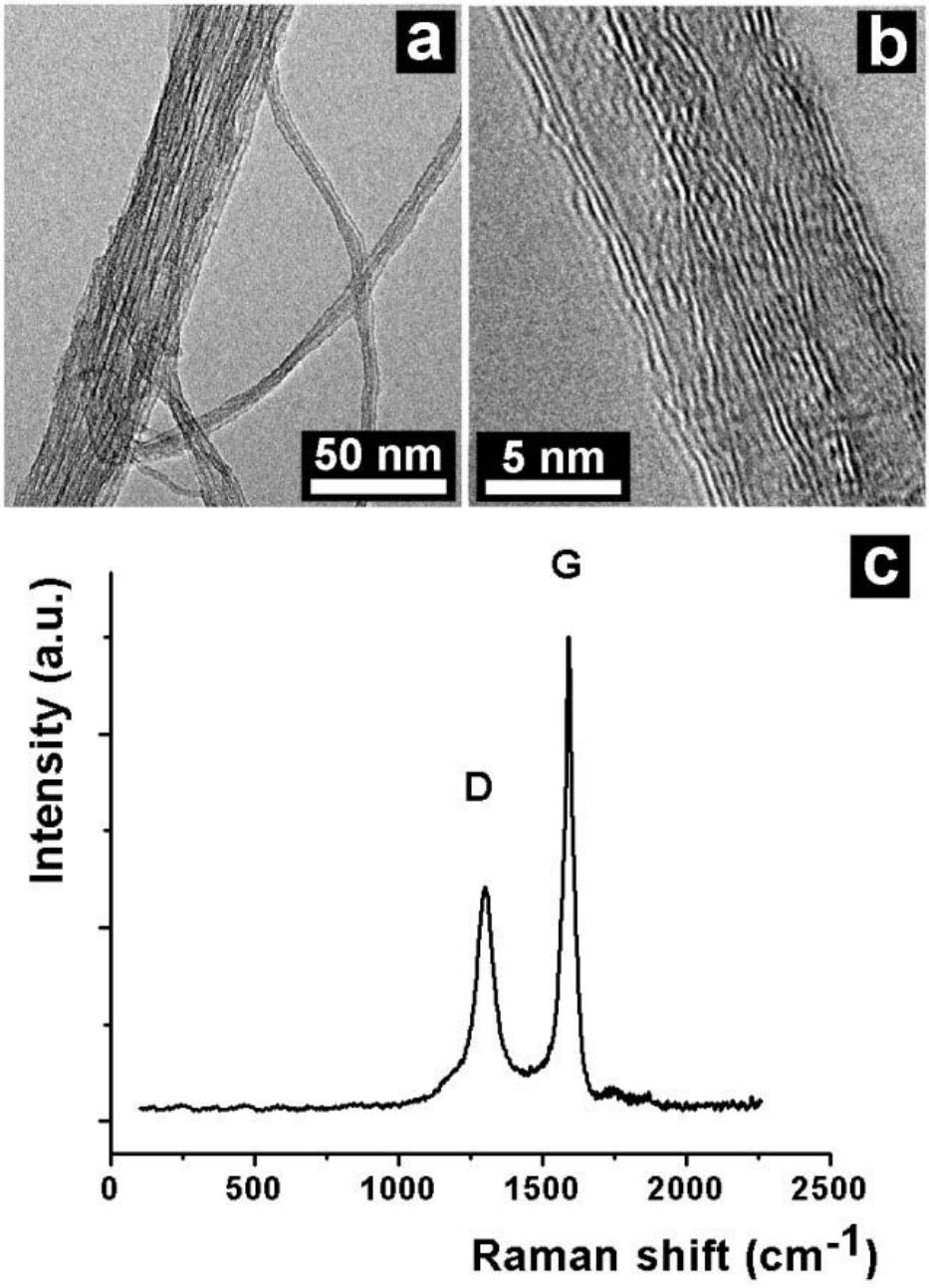

Figure 7.5 Characterization of the samples obtained for 3 nm catalyst thickness – Low magnification TEM image of the FWCNT bundles (a); Magnified TEM image of the FWCNTs (b); Raman spectrum of the FWCNTs (c).

Figure 7.5c shows Raman spectrum of the FWCNTs, in which radial breath modes (RBM) are absent and intensity of the D band relative to G band (I_D/I_G) is around 0.48. The disordered structure reflecting from the D band may originate from the defects and distortion of the graphene walls and from amorphous carbon on the nanotube surface. Figure 7.6 presents TEM images and Raman spectrum of the nanotubes with 1 nm thick Fe catalyst. The presence of CNT bundles is clearly visible while the tubes present a narrow diameter distribution in the range of 1-2 nm. The tubes have even diameters and appear clean and uncoated with amorphous carbon. The Raman spectrum with a clearly visible RBM region (Figure 7.6b) presents features related to a SWCNT spectrum. The RBMs (Figure 7.6c) reveal that the majority of peak positions are between 136 and 233 cm^{-1}. These correspond to tube diameters of 1.85 and 1.05 nm [38], which are consistent with the TEM observations. The spectrum in Figure 7.6d is acquired from a single bundle of nanotubes and shows an individual RBM peak at 233 cm^{-1}. This indicates a bundle of metallic-type SWCNTs. A lower I_D/I_G intensity ratio of 0.24 indicates a lower defect concentration within the SWCNTs compared to the FWCNTs. The results indicate that SWCNTs and FWCNTs can be selectively synthesized by tuning the catalyst thickness.

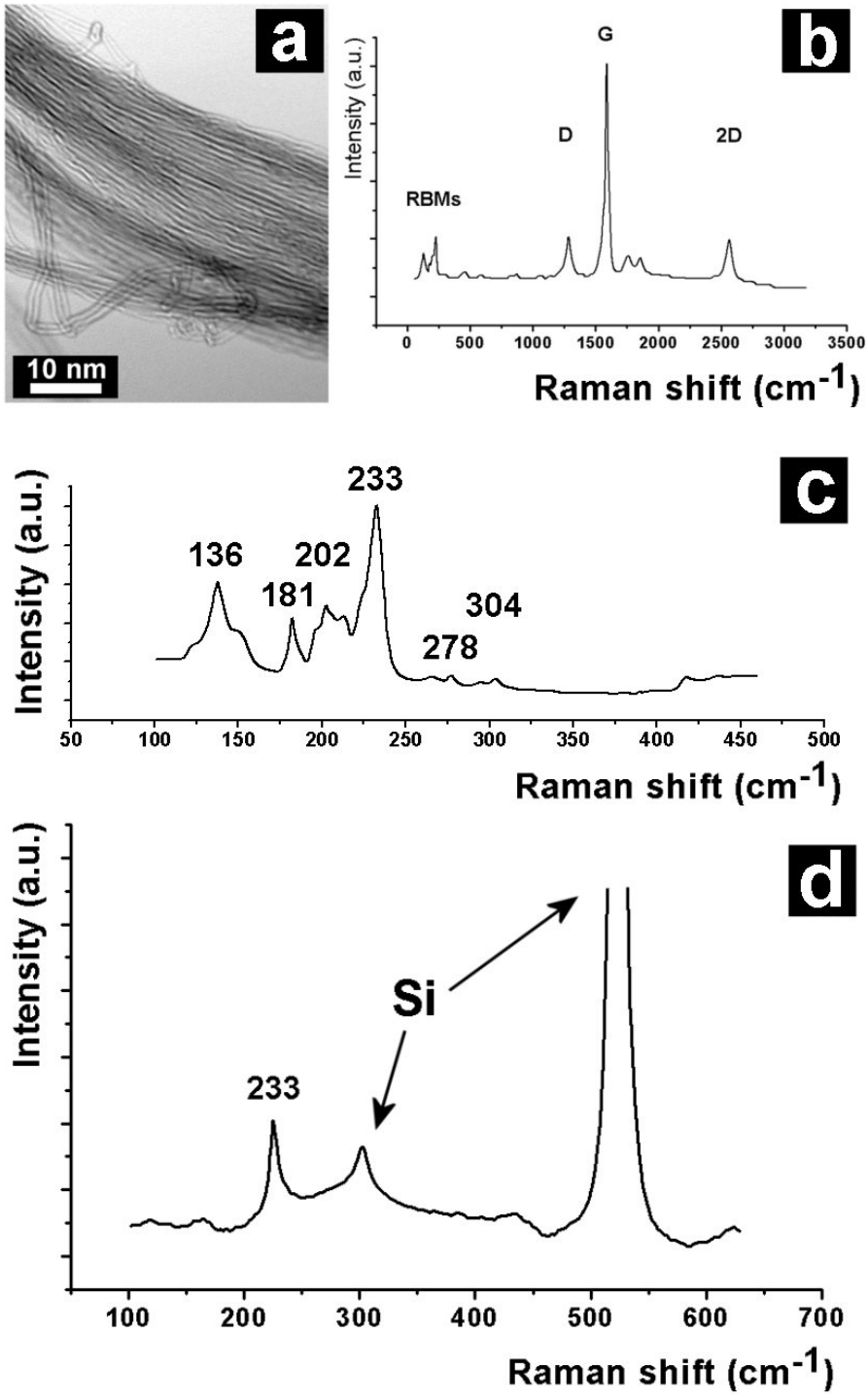

Figure 7.6 Characterization of the samples obtained for 1 nm catalyst thickness – TEM image of the nanotube bundles (a); Raman spectrum (b); RBM region (c); RBM from a single bundle of the CNTs (d).

7.4.5 Field emission performance of FWCNTs and SWCNTs

The correlation of current density versus electric field of the FWCNTs and SWCNTs is shown in Figure 7.7 along with linear Fowler-Nordheim plots, indicating field emission behaviour of both types of the nanotubes. The turn-on field, defined as the field under which a 10 $\mu A*cm^{-2}$ current density is extracted [25], was determined to be 0.417 $V*\mu m^{-1}$ and 1.237 $V*\mu m^{-1}$ for SWCNTs and FWCNTs, respectively. The current density of 1 mA/cm^2, required for most conventional flat panel displays, was determined to be achieved at field levels of 2.458 $V*\mu m^{-1}$ for FWCNTs and even at lower field levels of 0.938 $V*\mu m^{-1}$for SWCNTs. These findings imply that the obtained SWCNTs exhibit superior emission properties than the FWCNTs, and are in concordance with previously reports [28, 29].

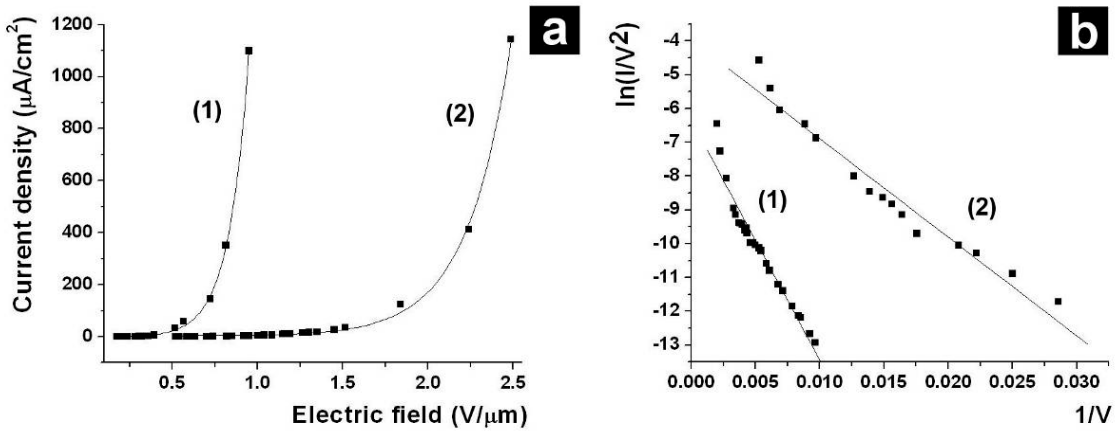

Figure 7.7 Curves of current density vs. electric field and Fowler-Nordheim plots for the SWCNTs (curve (1)) and for FWCNTs (curve (2)).

Figure 7.7b shows Fowler-Nordheim plots of the nanotubes. Fowler-Nordheim (F-N) equation is used as a mathematic interpretation of field emission for carbon nanotube arrays:

$$\ln(J/E^2) = \ln(A\beta^2/\phi) - B\phi^{3/2} / \beta E \qquad (1)$$

where J is the field emission current density in $A*cm^{-2}$, E the applied electric field in $V*cm^{-1}$, and ϕ is the work function of emitters in eV. The constants $A=1.54x10^{-6}$ $A*eV*V^{-2}$ and $B=6.83x10^3$ $eV^{-3/2}*V*mm^{-1}$ are derived from quantum statistics. β is the field enhancement factor and depends on the geometry and surface properties of CNT emitters. The slope of F-N equation is proportional to the field enhancement factor β. The field enhancement factor is proportional to the applied voltage V and the electric field E on the emitter tip ($\beta=E/V$) and thus depends on the geometry and surface properties of CNT emitters. As seen from the above TEM and Raman characterizations, defects and larger diameter of the FWCNTs have an impact on the geometry and radius curvature of field emitter tips. Moreover, SWCNTs have a lower defect concentration and are grown in bundles of smaller diameter tubes providing additional emission sites. The linear F-N plots indicate a smaller slope for SWCNTs caused by a larger field emission β factor than that for FWCNTs. The slope of F-N equation is also proportional to the work function of emitters ϕ, which might be another reason for the differences in emission properties between FWCNTs and SWCNTs. Unfortunately, precise values of the work functions for different types of CNTs are not yet known. Further research work is necessary to quantify the difference between the FWCNTs and SWCNTs.

7.5 Conclusions

Vertically aligned carbon nanotubes have been synthesized at relatively low temperature using an inductive coupled PECVD system. A parametric study of the nanotube growth has been carried out to investigate the effect of the involved factors on the nanotube growth, such as substrate temperature, plasma power, substrate to plasma distance, and catalyst thickness. VA-CNTs have been successfully synthesized at temperatures as low as 450 °C. FWCNTs and SWCNTs can be selectively obtained by tuning the catalyst thickness from 3-5 nm to 1 nm. The electron field emission measurement and calculation of the nanotubes indicates that the SWCNTs exhibit better field emission characteristics than the FWCNTs and their performances recommend both nanomaterials for field emission applications.

7.6 References

[1] M.S. Dresselhaus, G. Dresselhaus, and P.C. Eklund, *Science of Fullerenes and Carbon Nanotubes: Their Properties and Applications*, Academic Press, 1996.

[2] R. Saito, G. Dresselhaus, and M.S. Dresselhaus, *Physical Properties of Carbon Nanotubes*, World Scientific Publishing Company, 1998.

[3] J. Bernholc, D. Brenner, M. Buongiorno Nardelli, V. Meunier, and C. Roland, "Mechanical and electrical properties of nanotubes," *Annual Review of Materials Science*, vol. 32, 2002, pp. 347-375.

[4] A. Jorio, *Carbon Nanotubes: Advanced Topics in the Synthesis, Structure, Properties and Applications*, Springer, 2008.

[5] S. Iijima and T. Ichihashi, "Single-shell carbon nanotubes of 1-nm diameter,"

Nature, vol. 363, Jun. 1993, pp. 603-605.

[6] C. Journet, W. Maser, P. Bernier, A. Loiseau, M. Lamy de la Chapelle, S. Lefrant, P. Deniard, R. Lee, and J. Fischer, "Large-scale production of single-walled carbon nanotubes by the electric-arc technique," *Nature*, vol. 388, 1997, pp. 756-758.

[7] A. Thess, R. Lee, P. Nikolaev, H. Dai, P. Petit, J. Robert, Chunhui Xu, Young Hee Lee, Seong Gon Kim, A. Rinzler, D. Colbert, G. Scuseria, D. Tombnek, J. Fischer, and R. Smalley, "Crystalline ropes of metallic carbon nanotubes," *Science*, vol. 273, Jul. 1996, pp. 483-7.

[8] J. Kong, A.M. Cassell, and H. Dai, "Chemical vapor deposition of methane for single-walled carbon nanotubes," *Chemical Physics Letters*, vol. 292, Aug. 1998, pp. 567-574.

[9] A.M. Cassell, J.A. Raymakers, J. Kong, and H. Dai, "Large Scale CVD Synthesis of Single-Walled Carbon Nanotubes," *The Journal of Physical Chemistry B*, vol. 103, 1999, pp. 6484-6492.

[10] Jing Kong, N. Franklin, Chongwu Zhou, M. Chapline, Shu Peng, Kyeongjae Cho, and Hongjie Dai, "Nanotube molecular wires as chemical sensors," *Science*, vol. 287, Jan. 2000, pp. 622-625.

[11] S. Ghosh, A. Sood, and N. Kumar, "Carbon nanotube flow sensors," *Science*, vol. 299, Feb. 2003, pp. 1042-1044.

[12] W. Zhu, C. Bower, O. Zhou, G. Kochanski, and S. Jin, "Large current density from carbon nanotube field emitters," *Applied Physics Letters*, vol. 75, 1999, pp. 873-5.

[13] T. Rueckes, K. Kim, E. Joselevich, G. Tseng, C. Cheung, and C. Lieber, "Carbon nanotube-based nonvolatile random access memory for molecular computing," *Science*, vol. 289, Jul. 2000, pp. 94-97.

[14] H. Postma, T. Teepen, Zhen Yao, M. Grifoni, and G. Dekker, "Carbon nanotube single-electron transistors at room temperature," *Science*, vol. 293, Jul. 2001, pp. 76-9.

[15] A. Bachtold, P. Hadley, T. Nakanishi, and C. Dekker, "Logic circuits with carbon nanotube transistors," *Science*, vol. 294, Nov. 2001, pp. 1317-1320.

[16] K. Hata, D.N. Futaba, K. Mizuno, T. Namai, M. Yumura, and S. Iijima, "Water-assisted highly efficient synthesis of impurity-free single-walled carbon nanotubes,"

Science, vol. 306, 2004, pp. 1362-1364.

[17] V.K. Kayastha, S. Wu, J. Moscatello, and Y.K. Yap, "Synthesis of vertically aligned single- and double-walled carbon nanotubes without etching agents," *Journal of Physical Chemistry C*, vol. 111, 2007, pp. 10158-10161.

[18] T. Kato, G. Jeong, T. Hirata, and R. Hatakeyama, "Structure control of carbon nanotubes using radio-frequency plasma enhanced chemical vapor deposition," *16th Sympsoium on Plasma Science for Materials (SPSM-16), 4-5 June 2003*, Switzerland: Elsevier, 2004, pp. 2-6.

[19] Yiming Li, D. Mann, M. Rolandi, Woong Kim, A. Ural, A. Javey, Jien Cao, Dunwei Wang, E. Yenilmez, Qian Wang, J. Gibbons, Y. Nishi, and H. Dai, "Preferential growth of semiconducting single-walled carbon nanotubes by a plasma enhanced CVD method," *Nano Letters*, vol. 4, Feb. 2004, pp. 317-21.

[20] G. Zhong, T. Iwasaki, K. Honda, Y. Furukawa, I. Ohdomari, and H. Kawarada, "Very high yield growth of vertically aligned single-walled carbon nanotubes by point-arc microwave plasma CVD," *Chemical Vapor Deposition*, vol. 11, 2005, pp. 127-130.

[21] G. Zhang, D. Mann, L. Zhang, A. Javey, Y. Li, E. Yenilmez, Q. Wang, J. McVittie, Y. Nishi, J. Gibbons, and H. Dai, "Ultra-high-yield growth of vertical single-walled carbon nanotubes: hidden roles of hydrogen and oxygen," *Proceedings of the National Academy of Sciences of the United States of America*, vol. 102, Nov. 2005, pp. 16141-5.

[22] Z. Luo, S. Lim, Y. You, J. Miao, H. Gong, J. Zhang, S. Wang, J. Lin, and Z. Shen, "Effect of ion bombardment on the synthesis of vertically aligned single-walled carbon nanotubes by plasma-enhanced chemical vapor deposition," *Nanotechnology*, vol. 19, 2008.

[23] A. Gohier, T. Minea, A. Djouadi, A. Granier, and M. Dubosc, "Limits of the PECVD process for single wall carbon nanotubes growth," *Chemical Physics Letters*, vol. 421, Apr. 2006, pp. 242-5.

[24] S. Alexandrov, "Remote PECVD: a route to controllable plasma deposition," *Tenth European Conference on Chemical Vapour Deposition, 10-15 Sept. 1995*, France: 1995, pp. 567-82.

[25] J. Bonard, J. Salvetat, T. Stockli, W. de Heer, L. Forro, and A. Chatelain, "Field emission from single-wall carbon nanotube films," *Applied Physics Letters*, vol. 73, 1998, pp. 918-20.

[26] H. Murakami, M. Hirakawa, C. Tanaka, and H. Yamakawa, "Field emission from well-aligned, patterned, carbon nanotube emitters," *Applied Physics Letters*, vol. 76, Mar. 2000, pp. 1776-8.

[27] Y. Yang, C. Wang, U. Chen, W. Hsieh, Y. Chang, and H. Shin, "Large-area single wall carbon nanotubes: synthesis, characterization, and electron field emission," *Journal of Physical Chemistry C*, vol. 111, Feb. 2007, pp. 1601-4.

[28] A. Wadhawan, R. Stallcup, K. Stephens, J. Perez, and I. Akwani, "Effects of O2, Ar, and H2 gases on the field-emission properties of single-walled and multiwalled carbon nanotubes," *Applied Physics Letters*, vol. 79, Sep. 2001, pp. 1867-9.

[29] S. Boddepalli, S. Boddepalli, Kyungseok Noh, Minhyon Jeon, and Wonbong Choi, "Enhanced field emission from aligned multistage carbon nanotube emitter arrays," *Nanotechnology*, vol. 19, Feb. 2008, pp. 065605-065605-4.

[30] A. Gohier, T. Minea, M. Djouadi, J. Jimenez, and A. Granier, "Growth kinetics of low temperature single-wall and few walled carbon nanotubes grown by plasma enhanced chemical vapor deposition," *Physica E: Low-Dimensional Systems and Nanostructures*, vol. 37, 2007, pp. 34-39.

[31] Y. Chen, L.P. Guo, D.J. Johnson, and R.H. Prince, "Plasma-induced low-temperature growth of graphitic nanofibers on nickel substrates," *Journal of Crystal Growth*, vol. 193, Oct. 1998, pp. 342-346.

[32] P.E. Nolan, D.C. Lynch, and A.H. Cutler, "Carbon deposition and hydrocarbon formation on group VIII metal catalysts," *Journal of Physical Chemistry B*, vol. 102, 1998, pp. 4165-4175.

[33] D. Hash and M. Meyyappan, "Model based comparison of thermal and plasma chemical vapor deposition of carbon nanotubes," *Journal of Applied Physics*, vol. 93, Jan. 2003, pp. 750-2.

[34] M. Chhowalla, K.B.K. Teo, C. Ducati, N.L. Rupesinghe, G.A.J. Amaratunga, A.C. Ferrari, D. Roy, J. Robertson, and W.I. Milne, "Growth process conditions of vertically aligned carbon nanotubes using plasma enhanced chemical vapor

deposition," *Journal of Applied Physics*, vol. 90, 2001, p. 5308.

[35] M. Bell, K. Teo, and W. Milne, "Factors determining properties of multi-walled carbon nanotubes/fibres deposited by PECVD," *Journal of Physics D: Applied Physics*, vol. 40, 2007, pp. 2285-2292.

[36] Z. Tsakadze, I. Levchenko, K. Ostrikov, and S. Xu, "Plasma-assisted self-organized growth of uniform carbon nanocone arrays," *Carbon*, vol. 45, Sep. 2007, pp. 2022-30.

[37] A.R. Harutyunyan, N. Awasthi, A. Jiang, W. Setyawan, E. Mora, T. Tokune, K. Bolton, and S. Curtarolo, "Reduced carbon solubility in Fe nanoclusters and implications for the growth of single-walled carbon nanotubes," *Physical Review Letters*, vol. 100, May. 2008, p. 195502.

[38] M. Dresselhaus, G. Dresselhaus, R. Saito, and A. Jorio, "Raman spectroscopy of carbon nanotubes," *Physics Reports*, vol. 409, Mar. 2005, pp. 47-99.

CHAPTER 8

ONE-DIMENSIONAL/TWO DIMENSIONAL CARBON NANOSTRUCTURE HYBRID BY PLASMA ENHANCED CHEMICAL VAPOR DEPOSITION

8.1 Abstract

Large area of one-dimensional/two-dimensional nanostructured carbon hybrid has been synthesized in a single step by radio frequency plasma enhanced chemical vapor deposition (PECVD) method. The architecture of the hybrid shows carbon nanosheets suspended on vertically aligned carbon nanotubes. In the growth process, a mixture of methane and hydrogen was decomposed over silicon substrates covered with a film of alumina under-layer and a thin film of catalyst layer. The alumina under-layer plays a key role in the formation of the carbon hybrid nanostructure. The hybrid was analyzed by scanning electron microscopy, transmission electron microscopy, and Raman spectroscopy. The present work illustrates the potential of PECVD method in producing nanostructured carbon hybrids with different dimension and the understanding of the synthesis approach to ordered carbon nanostructures is expanded.

8.2 Introduction

Nanostructured carbon materials, including fullerenes, nanotubes, and graphene sheets have attracted great interest in recent years due to their novel properties [1, 2]. Because graphene sheets tend to self aggregate, it is difficult to process them in bulk quantities, unless the graphitic sheets are well separated from each other. Recently, attention has been focused on carbon nanosheet (CNS) materials which are two-dimensional (2D) self-supported networks of graphitic walls [3-5]. The most frequently used method of CNS synthesis is plasma enhanced chemical vapor deposition (PECVD) including microwave PECVD [6] and radio frequency PECVD assisted by hydrogen-radical injection [7, 8]. CNSs provide an important model of a two-dimensional graphite structure with strong anisotropy of physical properties. Free-standing and vertically oriented nanosheets have a high specific surface area which is of importance for applications in nanoelectronics [9], sensors [10], catalysis [11], and energy conversion and storage [12]. Combining these characteristics of CNSs with the unique properties of one-dimensional (1D) carbon nanotubes (CNTs) [13], a hybrid of 1D/2D nanostructured carbon hybrid with novel properties has been theoretically predicted [14]. This kind of hybrid would play a major role in future nanotechnology. Several experimental studies have been reported to obtain carbon hybrids containing both graphite sheets and nanotubes. These studies were mainly based on graphene reintegration around or inside pristine nanotubes [15] or on mixing the nanostructures [16]. However, up to present, CNTs and CNSs have been created separately. *In-situ* or direct fabrication of complex

carbon nanostructures with controlled dimension and surface architecture remains a significant challenge.

In this work, for the first time, a hybrid of free-standing CNSs anchored on CNTs was synthesized *in-situ*, on large substrate area, and in a single step by using radio frequency PECVD method.

8.3 Experimental

The hybrid of carbon nanostructures has been synthesized using a PECVD/sputtering hybrid system schematically illustrated in Figure 8.1.

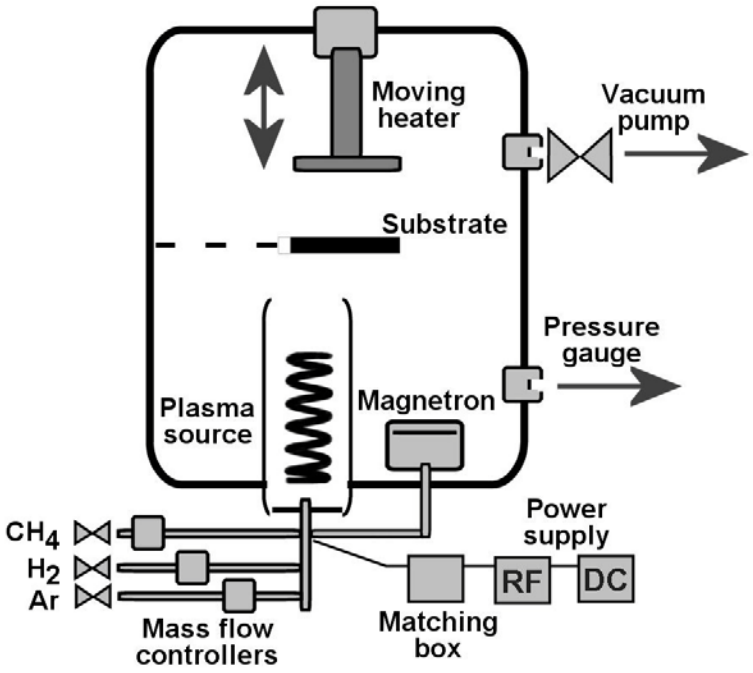

Figure 8.1 Schematic diagram of the PECVD/sputtering hybrid system

In this study, oriented n-type (1, 0, 0) silicon (Si) wafers were used as a substrate, without removing the native oxide layer. The substrate was fixed 10 cm above the magnetron and plasma source and 7 cm bellow the moving heater. Prior to deposition process of carbon, the vacuum chamber was evacuated to 10^{-5} Torr. A thin film of 10 nm alumina (Al_2O_3) was sputtered on the substrate followed by depositing a 5 nm molybdenum (Mo) and iron (Fe) film by magnetron sputtering at a pressure of 15 mTorr. Then, argon was fed at a flow rate of 50 sccm and the substrate was heated to 620 ^{o}C. Once the temperature was reached, the argon flow was stopped and hydrogen (H_2, 60 sccm) and methane gas (CH_4, 6 sccm) were introduced into the deposition chamber. The heater was moved 1.5 mm close to the substrate. The radio frequency plasma source was started and operated at the power of 200 W and the pressure was controlled at 1.2 Torr. After 10 min growth time, the reactor was allowed to cool down under vacuum before exposure to air. The samples were characterized by scanning electron microscopy (SEM - Hitachi S-4800), transmission electron microscopy (TEM - Philips CM-10), and Raman spectroscopy (LabRAM HR800 with laser excitation of 785 nm).

8.4 Results and discussion

SEM images show a top view (Figure 8.2a) of the hybrid material composed by nanosheets with CNTs attached on one side (Figure 8.2b), totally covering the silicon substrate. The material could be easily scratched and removed from the substrate. Seen from the top of the substrate, the nanosheet has a surface marked by irregularities (Figure

8.2c), while arrays of CNTs are formed on the other side (Figure 8.2d). A higher magnification image reveals that the CNS was grown and suspended on vertically aligned CNTs (Figure 8.2e). The tubes have an average length of 600 nm (Figure 8.2f).

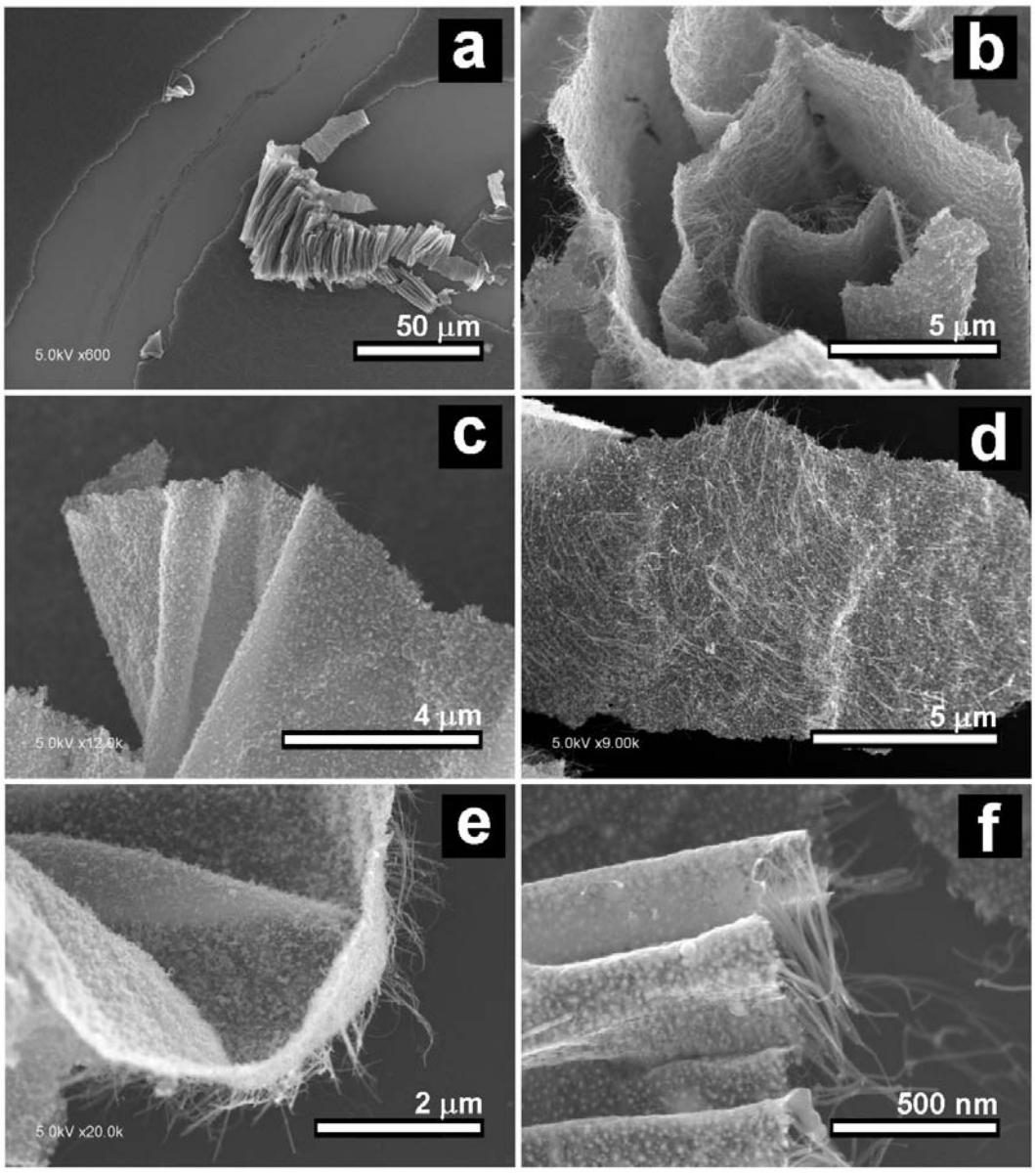

Figure 8.2 SEM images of hybrid carbon nanostructure at low magnifcation (a); a freestanding nanostructure at high magnification (b); view from nanosheet side (c); view from CNTs side (d); hybrid carbon nanostructure detached from the substrate (e) view of aligned CNTs at high magnification (f).

TEM images confirm the irregularities and protuberances seen on the CNSs and indicate numerous particles on the CNS structure with the particle diameter in the range of 3-40 nm (Figure 8.3a).

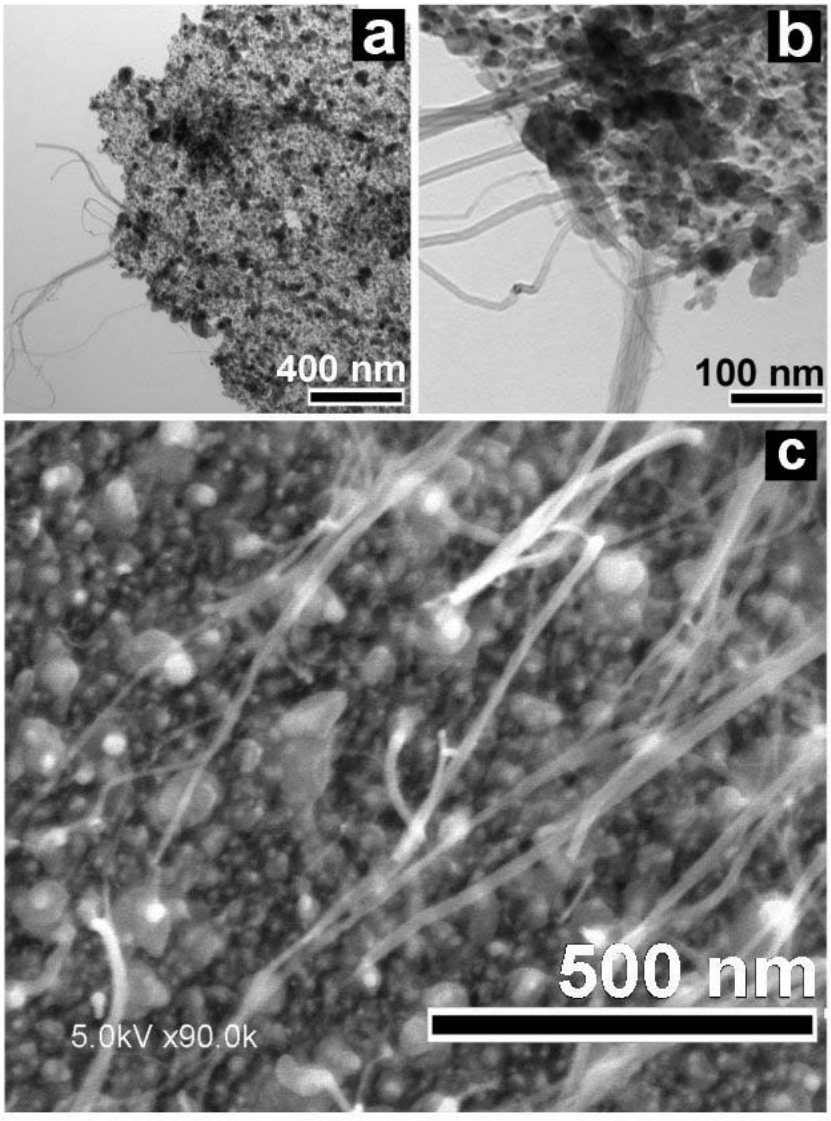

Figure 8.3 TEM image of hybrid carbon nanostructure showing the inclusion of numerous granular domains in the carbon nanosheet (a); TEM image indicating CNTs connected with nanoparticles (b); SEM image indicating CNTs connected with nanoparticles (c).

The CNTs have diameters in the range of 5-50 nm and are connected with these particles (Figure 8.3b). SEM observation confirms that CNTs are formed on the particles suggesting that they are catalyst particles (Figure 8.3c). The influence of growth time was studied by keeping the other parameters as previously described. By changing the deposition time, a direct correlation between CNT length and the growth time was observed. The average length of the CNTs changed from 300 nm for a growth time of 5 min, to 600 nm for a growth time of 10 min, and increased to 1.1 μm for a growth time of 20 min (Figure 8.4).

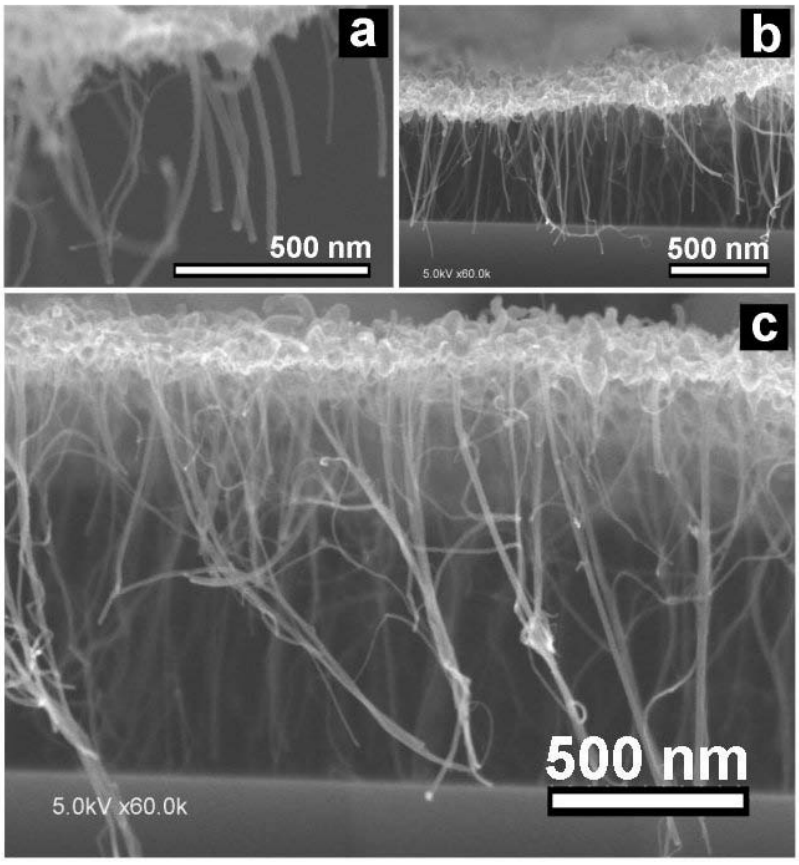

Figure 8.4 SEM images of hybrid carbon nanostructure showing the CNTs height for different deposition time: 5 min – 300 nm (a); 10 min – 600 nm (b); 20min – 1.1 μm (c).

SEM images show that during the growth process, the CNS was suspended on vertically aligned CNTs and it was pushed away from the substrate with increasing growth time. These observations were consistent with all experiments and indicated that the tubes grew downwards from CNS to the substrate, while the CNS morphology was almost unchanged.

In previous experiments, the substrate preparation process consisted in sputtering the Si wafer with a thin film of 10 nm Al_2O_3 followed by another film sputtering of 5 nm Mo and Fe. In the following experiment, the substrate was deposited only with Mo/Fe catalyst without the alumina under-layer. The other parameters and growth procedures were the same as in previous experiments. SEM images show the Si substrate totally covered (Figure 8.5a) by diaphanous sheets which could be easily scratched and removed from the substrate. During the scratching process, the material had the tendency to roll up (Figure 8.5b). In a close-up investigation, the nanosheet reveals an irregular structure with particle inclusion similar to previous experiments (Figure 8.5c). These findings confirm that the alumina layer is an effective under-layer support for Fe catalysts in the CNT growth [17]. When the alumina layer was removed, the Mo/Fe catalyst layer enhanced the CNS growth.

In order to explore the possibility of alternative growth of CNSs and vertical aligned CNTs, a subsequent experiment was carried out. For this purpose, the carbon hybrid nanostructure was deposited on Si substrate as previously. Without breaking the vacuum or changing the temperature, Fe was sputtered on the formed CNS at 15 mTorr in an argon protective atmosphere.

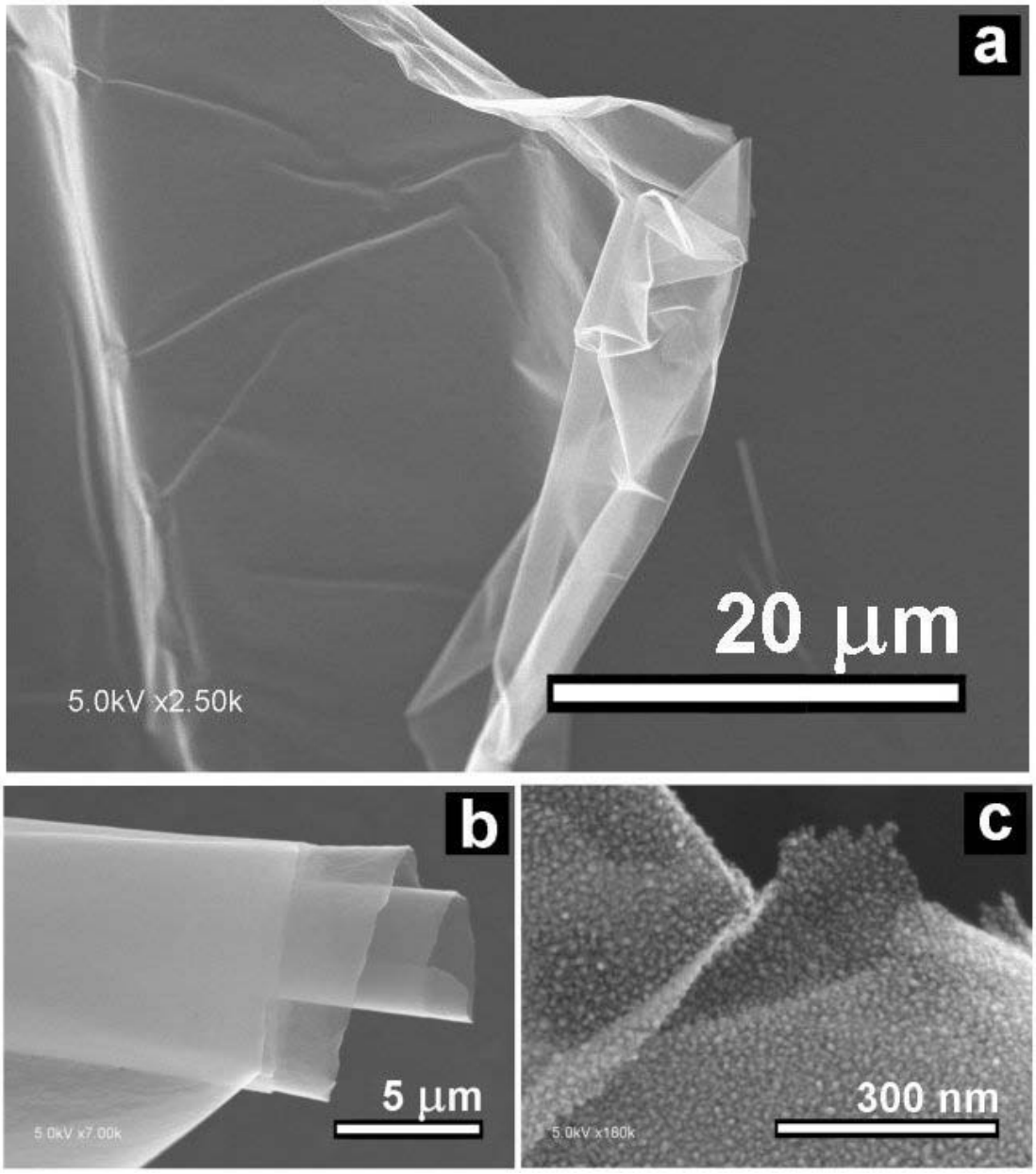

Figure 8.5 SEM images of carbon nanosheet obtained without Al_2O_3 underlayer.

Then the pressure was increased to 1.2Torr and H_2/CH_4 plasma was started for 10 min as described in the experimental section. The Si substrate was totally covered by the carbon hybrid nanostructure seen in the SEM images (Figure 8.6a). In the cross section view, the

carbon sheet, detached from the substrate by the first generation of vertical align CNTs, was covered by arrays of a new CNT generation (Figure 8.6b). The second generation of CNTs has approximately the same average diameter and length as that of the first generation of CNTs (Figure 8.6c).

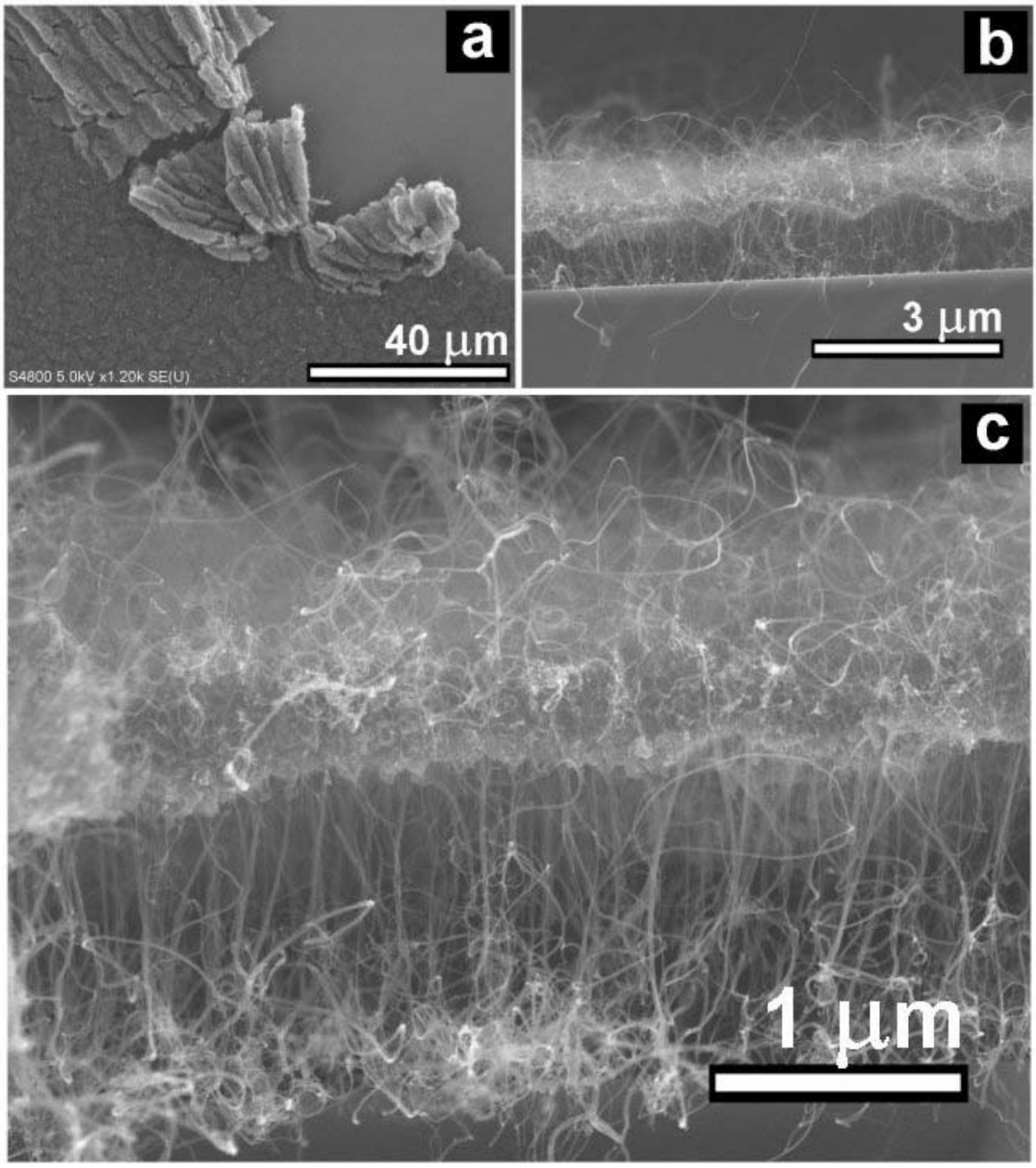

Figure 8.6 SEM images of carbon nanostructure hybrid obtained in two steps.

Raman spectra of the obtained CNS (Figure 8.7 curve (a)), CNS suspended on CNTs (Figure 8.7 curve (b)), and the hybrid nanostructure obtained in two steps (Figure 8.7 curve (c)) confirm the formation of graphitic carbon nanostructures by the occurrence of well-defined G-band around 1613 cm^{-1} [18]. The G-band of the carbon hybrid nanostructure obtained in two steps underwent a down-shift from 1613 cm^{-1} to 1597 cm^{-1}.

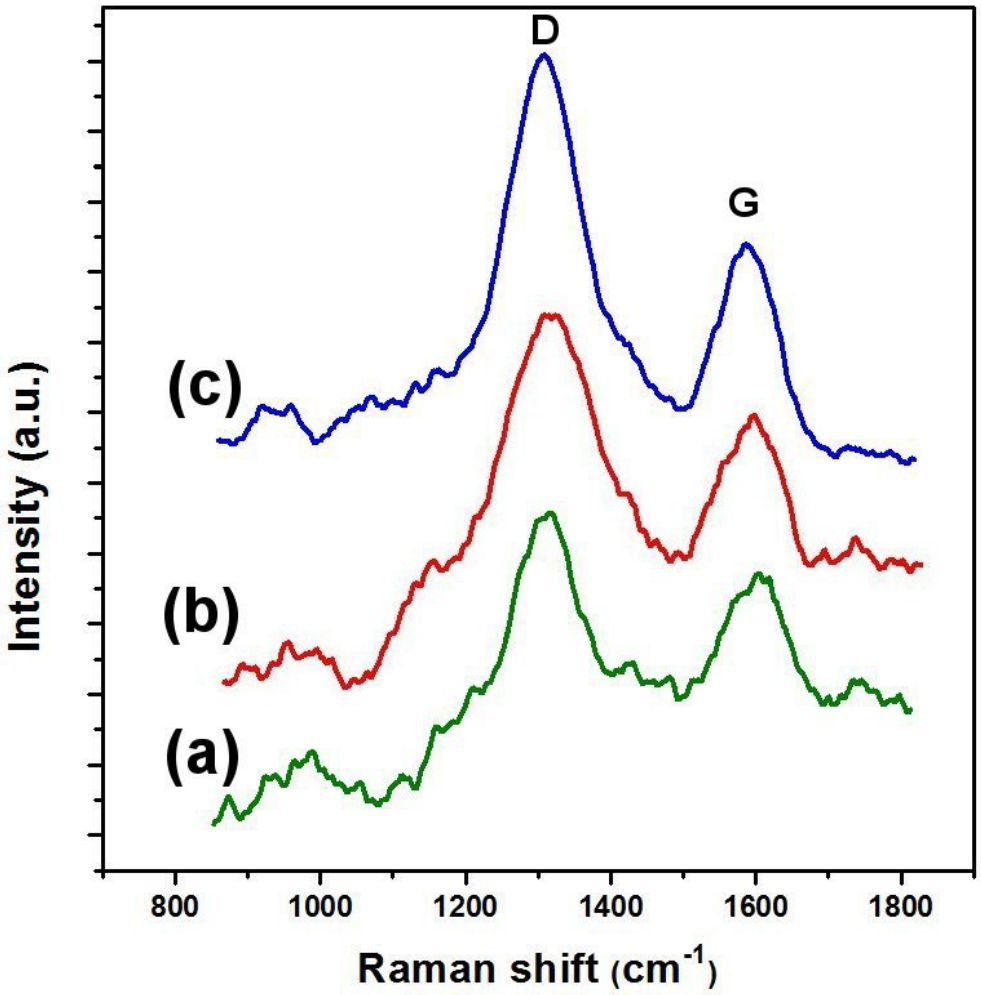

Figure 8.7 Raman spectra of carbon nanosheets (curve a); carbon nanosheet sustained on CNTs (curve b); carbon nanostructure hybrid obtained in two steps (curve c).

This is the characteristic of bond modification between carbon atoms in graphene sheets and could be ascribed to an increase in concentration of defects [19]. The D-band at around 1318 cm^{-1}, involves scattering from defects which change the symmetry of graphene sheet. The intensity of the D-band is stronger relative to the G-band for all studied nanostructures. This indicates the occurrence of impurities and symmetry breaking defects in the graphite monolayer [20] and is consistent with the TEM and SEM observations.

The presented findings suggest that the plasma decomposed carbon species cannot diffuse in the catalyst particles to nucleate and form CNTs in the initial growth stage when substrate temperature is still low. Instead, as the TEM images and Raman spectra suggest, the particles are covered and connected by low graphitized carbon to form the CNS layer. While the temperature on the substrate increases, the catalyst particles allow diffusion of carbon and CNTs are formed when the catalyst particles are supersaturated with carbon. The CNT growth detaches the CNS layer and pushes it away from the substrate forming the carbon hybrid nanostructure. When the catalyst activity is enhanced by the existence of an alumina under-layer [21], the CNTs and the carbon hybrid nanostructure are formed. Without the alumina under-layer, the catalyst particles are covered by low graphitized carbon. In this case only the carbon nanosheet is grown. The use of Mo/Fe co-catalyst instead of sole metals has been well studied and proved to have the advantage of enhancing the catalytic activity for CNT growth [22, 23]. Computer simulations suggested that bi-metallic catalysts improve the nanotube growth, molybdenum is the best catalyst responsible for nucleation, and iron is a good catalyst

responsible for growth [24]. However, further examination of the catalyst influence to the hybrid formation will be conducted in near future.

8.5 Conclusions

A nanostructured hybrid of two-dimensional carbon nanosheets suspended on vertically aligned carbon nanotubes has been synthesized in a single step by radio frequency PECVD method. Without a pre-deposited alumina under-layer film on the substrate, the nanotube growth was suspended and only carbon nanosheets were obtained. Depositing a catalyst film on the suspended nanosheet followed by nanotube growth, lead to synthesis of a carbon hybrid nanostructure. The structure was formed by the detachment of carbon nanosheets from the substrate pushed by the first generation of vertically aligned CNTs, being followed by a growth of a new generation CNT arrays on the carbon nanosheets. This study shows that the PECVD method is suitable for growing tailored carbon nanostructures and could play a major role in future nanotechnology.

8.6 References

[1] T. Hayashi, Y.A. Kim, T. Natsuki, and M. Endo, “Mechanical Properties of Carbon Nanomaterials,” *ChemPhysChem,* vol. 8, 2007, pp. 999-1004.

[2] M. Terrones, “Science and Technology of the Twenty-First Century: Synthesis, Properties, and Applications of Carbon Nanotubes,” *ChemInform,* vol. 35, 2004.

[3] Y. Wu, B. Yang, B. Zong, H. Sun, Z. Shen, and Y. Feng, "Carbon nanowalls and related materials," *Journal of Materials Chemistry*, vol. 14, 2004, p. 469.

[4] M. Hiramatsu and M. Hori, "Fabrication of Carbon Nanowalls Using Novel Plasma Processing," *Japanese Journal of Applied Physics*, vol. 45, 2006, pp. 5522-5527.

[5] K. Kobayashi, M. Tanimura, H. Nakai, A. Yoshimura, H. Yoshimura, K. Kojima, and M. Tachibana, "Nanographite domains in carbon nanowalls," *Journal of Applied Physics*, vol. 101, 2007, p. 094306.

[6] Y. Wu, P. Qiao, T. Chong, and Z. Shen, "Carbon Nanowalls Grown by Microwave Plasma Enhanced Chemical Vapor Deposition," *Advanced Materials*, vol. 14, 2002, pp. 64-67.

[7] M. Hiramatsu, K. Shiji, H. Amano, and M. Hori, "Fabrication of vertically aligned carbon nanowalls using capacitively coupled plasma-enhanced chemical vapor deposition assisted by hydrogen radical injection," *Applied Physics Letters*, 2004.

[8] M. Zhu, J. Wang, R.A. Outlaw, K. Hou, D.M. Manos, and B.C. Holloway, "Synthesis of carbon nanosheets and carbon nanotubes by radio frequency plasma enhanced chemical vapor deposition," *Diamond and Related Materials*, vol. 16, Feb. 2007, pp. 196-201.

[9] S. Wang, J. Wang, P. Miraldo, M. Zhu, R. Outlaw, K. Hou, X. Zhao, B.C. Holloway, D. Manos, T. Tyler, O. Shenderova, M. Ray, J. Dalton, and G. McGuire, "High field emission reproducibility and stability of carbon nanosheets and nanosheet-based backgated triode emission devices," *Applied Physics Letters*, vol. 89, 2006, p. 183103.

[10] Y.J. Hong, H.S. Jung, J. Yoo, Y. Kim, C. Lee, M. Kim, and G. Yi, "Shape-Controlled Nanoarchitectures Using Nanowalls," *Advanced Materials*, vol. 21, 2009, pp. 222-226.

[11] Y. Wu, B. Yang, G. Han, B. Zong, H. Ni, P. Luo, T. Chong, T. Low, and Z. Shen, "Fabrication of a Class of Nanostructured Materials Using Carbon Nanowalls as the Templates," *Advanced Functional Materials*, vol. 12, 2002, p. 489.

[12] C. Chen, C. Chen, I. Lee, and C. Lin, "Fabrication of high surface area graphitic nanoflakes on carbon nanotubes templates," *Diamond and Related Materials*, vol. 14, Nov. , pp. 1897-1900.

[13] J. Bernholc, D. Brenner, M. Buongiorno Nardelli, V. Meunier, and C. Roland, "Mechanical and electrical properties of nanotubes," *Annual Review of Materials Research*, vol. 32, 2002, pp. 347-375.

[14] E.F. Sheka and L.A. Chernozatonskii, "Graphene-carbon nanotube composites," Jan. 2009.

[15] Z. Zhu, D. Su, G. Weinberg, R. Jentoft, and R. Schlögl, "Wet-Chemical Assembly of Carbon Tube-in-Tube Nanostructures," *Small*, vol. 1, 2004, pp. 107-110.

[16] S. Yang, K. Chang, Y. Lee, C.M. Ma, and C. Hu, "Constructing a hierarchical graphene-carbon nanotube architecture for enhancing exposure of graphene and electrochemical activity of Pt nanoclusters," *Electrochemistry Communications*, vol. 12, Sep. 2010, pp. 1206-1209.

[17] G.D. Nessim, D. Acquaviva, M. Seita, K.P. O'Brien, and C.V. Thompson, "The Critical Role of the Underlayer Material and Thickness in Growing Vertically Aligned Carbon Nanotubes and Nanofibers on Metallic Substrates by Chemical Vapor Deposition," *Advanced Functional Materials*, vol. 20, 2010, pp. 1306-1312.

[18] M. Dresselhaus, G. Dresselhaus, R. Saito, and A. Jorio, "Raman spectroscopy of carbon nanotubes," *Physics Reports*, vol. 409, Mar. 2005, pp. 47-99.

[19] L. Zhang, H. Li, K. Yue, S. Zhang, X. Wu, J. Zi, Z. Shi, and Z. Gu, "Effects of intense laser irradiation on Raman intensity features of carbon nanotubes," *Physical Review B*, vol. 65, Jan. 2002, p. 073401.

[20] M. Dresselhaus and P. Eklund, "Phonons in carbon nanotubes," *Advances in Physics*, vol. 49, 2000, pp. 705-814.

[21] P.B. Amama, C.L. Pint, S.M. Kim, L. McJilton, K.G. Eyink, E.A. Stach, R.H. Hauge, and B. Maruyama, "Influence of Alumina Type on the Evolution and Activity of Alumina-Supported Fe Catalysts in Single-Walled Carbon Nanotube Carpet Growth," *ACS Nano*, vol. 4, Feb. 2010, pp. 895-904.

[22] A.J. Hart, A.H. Slocum, and L. Royer, "Growth of conformal single-walled carbon nanotube films from Mo/Fe/Al2O3 deposited by electron beam evaporation," *Carbon*, vol. 44, Feb. 2006, pp. 348-359.

[23] L. Delzeit, B. Chen, A. Cassell, R. Stevens, C. Nguyen, and M. Meyyappan, "Multilayered metal catalysts for controlling the density of single-walled carbon

nanotube growth," *Chemical Physics Letters*, vol. 348, Nov. 2001, pp. 368-374.

[24] W. Deng, X. Xu, and W.A. Goddard, "A two-stage mechanism of bimetallic catalyzed growth of single-walled carbon nanotubes," *Nano Letters*, vol. 4, Dec. 2004, pp. 2331-2335.

CHAPTER 9

SYNTHESIS OF FREESTANDING CARBON NANOWALLS BY MAGNETRON SPUTTERING

9.1 Abstract

Arrays of carbon nanowalls have been synthesized by physical vapor deposition in a radio frequency operated magnetron sputtering device. Carbon nanowalls were grown on silicon substrates without using catalyst. The deposit was formed at sputtering powers as low as 200 W and the involvement of hydrogen was found to play a key role in the nanowall formation. Morphology, structure, and vibrational properties of the nanowalls were analyzed by scanning electron microscopy, transmission electron microscopy and Raman spectroscopy. The present work illustrates the potential of magnetron sputtering method for the creation of ordered carbon nanostructures and extends the understanding of carbon based nanomaterial synthesis.

9.2 Introduction

Carbon nanowalls (CNWs) are two-dimensional self-supported networks of almost vertically aligned graphitic walls [1] and provide an important model of a two-dimensional graphite structure with strong anisotropy of physical properties. Free-

standing and vertically oriented CNWs have a very high specific surface area and sharp edges. These properties make the nanowalls attractive in various practical applications such as electron field emission devices [2] and catalyst support in proton exchange membrane fuel cells [3]. This type of carbon structure has been previously reported as byproduct during fullerene and nanotube preparation [4, 5]. It coexisted with other carbon forms and had low controllability. Recently, carbon nanowalls or nanosheets have been synthesized on various substrates using plasma enhanced chemical vapor deposition (PECVD). The existing synthesis methods include microwave PECVD [6] and radio frequency PECVD assisted by hydrogen-radical injection [7, 8]. Although the PECVD procedure has the advantage of assisting the precursor dissociation and facilitating the nanomaterials growth at lower temperatures, the condition of high plasma powers or long deposition time is necessary to obtain CNWs.

In this work, carbon nanowalls, approximately 1 nm thick, have been synthesized using a simple magnetron sputtering method for the first time, at low sputtering powers, without using any catalyst.

9.3 Experimental

CNWs were synthesized using a PECVD/sputtering hybrid system schematically illustrated in Figure 9.1. The system comprised of one radio frequency and two direct-current operated magnetron sputtering guns, a plasma source, and a resistively heated sample stage. The distance of the heating element to the magnetrons was adjustable.

In this study, oriented n-type (1, 0, 0) silicon (Si) wafers were used as a substrate, without removing the native oxide layer. The substrate was fixed in a resistively heated stage and positioned at 8 cm above the magnetron. The target used in the sputtering process was a graphite target with 99.999% purity. Prior to deposition process, the vacuum chamber was evacuated to 10^{-5} Torr. Argon was fed at a flow rate of 30 sccm and the Si substrate was heated to 700 ^{o}C under 30 sccm stream of hydrogen, and the pressure was fixed at 0.1 Torr. Once the temperature was reached, the radio frequency operated magnetron was started at a power of 200 W. After 30 min growth time, the reactor was allowed to cool down under vacuum before exposure to air.

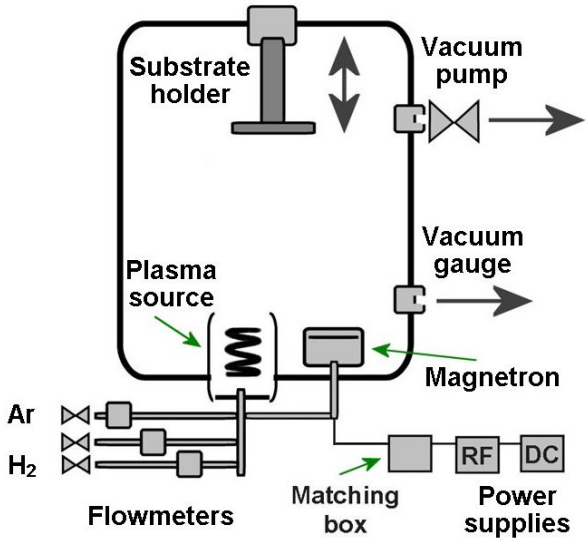

Figure 9.1 Schematic diagram of the PECVD/sputtering hybrid system deposition system.

The samples were characterized by scanning electron microscopy (SEM - Hitachi S-4800), Raman spectroscopy (LabRAM HR800 with laser excitation of 785 nm), and transmission electron microscopy (TEM - Philips CM-10).

9.4 Results and discussion

SEM images of a typical experiment show large scale arrays of carbon nanowalls deposited in a highly corrugated morphology, covering the entire substrate. The nanowalls are very thin and are deposited nearly vertical to the substrate (Figure 9.2a-b). Seen on a higher magnification, the sheet-like feature become evident. The translucent appearance suggests a smooth, uniform, and thin graphitic planes (Figure 9.2c). The wall thickness of the carbon nanosheet is approximately 1 nm (Figure 9.2d).

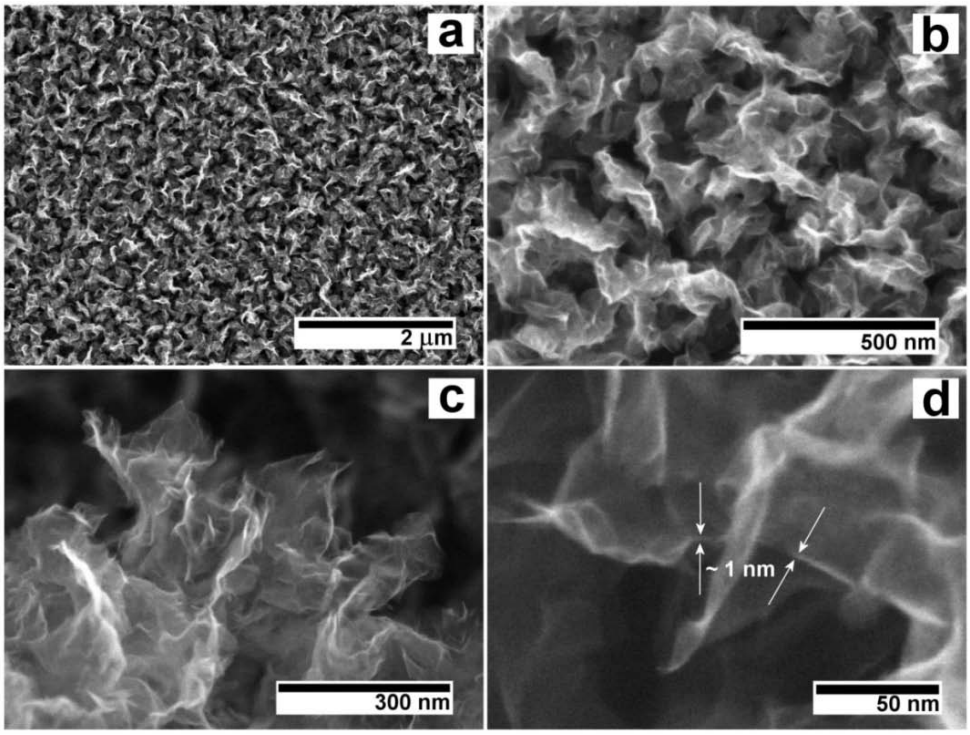

Figure 9.2 SEM images of carbon nanowalls at different magnifications.

TEM images confirm the high density of free-standing corrugated structure and reveal a large area of clean and unbroken graphitic sheets (Figure 9.3a-b).

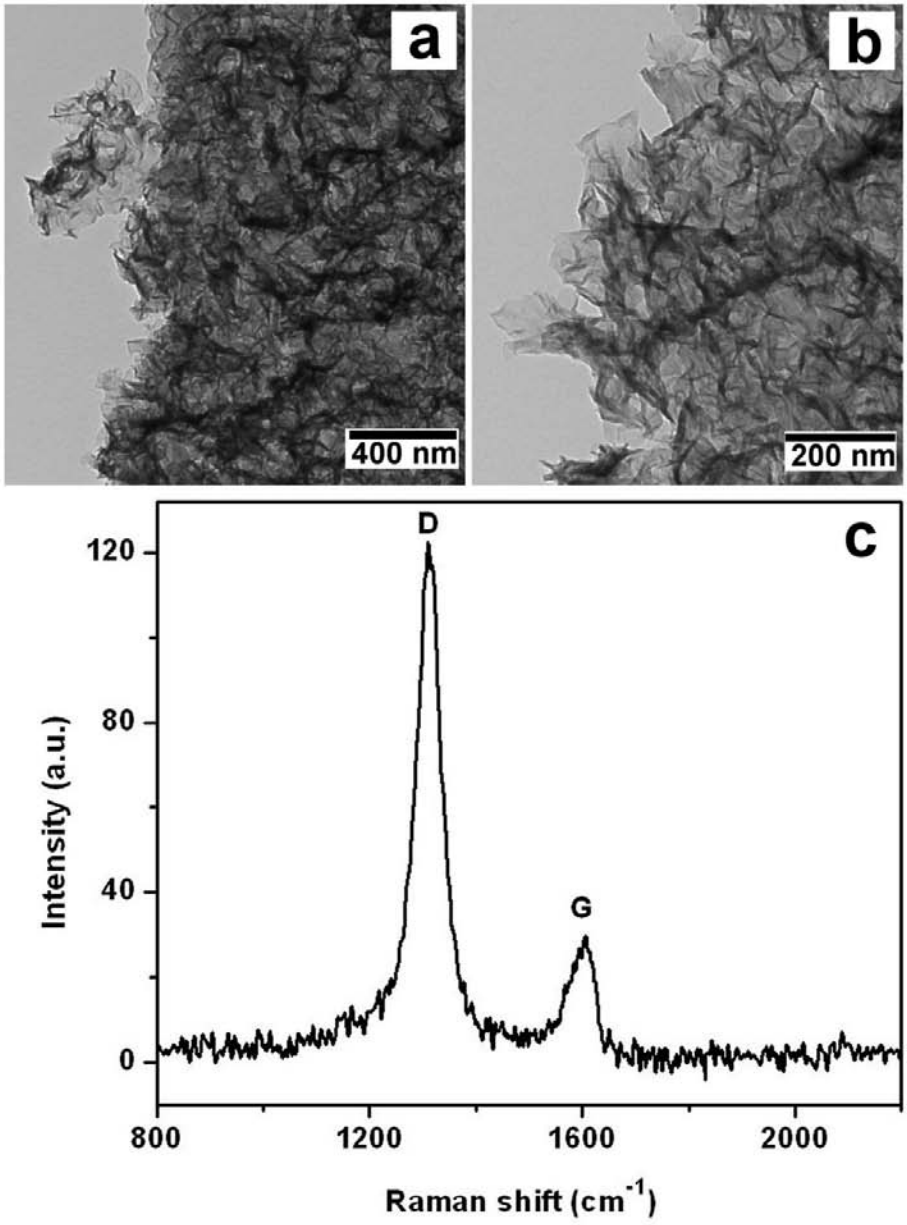

Figure 9.3 TEM images of carbon nanosheets show large area (a) of continuous and corrugated structure (b); Raman spectrum of the carbon nanowalls (c).

The Raman spectrum of carbon nanowalls (Figure 9.3c) has a well defined peak at 1590 cm^{-1} (G-band) indicating the formation of graphitic structure. The G-band peak at 1590 cm^{-1} is accompanied by a shoulder peak at 1610 cm^{-1}. The origin of the shoulder peak is

not clearly understood and could be a characteristic of carbon nanowalls as it was repeatedly seen on different reports [6, 7, 9]. The peak at 1310 cm^{-1} corresponds to the disorder induced mode (D-band). A strong D peak indicates a nanocrystaline structure and the presence of defects caused by distortions and vacancies in the graphitic layers. The corrugated and twisted structure, seen in the electron microscope images, can be attributed to strained sp^3 bonding arrangement in the graphite sheets [10, 11].

Hydrogen flow rate was found to have a key role in the carbon nanowall formation. In a typical experiment, a hydrogen flow of 30 sccm was used. It was observed that a decrease of hydrogen flow rate to 10 sccm led to the growth of amorphous carbon, while an increase of hydrogen flow to 50 sccm reduced the density and thickness of the nanowalls (Figure 9.4a). A further increase of hydrogen flow suppressed the carbon nanowall growth. The synthesis of carbon nanowalls on 304 stainless steel (SS) substrates brought similar macro morphology to that on the silicon substrate, but lowered growth rate (Figure 9.4b). This finding differs from the PECVD results which showed the same growth rate on either Si or SS [10]. Such a difference can be attributed to the plasma power difference between the two methods. While in the PECVD experiments plasma was generated at 900 W, in this study plasma was generated at 200 W. In a subsequent experiment, it was found that no nanowalls were formed when a 10 nm-thick thin iron layer was pre-deposited on the Si substrate. An iron film is commonly used for carbon nanotube growth [12]. SEM investigation of the obtained deposit demonstrates very thin tubes, with diameters smaller than 10 nm, randomly oriented on the substrate along with tubes of larger diameter (Figure 9.4c).

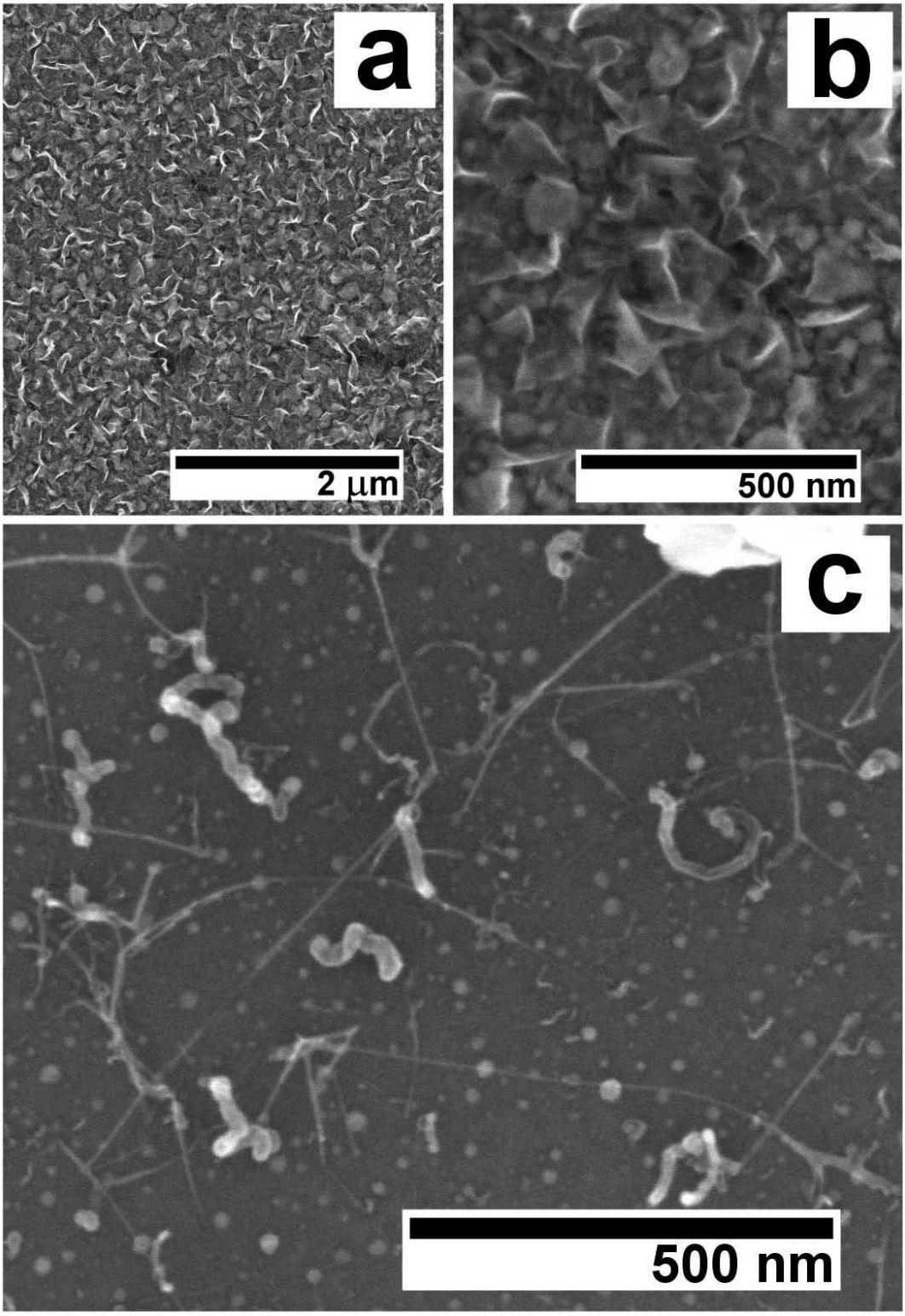

Figure 9.4 SEM images of CNWs grown under a hydrogen flow of 50 sccm (a); CNWs grown on a SS substrate (b); thin carbon nanotubes obtained on Si (c).

These findings suggest the possibility of growing carbon nanotubes using magnetron sputtering techniques. Further examination of nanotube growth using this method will be conducted in near future.

Previously, several growth mechanisms for carbon nanowalls have been proposed. By decomposing acetylene and hydrogen mixtures in a hot filament system, the structure starts as nanorod formation on the substrate and grows anisotropically into nanowalls [13]. A different mechanism has been proposed by using microwave plasma to decompose methane and hydrogen mixtures over a biased substrate. The nanowall growth was attributed to the existence of a strong lateral electric field which inhibited the tubular formation and connected the structure laterally to form continuous walls [14]. Hiramatsu et al. [15] have deposited nanowalls by decomposing mixtures of hexafluoroethane and hydrogen. It was suggested that, initially, carbon species condense to form nanoislands, which develop into nanoflakes with disordered orientation, and eventually grow into continuous wall-like structure. A similar growth mechanism could be attributed to this study, since no metal catalysts or bias voltage has been used. In addition, at the growth substrate temperature, atomic hydrogen and hydrogen radicals prevent the formation of additional graphene layers by etching weakly bonded carbon atoms and amorphous carbon [16, 17]. A study in this direction needs further investigation and will be performed in the near future.

9.5 Conclusions

Thin carbon nanowalls have been produced on Si substrates, by magnetron sputtering techniques for the first time, using graphite target as carbon source. The nanowalls have been synthesized at low sputtering powers without any catalyst. The importance of hydrogen in the nanowall growth was demonstrated and the possibility to obtain carbon nanowalls on stainless steel substrate was addressed. In addition, it was found that carbon nanotubes instead of carbon nanowalls were formed when a thin film of iron was deposited on the Si substrate. The present work indicates that sputtering procedure of growing CNWs is an efficient, catalyst-free, and easy to scale up route for production of high-quality two dimensional carbon nanostructures.

9.6 References

[1] A.T. Chuang, B.O. Boskovic, and J. Robertson, “Freestanding carbon nanowalls by microwave plasma-enhanced chemical vapour deposition,” *Diamond and Related Materials*, vol. 15, Apr. , pp. 1103-1106.

[2] A.T.H. Chuang, J. Robertson, B.O. Boskovic, and K.K.K. Koziol, “Three-dimensional carbon nanowall structures,” *Applied Physics Letters*, vol. 90, 2007, p. 123107.

[3] Y. Wu, B. Yang, B. Zong, H. Sun, Z. Shen, and Y. Feng, “Carbon nanowalls and related materials,” *Journal of Materials Chemistry*, vol. 14, 2004, p. 469.

[4] Y. Ando, X. Zhao, and M. Ohkohchi, “Production of petal-like graphite sheets by hydrogen arc discharge,” *Carbon*, vol. 35, 1997, pp. 153-158.

[5] S. Iijima, T. Wakabayashi, and Y. Achiba, “Structures of Carbon Soot Prepared by

Laser Ablation," *The Journal of Physical Chemistry*, vol. 100, Jan. 1996, pp. 5839-5843.

[6] Y. Wu, P. Qiao, T. Chong, and Z. Shen, "Carbon Nanowalls Grown by Microwave Plasma Enhanced Chemical Vapor Deposition," *Advanced Materials*, vol. 14, 2002, pp. 64-67.

[7] M. Hiramatsu, K. Shiji, H. Amano, and M. Hori, "Fabrication of vertically aligned carbon nanowalls using capacitively coupled plasma-enhanced chemical vapor deposition assisted by hydrogen radical injection," *Applied Physics Letters*, 2004.

[8] M. Zhu, J. Wang, R.A. Outlaw, K. Hou, D.M. Manos, and B.C. Holloway, "Synthesis of carbon nanosheets and carbon nanotubes by radio frequency plasma enhanced chemical vapor deposition," *Diamond and Related Materials*, vol. 16, Feb. 2007, pp. 196-201.

[9] K. Shiji, M. Hiramatsu, A. Enomoto, M. Nakamura, H. Amano, and M. Hori, "Vertical growth of carbon nanowalls using rf plasma-enhanced chemical vapor deposition," *Diamond and Related Materials*, vol. 14, Mar. , pp. 831-834.

[10] J. Wang, M. Zhu, R.A. Outlaw, X. Zhao, D.M. Manos, and B.C. Holloway, "Synthesis of carbon nanosheets by inductively coupled radio-frequency plasma enhanced chemical vapor deposition," *Carbon*, vol. 42, 2004, pp. 2867-2872.

[11] A.C. Ferrari and J. Robertson, "Interpretation of Raman spectra of disordered and amorphous carbon," *Physical Review B*, vol. 61, May. 2000, pp. 1313119-14107.

[12] C. Li, H. Zhu, K. Suenaga, J. Wei, K. Wang, and D. Wu, "Diameter dependent growth mode of carbon nanotubes on nanoporous SiO2 substrates," *Materials Letters*, vol. 63, Jun. 2009, pp. 1366-1369.

[13] N.G. Shang, F.C.K. Au, X.M. Meng, C.S. Lee, I. Bello, and S.T. Lee, "Uniform carbon nanoflake films and their field emissions," *Chemical Physics Letters*, vol. 358, May. 2002, pp. 187-191.

[14] Wu and Yang, "Effects of localized electric field on the growth of carbon nanowalls," *Nano Letters*, vol. 2, Apr. 2002, pp. 355-359.

[15] M. Hiramatsu, K. Shiji, H. Amano, and M. Hori, "Fabrication of vertically aligned carbon nanowalls using capacitively coupled plasma-enhanced chemical vapor deposition assisted by hydrogen radical injection," *Applied Physics Letters*, vol. 84,

Jun. 2004, pp. 4708-10.

[16] J. Mucha, D. Flamm, and D. Ibbotson, “On the role of oxygen and hydrogen in diamond-forming discharges,” *Journal of Applied Physics,* vol. 65, May. 1989, pp. 3448-52.

[17] Y. Muranaka, H. Yamashita, K. Sato, and H. Miyadera, “The role of hydrogen in diamond synthesis using a microwave plasma in a CO/H2 system,” *Journal of Applied Physics*, vol. 67, May. 1990, pp. 6247-54.

CHAPTER 10

CONCLUSIONS, FUTURE WORK, AND RECOMENDATIONS

10.1 Conclusions

This study has presented a systematic investigation on synthesis, structural characterization, and property evaluation of 1D and 2D as well as 1D/2D hybrid carbon based nanostructures, based on varied improved or unexplored carbon nanomaterial deposition methods, such as spray pyrolysis, PECVD, or magnetron sputtering. The main goals of this thesis have been to implement controllable synthesis procedures and to analyze the correlation between the applied growth parameters and the structure and properties of the obtained carbon based nanomaterial.

Vertically aligned CNTs have been achieved on semiconducting and conducting substrates using a modified spray pyrolysis CVD process. This method allowed the growth of CNTs by spraying mixtures of catalyst and carbonaceous liquids under low carrier gas flow rates. The nanotube growth was significantly affected by temperature, flow rate, precursor volume, and concentration of catalyst. Using a similar deposition method, vertically aligned CNTs with tuned nitrogen content have been synthesized on semiconducting substrates. The nitrogen concentration was controlled by changing the nitrogen/carbon source concentration during spraying process. It has been found that the nitrogen amount incorporated in CNTs significantly influences the tube structure, from straight to corrugated nanotubes, and affectes the CNT growth rate. Moreover, the

versatility of spray pyrolysis CVD method has been demonstrated by obtaining a novel multiple-level carbon nanostructure. The structure consists of aligned CNTs which possesses multiple-level branched tubes with increasing mean diameters. The branching process is highly controllable and the formation mechanism is attributed to the coalescence of the catalyst particles on the substrate during the growth process. The spray pyrolysis CVD method offers several significant advantages in CNT growth such as controlling the carrier gas flows without affecting the spraying process, making use of complex mixtures of volatile precursors, the absence of complex substrate preparation, and the setup simplicity.

A PECVD/sputtering hybrid system has been devised as a strategy to enhance the precursor dissociation and to facilitate the carbon nanostructure growth at lower temperatures. Controlling the plasma condition during the growth process, vertically aligned SWCNTs with a narrow diameter distribution have been synthesized at temperatures as low as 450 °C. The same system has been used in different experiments to deposit two-dimensional nanosheets. In addition, a hybrid of nanosheets suspended on vertically aligned CNTs has been obtained. The growth process of hybrid carbon nanostructure was conducted in a single step. An additional step was applied to deposit CNTs on the obtained structure, which led to the growth of a novel hybrid nanostructure consisting of a layer of carbon nanosheets detached from the substrate by a first generation of vertically aligned CNTs and covered by a new CNT generation.

Carbon nanowalls have been synthesized using a graphite target in the radio frequency operated magnetron of the PECVD/sputtering hybrid system. The nanowalls have been synthesized without any catalyst, on silicon and stainless steel substrates, at

low sputtering powers. These experiments have proved the advantages given by plasma and the flexibility of the deposition system for the synthesis of carbon based nanomaterials with controlled and complex architecture.

10.2 Future work

Despite the comprehensive approach of this study, further investigations are required for an exhaustive understanding of CBN synthesis processes. Further research will be focused on the optimization of growth process and the characterization of the obtained products. The growth conditions and parameters used in the spray pyrolysis described in Chapter 4 will be improved to achieve maximum efficiency for the synthesis of FWCNTs and SWCNTs. The enhancement of the nanotube formation with small diameters will include the substrate preparation prior to the deposition process and the consideration of precursors with low bond dissociation energy. This approach is essential in order to comprehend the formation of few–walled nanotubes, which is not completely understood. The growth process of doped CNTs and the increase of the nitrogen presented in Chapter 5 will be further inquired by using precursors with high content of nitrogen (i.e. melamine, ethylenediamine, or imidazole). Structure, composition, and chemical bonding characterization of the nanostructures will be done by using high-resolution TEM, XPS, and EELS. The same characterization methods will be used to examine the branched nanotube results outlined in Chapter 6. The experiments of nanotubes obtained in plasma (Chapter 7) will be continued to compare the effects of

different types of precursors and catalysts in the SWCNT formation. Furthermore, in order to detail the morphology of nanotubes, high-resolution TEM will be employed. The study of N-doped SWCNT synthesis will be developed by using precursors with high content of nitrogen. The hybrid structure described in Chapter 8 and the 2D carbon nanowalls presented in Chapter 9 necessitate further in depth morphological study. Thus, high-resolution TEM investigations will be performed. Special consideration will be given to the investigation and explanation of the CNW and N-doped CNW formation due to plasma enhancement. This endeavors will lead to the development of N-doped CNWs and CNW growth mechanism, which are absent in the current literature.

10.3 Recommendations

A thorough understanding of carbon nanomaterial growth mechanism would be reflected in finding optimum synthesis conditions. While the effect of several parameters has been investigated, the CVD method has many variables that can be explored to improve and control the carbon nanomaterial growth. A closer examination of the interaction between catalysts and substrates would be useful in understanding the growth of CNT arrays. Preparation of regular or doped carbon nanomaterials could be enhanced by considering precursors with low bond dissociation energy between carbon atoms and doping elements. Mass spectrometry, applied *in-situ* to characterize the plasma, could be used as a technique to identify the chemical radicals issued from the direct fragmentation of precursors and involved in the material growth. Other factors involved in the CVD

process that can be studied are the delivery mechanism of precursors and the growth influence of other additives. The spray pyrolysis CVD method can be improved by controlling the drop size distribution of carbon precursor over the substrate. This can be achieved by using an ultrasonic nozzle and controlling it with different frequency of vibration. This strategy enlarges the species of chemical precursors which can be exploited in the synthesis process since non-volatile liquids can be used.

The author hopes that the findings presented in this thesis will contribute to the further development of fundamental studies and applications of carbon based nanomaterials.

CURICULUM VITAE

Name: Mihnea Ioan Ionescu

Post-secondary Education and Degrees:

The University of Western Ontario
London, Ontario, Canada
2007-2011 Ph.D. - Mechanical & Materials Engineering

University of Bucharest
Bucharest, Romania
1998-2000 M.Sc. - Materials Science

University of Bucharest
Bucharest, Romania
1998-2000 B.Eng. - Materials Science & Engineering

Honours and Awards:

Province of Ontario Graduate Scholarship
2009-2011

Related Work Experience

Teaching Assistant
The University of Western Ontario, London, ON, Canada
Department of Mechanical & Materials Engineering
2008-2010

Teaching Professor
University of Bucharest, Bucharest, Romania
Department of Mechanics and Molecular Physics
2003-2006

Publications:

1. Meng, X., **Ionescu M.I.,**, Banis, M., Zhong, Y., Liu, H., Zhang, Y., Sun, S., Li, R., and Sun, X.. "Heterostructural coaxial nanotubes of CNT@Fe2O3 via atomic layer deposition: Effects of surface functionalization and nitrogen-doping". **Journal of Nanoparticle Research** (in press); 2010

2. Zhang, G., Sun, S., **Ionescu, M.I.**, Liu, H., Zhong, Y., Li, R., Sun, X., "Controlled growth/patterning of Ni nanohoneycombs on various desired substrates". **Langmuir**. 26: 4346–4350; 2010

3. **Ionescu M.I.,** Liu, H., Y. Zhong, Zhang. Y., Li, R., Sun, X., Sarkissian, A., Kpetsu, J., Côté, C., Jedrzejowski, C., Mérel, P., Laou, P., "Controlled synthesis of carbon nanotubes by various CVD and PECVD methods". **ECS Transactions (ECST)**. 25: 737-748; 2009

4. Zhong, Y., Jaidann, M., Zhang, Y., Zhang, G., Liu, H., **Ionescu, M.I.**, Li, R., Sun, X., Abou-Rachid, H., Lussier, L-S., "Synthesis of high nitrogen-doping of carbon nanotubes and modeling the stabilization of filled DAATO@CNTs (10, 10) for nanoenergetic materials". **Journal of Physics and Chemistry of Solids**. 71: 134-139; 2009

5. Nastase, C., Nastase, F., Dumitru, A., **Ionescu M.I.**, and Stamatin, I., "Thin film composites of nanocarbons-polyaniline obtained by plasma polymerization technique". **Composites Part A: Applied Science and Manufacturing**. 36: 481-485; 2005

6. **Ionescu, M.I.**, Stamatin, I., Nastase, F., Nastase, C., and Serban, C., "High-quality carbon nanotubes production using plasma-chemistry deposition method". **Molecular Crystals and Liquid Crystals**. 415: 133-140; 2004

7. **Ionescu, M.I.**, Stamatin, I., and Grecu, S., "SWNT Young modulus based on micromechanical simulation model". **Romanian Journal of Physics**. 46: 337-344; 2001

8. Dumitru, A., Stamatin, I., Grecu, S., and **Ionescu, M.I.,** "Plasma polymerization of thin films using aniline and p-xylene precursors". Published: **Frontiers of High Pressure Research II**, Kluwer Academic Pub. ISBN: 978-1-4020-0160-4. Pages 45-52; 2001

9. Stamatin, I., Grecu, S., **Ionescu M.I.**, and Kleps, I., "Field emission in diamond structures deposited onto Si-111 tips. **Romanian Journal of Physics**. 45: 111-119; 2000

10. **Ionescu, M.I.**, Grecu, S., and Stamatin I., "Tracing the 0K isotherm of graphite at compression in graphite - diamond System". **Analele Universitatii Bucuresti - Physics**. XLVIII: 45-48; 1999

Papers to be submitted:

1. **Ionescu, M.I.,** Zhang, Y., Li, R., Sun, X., Hakima, A.-R., and Lussier L.-S., "Parametric study on the growth of carbon nanotubes on electrically semiconducting and conducting substrates by spray pyrolysis chemical vapor deposition".

2. **Ionescu, M.I.,** Zhang, Y., Li, R., Sun, X., "Nitrogen-doping effects on the growth, structure and electrical performance of carbon nanotubes obtained by spray pyrolysis method".

3. **Ionescu, M.I.,** Zhang, Y., Li, R., Sun, X., "Selective growth, characterization and field emission performance of single-walled and few-walled carbon nanotubes by plasma enhanced chemical vapor deposition".

4. **Ionescu, M.I.**, et al., "Controlled synthesis of nitrogen-doped and multi-generation carbon nanotubes by spray pyrolysis".

5. **Ionescu, M.I.**, et al., "Nanostructured 1D/2D carbon hybrid by plasma assisted chemical vapor deposition".

6. **Ionescu, M.I.**, et al., "Synthesis of novel graphene sheets by reactive magnetron sputtering".

Patent:

Mihnea, M.I., Zhong, Y., Li, R., Abou-Rachid, H., Lussier, L-S.,and Sun, X., "Controlled synthesis of a novel class of carbon nanostructures: N-doped and multi-generation carbon nanotubes", U.S. Patent Application (on pending); 2009

Conferences:

1. **Ionescu, M.I.,** Geng, D., Zhang, Y., Li, R., and Sun, X., "Carbon Nanotubes/Graphene Nanocomposites as Supercapacitor Electrodes". 3rd International IUPAC Conference on Green Chemistry; refereed, Ottawa, Canada; 2010

2. **Ionescu, M.I.,** Li, R., and Sun, X., "Synthesis of advanced carbon nanomaterials and nanocomposites"; ECS Fall Symposium 2010, London, Canada; 2010

3. **Ionescu, M.I.,** Zhang, Y., Li, R., and Sun, X., "Synthesis of N-doped and Multiple-level Hierarchical Carbon Nanotubes". Ontario Nanoscience and Nanotechnology Workshop; London, Canada; 2010

4. **Ionescu, M.I**, Liu, H., Zhang, Y., Mérel, P., Désilet, S., Li, R., and Sun, X., "Temperature dependent resistivity of bulk multi-walled carbon nanotubes"; refereed, CSME Forum 2008, Ottawa, Canada; 2008

5. **Ionescu, M.I.**, Nastase, F., Nastase, C., Serban, C., and Stamatin, I., "High-quality SWNTs production using plasma-chemistry deposition method"; refereed, ICFPAM - 7th International Conference on Frontiers of Polymers and Advanced materials, Bucharest, Romania; 2003

6. Nastase, C., Stamatin, I., Nastase, F., and **Ionescu M.I.,** "The electrical properties of nanocomposites: pani-polysilicic acid"; refereed, ICFPAM, 7th International Conference on Frontiers of Polymers and Advanced Materials, Bucharest, Romania; 2003

7. Nastase, C., Stamatin, I., Nastase, F., **Ionescu, M.I.**, and Dumitru, A. "The effect of nanocarbon structures on the conductivity in a conductive polymer matrix"; refereed, Carbon 2003, Oviedo, Spain; 2003